earthscope

FACILITY OPERATION & MAINTENANCE

OCTOBER 1, 2008 – SEPTEMBER 30, 2018

Volume II – EarthScope Facilities

Volume III – EarthScope Science

Proposal to the National Science Foundation

March 2007

EarthScope Facility Operation and Maintenance

October 1, 2008–September 30, 2018

A Collaborative Proposal from:

the IRIS Consortium—for USArray
David Simpson, PI
Thorne Lay, University of California, Santa Cruz representing the IRIS Board of Directors

UNAVCO Inc—for Plate Boundary Observatory
Mike Jackson, PI
Charles Meertens, co-PI
Eric Calais, Purdue University representing the UNAVCO Board of Directors

Stanford University—for SAFOD
Mark Zoback, PI
Steven Hickman, USGS, co-PI
William Ellsworth, USGS, co- PI

Submitted to the
National Science Foundation
Division of Earth Sciences
EarthScope Program

March 2007

Volume III – EarthScope Science
Contributed Thematic Overviews and "One-Pagers"

Project Summary

EarthScope is a broad-based earth science initiative that is taking a multidisciplinary approach to studying the structure and evolution of the North American continent and the physical processes responsible for earthquakes and volcanic eruptions. The integrated observing systems that comprise the EarthScope Facility can be used to address fundamental questions at all scales—from the active nucleation zone of earthquakes, to individual faults and volcanoes, to the deformation along the plate boundary, to the structure of the continent and planet. EarthScope data will be openly available to maximize participation from the national and international scientific community and to provide ongoing educational outreach to students and the public.

The **intellectual merit** of the EarthScope Facility is derived from its link to the support of fundamental research throughout the earth sciences. Through an ambitious data collection scheme and broad geographic coverage, the EarthScope Facility will provide the observational resources to encourage cross-disciplinary investigations and stimulate the next generation of research scientists. The design and implementation plan for EarthScope was developed through extensive, decade-long engagement with the scientific and educational communities. Through numerous workshops and working groups, the research community, along with federal and state partners, defined the data and tools required for geoscience to take the next step in exploring the fundamental processes that shape the structure and evolution of our continents. As the MREFC-supported construction stage for the EarthScope Facility nears completion, exciting results are already emerging from the analysis of new EarthScope data, confirming the enhanced resolution provided by this powerful new suite of observational tools.

The **broader impacts** of EarthScope will be achieved through an integrated education and outreach program and applications in hazard assessment, land use, and resource management. While EarthScope is a national program, it is being operated and maintained at local levels through interactions with hundreds of universities, schools, and organizations across the nation. As EarthScope collects data and makes it available, students and the public will be introduced to key unanswered scientific questions and the role that their region or discipline plays in understanding the evolution of the North American continent and the active processes driving deformation and volcanic activity. Improved understanding of the natural environment is the first step toward improved land use, environmentally sound development, and resiliency to natural hazards. With over 3,000 geographical locations, the broad distribution of EarthScope facilities will engage traditionally under-represented groups, particularly students in rural areas that have under-resourced schools and Native Americans on tribal lands (where some of the EarthScope stations will be installed). EarthScope will provide a unique opportunity for students and the public to observe geological processes in real time and to measure geological change within the time frame of an academic school year. EarthScope is providing the public with practical examples of how science advances, as they see new data being collected and watch new theories being formulated and tested.

EarthScope Facility Operation & Maintenance
Volume III

EarthScope Science: Contributed Thematic Overviews and One-Page Essays

The EarthScope facilities are expected to enable research over the next ten to twenty years that radically departs from past investigations, thanks to an unprecedented abundance and resolution of data, all of which are freely and openly available and readily integrated with data of many different types. Less than four years after construction started, and with none of the facilities yet complete, one might expect new research results to be scarce. This volume demonstrates, instead, that while deep drilling is still underway and extensive new geodetic and seismological networks are still being installed, Earth scientists have already embraced these new data and, in concert with other geological and geophysical information, initiated research programs that will change our understanding of the structure and dynamics of North America and point to new ways to mitigate geologic hazards.

This volume is organized into two sections. The first section is a collection of thirteen thematic essays outlining nascent programs of discovery based on EarthScope data. The second section is comprised of about 100 one-page summaries of research projects that make use of EarthScope data, or that have been carried out on an exploratory scale using similar data, using new methods that promise to dramatically increase our understanding of Earth structure and processes when applied on a continental scale. These project summaries offer a taste of EarthScope science that will be accomplished as the facility is completed, new experimental avenues are explored and advanced analytical techniques evolve.

CONTRIBUTED THEMATIC OVERVIEWS

EARTHQUAKE SOURCE PHYSICS 1
Rachel Abercrombie · Boston University
Nadia Lapusta · California Institute of Technology
William Ellsworth · U.S. Geological Survey

EARTHQUAKE PROCESSES 5
Gregory Beroza · Stanford University
John Langbein · U.S. Geological Survey

SPATIAL AND TEMPORAL VARIATIONS IN FAULT LOADING AND STRAIN RELEASE RATES 9
James Dolan · University of Southern California

MODE OF DEFORMATION OF A CONTINENT 11
Lucy M. Flesch · Purdue University

RHEOLOGY OF THE LITHOSPHERE FROM POSTSEISMIC DEFORMATION CAPTURED WITH GPS 14
Elizabeth H. Hearn · University of British Columbia

FLUIDS AND FAULTING 17
Stephen Hickman · U.S. Geological Survey
Richard Sibson · University of Otago
Ronald Bruhn · University of Utah

CONTINENTAL DELAMINATION AND EARTHSCOPE 21
Craig Jones · University of Colorado
George Zandt · University of Arizona
Gene Humphreys · University of Oregon

THE GLOBAL REACH OF USARRAY DATA 24
Thorne Lay · University of California, Santa Cruz
Edward Garnero · Arizona State University

EPISODIC TREMOR AND SLIP 27
Timothy Melbourne · Central Washington University

A FIRST GLIMPSE OF CRUSTAL STRUCTURE FROM USARRAY 30
Morgan Moschetti, Michael Ritzwoller · University of Colorado, Boulder
Thomas Owens, Philip Crotwell · University of South Carolina

STRESS IN THE CRUST AND LITHOSPHERE: INSIGHT FROM EARTHSCOPE 33
Anne Sheehan · University of Colorado at Boulder
Paul Silver · Carnegie Institution of Washington, DTM

IMAGING DEEP STRUCTURE IN THE UPPER MANTLE UNDER NORTH AMERICA 35
Suzan van der Lee · Northwestern University
Barbara Romanowicz · University of California, Berkeley

STRENGTH, STRUCTURE AND RHEOLOGY OF FAULTS 38
Mark Zoback · Stanford University
Steve Roecker · Rensselaer Polytechnic Institute
Fred Chester · Texas A&M University

ONE-PAGE ESSAYS

CONVECTIVE INTERACTIONS IN THE MANTLE BENEATH THE PACIFIC NORTHWEST: THE FATE OF THE JUAN DE FUCA PLATE 43
Richard Allen, Mei Xue · University of California, Berkeley

A GROUND VELOCITY MAP FOR THE BASIN AND RANGE BASED ON INSAR 44
Falk Amelung, Noel Gourmelen · University of Miami

EXPLORING THE SEISMIC WAVEFIELD WITH THE TRANSPORTABLE ARRAY 45
Charles Ammon · Pennsylvania State University

ISOLATING SMALL, DISTANT SEISMIC EVENT SIGNALS WITH THE TRANSPORTABLE ARRAY 46
Charles Ammon · Pennsylvania State University
Thorne Lay · University of California, Santa Cruz

USING USARRAY DATA TO TOMOGRAPHICALLY IMAGE THE UPPER MANTLE 47
Heather Bedle, Suzan van der Lee · Northwestern University

UPPER MANTLE SEISMIC VELOCITY STRUCTURE IN THE GREAT BASIN 48
Caroline Beghein, Matthew Fouch · Arizona State University
Arthur Snoke · Virginia Polytechnic Institute and State University

THE EPISODIC TREMOR AND SLIP 2005 (ETS05) GPS CAMPAIGN, CASCADIA SUBDUCTION ZONE 49
R.A. Bennett · University of Arizona
S. Thompson, S. Hreinsdóttir, D. Johnson · Washington and Univ. Puget Sound

BROAD-BAND AMBIENT NOISE SURFACE WAVE TOMOGRAPHY ACROSS NORTH AMERICA USING EARTHSCOPE/USARRAY DATA . . 50
Gregory Bensen, Michael Ritzwoller · University of Colorado at Boulder
Nikolai Shapiro · Laboratoire de Sismologie, CNRS, Paris, France

FUNDAMENTAL STUDIES OF EARTHQUAKE AND STRUCTURE PROPERTIES BASED ON DATA ASSOCIATED WITH THE SAFOD FACILITY . 51
Yehuda Ben-Zion · University of Southern California

THE EARTHQUAKE ENERGY BALANCE. 52
Gregory Beroza · Stanford University

HIGH RESOLUTION MAPPING OF THE SOUTHERN SAN ANDREAS FAULT SYSTEM USING AIRBOURNE LASER SWATH MAPPING . . . 53
Mike Bevis · Ohio State University
Ken Hudnut · U.S. Geological Survey

OBSERVING SEISMIC WAVES USING HIGH-RATE GPS: THE 2002 DENALI FAULT EARTHQUAKE. 54
Andria Bilich, Kristine M. Larson · University of Colorado at Boulder

COLLABORATIVE RESEARCH: LOW TEMPERATURE THERMOCHRONOLOGY ON THE SAN ANDREAS FAULT OBSERVATORY AT DEPTH (SAFOD). 55
Ann Blythe · University of Southern California
Ken Farley · California Institute of Technology
Roland Burgmann · University of California, Berkeley

SEISMIC-ASEISMIC DEFORMATION REVEALED BY MICROSTRUCTURES OF THE SAN ANDREAS FAULT ROCKS 56
Anne-Marie Boullier, Jean-Pierre Gratier, François Renard · Université Joseph Fourier - CNRS, France
Muriel Andreani · Université Montpellier 2, France

CONTRIBUTIONS OF EARTHSCOPE TO EARTHQUAKE HAZARD ASSESSMENT IN NORTHERN CALIFORNIA 57
Tom Brocher, Bill Ellsworth, Steve Hickman, Diane Moore · U.S. Geological Survey

LONG-TERM MEASUREMENTS IN THE SAFOD BOREHOLE 58
Emily Brodsky · University of California, Santa Cruz

DEFORMATION OF THE NORTH AMERICAN PLATE INTERIOR FROM A DECADE OF CONTINUOUS GPS MEASUREMENTS 59
E. Calais · Purdue University
C. DeMets · University of Wisconsin

USING EARTHSCOPE DATA FOR ENVIRONMENTAL STUDIES 60
Philip Carpenter · Northern Illinois University

CONTEMPORARY DEFORMATION OF THE WASATCH FAULT, UTAH, FROM GPS MEASUREMENTS WITH IMPLICATIONS FOR INTER-SEISMIC FAULT BEHAVIOR AND EARTHQUAKE HAZARD 61
Wu-Lung Chang, Robert B. Smith · University of Utah

ACCELERATED UPLIFT OF THE YELLOWSTONE CALDERA, 2004-2006, FROM GPS AND INSAR OBSERVATIONS 62
Wu-Lung Chang, Robert B. Smith, Chuck Wicks, Christine M. Puskas · University of Utah

SAFOD DATA & COMPUTER SIMULATIONS TO CLARIFY EARTHQUAKE PHYSICS 63
Ting Chen, Nadia Lapusta · California Institute of Technology

INFLUENCE OF STRUCTURE AND COMPOSITION OF THE SAN ANDREAS FAULT ZONE ON ASEISMIC AND SEISMIC SLIP PROCESSES AT SAFOD 64
Judith S. Chester, Frederick M. Chester · Texas A&M University

PHYSICAL PROPERTIES OF SAFOD ROCKS. 65
Nikolas Christensen, Herb Wang · University of Wisconsin, Madison

ANISOTROPY IN THE SHALLOW CRUST OBSERVED AROUND THE SAN ANDREAS FAULT BEFORE AND AFTER THE 2004 MW6 PARKFIELD EARTHQUAKE 66
Elizabeth Cochran · University of California, Riverside
Yong-Gang Li · University of Southern California
John Vidale · University of Washington

EPISODIC TREMOR AND SLIP LOCATIONS USING EARTHSCOPE DATA 67
Kenneth Creager, Aaron Wech, Stephen Malone · University of Washington

TRANSIENT MOTIONS IN THE BASIN AND RANGE FROM BARGEN GPS DATA 68
J. L. Davis, E. Malikowski · Harvard-Smithsonian Center for Astrophysics
B.P. Wernicke, K. Mahan · California Institute of Technology

USING LIDAR DIGITAL TOPOGRAPHIC DATA TO DETERMINE FAULT SLIP RATES ALONG THE FISH LAKE VALLEY FAULT ZONE 69
James F. Dolan, Kurt L. Frankel · University of Southern California, Los Angeles

RESOLVING SUBTLE EPISODES OF TREMOR AND SLIP 70
H. Dragert · Geological Survey of Canada

STRUCTURAL AND PETROLOGIC ANALYSES OF THE SAN ANDREAS FAULT IN THE SAFOD REGION. 71
James Evans, Kelly Bradbury, Sarah Draper · Utah State University

MEASURING THE FLUID FLOW AND ELASTIC PROPERTIES OF CORE COLLECTED FROM SAFOD 72
Daniel Faulkner · University of Liverpool, UK
Ernest Rutter · University of Manchester, UK

FAULT SLIP RATES ON THE NORTHERN DEATH VALLEY FAULT ZONE: IMPLICATIONS FOR PACIFIC-NORTH AMERICA PLATE BOUNDARY DEFORMATION 73
Kurt L. Frankel, James F. Dolan · University of Southern California
Robert C. Finkel · Lawrence Livermore National Laboratory
Lewis A. Owen · University of Cincinnati

AUGUSTINE VOLCANO: PBO DATA 74
Jeff Freymueller · University of Alaska

DOES THE BERING PLATE EXIST? 75
Jeff Freymueller · University of Alaska
Mikhail Kogan · Columbia University

PLATE COUPLING VARIATIONS IN THE 1964 ALASKA EARTHQUAKE RUPTURE ZONE. 76
Jeff Freymueller · University of Alaska

POSTSEISMIC DISPLACEMENTS FROM PBO SITES NEAR THE DENALI FAULT 77
Jeff Freymueller · University of Alaska

NORTHERN CALIFORNIA AIRBORNE LIDAR IMAGERY ACQUISITION FOR GEOEARTHSCOPE 78
K. Furlong, R. Bruhn, D. Burbank, J. Dolan · GeoEarthScope LiDAR Working Group

CONSTRAINING THE CRUSTAL CONVEYOR: EARTHSCOPE IMAGING OF MENDOCINO TRIPLE JUNCTION (MTJ) TECTONICS 79
Kevin P Furlong, Gavin P Hayes · Pennsylvania State University
Todd Williams · UNAVCO

MAPPING UPPER-MANTLE ANISOTROPY BENEATH THE WESTERN US: TOWARD AN INTEGRATED SEISMIC AND GEODYNAMIC ANALYSIS OF CRUST-MANTLE COUPLING 80
James Gaherty, Arthur Lerner-Lam · Columbia University
Li Zhao · Academia Sinica, Taiwan
Mousumi Roy · University of New Mexico

LINEAMENTS IN CENTRAL-EASTERN OREGON 81
Gary Egbert · Oregon State University
Randy Mackie · GSY-USA, Inc.
Shane Ingate · IRIS
Dean Livelybrooks · University of Oregon

USARRAY IMAGES FOUNDERING LITHOSPHERE 82
Hersh Gilbert · Purdue University
George Zandt · University of Arizona
Craig Jones · University of Colorado at Boulder
Tom Owens · University of South Carolina

LABORATORY STUDIES OF THE FRICTIONAL BEHAVIOR OF MATERIALS CORED FROM THE SAN ANDREAS FAULT 83
David Goldsby · Brown University

MICROSTRUCTURAL ANALYSES OF GOUGE FROM THE SAFOD BOREHOLE IN RELATION TO BRITTLE FAULT MECHANICS: A COLLABORATIVE STUDY 84
Jafar Hadizadeh · University of Louisville
Hassan Babaie · Georgia State University
Karen Mair · University of Oslo, Norway
Giulio Di Toro · University of Padova, Italy

AN INTERACTIVE MAP TOOL FOR EARTHSCOPE EDUCATION AND OUTREACH 85
Michael Hamburger · Indiana University
Marianne Weingroff · Digital Library for Earth System Education/UCAR, Boulder
William Holt · State University of New York at Stony Brook
Lou Estey · UNAVCO

COMPARING GEODETICALLY AND GEOLOGICALLY INFERRED DEFORMATION OF THE WALKER LANE, WESTERN BASIN AND RANGE . 86
William C. Hammond, Corné Kreemer, Geoff Blewitt · University of Nevada, Reno

GEOTHERMS, FLUIDS AND LITHOSPHERIC STRUCTURE OF THE GREAT BASIN–COLORADO PLATEAU TRANSITION ZONE, 38.5N LATITUDE 87
Derrick Hasterok, David S. Chapman · University of Utah
Phillip E. Wannamaker · Energy and Geoscience Insititute
William Doerner · Quantech Geoscience

REAL-TIME DATA FEEDS FROM THE PLATE BOUNDARY OBSERVATORY BOREHOLE INSTRUMENTS AT ANZA TO THE CALTECH/USGS SOUTHERN CALIFORNIA SEISMIC NETWORK 88
Egill Hauksson · Seismological Laboratory, Caltech

REAL-TIME DATA SHARING BETWEEN USARRAY AND THE CALTECH/USGS SOUTHERN CALIFORNIA SEISMIC NETWORK 89
Egill Hauksson · Seismological Laboratory, Caltech

QUANTIFYING REGIONAL VELOCITY RATIO IN CALIFORNIA: USING SEISMIC DATA TO MAP SHALLOW STRUCTURE 90
Gavin Hayes, Kevin Furlong · Pennsylvania State University

CHARACTERIZING TRANSIENT STRAIN RATE DEPARTURES FROM A LONG-TERM STRAIN RATE FIELD. 91
Daniel Hernandez, William E. Holt · State University of New York at Stony Brook
A. John Haines · University of Cambridge, United Kingdom
Richard A. Bennett · University of Arizona

EARTHSCOPE AND TECTONICS STRESS ACROSS NORTH AMERICA 92
Robert Herrmann · Saint Louis University
Charles Ammon · Pennsylvania State University

WALLOWA MOUNTAIN UPLIFT AND ERUPTION OF THE COLUMBIA RIVER FLOOD BASALTS:
A GREEN'S FUNCTION DELAMINATION EVENT 93
Gene Humphreys · University of Oregon

USING LARGE APERTURE SEISMIC ARRAYS TO IMAGE THE RUPTURES OF THE NOVEMBER 15, 2006
AND JANUARY 13, 2007 KURIL EARTHQUAKES 94
Alexander Hutko · University of California, Santa Cruz

COPIOUS POSTSEISMIC SLIP FOLLOWING THE 2004 PARKFIELD EARTHQUAKE, CONSTRAINED BY GPS AND INSAR DATA. 95
Ingrid Johanson · U.S. Geological Survey
Eric Fielding · Jet Propulsion Laboratory
Roland Bürgmann · University of California, Berkeley
Frederique Rolandone · Universite Pierre et Marie Curie, France

EARLY TOMOGRAPHIC RESULT FROM THE BROADBAND FLEXARRAY DEPLOYMENT IN THE SIERRA NEVADA 96
Craig Jones · University of Colorado
Hersh Gilbert · Purdue University
George Zandt · University of Arizona
Tom Owens · University of South Carolina

EARTHQUAKE SOURCE PROPERTIES FROM NEAR-FIELD EARTHQUAKE MONITORING 97
Thomas Jordan, Yehuda Ben-Zion · University of Southern California
Ze'ev Reches · University of Oklahoma
Margaret Boettcher · U.S. Geological Survey

RESULTS OF ELEMENTAL, STABLE ISOTOPE, ORGANIC MATTER, AND FISSION-TRACK ANALYSES OF SAFOD DRILL-HOLE
CUTTINGS AND CORE MATERIAL 98
David Kirschner · Saint Louis University
Judith Chester · Texas A&M University
John Garver · Union College
Jim Evans · Utah State University

REFLECTION IMAGING THE 35°-DIPPING NORMAL FAULT THAT BOUNDS THE BASIN & RANGE PROVINCE 99
Simon Klemperer · Stanford University
Derek Lerch · Feather River College
Anne Egger · Stanford University
Joseph Colgan · U.S. Geological Survey

CRUSTAL STRUCTURE OF THE NORTHWESTERN BASIN AND RANGE PROVINCE AND ITS TRANSITION TO UNEXTENDED
VOLCANIC PLATEAUS. 100
Simon Klemperer · Stanford University
Derek Lerch · Feather River College
Jonathan Glen, David Ponce · U.S. Geological Survey

GEOLOGICAL INTERPRETATION OF MULTI-DIMENSIONAL GEOPHYSICAL MONITORING DATA BASED ON SELF-ORGANIZING MAPS . . 101
Christian Klose · Columbia University

NOISE IN GPS MEASUREMENTS FROM SOUTHERN CALIFORNIA AND SOUTHERN 102
John Langbein · U.S. Geological Survey

TIDAL CALIBRATION OF PBO STRAINMETERS LOCATED IN THE PACIFIC NORTHWEST 103
John Langbein · U.S. Geological Survey

WAVE GRADIOMETRY FOR EARTHSCOPE 104
Charles Langston · University of Memphis

IS IT ALL WET? SEARCHING FOR HYDRATED MANTLE ROCK WITHIN CASCADIA MEGATHRUST. 105
Vadim Levin, Alex Nikulin · Rutgers University
Jeffrey Park · Yale University

THE LITHOSPHERE-ASTHENOSPHERE BOUNDARY BENEATH THE WESTERN UNITED STATES 106
Xueqing Li, Xiaohui Yuan and Rainer Kind · GeoForschungsZentrum Potsdam, Germany

MONITOR PROPERTY VARIATIONS ON THE PARKFIELD SAN ANDREAS BY FAULT-ZONE TRAPPED WAVES 107
Yong-Gang Li · University of Southern California
Peter E. Malin · Duke University
Elizabeth S. Cochran · University of California, Riverside
John E. Vidale · University of Washington

HIGH RESOLUTION AMBIENT NOISE SURFACE WAVE TOMOGRAPHY OF THE WESTERN UNITED STATES USING EARTHSCOPE USARRAY DATA: PHASE VELOCITY MAPS FOR RAYLEIGH AND LOVE WAVES 108
Fan-Chi Lin, Morgan P. Moschetti, Michael H. Ritzwoller · University of Colorado at Boulder

DEFORMATION ASSOCIATED WITH ERUPTIVE ACTIVITY AT MOUNT ST. HELENS, WASHINGTON 109
Michael Lisowski, Larry Mastin, Daniel Dzurisin, Michael Poland · U.S. Geological Survey

FAULT SLIP IN C SHARP MINOR: FAULT SLIP RESONANCE AS A MECHANISM FOR SLOW SLIP 110
Anthony R. Lowry · Utah State University

LABORATORY STUDY OF THE MECHANICS AND PHYSICAL PROPERTIES OF THE SAN ANDREAS FAULT AND 3D SAFOD VOLUME. . . . 111
Chris Marone, Demian Saffer · Pennsylvania State University
Harold Tobin · University of Wisconsin, Madison

VELOCITY FIELD OF THE PACIFIC NORTHWEST 112
Rob McCaffrey · Rensselaer Polytechnic Institute
Robert W. King · Massachusetts Institute of Technology
Anthony Qamar · University of Washington

SUBDUCTION TREMOR AND SLOW SLIP RECORDED IN JANUARY 2007 IN CASCADIA ON THE PLATE BOUNDARY OBSERVATORY (PBO) BOREHOLE NETWORK 113
Wendy McCausland, Evelyn Roeloffs · U.S. Geological Survey

A 70+ STATION GPS RECORDING OF THE JANUARY, 2007 CASCADIA ETS 114
Timothy Melbourne, Marcelo Santillan, Walter Szeliga, Meghan Miller · Central Washington University

GPS CONSTRAINTS ON 34 SLOW SLIP EVENTS WITHIN THE CASCADIA SUBDUCTION ZONE 115
Timothy Melbourne, Marcelo Santillan, Meghan Miller · Central Washington University

TRACKING THE PROGRESS OF THE USARRAY TRANSPORTABLE ARRAY WITH AMBIENT NOISE TOMOGRAPHY 116
Morgan Moschetti, Michael Ritzwoller · University of Colorado at Boulder
Nikolai Shapiro · Institut de Physique du Globe de Paris, France

A MICROSEISMIC VIEW OF THE IMMEDIATE SAFOD TARGET ZONE 117
Robert Nadeau · University of California, Berkeley

ONGOING TRANSIENT DEFORMATION FROM A SHALLOW SOCORRO MAGMA BODY? 118
Andrew V. Newman · Georgia Institute of Technology
Timothy H. Dixon · University of Miami
Dave Love, Richard Chamberlain · New Mexico Bureau of Geology and Mineral Resources

THE EARTHSCOPE AUTOMATED RECEIVER SURVEY. 119
Thomas J. Owens, H. Philip Crotwell · University of South Carolina

ARRAY PROCESSING OF TELESEISMIC BODY WAVES WITH THE EARTHSCOPE TRANSPORTABLE ARRAY 120
Gary Pavlis · Indiana University
Frank Vernon · University of California, San Diego

MICROPLATE DEFORMATION OF THE WESTERN U.S. INTERIOR 121
C. M. Puskas, R. B. Smith · University of Utah

KINEMATICS AND CRUSTAL DEFORMATION OF THE YELLOWSTONE HOTSPOT FROM GPS MEASUREMENTS: 1987-2006 122
C. M. Puskas, R. B. Smith, W. L. Chang · University of Utah
C. M. Meertens · UNAVCO

STRUCTURE AND PHYSICAL PROPERTIES OF FAULT ROCKS OF THE SAN ANDREAS FAULT-ZONE AT SAFOD BOREHOLE AND EXHUMED, ACTIVE SEGMENTS 123
Ze'ev Reches, Randy Keller · University of Oklahoma

HIGH-RESOLUTION 3D ANISOTROPIC STRUCTURE OF THE NORTH AMERICAN UPPER MANTLE FROM INVERSION OF BODY AND SURFACE WAVEFORM DATA 124
Barbara Romanowicz · Berkeley Seismological Laboratory
Federica Marone · Paul Scherrer Institute, Switzerland

IMAGING SUBDUCTION AND RELATED FLUID PROCESSES IN THE PACIFIC NORTHWEST: CASCADIA ARRAYS FOR EARTHSCOPE (CAFE). 125
Stéphane Rondenay · Massachusetts Institute of Technology
Geoffrey Abers · Boston University
Kenneth Creager, Stephen Malone · University of Washington

EARTHQUAKE NUCLEATION 126
Allan Rubin · Princeton University

SOURCE PROCESSES AND EARTHQUAKE TRIGGERING USING SAFOD DATA 127
Justin Rubinstein · University of Washington

INTEGRATING CONTROLLED-SOURCE AND PASSIVE SEISMIC DATASETS 128
Eva-Maria Rumpfhuber, Randy Keller · University of Oklahoma
Aaron Velasco · University of Texas at El Paso

MODELING PLATE BOUNDARY STRESS CHANGES WITH INSAR AND CGPS 129
David Sandwell, Bridget Konter, Yehuda Bock · University of California, San Diego

CRUSTAL DEFORMATION AND THE SEISMIC CYCLE ACROSS THE KODIAK ISLANDS, ALASKA 130
Jeanne Sauber, Steven Cohen · National Aeronautics and Space Administration, Goddard Space Flight Center
Gary Carver · Humboldt University
Robert King · Massachusetts Institute of Technology

CLAY MINERAL REACTIONS IN THE SAFOD DRILLHOLE AND THEIR INFLUENCE ON THE SEISMIC BEHAVIOR OF THE SAN ANDREAS FAULT. 131
Anja M. Schleicher · Universität Würzburg, Germany
Laurence N. Warr · Centre de Géochimie de la Surface, France
Ben A. van der Pluijm, Sara Tourscher · University of Michigan

INVESTIGATIONS OF SLOW SLIP ALONG THE CASCADIA SUBDUCTION ZONE USING GPS AND STRAINMETER TIME SERIES 132
David Schmidt, Haiying Gao · University of Oregon

EARTHSCOPE ENGAGES AMERICAN INDIAN STAKEHOLDERS IN ARIZONA 133
Steven Semken, Peterson Zah, Matthew Fouch, Edward Garnero · Arizona State University

INTERFEROMETRIC TECHNIQUES FOR FAULT ZONE IMAGING AND MONITORING 134
Roel Snieder, Ivan Vasconcelos, Alexandre Gret · Colorado School of Mines

CONSTRAINING THE COMPOSITION AND BEHAVIOR OF FAULT ZONES AT SAFOD 135
John Solum · Sam Houston State University
David Lockner, Stephen Hickman, Diane Moore · U.S. Geological Survey

GPS CONSTRAINTS ON CONTINENTAL INTRAPLATE EARTHQUAKES AND HAZARDS 136
Seth Stein · Northwestern University

MAPPING THE PV-PPV BOUNDARY BENEATH CENTRAL AMERICA 137
Daoyuan Sun, Don Helmberger · California Institute of Technology

MULTI-PARAMETER SEISMIC IMAGING OF THE CRUST AROUND SAFOD, PARKFIELD, CALIFORNIA. 138
Clifford Thurber, Haijiang Zhang, Ninfa Harrington · University of Wisconsin, Madison
Steven Roecker · Rensselaer Polytechnic Institute

LOCATING THE SAFOD DRILLING TARGET EARTHQUAKES 139
Clifford Thurber, Haijiang Zhang, Yunfeng Liu · University of Wisconsin, Madison
Steven Roecker · Rensselaer Polytechnic Institute

EARTHQUAKE SOURCE STUDIES USING ANZA AND PBO BOREHOLE DATA 140
Frank Vernon · University of California, San Diego

USARRAY HELPS UPGRADE THE PACIFIC NORTHWEST SEISMIC NETWORK 141
John Vidale, Paul Bodin, Steve Malone · University of Washington

ALONG-STRIKE VARIATION IN LOCKING ON THE CASCADIA SUBDUCTION ZONE, OREGON AND NORTHERN CALIFORNIA 142
Ray Weldon, David Schmidt, Reed Burgette · University of Oregon

SUBCONTINENTAL-SCALE STRAIN WAVES ACROSS THE PACIFIC-NORTH AMERICA PLATE BOUNDARY DEFORMATION ZONE: A JOINT EARTHSCOPE-TECTONICS OBSERVATORY STUDY IN CENTRAL NEVADA. 143
B. Wernicke, K. Mahan, M. Simons, R. Briggs · California Institute of Technology

ON THE ORIGIN, CONCENTRATION AND SPATIAL DISTRIBUTION OF GASES AT SEISMOGENIC DEPTHS 144
Thomas Wiersberg, Jörg Erzinger · GeoForschungsZentrum Potsdam, Germany

SEISMIC TRAVEL TIMES AND ATTENUATION MEASUREMENTS:AN EARTHSCOPE DATA PRODUCT 145
Michael Wysession · Washington University

AMBIENT NOISE AND TELESEISMIC TOMOGRAPHY TO INFER THE PHYSICAL STATE AND STRUCTURE OF THE CRUST AND UPPER MANTLE IN THE WESTERN US 146
Yingjie Yang, Michael Ritzwoller, Morgan Moschetti · University of Colorado at Boulder
Donald Forsyth · Brown University

TESTING THE FIVE SIMPLEST UPPER MANTLE ANISOTROPIC VELOCITY PARAMETERIZATIONS USING TELESEISMIC S AND SKS DATA FROM THE BILLINGS, MONTANA PASSCAL ARRAY 147
Huaiyu Yuan, Ken Dueker, Derek Schutt · University of Wyoming

SEISMIC IMAGING OF SOUTHERN CALIFORNIAN CRUST USING DEFORMABLE-LAYER TOMOGRAPHY AND PRESTACK DEPTH MIGRATION: INNOVATIVE APPLICATIONS FOR EARTHSCOPE/USARRAY PROJECTS 148
Hua-wei Zhou, Michael Thornton, Li Li, Chris Gantela, Tom Bjorklund · University of Houston

EARTHQUAKE SOURCE PHYSICS

Rachel Abercrombie • Boston University
Nadia Lapusta • California Institute of Technology
William Ellsworth • U.S. Geological Survey

SAFOD will provide us with the first data from within the earthquake source zone, that is essential for us to understand earthquake source physics, and thus to develop the physics-based models of earthquakes required to evaluate strong ground motion and seismic risk.

Understanding the physical processes that occur during an earthquake has been a central objective of seismology since the instrumental study of earthquakes began over a century ago. The field has made major strides in understanding both the wave motions that occur when a fault suddenly slips (the "earthquake") and the kinematics of the phenomena that occur on the fault (the "earthquake source" processes) that creates the seismic waves. Seismological data and methods have been particularly effective, as elasticity provides a quantitative theoretical framework for the analysis of wave phenomena. The processes that control occurrence of slip on the fault, however, are less well understood. How do earthquakes nucleate and arrest? What controls the spatio-temporal distribution of slip on faults? What are the appropriate description and parameters of fault friction? How do thermal effects due to shear heating in rapid slips influence dynamic rupture propagation? How is energy released in an earthquake partitioned between radiated energy and energy dissipated in fault processes? How do earthquake energetics scale with magnitude? What is the stress state on faults? How much slip on faults occurs seismically vs. aseismically? How predictable are earthquake characteristics such as rupture direction? Numerical simulations of earthquake processes and interpretation of laboratory rock experiments are currently limited by the lack observations from near to the earthquake source that SAFOD will provide.

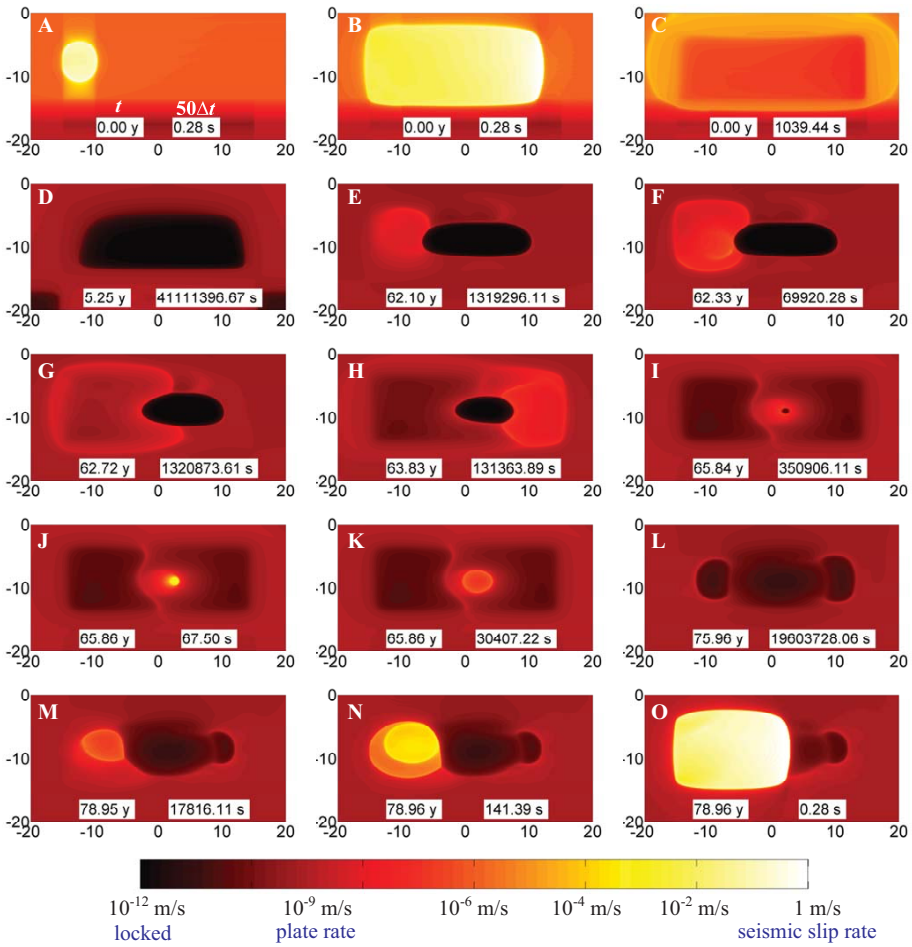

Figure 1: State-of-the-art simulation of the seismic cycle of strain accumulation and release valid over time and slip rate scales of interseismic loading, nucleation and dynamic rupture. Each panel shows the elapse time t and the time increment Δt. Locked portions of the model fault (40 by 20 km) are black, creeping portions red and seismically slipping portions yellow and white. The first event (panels A and B) is followed by rapid post-seismic creep (panel C) that gives away to an evolving pattern of accelerating and decelerating aseismic slip. Nucleation processes (panels M and N) eventually succeed in initiating the second event (panel O) (Lapusta and Liu, 2006).

A natural laboratory in which synoptic studies of the earthquake process are conducted through multi-parameter observations is needed to study the physical processes that occur during fault rupture. By placing seismometers and accelerometers within or adjacent to the fault, we will obtain information on the physical phenomena that occur during nucleation, rupture and arrest of earthquakes. By also emplacing instruments that measure tilt, pore pressure and temperature within or immediately adjacent to active sliding surfaces, we can study connections between displacements, deformation, variations in pore pressure and heat generated during sliding.

In the report *Living on an Active Earth: Perspectives on Earthquake Science* (2003) the Committee on Earthquake Science of the National Research Council underscored the critical need for near-field observations to develop and test theoretical and numerical models of the earthquake generation process. They argued that the understanding of earthquake source

physics on short time scales is essential for understanding a broad spectrum of processes ranging from how dynamic slip is initiated and sustained to how strong ground motions are generated. Ultimately, the validation of theories and models of earthquake source processes including earthquake nucleation, earthquake interaction and recurrence depend on observations that can only be made within the process zone of the underlying phenomena.

SAFOD represents a unique facility for conducting near-field observational studies of the earthquake source. Its location ensures that seismic, pore-pressure, tilt, and temperature data will be captured in unprecedented proximity for multiple earthquakes and processes before and after them. Proximity is an important advantage of SAFOD, as it not only allows to capture variations that may not be observable at a greater distance but also significantly improves the ability to separate the signal into path effects and source contributions. Following the completion of the Phase 3 core drilling, the multi-parameter long-term monitoring system will be installed within the fault core and damage zone of the San Andreas Fault at the location of a repeating microearthquake (M 1.8 – 2.0). The details of the emplacement will not be known until drilling has been completed, but each of the candidate earthquake sources has been observed to repeat multiple times over the past

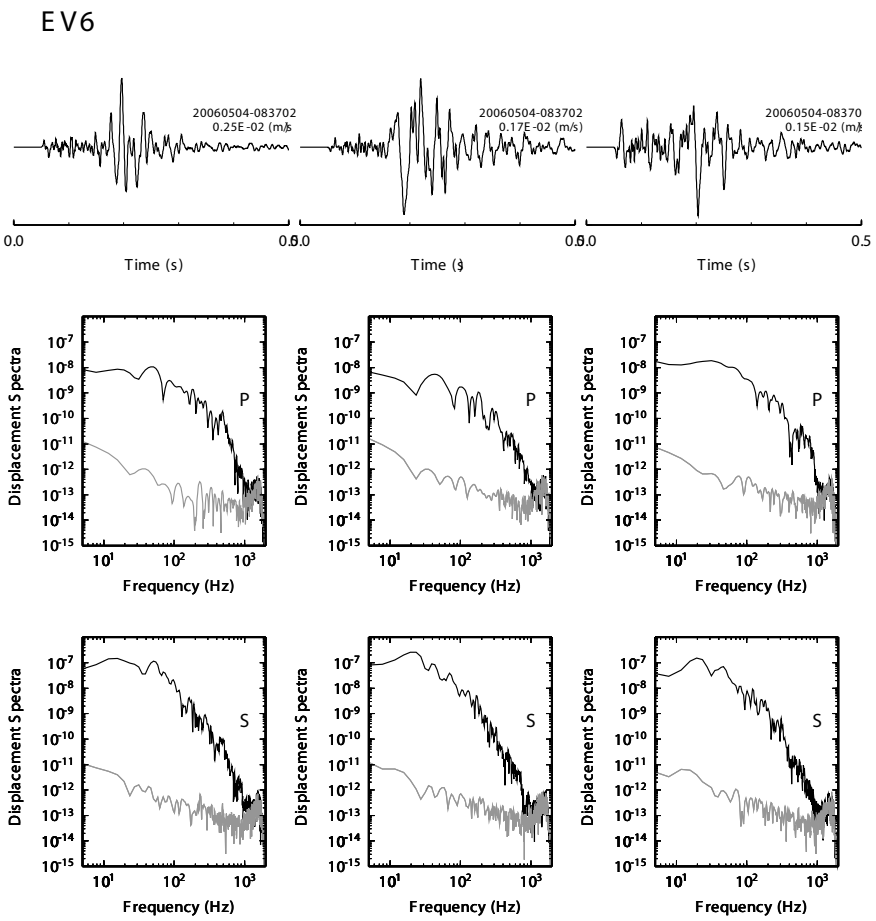

Figure 2: Seismograms and spectra of M 1.1 earthquake of May 4, 2007 08:37 recorded at a depth of 2660 m in the SAFOD main hole. The event occurred about 600 m from the instrument. Note the very broad bandwidth of the P and S body waves (black line) with energy above the noise (gray line) at frequencies up to 1000 Hz. A stress drop of 30 MPa was determined for this event using the method of Imanishi and Ellsworth (2006).

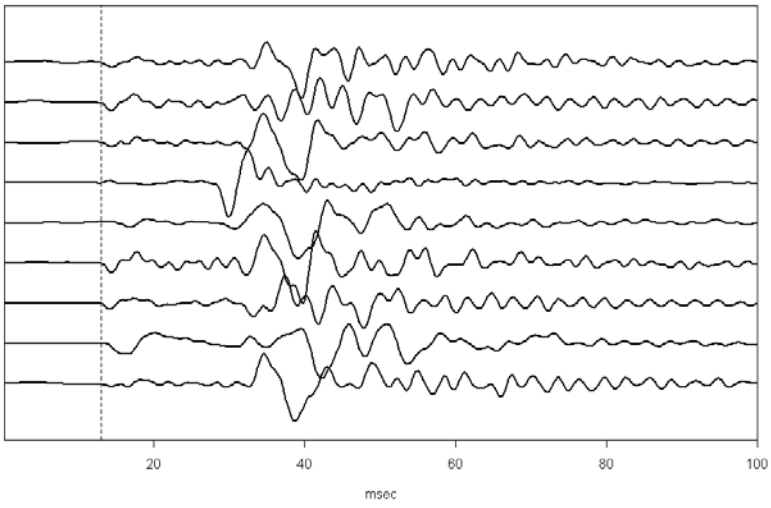

Figure 3: Seismograms of microearthquakes, M -1.5 to -3, recorded at a depth of 2660 m in the SAFOD main hole. Seismograms aligned on the P-wave arrival. The S-P intervals range from 15 to 23 msec indicating that the earthquakes occurred between 90 and 140 m from the sensor.

2 decades. Currently, the recurrence interval for the sources stands at slightly over 1 year. They are slowly lengthening toward their long-term values of between 2 and 3 years as the post seismic slip rate transient of the 2004 Parkfield earthquake fades away. Over the course of the planned 15 year lifetime of the SAFOD monitoring program, multiple recurrences of the target earthquake will be observed.

The process by which a fault becomes unstable and initiates a dynamically propagating rupture is central to the understanding of how earthquakes work. It has long been understood, on the basis of theoretical and laboratory-based models, that aseismic (stable) sliding must precede dynamic rupture. Critical issues that continue to be vigorously debated and that can be addressed with SAFOD data include 1) the process of transition from aseismic nucleation to seismic sliding, which could be called seismic nucleation, and 2) the potential scaling of aseismic and seismic nucleation processes with

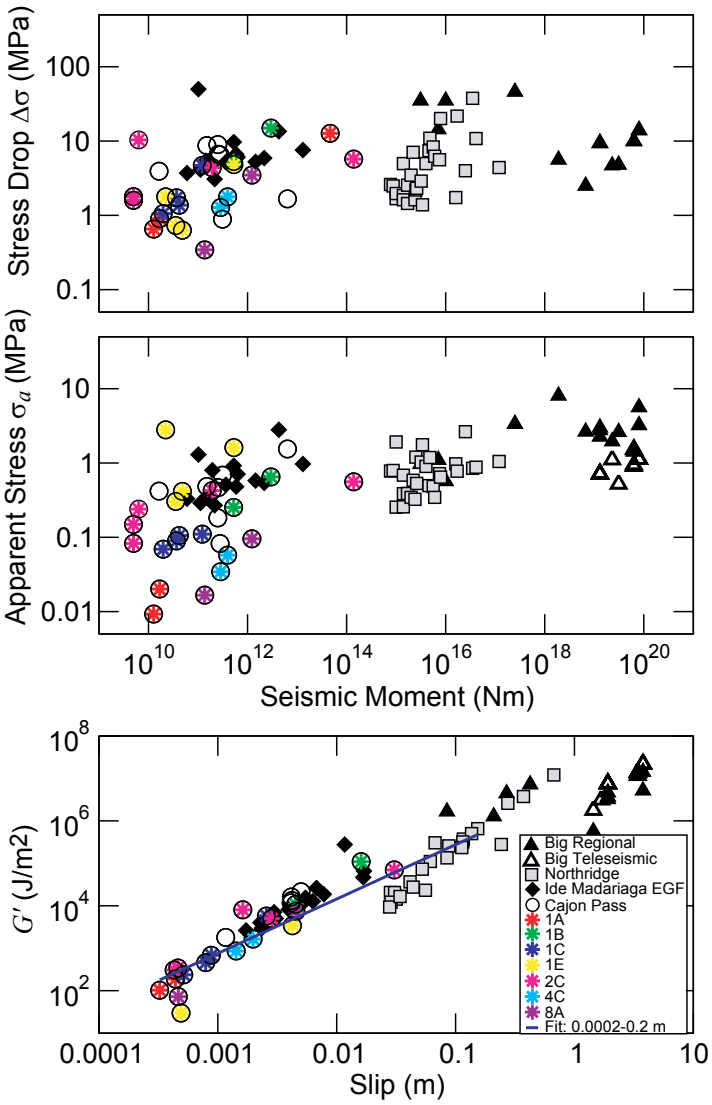

Figure 4: How do earthquake sources scale, and what is the energy budget? Abercrombie (1995) showed that the static stress parameters of small earthquakes were similar to those of larger ones, but found that there could be scale dependence to the energy budget. A decade of ongoing work using far-field recordings has still failed to determine whether this is a real earthquake source effect, or simply reflects the limitation of the observations. The figure combines some of the best estimates of (a) static stress drop, (b) apparent stress and (c) G', an estimate of fracture energy. The least squares fit (blue line) is between 0.2mm and 0.2 m slip. The circles are earthquakes recorded 2.5 km down the Cajon Pass borehole (earthquakes from the same cluster are the same color), the black diamonds are from the Long Valley borehole Ide et al. (2003), the grey squares are the larger Northridge aftershocks (Mori et al. 2003) and the black triangles are estimates of source parameters of larger, mostly Californian earthquakes (solid symbols are regional estimates of energy and open symbols, teleseismic)., Abercrombie and Rice (2005).

earthquake size. Unfortunately, far field observations of the initiation of rupture have thus far proven inadequate to address those issues. The near field data to be collected at SAFOD has the potential to illuminate the processes leading to earthquake initiation and, in particular, to resolve whether or not the initial growth of dynamic rupture represents the end-stage of a slow growth to instability or a cascade of crack-like subevents. In addition, by comparing SAFOD data with laboratory rock measurements and outputs of numerical models that simulate earthquake nucleation, one might be able to infer constitutive assumptions such as fault friction laws that best reproduce earthquake behavior. For example, the validity of rate and state friction models for earthquake nucleation can be assessed.

The physics of earthquake rupture propagation has also been the subject of intensive observational, experimental and theoretical investigations in recent years. Again, we are limited by the lack of observations from the near-field of the earthquakes. The energy budget, fundamental to understanding the dynamics of a system, is very poorly known, as is whether it varies with earthquake size. New data has again drawn into question the standard model of a dynamically expanding crack that heals inward from its outer boundary. Evidence from kinematic studies of large earthquakes shows that the rupture may propagate as a self-healing slip pulse, yet there is no consensus on how such a concentrated slip zone is generated or maintained, or why the fault comes to rest so abruptly. Several mechanisms have been shown by numerical models to result in pulse-like rupture propagation, including: significant dynamic weakening of the fault friction coefficient with seismic slip rates, supported by laboratory rock experiments; dynamic variation of pore pressure and hence normal stress during sliding: normal stress variations during sliding due to material contrast across the fault; tensile opening of the fault within the pulse as observed in foam-rubber experiments; local wave arrests due to heterogeneous stress or strength distributions or geometric effects. These mechanisms would all result in significant reduction of fault strength during sliding and hence could explain how a fault can have high static strength, but slide without generating much heat. However, sliding at near-zero values of stress implies that the dynamic stress change should nearly equal the tectonic stress. Thus, using high-quality near-field SAFOD data to infer dynamic stress changes, will give us a direct test of the high static strength/low dynamic strength hypothesis for the range of earthquake slips that can be observed at SAFOD. This will provide a constraint on how much the fault needs to slide before the weakening mechanisms can be engaged and will contribute to the understanding of energy partition between radiated energy and energy dissipated on the fault in processes that resist sliding. From the detailed velocity logs across the fault collected in the Phase 2 drilling in 2005 and the logs and core samples to be collected in Phase 3 drilling, SAFOD will have unique constraints on the physical system that hosts the repeating

earthquakes, opening new opportunities for research on the modes and mechanics of rupture propagation. In part, it will help further constrain some of earthquake physics hypotheses such as the importance of material contrast across the fault for rupture modes and rupture direction.

Completeness of earthquake catalogs and a related issue of whether earthquakes have a minimum size is an important question in earthquake studies with direct implications for processes governing earthquake nucleation. Observations of microearthquakes in moderately deep boreholes (2–2.5 km) at Cajon Pass, California, the SAFOD pilot hole and in Long Valley, California, demonstrate that ultra high-fidelity recordings can be made in downhole observatories. Instrumentation in the SAFOD Main Hole will extend the potential range of observable earthquakes to M -2 or even M -3, bringing the observational base of natural earthquakes into the size range of laboratory earthquakes. The ability to capture such small earthquake sizes over a period of time will extend the range of earthquake statistics and address the question of whether there is a cut-off in earthquake sizes as predicted by some models. Such ability is also important for studying earthquake source properties over a range of earthquake magnitudes.

SAFOD data will provide a benchmark for theoretical and numerical models of earthquake processes and laboratory rock experiments, and complementary data to near-source observations of large magnitude earthquakes. Numerical simulations of the earthquake on rate-and-state faults have now advanced to the point that they can produce numerically accurate models that span the slow earthquake loading cycle and dynamic rupture on fault patches of comparable dimension to the SAFOD target earthquakes. We should anticipate a productive interchange between observations, theories, models and laboratory experiments, as we begin to gather data in the near field of the target earthquakes.

Abercrombie, R. E. (1995), Earthquake source scaling relationships from -1 to 5 ML, using seismograms recorded at 2.5 km depth, J. Geophys. Res., 100, 24015-24036.

Beeler, N. M., D. L. Lockner, and S. H. Hickman, (2001), A Simple Stick-Slip and Creep-Slip Model for Repeating Earthquakes and its Implication for Microearthquakes at Parkfield, Bull. Seism. Soc. Am. 91, 1797–1804.

Ben-Zion, Y. (2001), Dynamic ruptures in recent models of earthquake faults, J. Mech. Phys. Solids 49, 2209-2244.

Beroza, G. C. and T. Mikumo (1996), Short slip duration in dynamic rupture in the presence of heterogeneous fault properties, J. Geophys. Res., 101, 22449-22460.

Earthquakes: Radiated Energy and the Physics of Faulting (2006), R.E. Abercrombie, A. McGarr, G. Di Toro, and H. Kanamori, eds., Geophysical Monograph 170, Amer. Geophys, U., Washington, D.C., ISBN-13:978-0-87590-435-1.

Heaton, T.H. (1990), Evidence for and implications of self-healing pulses of slip in earthquake rupture, Phys. Earth Planet. Inter. 64, 1-20.

Ide, S., G.C. Beroza, S.G. Prejean, and W. L. Ellsworth. (2003), Apparent break in earthquake scaling due to path and site effects on deep borehole recordings, J. Geophys. Res, 108, DOI 10.1029/2001JB001617.

Imanishi, K., and W.L. Ellsworth (2006), Source scaling relationships of microearthquakes at Parkfield, CA, determined using the SAFOD pilot hole array, in Earthquakes: Radiated Energy and the Physics of Faulting, R.E. Abercrombie, A. McGarr, G. Di Toro, and H. Kanamori (Editors), Geophysical Monograph 170, Amer. Geophys. U., Washington, D.C., p. 81-80.

Kanamori, H., and E. Brodsky (2004), The physics of earthquakes, Rep. Prog. Phys. 67, 1429–1496.

Lapusta, N., and Y. Liu (2006), Three-dimensional elastodynamic simulations of seismic and aseismic slip history of a planar strike-slip fault, EOS Trans. Am. Geophys. U., v. 87, no. 52, Abstract S34A-07.

Lapusta, N. and J.R. Rice (2003), Nucleation and early seismic propagation of small and large events in a crustal earthquake model, J. Geophys. Res. 108, DOI 10.1029/2001JB000793.

Living on an Active Earth, Perspectives on Earthquake Science (2003), Committee on the Science of Earthquakes, Board on Earth Sciences and Resources, Division on Earth and Life Studies, National Research Council of the National Academies, ISBN 0-309-06562-3.

Marone, C. (1998), Laboratory-derived friction laws and their application to seismic faulting, Ann. Revs. Earth & Plan. Sci., 26, 643-696.

Mori, J., R.E. Abercrombie, and H. Kanamori (2003), Stress drops adn radiated energies of aftershocks of the 1994 Northridge, California, earthquake, J. Geophys. Res, v. 108, DOI 10.1029/2001JB000474.

Nadeau, R. M. and L. R. Johnson (1998), Seismological studies at Parkfield VI: Moment release rates and estimates of source parameters for small repeating earthquakes, Bull. Seism. Soc. Am. 88, 790-814.

Nielsen, S.B., J.M. Carlson and K.B. Olsen (2000), Influence of friction and fault geometry on earthquake rupture, J. Geophys. Res. 105, 6069-6088.

Rice, J.R. (2006), Heating and weakening of faults during earthquake slip, J. Geophys. Res. 111, DOI 10.1029/2005JB004006.

Funding from the NSF (REA, NL) is gratefully acknowledged.

EARTHQUAKE PROCESSES

Gregory Beroza • Stanford University
John Langbein • U.S. Geological Survey

Understanding Episodic Tremor and Slip

Understanding the recently discovered phenomena of deep, non-volcanic tremor, and related large-scale slow slip events, found both in subduction and strike slip environments, is a prime scientific target for Earthscope, and data from each component of Earthscope have the potential to shed light on these processes. Episodic tremor has been clearly recorded on seismometer strings in the SAFOD experiment. Because of the great depth at which tremor signals are recorded, and due to the many sensors on the SAFOD array, these recordings have a sensitivity and density of recording that has not been achieved elsewhere. For this reason they are well-suited for determining the spectral character of tremor, particularly at frequencies in excess of 10 Hz. Many of the PBO borehole instruments are located near areas known to produce deep tremor. Their unique combination of high resolution borehole strain measurements, which can detect slow slip events and high frequency velocity transducers, which can detect tremor, should allow unprecedented resolution of the relative timing of these two phenomena.

In Cascadia and in Japan, episodic tremor and slip events have been shown to be strongly correlated. In the case of Japan, at least, both slow slip events and deep tremor appear to be generated as shear slip on the plate interface (Shelly et al., 2007), and occur at depths at which slab metamorphism leads to dehydration reactions and provides a source of pore fluids (Figure 1). A key question is whether or not a similar relationship holds in Cascadia. In Cascadia the depth distribution of tremor (Kao et al., 2005) shows a much wider range (Figure 2), which suggests a different generation mechanism. Data from the Flexible Array component of US Array has the potential to resolve this issue. Because the tremor in Cascadia occurs with

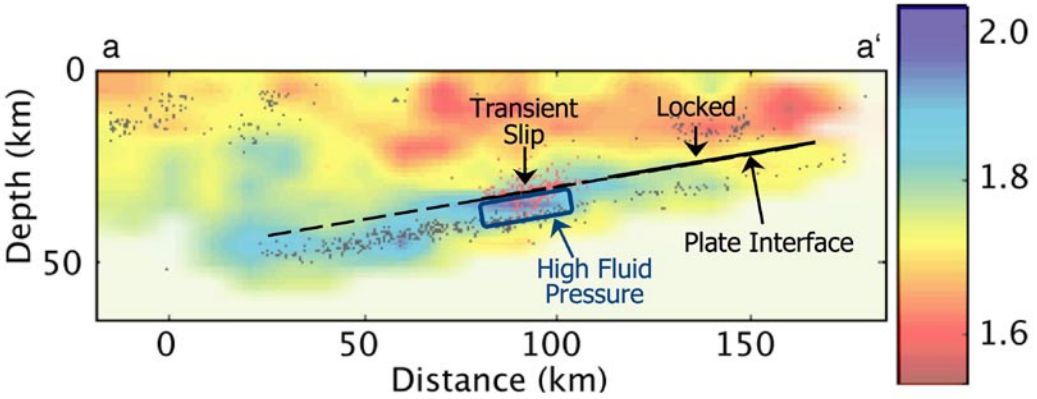

Figure 1: Cross section of Vp/Vs ratio under SW Shikoku, Japan (Shelly et al., 2006). Relocated Benioff zone earthquakes in the downgoing slab are shown as black dots while relocated LFEs are shown as red dots. LFEs represent shear slip on the plate interface and occur during silent slip events. The high Vp/Vs area under the LFE zone may indicate high fluid pressure. If so, fluids may play an enabling (indirect) role in tremor occurrence.

such regularity, it has been an ideal target for temporary seismic deployments. If recently discovered very low frequency earthquakes (Ito et al., 2006), intermediate in size between tremor and slow slip events, occur in Cascadia, they should be detectable using transportable array data.

The deep tremor observed under Cholame (Nadeau and Dolenc, 2004) is unusual in several respects. Deep tremor, in this case, is occurring in a strike-slip environment, where there is no obvious source of fluids. Moreover, while tremor has been observed in Cholame, there has been no corresponding measurement of deformation arising from deep slow slip (Johnston et al., 2006). This leads to the question of whether the tremor under Cholame, which has a character identical to that observed in Cascadia and Japan, might differ somehow. The long-baseline laser strainmeter being installed in Cholame, will provide an increased capability for detecting any strain

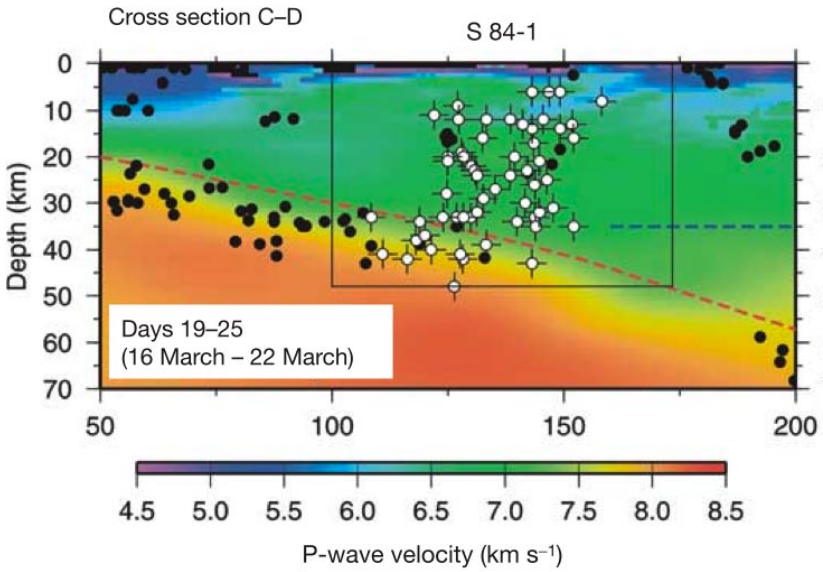

Figure 2: Cross section (Kao et al., 2005) of Cascadia showing the spatial distribution of deep tremor locations (open symbols), background seismicity (filled symbols), with regional P-wave tomography model and reflectivity from seismic reflection surveys.

transients that might occur in Cholame in association with the observed. The higher stability of this instrument relative to the borehole strainmeters over long time periods may prove critical in this instance.

Hybrid Seismic and Geodetic Earthquake Modeling

Many studies of earthquake processes are based upon estimates of the distribution of slip on faults. These distributions can be derived solely from GPS or solely from seismic data, or more recently, using hybrid data sets. With GPS data, both the interseismic slip and, where it exists, postseismic slip are estimated. Interseismic slip, coupled with geologically determined long-term slip rates, provides an estimate of the strain-energy that is being built-up in this part of the earthquake cycle. Inversion of GPS data can provide insight on the distribution of slip on a fault; and if aseismic transients occur, then the combination of data from GPS and strainmeters can provide constraints on these events.

With inversions of seismic data, the features of the dynamic rupture from earthquakes are determined. Inversion of GPS data of deformation occurring during the postseismic interval provides some constraints upon fault-zone friction-laws and/or rheology of the lower crust and upper mantle. However, without prior knowledge of the seismicity, surface geology guides the modeler in the location of the fault.

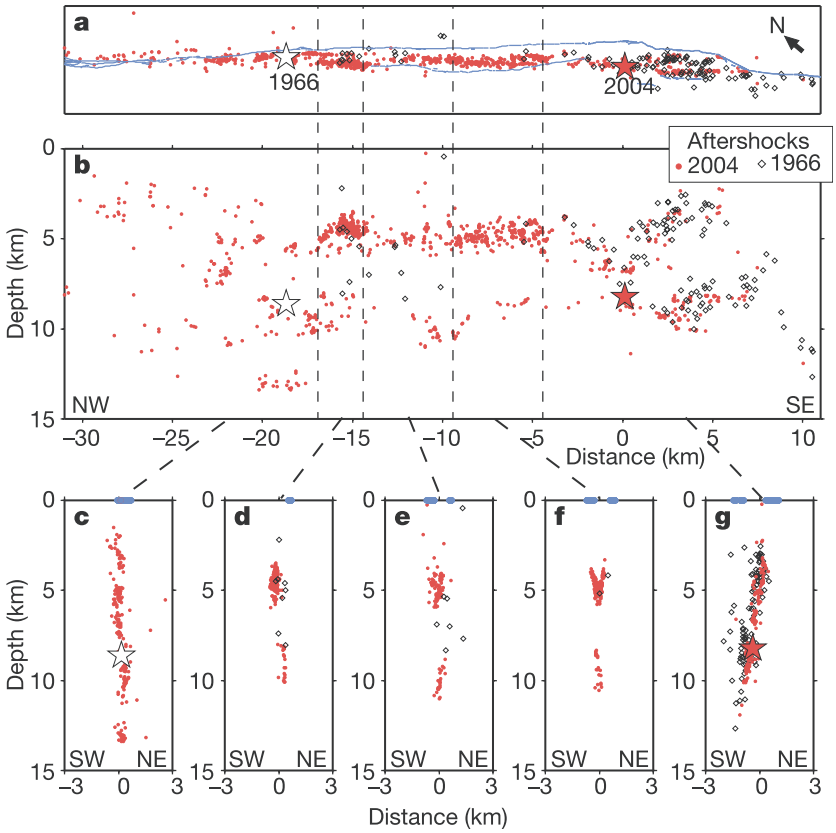

Figure 3: Earthquake locations showing the complexity of faulting at depth for Parkfield from the period 1966 through 2004 (Bakun et al., 2005). The top panel shows the map view of the main trace of the San Andreas and its relation to earthquake epicenters. The middle panel is along-fault cross section of seismicity with depth. The bottom panels show vertical cross-sections that correspond fault segments in the top two panels. The blue triangles in the bottom panel illustrate the location of the mapped surface traces relative to seismicity at depth. The bottom panel reveals multiple strands of the fault are active.

Improved earthquake relocation techniques have led to detailed maps of earthquake locations, which reveal that the fault geometry at depth is complex and can differ from that implied by downward continuation of surface geology (Figure 3). The complexity for the Parkfield segment of the San Andreas Fault, for example, has been revealed by such techniques Thurber et al. (2006). Both Murray and Langbein (2006) and Simpson et al. (2006) incorporated the observed fault zone complexity at depth in their analyses of crustal deformation data. As better earthquake location data become more widely available through Transportable and Flexible Array deployments and as denser geodetic coverage through PBO provides better resolution of crustal motion, we anticipate future studies of the earthquake process will be able to incorporate increasingly complex, and realistic, models of earthquake faulting at depth.

High Sample-Rate GPS

Using the combination of waveform data from seismic instruments and GPS to estimate the dynamic rupture of earthquakes is an emerging technique. It has only been recently that position changes estimated from GPS data have been used to augment seismic data in the recordings of moderate-sized earthquakes. The key are 1 to 10 Hz measurements of position changes from GPS that are accurate to a few centimeters. Currently, the mixing of both near-field GPS and seismic data have only been done in a few cases for moderate-size, circa M6 earthquakes (Ji et al., 2004) or from distant, large earthquakes. The limitation for GPS is its low sensitivity at high sample rates. The seismic data is limited at the low frequency end where source inversions require double integration of accelerometer records to obtain displacements needed to get the final values of fault slip. For moderate-sized earthquakes, which happen quickly, the loss of precision from double integration is a minor problem; for large earthquakes that take minutes to rupture, getting accurate displacement records from accelerometers can be problematic. Complimentary measurements of displacement using high-rate GPS data, which are "flat" at zero-frequency and seismic data should provide better estimates of both the dynamic part of the fault rupture and the final distribution of slip. For moderate-sized earthquake, using "straingrams" from borehole, PBO strainmeters should provide complimentary data to accelerometer data since the strainmeters are "flat" at zero-frequency and have much better sensitivity than GPS.

Earthquake Source Parameters and Scaling

The different components of Earthscope have the potential to make critical contributions to the understanding of seismo-tectonics and to resolve longstanding questions about the nature of earthquake scaling. The broadband data of the transportable component of the US Array will greatly increase our ability to determine the source parameters of moderate earthquakes, for example with moment-tensor inversion, and to the extent that the elements of the array will be "adopted" by local agencies, this capability will persist after the array has moved on.

The magnitude of the stress that drives earthquake faulting is a long-standing, unresolved, and fundamental question in earthquake science (Zoback et al., 1987; Scholz, 2000). By measuring stress at the depths of the shallowest earthquakes, the

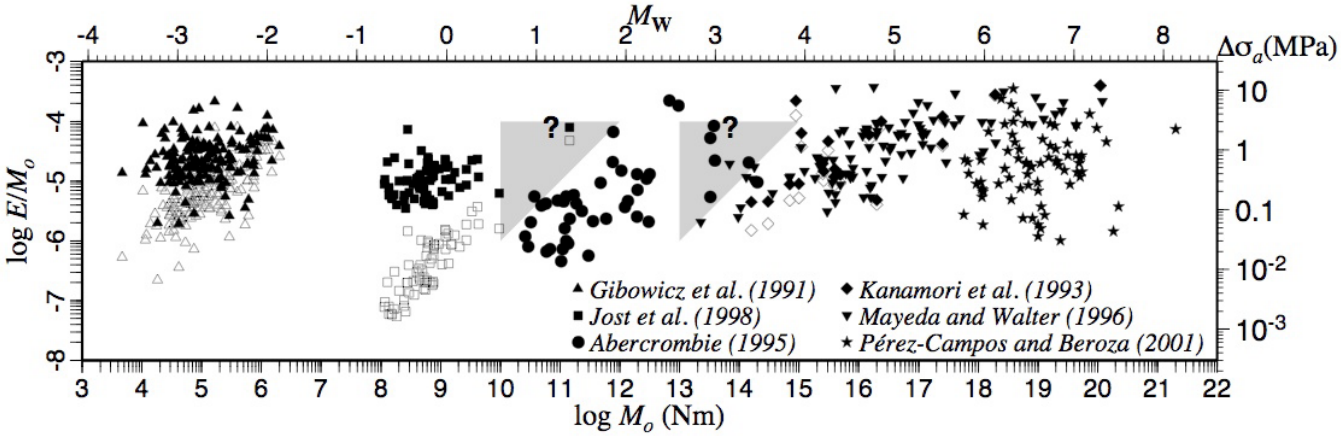

Figure 4: Es/M_0 vs. M_0 from various studies (Ide and Beroza, 2001). Open symbols show original measurements. filled symbols show values once seismic energy possibly missing due to limited bandwidth is restored. Gray triangles show areas where earthquakes are excluded from two studies due to limited bandwidth. After the correction, no clear break in scaling is apparent.

SAFOD project will provide direct constraints on stress levels. Earthquakes relieve shear stress acting across faults within the Earth, and for that reason, earthquake stress drops provide a bound of the level of shear stress at seismogenic depths in the Earth's crust. It is reasonable to expect that as depth increases, and the stress due to overburden changes with it, earthquake stress drops should also increase. By stacking over thousands of earthquakes, Shearer et al. (2006) have discerned such a correlation, but it is much weaker than would be expected if stress drops scaled with the overburden.

Stress drops are usually determined from a combination of the seismic moment, M_0, and a measure of characteristic dimension based on the corner frequency. Most studies indicate that data from earthquakes of all sizes follow a constant stress drop scaling relation of the form $M_0 \sim r^3$. Stress drops have also been estimated using repeating earthquakes, under the assumption that these areas slip only seismically and keep up with long-term steady slip. For a given seismic moment, one can then determine the fault dimension required to match the long-term rate. Stress drops determined by this approach (Nadeau and Johnson, 1998) for earthquakes of magnitude ~ 6 are similar to those based on corner frequency measurements, but stress drops measured using slip-rate matching of repeating earthquakes increase rapidly with decreasing earthquake size such that for the smallest earthquakes they are 1 to 2 orders of magnitude higher than those obtained by corner frequency techniques. By measuring earthquakes, in particular repeating earthquakes, in the extreme near field, SAFOD will allow essentially direct measurements of the radiated field before it has been altered by, possibly nonlinear, wave propagation effects that might otherwise obscure the magnitude of earthquake stress drops.

Another parameter of great interest is the efficiency with which earthquakes radiate seismic energy. There is a lot of scatter in measurements of this quantity, but representative values of Es/M_0, suggest a representative value of $Es/M_0 \sim 5 \times 10^{-5}$. Some studies find Es/M_0 increases with earthquake size (Kanamori and Heaton, 2000), while others suggest it does not (Ide and Beroza, 2001). Thus, whether or not the efficiency with which earthquakes generates seismic waves scales with earthquake size remains an important open question.

Borehole observations of earthquakes yield measurements of small earthquake processes that are relatively uncontaminated by propagation effects; however, even borehole recordings can be affected by propagation effects. The SAFOD project, by making observations in the extremely near field of micro-earthquakes, will allow seismic energy measurements that are essentially free from the propagation effects. Direct measurements of temperature, pore pressure, and strain will also help constrain the different components that control the efficiency of seismic wave generation. As for the stress drop, the seismic efficiency of extremely important to understand, as it bears directly on the potential of an earthquake to generate damaging strong ground motion.

Bakun, W. H., B. Aagaard, B. Dost, W. L. Ellsworth, J. L. Hardebeck, R. A. Harris, C. Ji, M., J. S. Johnston, J. Langbein, J. J. Lienkaemper, A. J. Michael, J. R. Murray, R. M., Nadeau, P.A. Reasenberg, M. S. Reichle, E. A. Roeloffs, A. Shakal, R. W. Simpson, and F. Waldhauser, Implications for prediction and hazard assessment from the 2004 Parkfield earthquake, Nature,

437, doi:10.1038/nature04067, 2005.

Ide, S., and G. C. Beroza, Does apparent stress vary with earthquake size? Geophys. Res. Lett., 28, 3349-3352.

Ito, Y., Obara, K, Shiomi, K., Sekine, S. & Hirose, H. Slow Earthquakes Coincident with Episodic Tremors and Slow Slip Events, Science, doi:10.1126/science.1134454, 2006.

Ji, C., K. M. Larson, Y. Tan, K. W. Hudnut, and K. Choi, Slip history of the 2003 San Simeon earthquake constrained by combining 1-Hz GPS, strong motion, and teleseismic data, Geophys. Res. Lett., 31, L17608, doi:10.1029/2004GL020448, 2004.

Johnston,M. J. S. , R. D. Borcherdt, A. T. Linde, and M. T. Gladwin, Continuous Borehole Strain and Pore Pressure in the Near Field of the 28 September 2004 M 6.0 Parkfield, California, Earthquake: Implications for Nucleation, Fault Response, Earthquake Prediction, and Tremor, Bull Seism Soc Amer 2006 96: S56-S72

Kanamori, H., and T. H. Heaton, Microscopic and macroscopic physics of earthquakes, Geophyiscs and the Complexity of Earthquakes, Geophysical Monograph 120, American Geophysical Union, 147-163, 2000.

Kao, H., S.-J. Shan, H. Dragert, G. Rogers, J. F. Cassidy, and K. Ramachandran, A wide depth distribution of seismic tremors along the northern Cascadia margin, Nature, 436, 841-844, 2005.

Murray, J., and J. Langbein, Slip on the San Andreas Fault at Parkfield, California, over two earthquake cycles, and the implications for seismic hazard, Bull. Seismol. Soc. Am., 96, S283-S303, 2006.

Nadeau, R. M. and D. Dolenc, Nonvolcanic tremors deep beneath the San Andreas fault. Science, 307, 389 (2005); published online 9 December 2004 (10.1126/science.1107142), 2004.

Nadeau, R. M., and L. R. Johnson, Seismological studies at Parkfield VI: moment release rates and estimates of source parameters for small repeating earthquakes, Bull. Seismol. Soc. Am., 88, 790-814, 1998.

Rogers, G., and Dragert, H., Episodic tremor and slip on the Cascadia subduction zone: The chatter of silent slip. Science, 300, 1942-1943, 2003.

Scholz, C. H., Evidence for a strong San Andreas Fault, Geology, 28,163-166; DOI: 10.1130/0091-7613, 2000.

Shearer, P. M., G. A. Prieto, and E. Hauksson, Comprehensive analysis of earthquake source spectra in southern California, J. Geophys. Res., 111, B06303, doi:10.1029/2005JB003979, 2006.

Shelly, D. R., G. C. Beroza, S. Ide, and S. Nakamula, Low-frequency earthquakes in Shikoku, Japan and their relationship to episodic tremor and slip. Nature, 442, 188-191, 2006.

Shelly, D. R., G. C. Beroza, and S. Ide, Non-volcanic tremor and low frequency earthquake swarms, Nature, (in press), 2007.

Simpson, R. W., M. Barall, J. Langbein, J. R. Murray, and M. J. Rymer, San Andreas Fault geometry in the Parkfield, California, region, Bull. Seismol. Soc. Am., 96, S28-S37, 2006.

Thurber, C., H. Zhang, F. Waldhauser, J. Hardebeck, A. Michael, and D. Eberhart-Phillips, Three-dimensional compressional wavespeed model, earthquake relocations, and focal mechanisms for the Parkfield, California, region, Bull. Seismol. Soc. Am., 96, S38

Zoback, M. D., M. L. Zoback, V. Mount, J. Eaton, J. Healy, D. Oppenheimer, P. Reasenber, L. Jones, B. Raleigh, I. Wong, O. Scotti, and C. Wentworth, New evidence on the state of stress on the San Andreas fault system, Science, 238, 1105-1111, 1987.

Funding from the NSF (GB) is gratefully acknowledged.

SPATIAL AND TEMPORAL VARIATIONS IN FAULT LOADING AND STRAIN RELEASE RATES

James Dolan • University of Southern California

The degree to which fault loading and strain release rates are constant (or non-constant) in time and space is one of the most fundamental, unresolved issues in modern geodynamics, with critical implications on our understanding of earthquake hazard. Comparisons of short-term geodetic data with very long-term (million year) global plate motion data indicate that, along many plate boundaries, strain storage and release are relatively continuous over a wide range of time scales (Sella et al., 2002). Moreover, on at least parts of the few major faults where sufficiently detailed geologic rate data are available (e. g., North Anatolian fault, central San Andreas fault (SAF) [Sieh and Jahns, 1984; McClusky et al., 2000; Argus and Gordon, 2001; Hubert-Ferrari et al., 2002; Kozaci et al., 2004; in review]), strain release appears to be relatively constant over a variety of time scales. In contrast, recent comparisons of geodetic and geologic rate data across some faults (e.g., the Mojave section of the SAF, eastern California shear zone [ECSZ]) reveal pronounced variations in rates of strain storage and release. For example, rapid geodetic rates measured in the Mojave region of the ECSZ (12±2 mm/yr) are much faster than longer-term geologic rates (on the order of ~5-7 mm/yr) (Dixon et al., 2000; Rockwell et al., 2000; McClusky et al., 2001; Peltzer et al., 2001; Oskin and Iriondo, 2004, Oskin et al., 2004), indicating a pronounced strain transient.

Such observations raise several fundamentally important questions. Most basically, how spatially and temporally constant is plate boundary strain accumulation and release? Are geologic fault slip rates averaged over thousands to hundreds of thousands of years commensurate with short-term geodetic rates of elastic strain accumulation, or do strain transients commonly occur? If transients do occur, over what time scales do they operate? Are strain transients localized features, perhaps tied to regions of structural complexity? Or are they more fundamental features of plate-boundary motion, particularly where two or more mechanically complementary fault systems accommodate plate-boundary motion? Finally, do different plate boundaries store and release strain differently, perhaps as a consequence of relative structural complexity or simplicity?

EarthScope is ideally poised to address these fundamentally important geodynamical questions. Specifically, a variety of data types are needed to understand the spatial and temporal constancy of plate-boundary deformation: (1) short-term geodetic observations of elastic (and anelastic) strain accumulation and release, provided by GPS, strain meters, and InSAR observations, with temporal resolution ranging from minutes to years; and (2) longer-term geologic rate data, which are provided by a combination of observations of offset landforms and other geological features, and age-dating of the deformed features (Figs. 1 and 2).

These short-term rate data are being complemented by Airborne Laser Swath Mapping (ALSM) and age data acquired as part of the

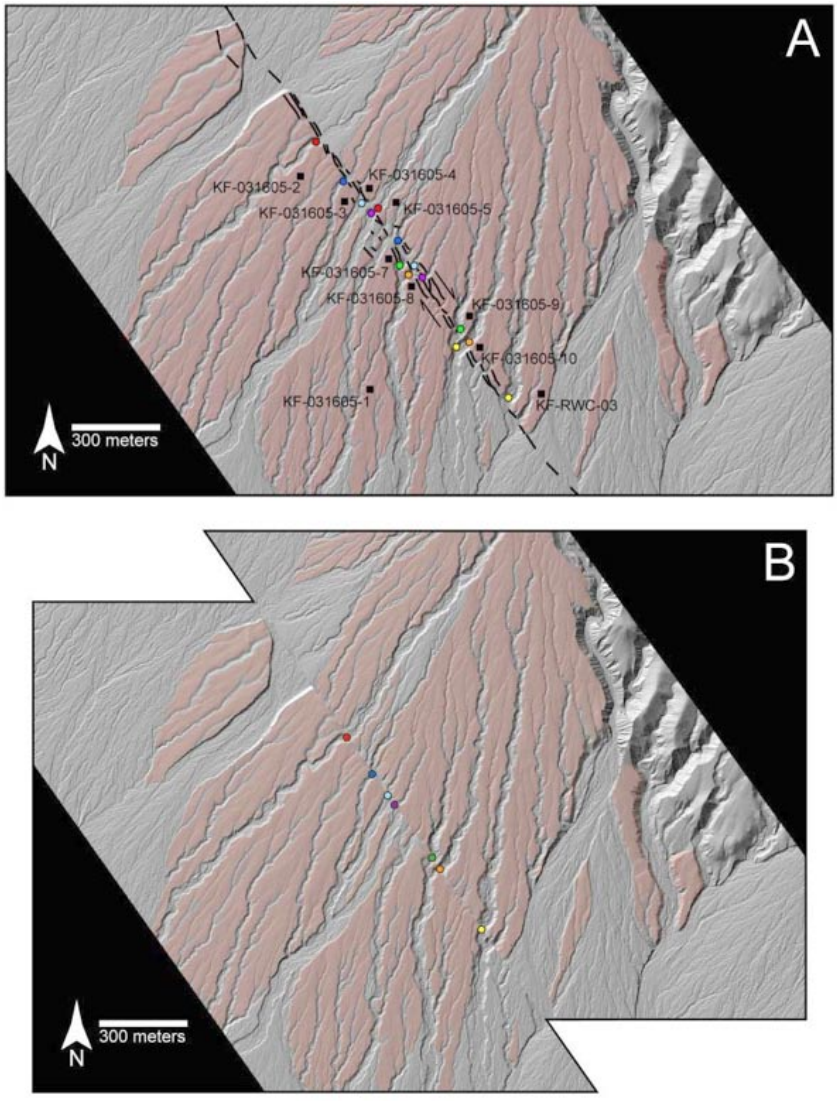

Figure 1: A. Airborne laser swath mapping (ALSM) images of the Red Wall Canyon alluvial fan along the northern Death Valley fault zone. The dextrally-offset Q2c surface is shown in red (after Klinger, 2001). Cosmogenic 10Be sample locations are shown by black squares. Colored circles indicate correlative channels. B. Restoration of the Q2c surface offset. Colored circles indicate correlative channels from A. Slip rates for the northern Death Valley fault zone based on 297 ± 9 m of offset and a Q2c surface age = 4.3 mm/yr. After Frankel et al. [in press, JGR].

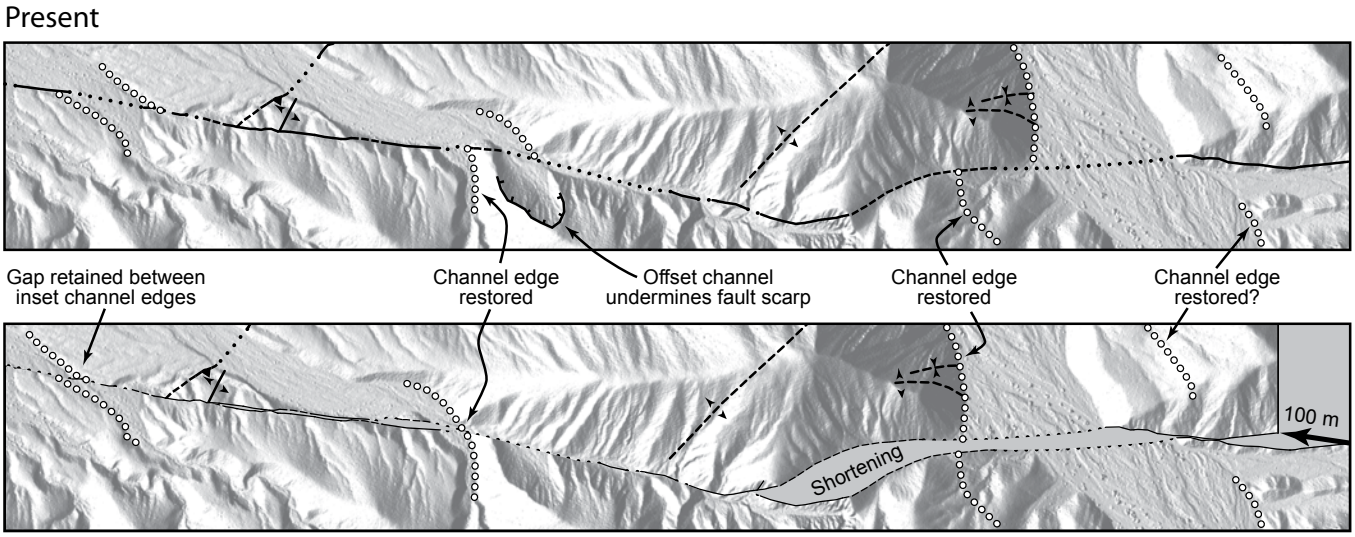

Figure 2: Restoration of 100 m of slip of the Calico fault since incision of the alluvial terrace ca. 56 ± 8 ka. Hillshade image derived from airborne laser swath topography. Lines of white dots indicate restored features, as denoted in figure. Gaps in restoration indicate areas of shortening during fault slip that are consistent with folding northeast of Calico fault.

GeoEarthScope program. The ALSM project will result in acquisition of detailed digital topographic data from most of the major active faults across the entire plate boundary, and will allow mapping of deformed geological features in unprecedented detail (see, for example, the results of two early ALSM-based slip-rate studies in figures 1 and 2). Age dating of these features, under the auspices of GeoEarthScope Geochronology Infrastructure, will facilitate the determination of the large numbers of precise geologic slip rates necessary for meaningful comparison with the shorter-term geodetic data. Together, the geodetic, geologic, and geochronologic efforts within the EarthScope experiment will provide the data necessary to begin to unravel the complex set of geodynamical questions posed above.

Argus, D. F., and Gordon, R. G., 2001, Present tectonic motion across the Coast ranges and San Andreas fault system in central California: Geol. Soc. Amer. Bull., v. 113, p. 1580-1592.

Dixon, T. H., Miller, M., Farina, F., Wang, H., and Johnson, D., 2000, Present-day motion of the Sierra Nevada block and some tectonic implications for the basin and Range province, North American Cordillera: Tectonics, v. 19, p. 1-24.

Hubert-Ferrari, A., Armijo, R., King, G., Meyer, B., and Barka, A., 2002, Morphology, displacement, and slip rates along the North Anatolian fault, Turkey: Jour. Geophys. Res., v. 107, p. X-1 to x-32.

Kozaci, Ö., Dolan, J. F., Finkel, R., Hartleb, R. D., Frankel, K. L., and Hubert-Ferrari, A., 2004, Long-term slip-rate study along the North Anatolian fault, Eksik, Turkey, using cosmogenic 36Cl: EOS, v. 85.

McClusky, S., Balassanian, S., Barka, A., Demir, C., Ergintav, S., Georgiev, I., Gurkan, O., Hamburger, M., Hurts, K., Kahle, H., Kastens, K., Kekelidize, G., King, R., Kotsez, V., Lenk, O., Mahmoud, S., Mishin, A., Nadariya, M., Ouzounis, A., Paradissis, D., Pter, Y., Prilepin, M., Reilinger, R., Sanli, I., Seeger, H., Tealeb, A., Toksöz, M. N., and Veis, G., 2000, Global positioning system constraints on plate kinematics and dynamics in the eastern Mediterranean and Caucusus: Jour. Geophys. Res., v. 105, p. 5695-5719.

Oskin, M., and Iriondo, A., 2004, Large magnitude transient strain accumulation on the Blackwater fault, Eastern California shear zone: Geology, v. 32, p. 313-316.

Oskin, M., Perg, L., Blumentritt, D., and Mukhopadyay, S., 2004, Slip rate of the Calico fault: Implications for anomalous geodetic strain accumulation across the Eastern California shear zone: EOS (Transactions, American Geophysical Union), v. 85, Fall Meeting Supplement, abstract G11A-0776.

Peltzer, G., Crampe, F., Hensley, S., and Rosen, P., 2001, Transient strain accumulation and fault interaction in the Eastern Californioa shear zone: Geology, v. 29, p. 975-978.

Rockwell, T. K., Lindvall, S., Herzberg, M., Murbach, D., Dawson, T., and Berger, G., 2000, Paleoseismology of the Johnson Valley, Kickapoo, and Homestead Valley faults: Clustering of earthquakes in the eastern California shear zone: Bull. Seismol. Soc. Amer., v. 90, p. 1200-1236.

Sella, G. F., Dixon, T. H., and Mao, A., 2002, REVEL: A model of Recent plate velocities from space geodesy: Jour. Geophys. Res., v. 107, 10.1029/2000JB000033, 2002.

Sieh, K. E., and Jahns, R. H., 1984, Holocene activity of the San Andreas fault at Wallace Creek, California: Geological Society of America Bulletin, v. 95, p. 883-896.

MODE OF DEFORMATION OF A CONTINENT

Lucy M. Flesch • Purdue University

Understanding the forces and factors that are responsible for deforming and driving the continental lithosphere remains a fundamental question in geophysics. Over the past 15 year there has been a proliferation of GPS measurements in the western United States, which have been used by several workers to place bounds on the long-term surface motions and strain rates over the North American plate boundary zone. These results have allowed for the quantification of the large-scale forces driving continental deformation. As the Plate Boundary Observatory (PBO) continues deployment over the entire deforming western United States, with high density station distribution and smaller uncertainties, exciting questions relating to size of allowable crustal blocks, local driving forces, along strike variations in fault strength, strength of the continental lithosphere, and levels of basal tractions can be addressed in detail.

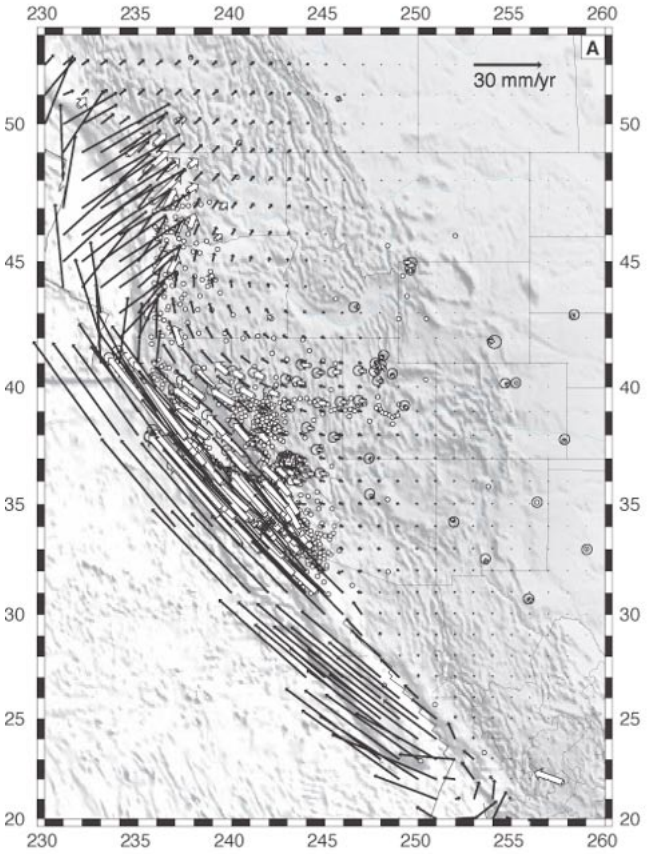

Figure 1: The continuous model velocity field from Flesch et al. (2007) (black vectors), and GPS data (white vectors) from Bennett et al. [1999] plotted relative to a North American frame of reference. White dots (without vectors for clarity) represent the additional GPS data used in that study. Error ellipses represent the 95% confidence limits.

The kinematics of the large-scale deformation of western North America have been quantified assuming that the lithosphere is composed of a finite number of rigid blocks (McCaffrey, 2005; Hammond and Thatcher, 2005; Thatcher, 2003) and allowing strain to be continuous (Flesch et al., 2007) (Figure 1). The large-scale picture of western US deformation can be thought of as dilation of the Basin and Range and translation of the Sierra Nevada block, where both are accommodated by the retreat of southern Cascadia (Humphreys and Coblentz, 2007). Both the block-like and continuous modes of deformation are able to produce a statically robust fit to the GPS observations, implying that the current distribution of GPS does not have sufficient density to delineate absolute block motions. Future PBO data should be able to isolate the scale (if any) of undeforming crustal blocks and/or regions of increased lithospheric strength that are deforming at much slower rates then along the fault zones at the boundaries of these regions. Additionally, there are large uncertainties within regions of very low strain rate in Figure 1 (~5 nano-strain per year), these uncertainties manifest into larger errors when quantifying the dynamics. Therefore, precise PBO observations of low velocity regions will help isolate individual driving forces in these regions.

Recently, two studies have used deformation indicators described above (Flesch et al., 2007) and the World Stress Map data (Humphreys and Coblentz, 2007) to directly quantify the relative importance of lithospheric buoyancy forces, relative plate motions and basal tractions in driving deformation in western North America plate boundary zone. Both found that gravitational potential energy (GPE) variations and plate interactions were the main deformational components, while effects from basal tractions were minimal (Figure 2). These results were determined using a GPS data clustered in Southern California, a swath through the Basin and Range and along western Oregon and Washington. As the GPS data from PBO becomes denser we may begin to quantify the relative importance of driving forces for individual areas, and identify regions where tractions associated with local convective systems, such as the Sierra Nevada drip (Zandt et al., 2004), may be playing a larger role in deforming the lithosphere.

Estimates of both deviatoric stress and strain rates show that stress is relatively constant throughout deforming western North America however, strain rates vary by two orders of magnitudes. As a result, it is possible to estimate the vertically averaged effective viscosity for the lithosphere, which also varies by two orders of magnitude (10^{20}-10^{22} Pas over 100 km) (Flesch et al., in prep). With a known viscosity distribution it is then possible to begin to explore the nature of the rheology of deforming continental lithosphere.

If the dynamics of the continental lithosphere is indeed controlled simply by gravitational collapse and plate interactions, then the standard forward modeling using the lithospheric body force distribution (GPE), lateral variations in effective viscosity, and velocity boundary conditions (boundary of Figure 1) should be able to reproduce the PBO observations. Figure 3 shows the model velocity results from such a standard forward model assuming n=3 for a power law rheology for the southwestern Unit-

ed States (Flesch et al., in prep). Additionally, GPS observations from the recent PBO solution and E. Calais (personal comm.), which were not used in the model, are plotted. Both the model and data show small velocities on the order of 1-3 mm/yr that start east of the Rio Grande rift and show a clockwise rotation of the region. This first order agreement between velocities prescribed by the dynamics and observed small GPS motions is very exciting and allows us to begin the investigation of regions that were previously thought to be undeforming. For example, why are velocities in Figure 3 continuous across the Rio Grande rift and not focused around the large geologic feature? If compressional basal tractions resulting from eastward mantle flow associated with the subducted Farallon plate were included, would the tractions cancel these small motions out?

Although it has been widely accepted that the driving forces associated with gravitational potential energy and plate interactions drive western US deformation (Figure 2) how each of these driving forces are applied throughout the region remains controversial, specifically, the level of shear stresses that are supported along the San Andreas fault. Results from several studies remain conflicting (Li and Liu, 2006; Fay and Humphreys, 2006;

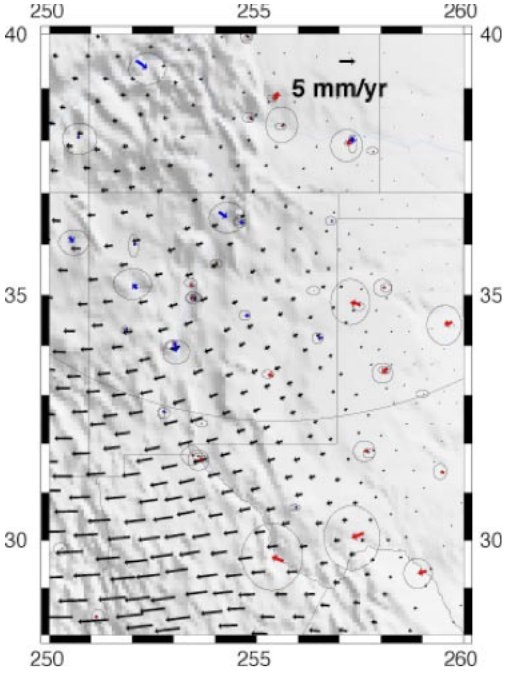

Figure 3: Preliminary forward modeled velocity field (black vectors) (Flesch et al., in prep) and GPS observations, PBO MIT solution (blue vectors) and E. Calais solution (red vectors) for the Rio Grande rift region.

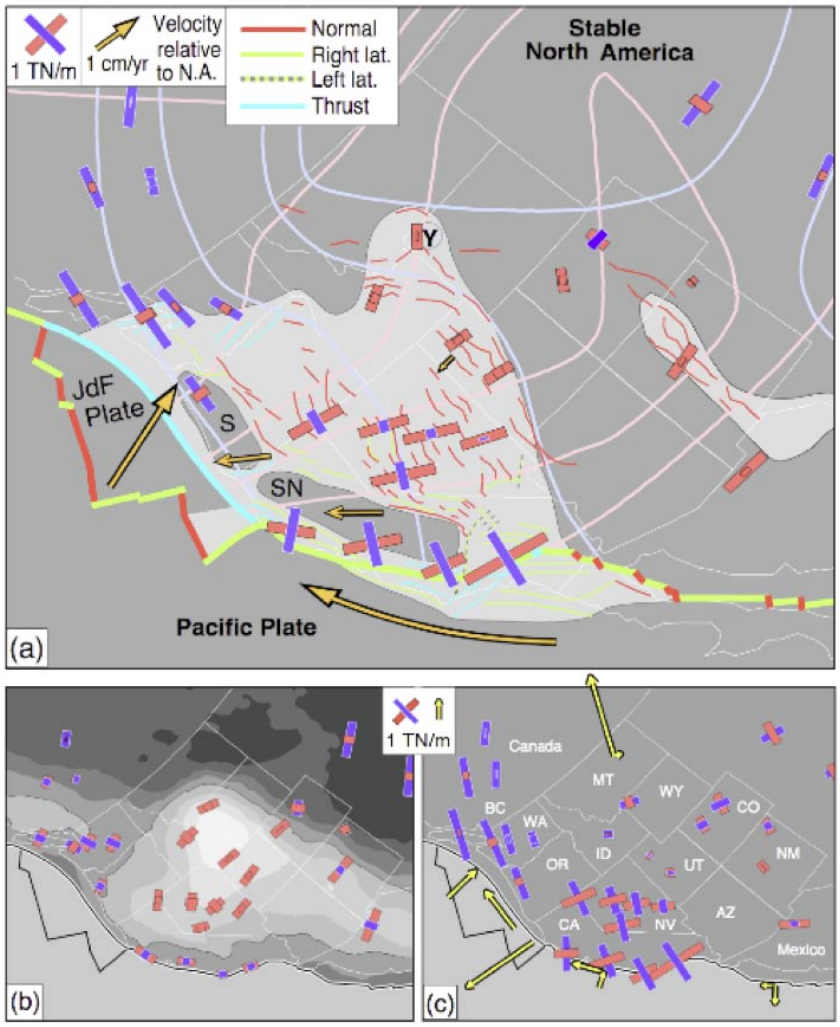

Figure 2: Western U.S. Geodynamics from Humphreys and Coblentz, 2007. (a) Red and blue bars show modeled stress with red indicating tension and blue compression relative to local pressure. The colored line segments represent active faults (thick for major plate-boundary faults). Gold arrows show velocity relative to North America for the Pacific and Juan de Fuca (JdF) Plates, and for selected points within the deforming western U.S. Stress trajectories represent the observed stress field, red for tension and blue for compression. (b) Gravitational potential energy and resulting modeled stresses. Contour level is 1 TN/m. Note extension within the regions of high GPE and compression in the regions of low GPE, with the compressive axis oriented with the GPE gradient. In the Basin and Range and California these stresses are responsible for most of the non-strike-slip deformation. (c) Boundary and basal loads and resulting modeled stresses. Note the shear stress field established across California and western Nevada caused by transform interaction, the compression north of California, and the tension common in the western U.S. interior.

Flesch et al., in prep). For example, Fay and Humphreys (2006) argue that shear stress associated with the Pacific plate are not transmitted any farther east than the Sierra Nevada block. However, Flesch et al (in prep) show if this were the case, there would be no opening in the Basin and Range. Knowledge of detailed surface motions proved by PBO will provide important constraints needed to answer these questions and solve for the magnitudes and origins of continental driving forces in order to better understand the dynamics of the deforming western North American continental lithosphere.

Bennett, R.A., J.L. Davis, and B.P. Wernicke, Present-day pattern of Cordilleran deformation in the western United States, Geology, 27 (4), 371-374, 1999.

Fay, N., and E.D. Humphreys, Dynamics of the Sierra Nevada block and implications for western U.S. fault mechanics and continental geodynamics, EOS Trans. AGU, 87(52) Fall Meet. Suppl., Abstract S54A-02, 2006.

Flesch, L.M., W.E. Holt, A.J. Haines, L. Wen, and B. Shen-tu, The dynamics of western North America: Stress magnitudes and the relative role of gravitational potential energy, plate interaction at the boundary and basal tractions, Geophys. J. Int., in press, 2007.

Hammond, W.C., and Thatcher W., Northwest basin and range tectonic deformation observed with the global positioning system, 1999-2003, J. Geophys. Res., 110, B10405, 2005.

Humphreys, E.D., and D.D. Coblentz, North America Dynamics and Western U.S. Tectionics, Reviews of Geophysics, in press, 2007.

Li, Q. and M. Liu, Geometrical impact of the San Andreas Fault on stress and seismicity in California, G.R.L., 33, L08302, doi:10.1029/2005GL025661, 2006.

McCaffrey R., Block kinematics of the Pacific-North America plate boundary in the southwestern United States from inversion of GPS, seismological, and geologic data, J. Geophys. Res., 110, B07401, doi:10.1029/2004JB003307, 2005.

Thatcher, W., GPS constraints on the kinematics of continental deformation, Int. Geol. Rev., 45(3), 191-212, 2003.

Zandt, G., H. Gilbert, T.J. Owens, M. Ducea, J. Saleeby, and C.H. Jones, Active foundering of a continental arc root beneath the southern Sierra Nevada in California, Nature, 431, 41-46, 2004.

RHEOLOGY OF THE LITHOSPHERE FROM POSTSEISMIC DEFORMATION CAPTURED WITH GPS

Elizabeth H. Hearn • University of British Columbia

When an earthquake occurs, it changes stresses in the surrounding lithosphere. Since the litho-sphere's elasticity and the earthquake slip distribution may be inferred from seismic, inSAR, and GPS data, this coseismic stress change may be estimated fairly accurately. The Earth's response to a known stress step can tell us a great deal about the rheology of the crust and mantle, and about how aseismically deforming material is distributed along a plate boundary zone. For ex-ample, is the lithosphere essentially rigid, and cut by creeping surfaces which extend brittle faults downward into the asthenosphere? Or does the lower crust and uppermost mantle beneath tectonically active regions flow, making the upper crust the "lithosphere"? What rheology governs slip on the deep fault zone extensions, or flow of the lower crust? A better understanding of litho-sphere structure and rheology is key to fundamental science questions (e.g., understanding stresses driving and resisting the motion of tectonic plates) and practical concerns (modeling time-dependent stress transfer for time-dependent probabilistic seismic hazard estimates). One way to address these questions is to develop numerical models of postseismic deformation, cali-brated to GPS, InSAR, or other surface deformation data. Thanks to Earthscope, we are poised to make significant advances in this area.

The Past and Present

Early studies of postseismic deformation showed that shallow afterslip along the fault may fol-low an earthquake (Stein and Lisowski, 1983), and that widespread relaxation of the mantle or lower crust may occur after large earthquakes (Nur and Mavko, 1974; Wahr and Wyss, 1980). With the advent of space geodesy, denser and more precise deformation data became available, and advances in computer technology allowed more sophisticated models of the lithosphere to be developed and tested. However, due to still-limited precision and sparse GPS site coverage in many areas, discerning even end-member hypotheses has remained a challenge. For example, postseismic deformation after the 1992 Landers, California earthquake was interpreted as viscoelastic relaxation of lower crust or upper mantle (with a variety of rheologies), afterslip, poroelastic deformation, or a combination of these processes. Following the 1999 Hector Mine earthquake in the same region seven years later, an narrower array of models was posited, because some possibilities (linear viscoelastic relaxation of lower crust or upper mantle) have been elimi-nated by the later post-Landers GPS velocity data and the improved, post-Hector Mine GPS data.

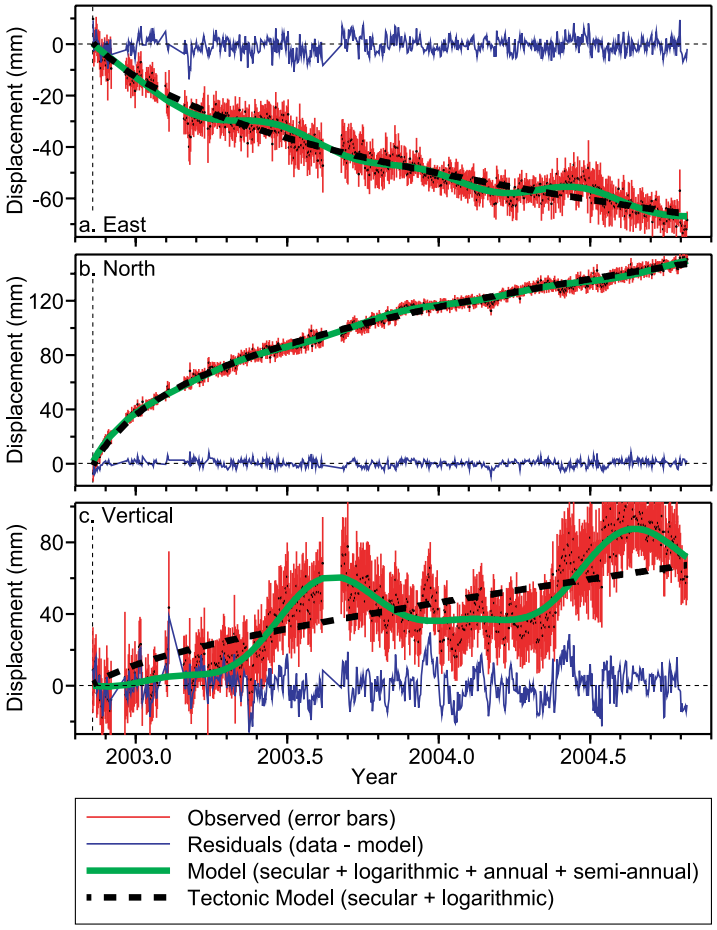

As GPS analysis techniques have evolved, we have begun to better understand the temporal complexity of postseismic deformation following large earthquakes (Figure 1). For example, components with characteristic decay times of 1 day, 1 to 2 months, and at least seven years appear to be present in postseismic data from the Izmit, Turkey earthquake (Ergintav et al., 2006). Debate now focuses on whether these timescales represent one complicated process (such as relaxation of nonlinear or "transient" viscoelastic material), or a combination of processes (e.g., rapid afterslip plus slower viscoelastic relaxation of mantle and lower crust layers). In the case of the Izmit earthquake, the spatial patterns of deformation during the first month after the quake differed markedly from that of later deformation (Ergintav et al., 2006), suggesting two distinct processes (rapid afterslip and slower viscoelastic relaxation).

Advances in computation have permitted us to test increasingly detailed postseismic deformation models. For example, early afterslip models were kinematic - that is, GPS velocities were in-verted for afterslip rates, whether or not such afterslip was

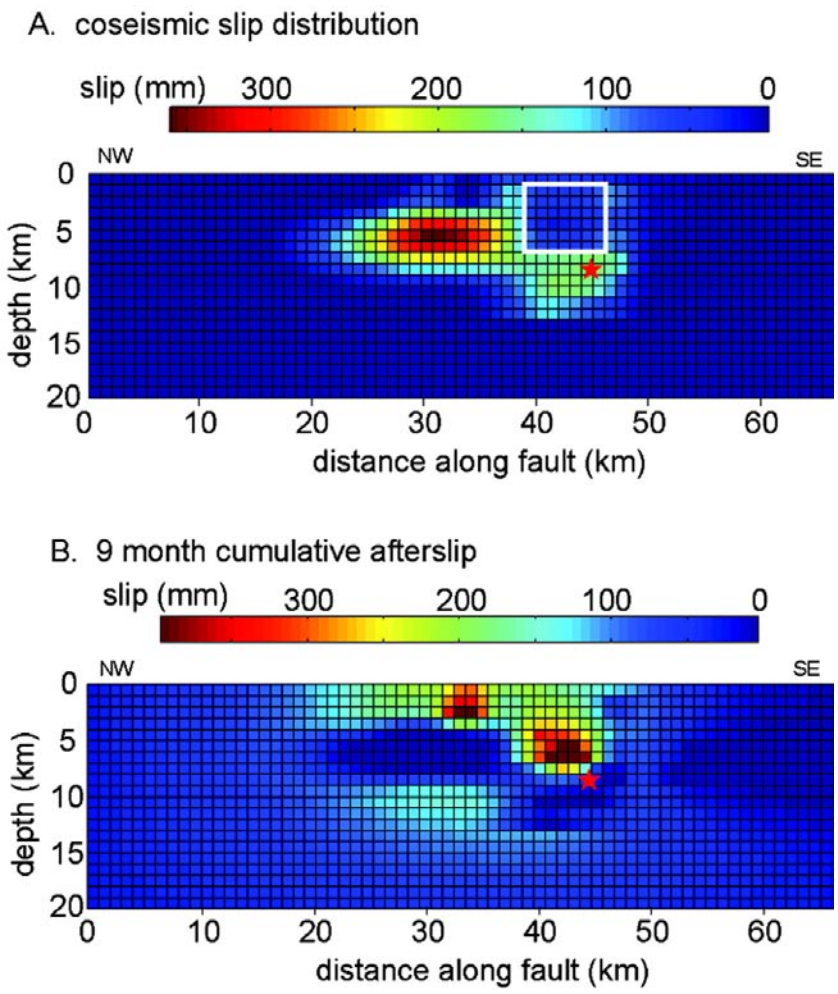

consistent with the subsurface stress conditions and fault zone rheologies. Now, afterslip is more frequently modeled as the response of faults to coseismic stresses caused by the earthquake (e.g., Johnson et al., 2006; Hearn et al., 2002; Linker and Rice, 1997). Figure 2 illustrates just what can be resolved with a dense network of CGPS sites close to a fault. Shallow afterslip after the 2004 Parkfield earthquake (modeled dynamically, with rate- and state-dependent friction, by Johnson et al. [2006]) is well-resolved and clearly anti-correlated with coseismic slip. The temporal evolution of the afterslip is com-patible with rate- and state-dependent friction (for a low effective normal stress on the fault), and the model produces the decay in velocities at GPS sites well. Such conclusions would simply not be possible without CGPS instrumentation.

In the past, nearly all early models of post-seismic deformation treated the Earth as a uniform elastic halfspace, and publications often described one (non-unique) explanation for postseismic displacements over a single time interval. Now, most models incorporate layered elastic struc-ture and realistic fault geometry, and multiple hypotheses can be tested in a timely manner. One example of this is the recent study by Freed et al. (2006) of postseismic deformation following the 2002 Denali, Alaska earthquake (Figure 3). In this study, geologically plausible lithosphere models incorporating creeping fault zones, poroelastic upper crust, and viscoelastic lower crust and upper mantle layers in combination were tested. Of these, several seemingly reasonable lithosphere models could not reproduce the observed surface deformation and were conclusively ruled out. Freed et al. found that shallow afterslip, deep fault zone creep (or viscoelastic relaxation of lower crust), and relaxation of viscoelastic mantle were all required by the Denali post-seismic deformation data.

Another new development is using earthquake-cycle models of "secular" deformation around faults to select among a suite of candidate models which can all explain early postseismic defor-mation. A transient mantle rheology with an initially low effective viscosity may explain rapid postseismic deformation followed by highly localized, essentially constant strain rates around a fault zone through most of the earthquake cycle (Hetland and Hager, 2006). For the specific example of the Izmit earthquake, relaxation of mantle with a transient viscoelastic rheology, and rapid frictional afterslip, are required to explain GPS velocities around the fault during the post-seismic and interseismic intervals (Hearn et al., 2006).

The Future and Earthscope's Role

Continued advances in computation promise to improve model resolution near faults, and allow seamless integration of coseismic, postseismic, and interseismic deformation with longer-term tectonic processes. New modeling codes which take advantage of parallel computation (e.g., PyLith and GeoFEST) will accelerate this trend. However exciting these models may be, the largest potential for advancing knowledge in our field is from better constraints: improved GPS surface deformation data (from PBO) and better-resolved subsurface structure (from the Earth-scope array). Key features of the PBO CGPS data include improved resolution of:

- Vertical deformation. Afterslip and relaxing viscoelastic layers at different depths produce distinct patterns of vertical motion (e.g., Pollitz, 1997; Hearn, 2003). This is even the case for nonlinear viscoelastic layers which may be hard to distinguish from afterslip based on horizontal GPS data only (e.g., Freed, 2006).
- Temporal evolution of velocities. This is important for resolving thickness and viscosity of relaxing layers (Hearn, 2003) or for distinguishing early afterslip from later viscoelastic re-laxation (e.g. Reilinger et al., 2006).

- Spatial distribution of observations. For example, fault-normal motions beyond the rupture are smoking-gun evidence for relaxing viscoelastic layers at depth (for strike-slip earthquakes; Hearn 2003).
- The secular velocity field. The secular (pre-earthquake) velocity field must be known to (1) correct later postseismic GPS site velocities for "secular" deformation, (2) to capture the earliest part of the postseismic transient and (3) to constrain earthquake cycle models. Later postseismic data are those which will tell us the effective viscosity of the lower crust and/or upper mantle, and errors in the secular velocity correction can invalidate these data. Having CGPS equipment deployed when the earthquake occurs is key to distinguishing the coseismic slip from rapid, early postseismic fault slip. Earthquake cycle models can tell us how (or whether) the effective mantle viscosity immediately after an earthquake increases with time, and whether this indicates a transient or a nonlinear mantle rheology.

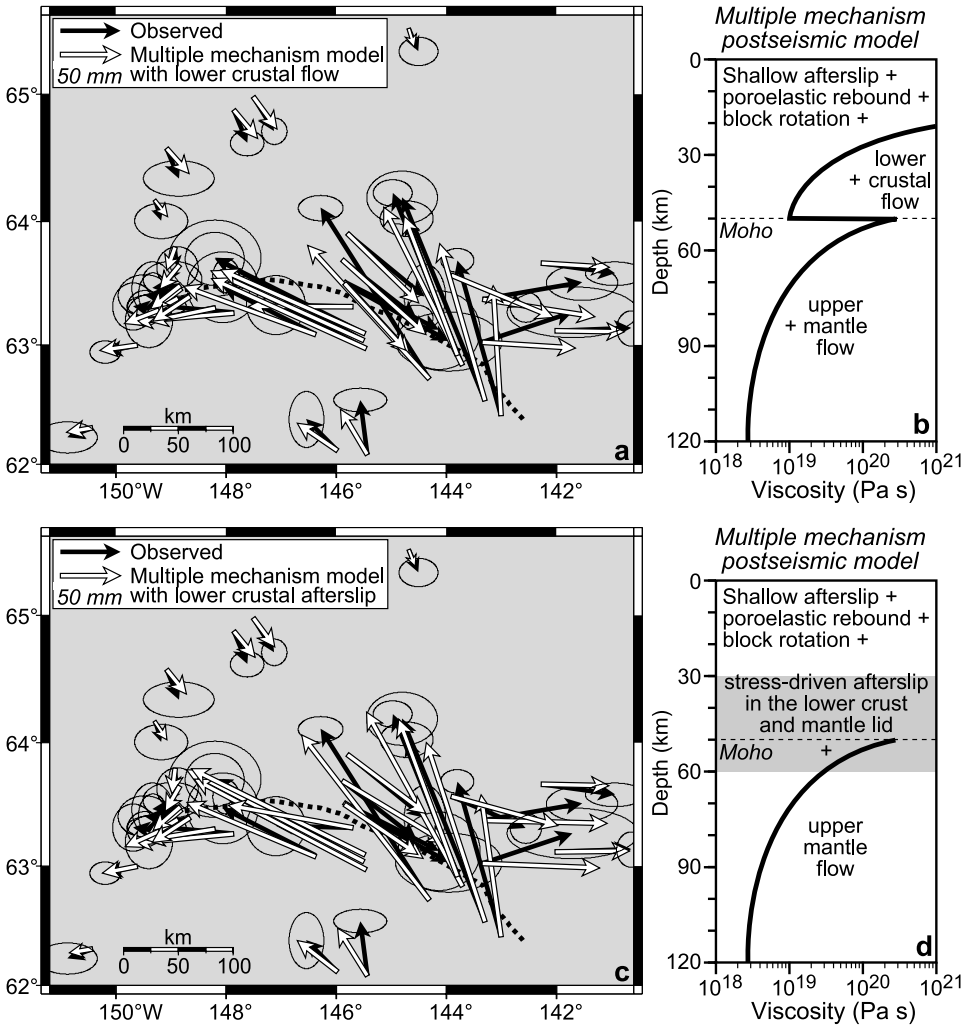

For a future earthquake in the western U.S., all of these factors will be addressed thanks to EarthScope. In addtion, the PBO CGPS network will provide a reference frame anchor for campaign-mode, postseismic GPS surveys. We do not look forward to the next large earthquake in the western U.S., but thanks to EarthScope, it will teach us an unprecedented amount about the mechanics of fault systems at depth.

Ergintav, S., S. McClusky, E. Hearn, and R. Reilinger, Postseismic Deformation following the 1999 Izmit, Turkey Earthquake: The First Seven Years, Eos Trans. AGU, 87(52), Fall Meet. Suppl., Abstract G32A-02, 2006.

Freed, A. M., R. Bürgmann, E. Calais, J. Freymueller, and S. Hreinsdóttir, Implications of de-formation following the 2002 Denali, Alaska, earthquake for postseismic relaxation proc-esses and lithospheric rheology, J. Geophys. Res., 111, B01401, doi:10.1029/2005JB003894, 2006.

Hearn, E.H., R. Bürgmann, R., and R.E. Reilinger, Dynamics of Izmit Earthquake Postseismic Deformation and Loading of the Duzce Earthquake Hypocenter, Bull. Seis. Soc. Am., 92, 172-193, 2002.

Hearn, E.H., What can GPS Tell us About the Dynamics of Postseismic Deformation?, Geo-phys. J. Int., 155, 753-777, 2003.

Hearn, E., S. McClusky, R. Reilinger, and S. Ergintav, Earthquake-cycle models as tie-breakers: Assessing candidate rheologies for ongoing Izmit earthquake postseismic deformation, Eos Trans. AGU, 87(52), Fall Meet. Suppl., Abstract G32A-03, 2006.

Hetland, E. and B. Hager, Postseismic and interseismic displacements near a strike-slip fault: A two-dimensional theory for general linear viscoelastic rheologies, J. Geophys. Res., 110, 10.1029/2005JB003689, 2005.

Johnson, K., R. Burgmann, and K. Larson, Frictional Properties on the San Andreas Fault near Parkfield, California, Inferred from Models of Afterslip following the 2004 Earthquake, Bulletin of the Seismological Society of America; v. 96; no. 4B; p. S321-S338; DOI: 10.1785/0120050808, 2006.

Linker, M. and J. R. Rice, Models of postseismic deformation and stress transfer associated with the Loma Prieta earthquake, in U.S. Geological Survey Paper 1550-D: The Loma Prieta, California Earthquake of October 17, 1989: Aftershocks and Postseismic Effects, D253-D275, 1997.

Nur, A. and G. Mavko, Postseismic viscoelastic rebound, Science, 183, 204-206, 1974.

Pollitz, F., Gravitational viscoelastic postseismic relaxation on a layered spherical Earth, J. Geophys. Research, 102, 17921-17942, 1997.

Stein, R. and M. Lisowski, The 1979 Homestead Valley earthquake sequence, California: Con-trol of aftershocks and postseismic deformation, J. Geophys. Res., 88, 6477-6490, 1983.

Wahr and Wyss, Interpretation of postseismic deformation with a viscoelastic relaxation model, J. Geophys. Res., 85, 6471-6477, 1980.

FLUIDS AND FAULTING

Stephen Hickman • U.S. Geological Survey
Richard Sibson • University of Otago
Ronald Bruhn • University of Utah

Among the many compelling reasons for drilling into active faults is the opportunity to study the role of fluid pressure, fluid flow and chemical fluid-rock interactions in earthquake processes. A long-standing (and still-growing) body of evidence suggests that fluids are intimately linked to a variety of faulting processes. These include the long-term structural and compositional evolution of fault zones; fault creep; and the nucleation, propagation, arrest and recurrence of earthquake ruptures.

The concept that high fluid pressures and the localization of deformation are often linked is widely accepted in the structural geology literature, and has been reinforced by studies of active accretionary prisms in subduction complexes and their fossil equivalents. A point to note is that there is good evidence that seismic rupturing, in at least some instances (e.g., the Western Taiwan fold and thrust belt and the western margin of the Great Valley adjacent to the San Andreas Fault), is occurring in fluid-overpressured crust.

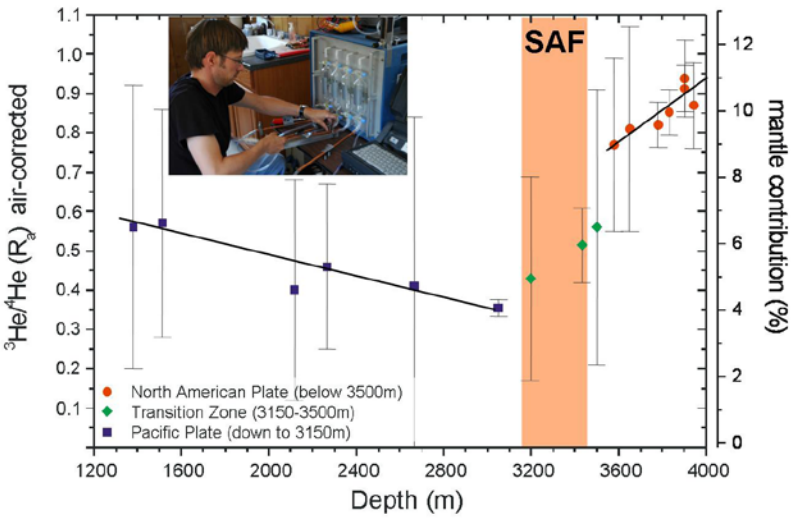

Figure 1: Air-corrected helium isotopic composition versus measured depth along the SAFOD borehole, as determined from real-time analysis of drilling mud gas (inset photograph). Highlighted is the core and damage zone of the San Andreas Fault Zone as identified by casing deformation and geophysical well logs (see Figure 2, below). The percentage contribution of mantle helium to total helium is also indicated (from Wiersberg and Erzinger, 2007).

Sources of Fault-Zone Fluids - Potential sources of fluids in brittle faults and shear zones include metamorphic fluid generated by dehydration of minerals during prograde metamorphism (including shear heating), fluid trapped in pore space as sedimentary formation brines, meteoric water carried downward by circulation and release of volatiles from molten magma or the upper mantle. The high fluid pressures that have been postulated within the San Andreas Fault Zone (being tested as part of the SAFOD project) might be generated and maintained by continued upwelling of overpressured fluids within the fault zone and leakage of these fluids into the country rock. Alternatively, high fluid pressures might result from the sealing of locally derived high-pressure fluids within the fault zone once pressure gradients drop below a critical "threshold" required to overcome forces between molecular water and mineral surfaces in very small cracks and pores.

The possibility of major active faults acting as conduits for high-pressure fluids derived from the mantle or lower crust has been raised by a number of workers. Elevated 3He/4He ratios observed in springs and wells located along a broad zone encompassing the San Andreas Fault system indicate that significant quantities of mantle-derived fluids are entering the overall plate boundary through the ductile lower crust at near lithostatic pressure. Some workers have suggested that these fluids are then focused in the relatively narrow deforming core of the San Andreas Fault and, hence, are intimately involved in the physics of faulting and earthquake generation. However, direct sampling of gases dissolved in the drilling mud during SAFOD Phases 1 and 2 (Figure 1) indicates that mantle-derived fluids are preferentially ascending along the northeast side of the fault and that the core of the San Andreas Fault is actually a barrier to cross-fault fluid flow.

Fault Zone Permeability -The permeability structure of shear zones and brittle faults has recently been the focus of field studies that both confirm and extend observations made years ago by mining geologists. Large faults are not discrete surfaces but rather are a braided array of slip surfaces encased in a highly fractured and often hydrother¬mally altered transition or damage zone. Structural and mineralogical textures indicate that episodic fracturing and brecciation are followed by cementation and crack healing, leading to cycles of permeability enhancement and reduction accompanied by episodic fluid flow along faults.

Laboratory and field observations demonstrate that dilatant pores and microcracks form within fault zones during episodic fault slip and that this porosity should then diminish over time through a variety of fluid-enhanced compaction creep processes, even at temperatures as low as 100° C. Under the right conditions, this will cause fluid pressure within the deforming fault core to increase as strain reaccumulates and then decrease when the fault slips again. In a hydraulically isolated fault zone, theoretical models have shown that the generation and subsequent compaction of these dilatant pores and microcracks can lead to temporal variations in fluid pressure within the fault that may be important in controlling earthquake periodicity and

stress interactions between nearby faults. Using these models to predict the behavior of real faults in the Earth, however, will require direct in-situ measurements and sampling in active fault zone materials at seismogenic depths, as made possible by SAFOD.

A possibly relevant development from studies of fluid pressure in sedimentary basins has been the revelation from borehole measurements of abrupt transitions, both vertically and laterally, between distinct fluid pressure regimes in some sedimentary basins. These fluid pressure compartments are bounded by seals which in some cases are stratigraphic (e.g., shale horizons) but in others are gouge-rich faults or thin zones of hydrothermal cementation which cut across stratigraphy. By analogy with these observations, contiguous vertical and horizontal seals within a fault zone have been proposed to lead to discrete fluid pressure compartments (i.e., tabular lenses), the rupture of which might be important in earthquake nucleation and rupture propagation. Although direct evidence for these fault zone fluid compartments in active fault zones is lacking, negative polarity reflections (bright spots) on seismic reflection images acquired over some accretionary prisms have been interpreted to indicate the existence of high-pressure fluid compartments along the basal decollements. Observations of calcite veining juxtaposed with cataclasites in drill cuttings collected during SAFOD Phase 2 suggest episodic hydrothermal sealing and refractuing within the San Andreas Fault Zone at depth. These cuttings display a distinct isotopic signature for veins associated with the actively deforming fault core (at a measured depth of ~3300 m) relative to the adjacent damage zone and country rock, suggesting upward flow of relatively deeply derived fluids along the active trace of the San Andreas Fault (Figure 2).

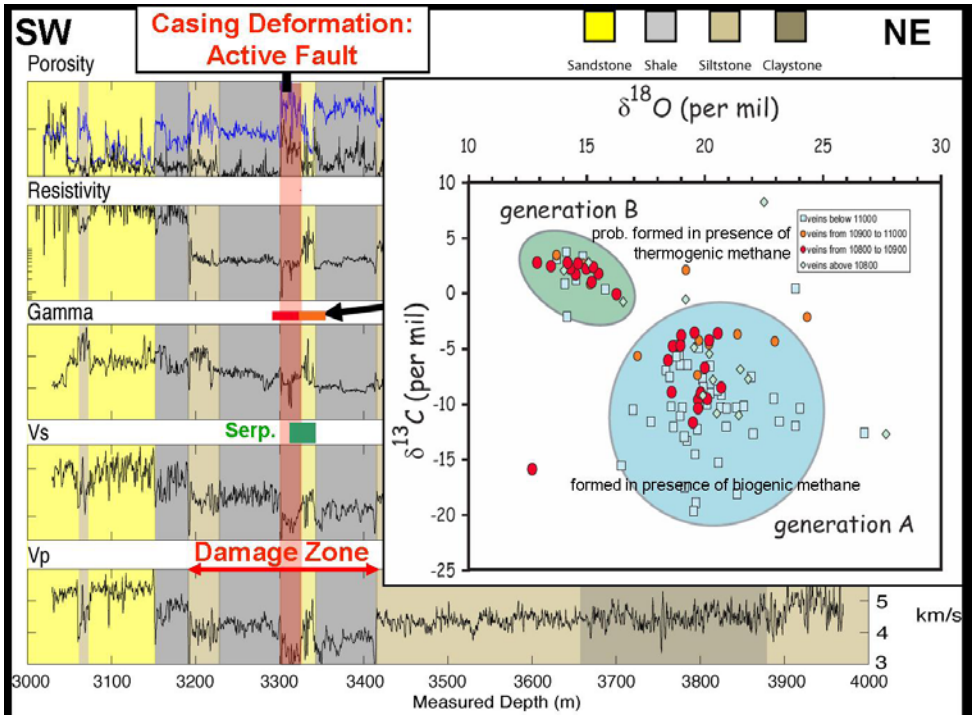

Figure 2: Carbon and oxygen isotopic composition of calcite veins from drill cuttings acquired during SAFOD Phase 2 (David Kirschner, written comm., 2006), superimposed on wireline geophysical logs and major lithologies from cuttings analysis. Depths are as measured along the borehole, which is inclined at 54-60° from the vertical. The currently active core of the San Andreas Fault is indicated by ongoing casing deformation and is embedded within an ~200-m-wide damage zone indicated by anomalously low P- and S-wave velocities. Red and orange symbols denote samples obtained within and immediately adjacent to the deforming fault core, whereas open symbols denote samples acquired from the relatively undeformed country rock. Note that samples from near the fault core tend to be isotopically distinct (generation B) from the country rock samples (generation A). Isotopic studies of drilling mud gas by Wiersberg and Erzinger (2007) suggest that calcite veins from generation B probably formed in the presence of thermogenic methane and, hence, were precipitated by more deeply derived fluids than were generation A.

Transient Fluid Pressure Effects - A range of physical effects arising from the mechanical response of fluid-saturated crust has been invoked to account for time-dependent phenomena associated with faulting such as slow earthquakes, creep events, earthquake swarms and aftershock activity and its decay. Transient changes in fluid pressure and effective stress have also been suggested to play a direct role in rupture propagation and arrest. Shear resistance on the rupture surface may be dramatically lowered by localized increases in fluid pressure from frictional heating or locally elevated as a consequence of pore fluid diffusion and dilatant hardening at fault jogs and other irregularities. Continuous monitoring of fluid pressure within active, seismogenic faults are needed to test these hypotheses and are a critical objective of the SAFOD monitoring program.

Chemical Effects of Fluids on Fault Zone Rheology - Over the past several years a number of fault mechanics models have either been developed or refined that incorporate solution transport deformation mechanisms that may weaken and/or destabilize the fault zone. However, complicating this issue enormously is the fact that under only slightly varied environmental and mineralogical conditions similar processes can act to cement the fault zone together, thereby increasing fault strength. The experimental and theoretical studies on which these models are based are now focusing on processes that have long been inferred as being important from field observations of natural fault and shear zones, such as pressure solution, fluid-assisted retrograde mineral reactions, crack healing and cementation. These deformation mechanisms are all interrelated, in that they depend upon ther¬mally activated chemical reactions between the rock and pore fluid as well as the rates at which dissolved species are trans¬ported through the pore fluid.

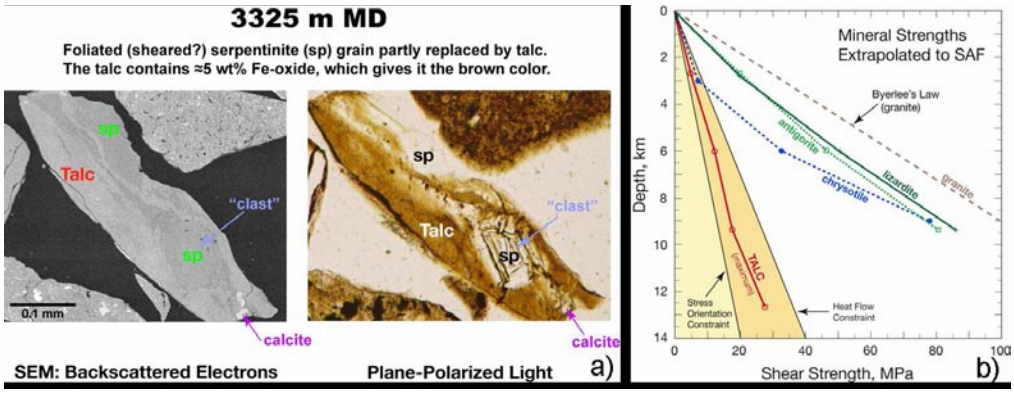

Figure 3: a) SEM image and photomicrograph of SAFOD drill cuttings from a measured depth of 3325 m (Diane Moore, pers. comm., 2007). Note the presence of serpentine minerals partially replaced by talc, with a calcite vein fragment also shown. b) Shear strength vs depth for a variety of serpentine minerals and talc, as extrapolated from laboratory deformation tests conducted at elevated temperatures and pressures (Moore et al., 1997; Diane Moore, pers. comm., 2007). Also shown for reference are strengths extrapolated from measurements on typical granitic rocks (Byerlee's Law) and the maximum shear stresses allowed by measurements of heat flow and maximum horizontal stress directions adjacent to the San Andreas Fault. Of the minerals shown, only talc is weak enough (coefficient of friction ~0.1-0.2 at slip velocities of 0.1 μm/sec) to be consistent with both the heat flow and stress orientation constraints.

Laboratory and theoretical investigations have shown that pressure solution may be important in reducing long-term fault strength and in promoting aseismic slip (i.e., creep) along faults. In contrast, solution transport processes such as crack healing and sealing and cementation may cause the welding together of asperities or fault gouge, leading to time-dependent fault strengthening between earthquakes. Laboratory friction experiments conducted under hydrothermal conditions suggest that a change in dominant deformation mechanism with increasing depth from brittle deformation to solution transport creep might control the depth at which the seismic-to-aseismic transition occurs in the crust. Observations of aligned fibrous serpentine in an exhumed branch of the San Andreas Fault system suggest that dissolution-diffusion-crystalization processes may be important in reducing fault strength and promoting aseismic slip (creep) along faults.

Hydrothermal mineral reactions can also weaken crustal rocks when the reaction products are weaker than the reactants. Some observations of exhumed shear zones in granite suggest that muscovite formed from the breakdown of feldspar might dramatically lower the ductile shear strength of the granite, even at temperatures well below those necessary for the plastic flow of quartz. At least at shallow depths, fault zones such as the San Andreas are mostly composed of clay- and mica-rich gouge resulting from the hydrolysis of feldspar, suggesting an enhancement of the feldspar breakdown reaction within the fault zone. Reactions in the olivine-talc-serpentine-water system have been demonstrated to dramatically lower the shear strength of ultramafic rocks in laboratory friction experiments.

A key result from SAFOD Phase 2 was the discovery of serpentine and talc in the drill cuttings, but only in close proximity to the actively deforming fault trace (Figures 2 and 3a). The occurrence of serpentine and talc along the active trace of San Andreas Fault at depth is particularly significant because these minerals tend to promote aseismic fault slip (i.e., creep). Furthermore, laboratory tests on compositionally similar talc indicate that it has extremely low shear strength at in-situ conditions (Figure 3b). Thus, although the mechanical significance of these minerals remains to be confirmed by microstructural observations and mechanical tests on core to be acquired within the fault zone during SAFOD Phase 3, the presence of talc (and associated serpentine minerals) at depth may explain both the overall creeping behavior of the fault at this location as well as its low long-term shear strength, as indicated by nearby heat flow and stress measurements.

Andreani M., A.-M. Boullier and J.-P. Gratier (2005), Development of schistosity by dissolution-crystallization in a California serpentinite gouge. J. Struct. Geol., 27, 2256-2267.
Andrews D. (2002), A fluid constitutive relation accounting for thermal pressurization of pore fluid. J. Geophys. Res., 107(B12), 2363, doi:10.1029/2002JB001942.
Bruhn R.L., W.A. Yonkee and W.T. Parry (1990), Structural and fluid-chemical properties of seismogenic normal faults. Tectonophysics, 175, 139-157.
Byerlee J.D. (1993), A model for episodic flow of high pressure water in fault zones before earthquakes. Geology, 21, 303-306.
Byrne T., and D. Fisher (1990), Evidence for a weak and overpressured décollement beneath sediment-dominated accretionary prisms. J. Geophys. Res., 98, 9081-9097.
Chester F.M., J.P. Evans, and R.L. Biegel (1993), Internal structure and weakening mechanisms of the San Andreas fault. J. Geophys. Res., 98, 771-786.
Evans, J.P., and F.M. Chester (1995), Fluid-rock interaction in rocks of the San Andreas system: Inferences from San Gabriel fault rock geochemistry and microstructures. J. Geophys. Res., 100, 13007-13020.
Hickman, S, R. Sibson and R. Bruhn (1995), Introduction to special section: Mechanical involvement of fluids in faulting. J. Geophys. Res., 100, 12831-12840.
Janecke, S.U., and J.P. Evans (1988), Feldspar-influenced rock rheologies. Geology, 16, 1064-1067.
Karner, S, C. Marone, B. Evans (1997), Laboratory study of fault healing and lithification in simulated fault gouge under hydrothermal conditions. Tectonophysics, 277, 41-55.
Kennedy, B.M., Y.H. Kharaka, W.C. Evans, A. Ellwood, D.J. DePaolo, J. Thordsen, G. Ambats and R.H. Mariner (1997), Mantle fluids in the San Andreas fault system, California. Science, 278, 1278-1281.
Moore, D E, D.A. Lockner, R. Summers, M. Shengli and J.D. Byerlee (1997), Strengths of serpentinite gouges at elevated temperatures. J. Geophys. Res., 102, 14787-14801.
Rice, J.R. (1992), Fault stress states, pore pressure distributions, and the weakness of the San Andreas fault. Fault Mechanics and Transport Properties of Rocks, B. Evans and T.-F. Wong (eds.), pp. 475-503, Academic, San Diego, Calif.
Robert, F., A-M. Boullier, K. Firdaous (1995), Gold-quartz veins in metamorphic terranes and their bearing on the role of fluids in faulting, J. Geophys. Res., 100, 12,861-12,879.
Segall, P, and J. R. Rice (1995), Dilatancy, compaction and slip instability of a fluid-infiltrated fault. J. Geophys.Res., 100, 22155-22171
Shipley, T. H., G. F. Moore, N. L. Bangs, J. C. Moore, and P. L. Stoffa (1994), Seismically inferred dilatancy distribution, northern Barbados Ridge decollement: Implications for fluid migration and fault strength. Geology, 22, 411-414.

Sibson, R. H. (1990), Rupture nucleation on unfavorably oriented faults. Bull. Seis. Soc. America, 80, 1580-1604.

Sleep, N. H., and M. L. Blanpied (1994), Ductile creep and compaction: A mechanism for transiently increasing fluid pressure in mostly sealed fault zones. Pure Appl. Geophys., 143, 9-40.

Solum J. G., S. H. Hickman, D. A. Lockner, D. E. Moore, B. A. van der Pluijm, A. M. Schleicher, J. P. Evans (2006), Mineralogical characterization of protolith and fault rocks from the SAFOD Main Hole, Geophys. Res. Lett., 33, L21314, doi:10.1029/2006GL027285.

Wiersberg T., and J. Erzinger (2007), A helium isotope cross-section study through the San Andreas Fault at seismogenic depths, Geochem. Geophys. Geosyst., 8, Q01002, doi:10.1029/2006GC001388.

Funding from NSF (RB) is gratefully acknowledged.

CONTINENTAL DELAMINATION AND EARTHSCOPE

Craig Jones • University of Colorado
George Zandt • University of Arizona
Gene Humphreys • University of Oregon

One of the great post-plate-tectonics challenges in tectonics and geochemistry is to understand the role played by and the process by which mantle lithosphere is recycled independently of overlying crust. A group of processes ranging from slab rollbacks to delaminations to convective instabilities have been proposed over the past twenty years to separate mantle lithosphere from the crust and replace it with asthenosphere. The structure, dynamics and implications of these processes are being addressed, and many basic questions have emerged. Such processes are being invoked for orogens around the world and through most of geologic time as geological events are recognized that have been difficult to explain by plate tectonic processes alone. The invocation of these processes appear to solve problems difficult to explain with plate tectonics, but without a solid set of observations bearing on the process of lithospheric removal, the inference of such removal is ad hoc. Our progress in understanding this cryptic continental deformation depends upon gaining more direct observations. EarthScope is well poised to provide such insights.

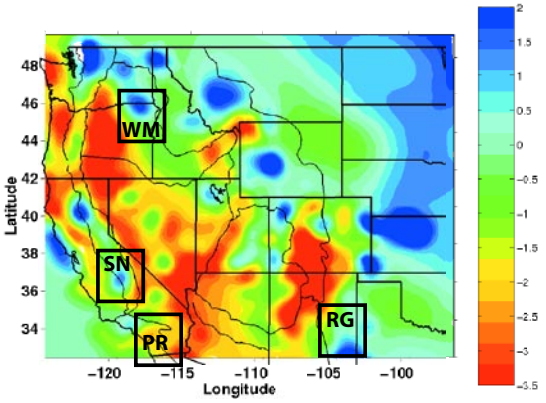

Figure 1: Pre-EarthScope P-wavespeed map at 100 km depth (modified from Dueker et al., GSA Today, 2001). How many blue and green dots are downwelling mantle lithosphere? How many are artifacts or variations in stationary lithosphere? SN= Sierra Nevada, PR= Peninsular Range, WM= Wallowa Mountains, RG= Rio Grande Rift flank.

The western United States was the launching pad for ideas about lithospheric removal and provides three environments increasingly tied to foundering of mantle lithosphere (Fig. 1). Delamination of mantle lithosphere arose as Peter Bird first suggested it to explain the elevation of the Colorado Plateau, although most of the western Cordillera experienced epeirogenic uplift that might have resulted from some style of lithospheric foundering. The western part of the Cordillera was built by large Mesozoic silicic batholiths, which are increasingly thought to develop over dense mafic to ultramafic roots likely to become gravitationally unstable. The compositional negative buoyancy may be an essential aspect of delamination, and removal of such roots might be a critical element in the process of generating continental crust. A third environment that appears related to lithospheric removal are flood basalt provinces such as the Columbia River Basalts in the Pacific Northwest.

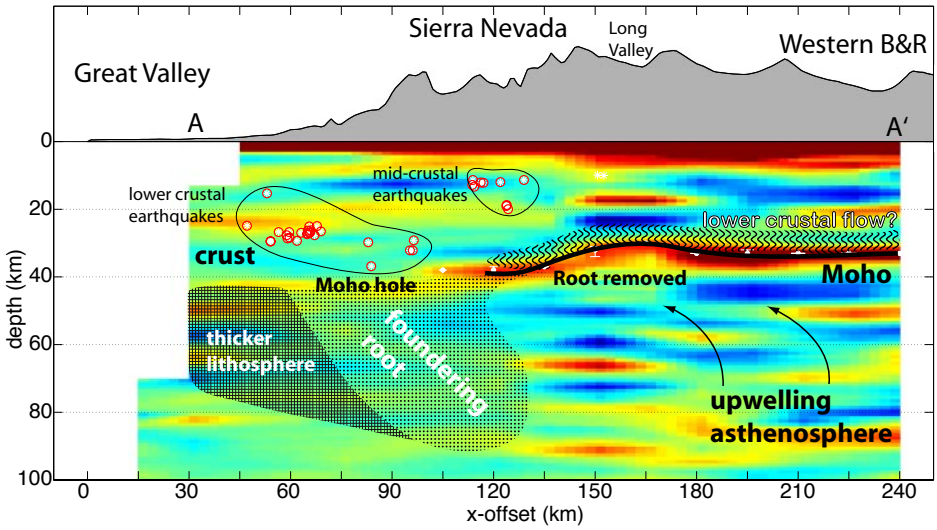

Figure 2: Southwest-northeast oriented receiver function cross-section across the Sierra Nevada with interpretations. Surface topography along this profile is plotted along the top of the cross-section. Red colors correspond to positive polarity arrivals while blues mark negative polarities. Earthquakes located near this profile are plotted as white asterisks within red circles. The interpretation of flow within the lower crust is based on observations of anisotropy at the base ofthe crust towards the eastern part of the SNEP array. The lack of a Moho arrival along the southwestern portion of the cross-section can be explained by a gradual increase in seismic velocities between the base of the crust and still intact portion of the batholithic root. The bright Moho present to the northeast marks the sharp contrast between the crust and inflowing asthenosphere that replaces the root following removal. [from Gilbert et al., EOS, in review].

Key questions need answers: how is such lithosphere made, what processes lead to lithosphere destabilization and control its removal, how much lithosphere might founder, precisely how does lithosphere get removed, what kind of tectonic and geochemical signals are produced as the lithosphere founders, and what kind of signatures will remain for many millions of years after a removal event? The diversity of environments and existing geologic data all suggest that this process will be far better constrained as EarthScope covers the United States.

EarthScope addresses delamination processes in several ways. The breadth of the Transportable Array will provide seismic images of moderate resolution into the Transition Zone and below, locating blobs that might have been removed from the lithosphere above. This wide aperture also permits identification of possible long-wavelength processes that act to cycle lithosphere to greater depth. FlexArray deployments within the Transportable Array will provide detailed imaging in places where lithosphere was removed, and this provides critical information necessary to interpret older orogens. Finally, the recent timing of proposed foundering events suggests uplift histories that would differ: foundering should produce rapid initial uplift slowing with time, while competing ideas (such as thermal reequilibration of the lithosphere following subduction or plume emplacement) should produce increasing uplift rates over time (e.g., Hales et al., 2005). Such differences are likely to become evident as vertical uplift rates become available from the Plate Boundary Observatory.

We are aware of four potential Late Cenozoic foundering events that are presently being studied: The Sierra Nevada, the Peninsular Ranges, the Wallowa Mountains, and the Rio Grande Rift. We discuss some of these recent and ongoing investigations to illustrate how EarthScope tools can bear on these problems, noting now that we expect applications to extend beyond these initial examples as EarthScope matures.

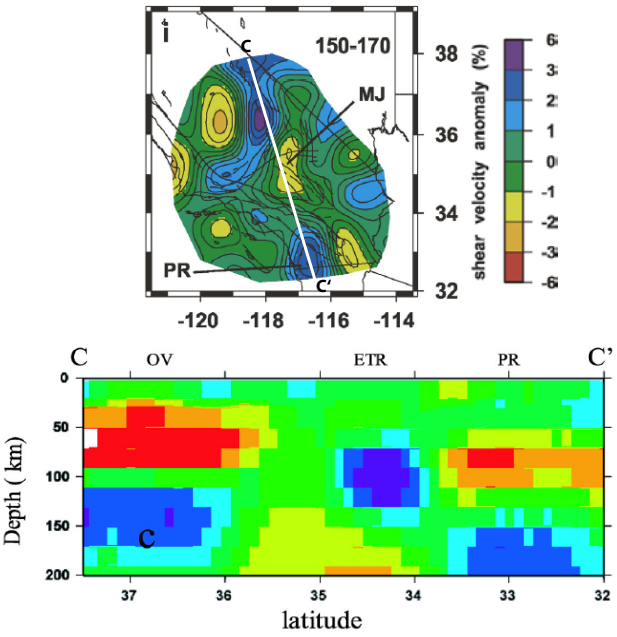

Figure 3: S-wave velocity variations from Yang and Forsyth (2006) inferred from teleseisms recorded at Transportable Array stations in southern California. Section C-C' shows both descending high-wavespeed material under the Sierra (blue below 100 km at left of section) and low wavespeed material (asthenosphere?) just below the crust. A similar pattern under the Peninsular Ranges (at right of section) suggests that a similar event might be occurring or have occurred in this area.

Sierra Nevada Batholith

Studies in the Sierra Nevada batholith in eastern California have found that the dense eclogitic and peridotitic mantle lithosphere that was present since the Mesozoic was removed by ~3.5 Ma and now sinks at one or more locations beneath the Great Valley. This foundering process is the target for the ongoing Sierra Nevada EarthScope Project (SNEP) FlexArray deployment in eastern California. The removal of dense eclogitic material from the Sierra Nevada has been proposed to explain the late Cenozoic rise of the southern Sierra, extension along the eastern Sierra, subsidence of the western foothills, and Quaternary volcanism. The SNEP array is a 30-month deployment of broadband seismometers at over 80 locations embedded within the initial footprint of the USArray Transportable Array. The closer spacing of SNEP permitted by the FlexArray deployment allows the creation of a cross-section of stacked receiver functions that clearly illustrates many of the large-scale changes in lithospheric structure observed across the central Sierra Nevada. Receiver functions are sensitive to discontinuities in densities and seismic wavespeeds. In cross-section, receiver functions can be viewed in a manner similar to seismic reflection style images (Fig. 2). Structures visible in this type of image suggest an asymmetric removal of lithosphere with the generation of new structures at the Moho. Further imaging, in conjunction with other approaches, will constrain the process triggering foundering.

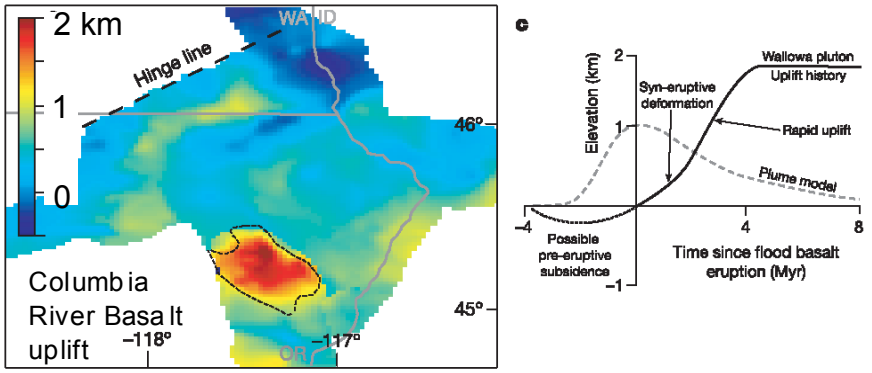

Figure 4: Uplift following eruption of the Columbia River flood basalts, based on current elevations of flow interfaces. Post-eruption uplift creates the bull's eye pattern, with Wallowa pluton (dotted line) experiencing ~2 km of uplift that is confined to the granitic mass, implying a large local change in density structure there.

Peninsular Ranges

The Peninsular Ranges of southern California represent a continuation of the Sierran arc to the south, so they present a likely place to investigate the association of lithospheric foundering with Mesozoic batholith formation. This region has only been covered at a spacing typical of the Transportable Array, so receiver function images are crude at best, but Yang and Forsyth (2006) have applied an innovative surface wave technique to early EarthScope data to develop a 3-D shear wavespeed model

(Fig. 3). This shows low- and high-wavespeed bodies under the Sierra consistent with body-wave tomography and the receiver functions, but to the south, under the Peninsular Ranges, a similar pair of low- and high-wavespeed bodies suggests that some similar foundering process might be underway. This is echoed by vertical uplift in the Peninsular Ranges seen with GPS (T. Dixon, pers. comm.) and uplift of marine terraces on the west flank of the range (Mueller et al., ms in prep.). This work, and the associated GPS uplift, indicates that the Transportable Array and PBO will both yield significant results outlining areas where foundering might be an ongoing process.

Wallowa Mountains, NE Oregon

In a region of few granitic plutons, the Wallowa pluton rose ~2 km rapidly following the flood eruptions of the Columbia River Basalts (CRB) ~16 Ma. The isolated and prominent uplift of this pluton (Fig. 4) suggests a delamination origin. The associated intense magmatism suggests that plume mantle was involved with the inferred delamination-driven flow. EarthScope data are being collected in this region to search for the proposed delaminates mass and to image the crustal, lithospheric and asthenospheric modifications that resulted.

Rio Grande Rift

Unlike the other locales, the Rio Grande Rift has had a more limited igneous history. Yet body wave tomographic images (Gao et al., 2004) have been interpreted to show lithosphere descending adjacent to the rift (Fig. 5). This high wavespeed body is imaged well into the Transition Zone. The large aperture of the Transportable Array will permit detection of such deep bodies throughout the western U.S. in three dimensions, better associating such bodies with surface geologic features and better limiting the processes producing such seismic anomalies (Fig. 1).

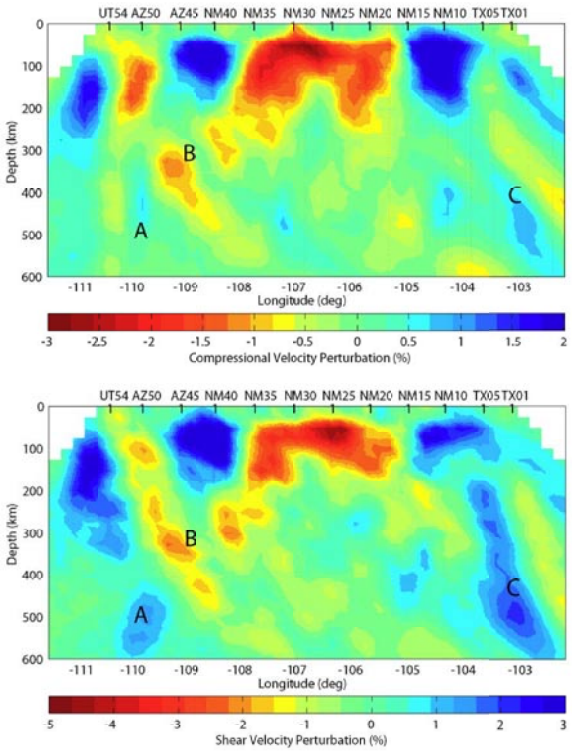

Figure 5: P-wave (top) and S-wave (bottom) wavespeeds along the RISTRA profile (Gao et al., 2004). Body A, at left is thought to be a fragment of the Farallon plate, while anomaly C (right) is inferred to be lithosphere descending from under the Rio Grande Rift.

Dueker, K., H. Yuan, and B. Zurek (2001), Thick-structured Proterozoic lithosphere of the Rocky Mountain region, GSA Today, 11 (12), 4-9.

Gao, W., S. P Grand, W. S. Baldridge, D. Wilson, M. West, J. F. Ni, and R. Aster (2004), Upper mantle convection beneath the central Rio Grande rift imaged by P and S wave tomography, Journal of Geophysical Research-Solid Earth, 109 (B3), B03305, doi:03310.01029/02003JB002743.

Gilbert, H., C. Jones, T.J. Owens, G. Zandt, Initial Earthscope FlexArray Deployment Images Foundering Sierra Nevada Lithosphere (2007), EOS, submitted.

Hales, T. C., D. L. Abt, E. D. Humphreys, and J. J. Roering (2005), A lithospheric instability origin for Columbia River flood basalts and Wallowa Mountains uplift in northeast Oregon, Nature, 438 (7069), 842-845.

Yang, Y., and D. W. Forsyth (2006), Rayleigh wave phase velocities, small-scale convection, and azimuthal anisotropy beneath southern California, J. Geophys. Res., 111, B07306, doi:10.1029/2005JB004180.

Zandt, G., H. Gilbert, T. J. Owens, M. Ducea, J. Saleeby, and C. H. Jones (2004), Active foundering of a continental arc root beneath the southern Sierra Nevada in California, Nature, 431 (7004), 41-46.

We thank our colleagues who have influenced our thinking on this topic. Our work has been supported by the Geophysics, Continental Dynamics, and Earthscope Programs of the EAR Division of NSF. Support for data collection and archiving by IRIS PASSCAL and DMC have been critical in the development of these ideas.

THE GLOBAL REACH OF USARRAY DATA

Thorne Lay • University of California, Santa Cruz
Edward Garnero • Arizona State University

Broadband seismic stations record ground shaking produced by both nearby and teleseismic sources, making them quintessentially multi-purpose tools for investigating earthquake processes and Earth structure throughout the globe. USArray will gather an immense seismic data set that can be exploited for many new research applications as the TA migrates across the United States, as the fixed ANSS Backbone accumulates data, and as deployments of dense arrays of FA stations occur for times scales from days to years. In combination with US regional network stations, these USArray data collection efforts will provide unprecedented aperture and wave field sampling that will enable new approaches and insights to fundamental problems.

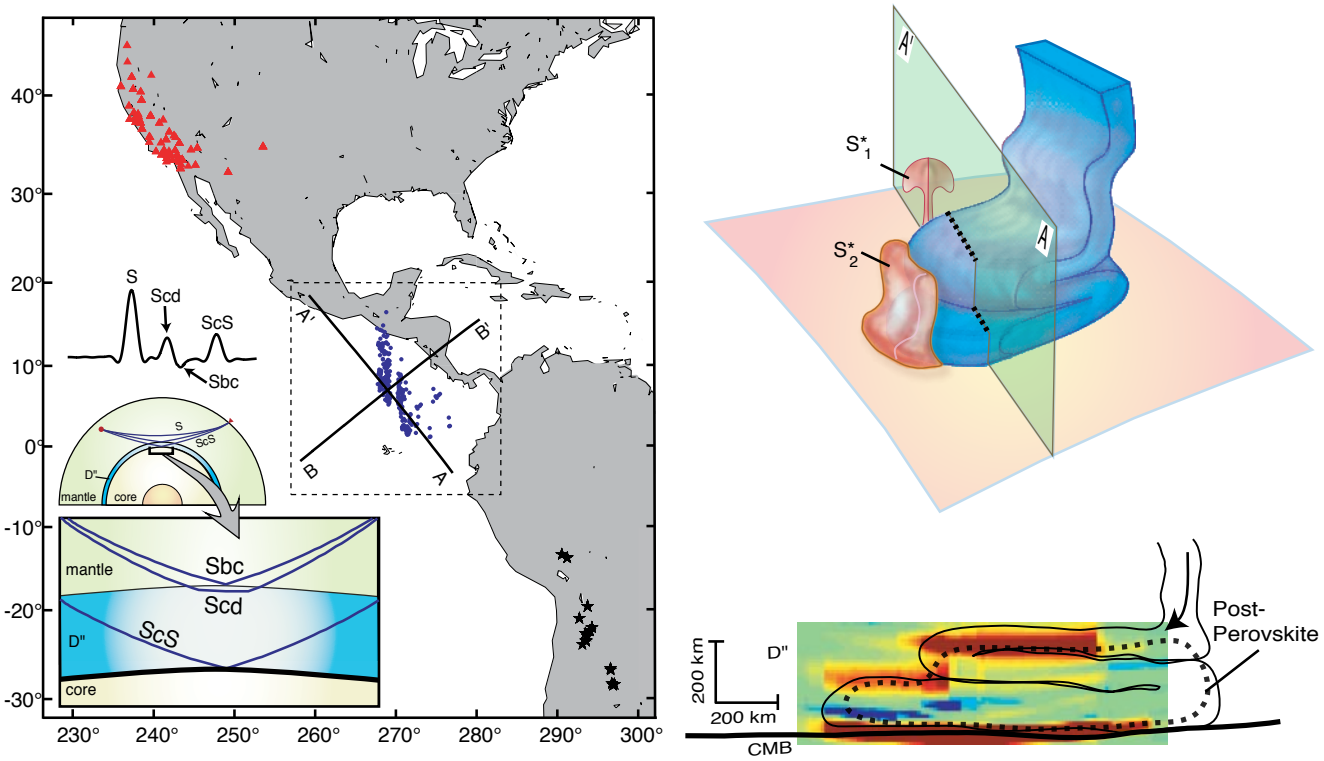

Figure 1: The deep mantle corridor sampled by paths from deep South American events to the initial TA deployment in the western US is shown on the left. S and ScS observations were migrated to form the image on the right along profile A'-A, which is interpreted as having a reflector above the CMB caused by post-perovskite phase transition in a cold, folded and piled relic Farallon slab. [Hutko et al., 2006].

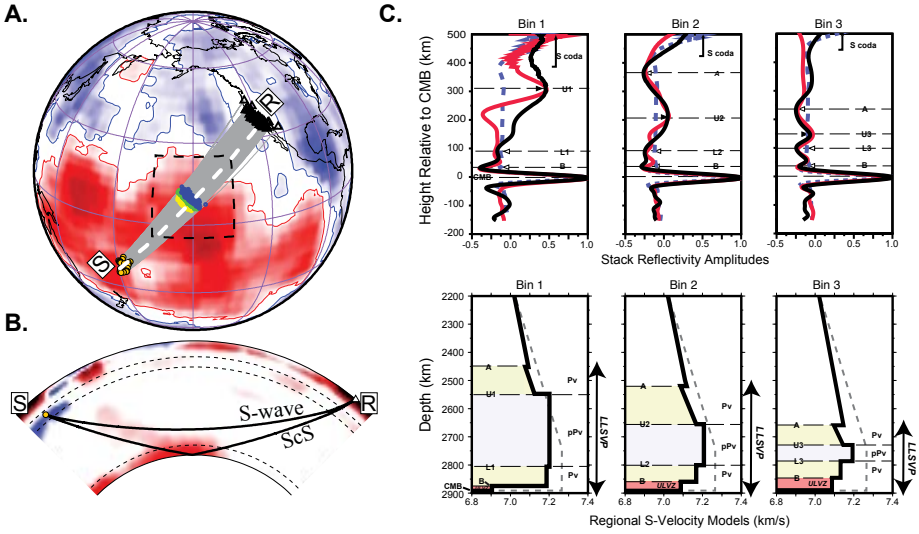

Figure 2: Paths to USarray TA stations in the western U.S. from deep focus events in the Tonga-Fiji region (A), illuminate the lowermost mantle beneath the central Pacific (B) in a region of lower than average shear velocities (red regions). (C) Stacking of broadband SH waves aligned on the core-reflection ScS (top right), reveals reflectivity (black lines) in the lowermost 300 km of the mantle, modeled (red lines) by small velocity increases and decreases for the velocity profiles shown on the lower right. A lens of post-perovskite material that thins toward the northeast is one interpretation of the velocity structure. In this scenario, the double intersection with the phase boundary provides an estimate of the regional temperature gradient, and by assuming a thermal conductivity, the heat flow through the CMB can be estimated [Lay et al., 2006].

While the principle scientific focus of USArray data collection is centered on earthquake processes and crustal, lithospheric, and upper mantle structure beneath the continental United States, a host of exciting investigations of other parts of the globe are possible using USArray data. These include studies of remote earthquake sources, as well as imaging of Earth structure far from North America, from the crust down to the planet's center. The density and quality of the USArray data are primary factors in the types of studies that are enabled. Here we highlight how USArray data can address fundamental questions in Earth science beyond those associated with the North American continent. Among a long list of possible applications, USArray can contribute significantly to our understanding of the nature of great earthquakes, the mode and style of mantle convection, the fate of subducting slabs, the genesis of mantle plumes, heat flux across the core-mantle boundary (CMB), the age and rotation rate of the inner core, the nature of Earth's magnetic field, and the mineralogical and petrological structure of the planet.

The global distribution of earthquake sources intrinsically ensures that USArray data have seismic wave paths that extensively sample Earth structure outside of the continental US. Seismologists have developed many approaches for isolating near-source, deep path, and near-receiver contributions to the seismic signals. Well-sampled wave fields with large spatial aperture are key to isolating the effects, and the TA plus ANSS backbone satisfies both criteria to an extent never before achieved. Global distributions of seismic observations are critical to many studies, and the concentration of North American observations provides particularly good sampling and signal-to-noise enhancement over a range of paths for studies of global mantle tomography, earthquake source mechanism inversions, and studies of deep Earth structure. The open access and high quality of the USArray data ensures its incorporation into such research applications. In this sense, the USArray broadband observations augment the global station distributions of the GSN and FDSN, and all the USArray recordings of larger earthquakes around the world can and will be routinely incorporated into important research efforts.

The more innovative value of USArray observations is their collective use in array approaches, which directly exploit the dense wavefield sampling. For example, investigations of deep Earth structure are commonly focused on localized corridors through the Earth sampled by specific earthquake and station concentrations. For studies that use deep earthquake sources, the well-illuminated corridors are limited; USArray in particular provides dense sampling of corridors under the Central Pacific, under Central America, and under Alaska and the Aleutians. Each of these three corridors has regions of deep seismicity at ideal distances from the US for analyses of seismic waves (e.g., direct and diffracted S and P, ScS, PcP, SKS, SKKS, SPdKS, and PKiKP) that sample the lowermost mantle (D" Region), the core-mantle boundary, and the outer core. As the TA migrates, the well-sampled corridors will expand spatially, unveiling structure over increasing length scales. This is a particularly exciting prospect, as it will transform tantalizing limited exposures to broadly sampled domains that can be more robustly interpreted.

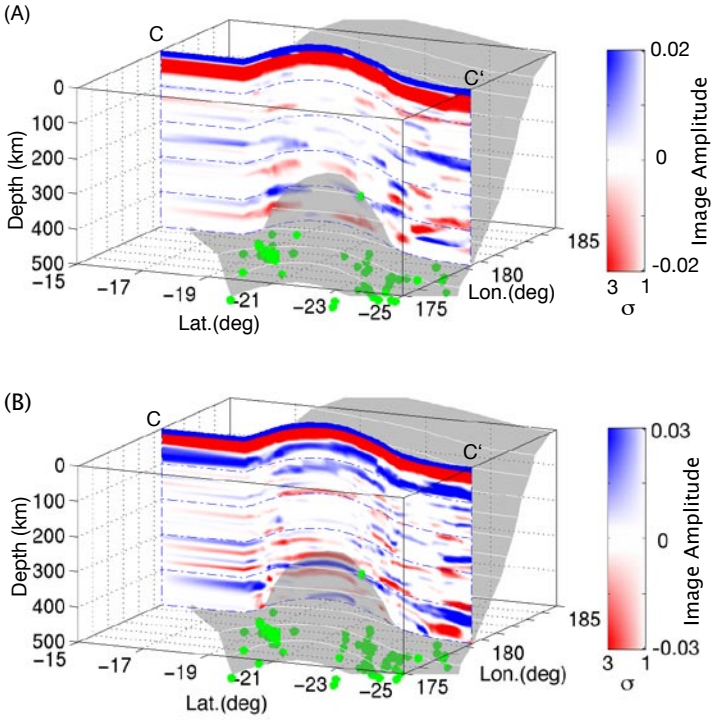

Figure 3: Migration of upper mantle reflectivity for P waves (A) and SH waves (B) above the subducting Tonga slab (gray surface) using globally distributed data including TA data in the western U.S.. The surface reflections pP and sSH produce blue stripes at the surface, with a red side-lobe below. Other blue features correspond to impedance increases with depth, while red features are impedance decreases with depth. The hues are scaled so that color saturation is only for features more than 3 standard deviations above the background level. [Zheng et al., 2007, in review].

Deep South American events recorded by the initial deployment of TA stations in the western US sample D" beneath the Cocos plate and Central America. Studies of P and PcP, and S and ScS phases in this corridor reveal complex lowermost mantle structure (Figure 1). Differential travel time analysis, differential shear wave splitting of ScS relative to S, and wavefield stacking and migrating algorithms that utilize the array aperture to isolate ray-parameter dependence of the wavefield are some of the methods used to isolate deep mantle structure in this corridor. The seismic wave reflector above the core-mantle boundary imaged by stacking of broadband data from the western US in Figure 1 is commonly attributed to the phase change from perovskite to post-perovskite phase predicted to exist some 200 to 400 km above the CMB, with the abrupt offset in the reflector interpreted as the result of folding and piling of cold Farallon slab material that has penetrated to the base of the mantle. As the TA migrates eastward, it will expose a broader region to high resolution imaging, allowing the folded slab interpretation to be tested. The TA data are already being incorporated into massive migrations of all seismic recordings sampling the deep mantle beneath the Caribbean that will resolve the details of what may be a large slab graveyard below North America.

Deep events in the Tonga-Fiji region recorded by USarray provide paths through the lower mantle beneath the central

Pacific (Figure 2), allowing detailed investigation of the large low shear velocity province (LLSVP) under the Pacific. This LLSVP and that beneath Africa, appear to be massive chemically distinct regions in the lower mantle. Past studies have suggested a variety of structures beneath the Pacific LLSVP, including changes in anisotropy related to the root of the Hawaiian plume, ultra-low velocity zone (ULVZ) layering right at the CMB, containing partial melt and giving rise to plume instabilities, as well as strong lateral gradients near the edges of the LLSVPs. Figure 2 shows array stacking of USArray data and synthetic modeling to image a layered D" structure which is interpreted as having a velocity drop at the top of the LLSVP, an entrance into (velocity increase) and exit from (velocity decrease) a lens of post-perovskite phase, and a mild ULVZ at the CMB. The laterally varying post-perovskite lens structure was used to infer regional heat flux through the core-mantle boundary of about 80 mW/m^2. Approaches like this that draw upon seismic, mineral physics, and geodynamics constraints are a promising tool for resolving major problems in deep Earth geophysics.

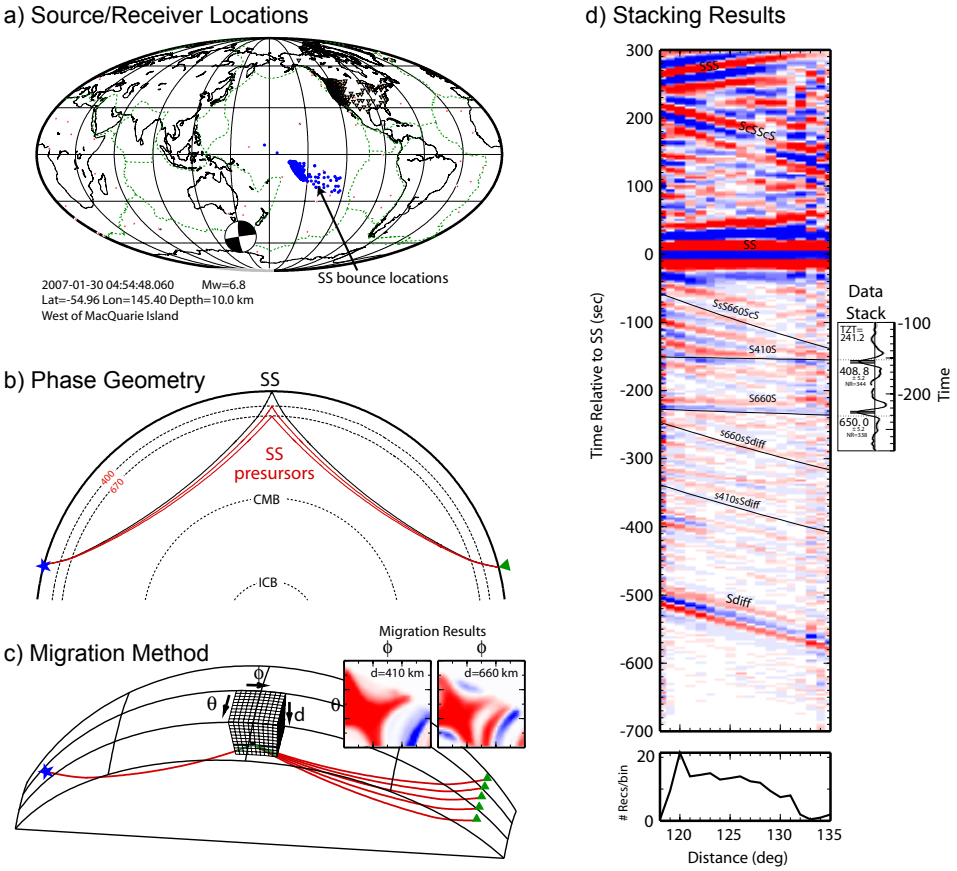

Figure 4: (a) The January 30, 2007 earthquake west of MacQuarie Island has SS surface bounce points (blue dots) in the central Pacific, for USArray TA and backbone stations (triangles in the US). (b) SS precursors reflect off of discontinuities between the event (blue star) and station (green triangle). (c) Migration analyses recover the mini-max Fresnel zone shape for both the 410 and 660 km depth discontinuities (schematics are shown in the inset panels, for synthetic seismograms of the PREM model), and have the ability to resolve fine scale structure. (d) Double array stacking of the data in (a) are shown versus distance, aligned on the SS wave (at time = 0). Travel times of dominant precursors are shown, with the waveforms for the stack of the entire data set shown to the right. Both the '410' and '660' precursors are clearly recovered, and sub-array analyses for this event would reveal the lateral variations of the discontinuity topography [Schmerr and Garnero, 2006].

Isolation of near-source structure can be done by designing the seismic analysis appropriately. Reflections from structure above the deep focus sources in the Tonga-Fiji regions are detected by migrations of P and SH waves in Figure 3. The dense sampling of the wavefield by TA stations plays an important role in forming these images, with additional coverage being provided by other global broadband stations. Imaging like that in Figures 2 and 3 is greatly enhanced by having large numbers of recordings for individual events because that allows elimination of source rupture characteristics and great signal-to-noise enhancement by stacking.

The large number of available stations in USArray and regional seismic networks provides resolution of Earth structure from single event studies – usually this is not possible with sparse data sets. Figure 4 show an example of stacking data from a recent teleseismic event (January 30, 2007) to study precursors of the SS wave. SS precursors have been demonstrated to be sensitive to upper mantle discontinuity structure – topography on the 410 and 660 km deep phase boundaries provide important clues to the temperature and mineralogy of the mantle. This single event shows that migration as well as double array stacking can be used to infer discontinuity depths, in this case in the central Pacific beneath previously noted hotspot volcanoes that may be related to mantle plumes.

These examples highlight just a few of the many exciting possibilities for using USArray data in studies of global structure and earthquake source retrieval. As the TA rolls east, new structures will be imaged, old structures will be viewed through a larger lens, and new earthquake processes will be revealed. These analyses will bring a deeper understanding to how Earth works as a system – how the evolution, structure, and dynamics of the interior relates to the tectonic processes manifested at Earth's surface.

Hutko, A., T. Lay, E. J. Garnero, and J. S. Revenaugh (2006). A folded slab at the base of the mantle imaged by migration, Nature, 441,333-336, doi:10.1038/nature04757.
Lay, T., J. Hernlund, E. J. Garnero, and M. S. Thorne (2006). A lens of post-perovskite and CMB heat flux in an iron-rich pile in D" beneath the Central Pacific, Science, 314, 1272-1276.
Zheng, Y., T. Lay, M. P. Flanagan, and Q. Williams (2007). Pervasive seismic wave reflectivity and metasomatism of the Tonga Mantle wedge, manuscript in review.

These research examples have been supported by NSF grants EAR-0125595 (Geophysics), EAR-0453884 (EarthScope), and EAR-0453944 (EarthScope).

EPISODIC TREMOR AND SLIP

Timothy Melbourne • Central Washington University

One of the most exciting avenues of research to emerge from joint GPS and seismic monitoring is transient creep inferred along the down-dip edge of subduction seismogenic zones, particularly in Cascadia. Japan led the way in first identifying these events, based on obvious transients in borehole strainmeter measurements from the early 1990s that were inferred to arise from slow slip episodes along the subduction fault [Hirose et al., 1999; Kawasaki et al., 1995]. However, due largely to sparse instrumentation coverage, these were assumed to be isolated occurrences. The ongoing proliferation of GPS, however, has afforded their routine detection in Japan, Cascadia and many other subduction zones [Larson et al., 2004; Lowry et al., 2001; Ohta et al., 2006; Ozawa et al., 2002]. In Cascadia, the initial recognition with GPS of transient slow faulting along the megathrust [Dragert et al., 2001] led to identification of 8 additional events with a regular, 13.9+0.9-month periodicity [Miller et al., 2002] and the forecasting of future events, 5 of which have occurred to date with the same periodicity, as detected on EarthScope Nucleus stations. It was originally assumed these events release large amounts of strain energy without detectable seismic shaking, but independent confirmation of Cascadia events came jointly from the discovery of subduction-related tremor signals in Japan [Obara, 2002] and their subsequent correlation in Cascadia with GPS-inferred slow slip events (Figure 1, [Rogers and Dragert, 2003]). Subsequent analysis of GPS from elsewhere in Cascadia shows that the slow slip events, also known as episodic tremor and slip (ETS, after [Rogers and Dragert, 2003]) likely occur throughout the Cascadia subduction zone, including beneath northern California, but with a different and distinctive 10.9+1.2-month periodicity, and offshore central Oregon with a 18+-2 month periodicity [Szeliga et al., 2007]. Most recently, reanalysis of EarthScope-Nucleus GPS data has shown that at least 35 slow slip events have occurred between 1997 and 2006 and that the region known for its regular, 14-month periodicity is largely confined to the northwest Washington and SW BC (Figure 2 [Szeliga et al., 2007].

The ongoing construction of the Plate Boundary Observatory promises to yield ever tighter constraints on this recently discovered, but evidently fundamental, process routinely occurring within many subduction zones. The most recent event in Cascadia, which initiated January 15, 2007 to the southwest of Seattle and propagated north into Canada over the ensuing three weeks, was by far the best measured event yet (Figure 3). Compared with previous events recorded on a handful of stations, this event took place within more than 70 GPS instruments and caused resolvable deformation on 40 of them. The event nucleated to the west of the southern Puget Basin and propagated only northwards: transient deformation appears in the southern Puget Basin for at least 14 days prior to its onset around the Strait of Juan de Fuca. The unprecedented coverage provided by PBO has yielded a very compact slip distribution not attainable without PBO. The greatest offsets are found along a swath beneath the eastern Olympic Mountains and overlying the 30 km depth contour, west of the southern Basin. The largest of these measure 6+-1.8 mm and is directed towards the southwest, characteristic of previous Cascadia events. The total effective moment of the event appears to be Mw=6.6, as estimated by inverting transient offsets for thrust-only slip; this number is also typical of past events in this region. Slip appears to be more concentrated, with best-fitting inversions yielding 3 cm of slip. Qualitatively, this event looks like the northern half of the Feb-March 2003 ETS, which also nucleated in the SW Puget Basin but propagated bidirectionally to the north and south. PBO GPS stations have also shown that many smaller events occur routinely outside the 14-month periodicity both within and outside of the northern Puget Sound area, a result confirmed by seismic tremor measurements. [Kao et al., 2005; McCausland et al., 2005].

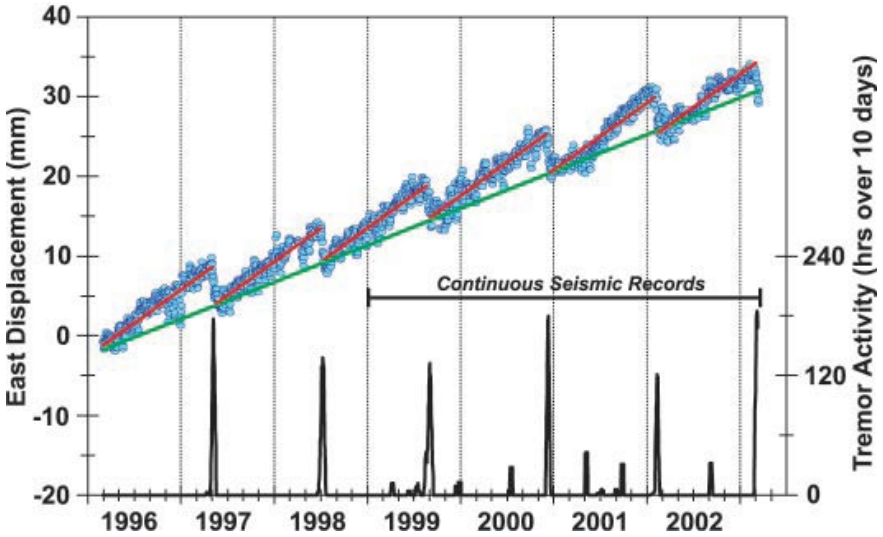

Figure 1: Comparison of slip and tremor activity observed for the Victoria area. Blue circles show day-by-day changes in the east component of the GPS site ALBH (Victoria) with respect to the GPS site near Penticton, which is assumed to be fixed on the North America plate. The continuous green line shows the long-term (interseismic) eastward motion of the site. Red line segments show the mean elevated eastward trends between the slip events, which are marked by the reversals of motion every 13 to 16months. The bottom graph shows the total number of hours of tremor activity observed for southern Vancouver Island within a sliding 10-day period (continuous seismic data were examined from 1999onward). Ten days corresponds to the nominal duration of a slip event. The graph ends 10 March 2003, with the slip and tremor activity that was predicted for the spring of 2003. After [Rogers and Dragert, 2003]

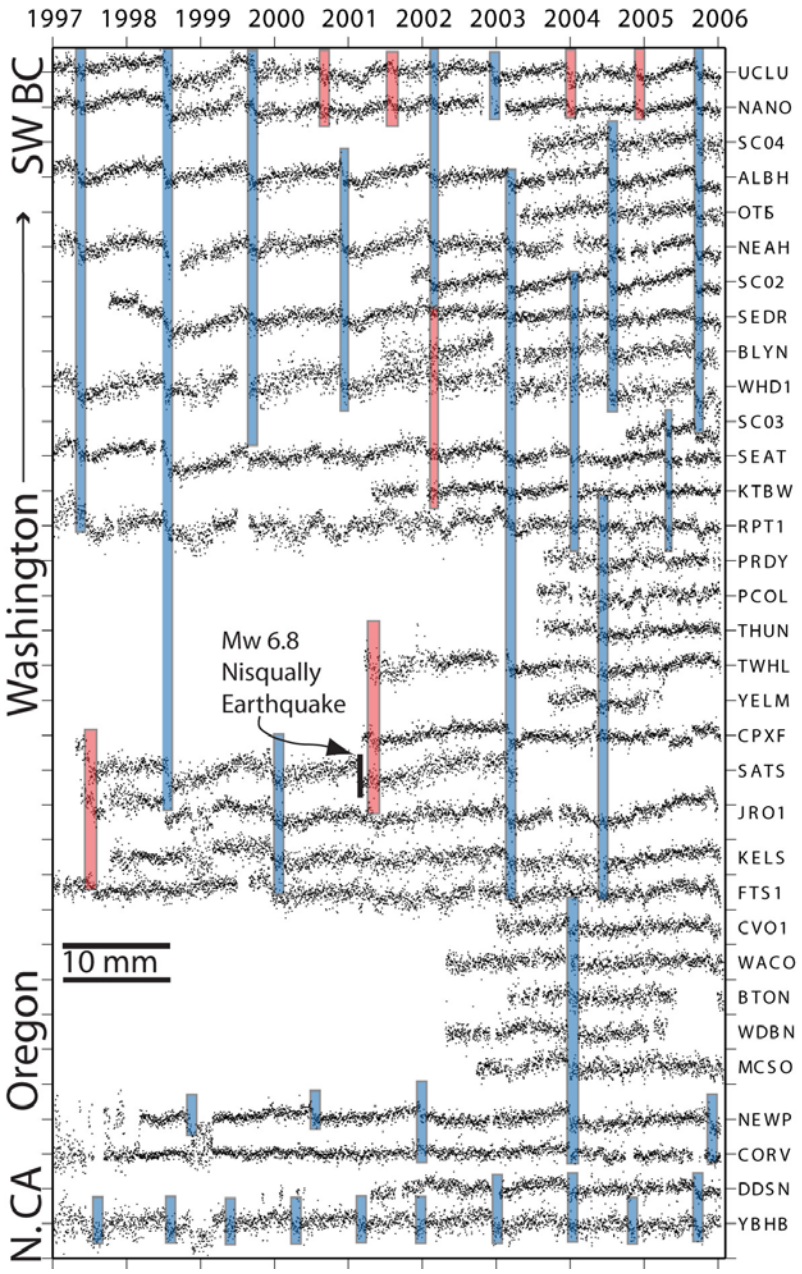

Figure 2: 9 years of GPS longitude measurements from the Cascadia subduction zone show evidence of over 30 slow slip events localized throughout the convergent margin. Vertical tick marks are 10 mm. Blue boxes indicate slip events either well-recorded with GPS or corroborated by observations of subduction-zone tremor. Red lines indicate spatially coherent transient GPS deformation typical of slow-slip events but recorded on less than four stations and uncorroborated at this time by tremor. Maximum geodetic offsets are 6 mm and correspond to the spatially largest event in early 2003, the smallest discernible events show 2 mm of deformation. Horizontal deformation for the 12 largest transients is shown in Figure 7. The February, 2001 Nisqually earthquake appears only on station SATS closest to the epicenter.

The mechanism by which slow slip occurs remains uncertain at the present time, but continued PBO and USArray observations will certainly provide the data needed to infer an answer. Three end-members mechanisms are all plausible and fit the available data: These are a) aseismic creep that triggers microseismicity, b) creep occurring simultaneous with seismicity, or c) no creep at all; meaning transient surface deformation represents only the integrated deformation from a large number of discrete, conventional seismic slip events. Depth estimations from both Cascadia and Japan show epicentral locations that consistently overlie the 25 to 40 km depth contours and 350oF isotherm of the subducted plate [Kao et al., 2005; McCausland et al., 2005; Obara, 2002], suggesting eclogitic dehydration-derived fluids process may play a role in promoting transient slip. Complicating this picture are tremor hypocentral depth estimates in Cascadia, however, which appear over a 40 km vertical range centered around the plate boundary [Kao et al., 2005; McCausland et al., 2005; Obara, 2002; Royle et al., 2006]. These depths imply that either tremor sources, and presumably slip, are spread radially over a wide range, or unmodeled diffraction of high frequency tremor (typically 1-6 Hz) bias the depth estimates. Along the Nankai Trough in Japan, however, hypocentral locations of very-low-frequency events that occur simultaneously with tremor both locate to the subducting plate interface [Ide et al., 2007; Ito et al., 2006; Shelly et al., 2006] and show thrust-fault mechanisms [Ide et al., 2007]. These inferences suggest, as of the present time, the theory that tremor originates from impulsive thrust-slip sources along the plate interface and thus are not likely scattered radially.

GPS-measured deformation is insensitive to the details of slip and cannot resolve the source process. However, it is currently the sole method for constraining the total equivalent moment of slip for a given episode of tremor, which eludes seismic and strainmeter analysis at the present time. Since transient plate interface slip impacts the developing moment budget, either by reducing the size of a future earthquake or delaying its recurrence, it is important to systematically document the sizes and characteristics of known slow slip events inferable from existing geodetic measurements. One of the most exciting observational confirmation of this theory comes from the most recent EarthScope-measured Cascadia ETS. Figure 3 shows the close correspondence between slip inverted from PBO GPS measurements and hypocentral locations of the accompanying tremor (white stars). Not only do the hypocenters generally overlie the slip patch, but the greatest concentration of tremor origins also overlies the regions showing greatest slip. This spatial and slip/tremor-density correspondence, the fact that no transient strain appears on PBO borehole strainmeters until tremor initiates, and the

fact that strain and deformation cease when tremor desists all lend credence to the theory that subduction zone slow slip events are in fact simply clustered microseismicity.

A current enigma stems from the fact that nowhere in the Cascadia subduction zone is there evidence of longer-term transients such as seen along Japan's Nankai Trough, the Middle-America trench offshore Mexico, or the Pacific subduction zone in Alaska [Larson et al., 2004; Ohta et al., 2006; Ozawa et al., 2002] suggesting that something about the Cascadia subduction zone favors more frequent but smaller creep transients than other regions. For all Cascadia events, anomalous station offsets rarely exceed 10 days at any given station and 4-6 weeks network-wide. Moreover, cumulative deformation from transient creep rarely exceeds 5 mm, and no offsets exceed 6 mm, which is in stark contrast to the Nankai Trough and Middle America Trench, where several cm of transient deformation are observed [Larson et al., 2004; Ohta et al., 2006]. The ongoing densification of GPS, strainmeters and seismometers in Cascadia will doubtless be fundamental in resolving this enigma.

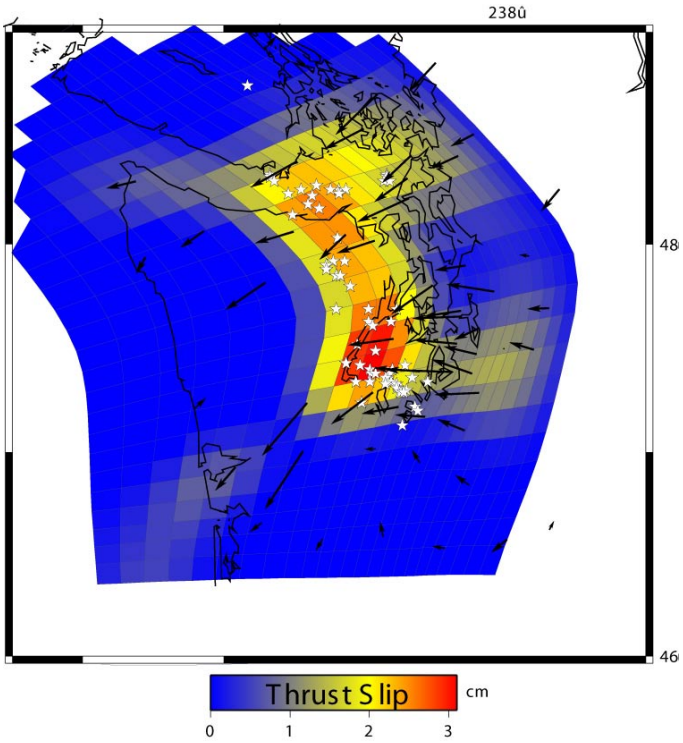

Figure 3: GPS-measured deformation (black arrows), inverted slip distribution (color) [Creager et al., 2007] and tremor epicentral estimates (white stars) [Creager et al., 2007] for the January 15-February 2 2007 Cascadia slow slip event. This transient produced measurable deformation on 40 of 70 PBO GPS stations and tremor recorded throughout the EarthScope TA stations. Maximum inverted slip is 3.1 cm and equivalent moment magnitude is Mw=6.6.

Creager, K., A. Wech, S. Malone, G. Abers, S. Rondenay, T. Melbourne, B. Hacker, and Z. Zhang, Locating Cascadia Deep Tremor Using Envelope Cross Correlation, in 2007 EarthScope National Meeting, Monterey, California, 2007.

Dragert, H., K. Wang, and T.S. James, A silent slip event on the deeper Cascadia subduction interface, Science, 292 (5521), 1525-1528, 2001.

Hirose, H., K. Hirahara, F. Kimata, N. Fujii, and S.i. Miyazaki, A slow thrust slip event following the two 1996 Hyuganada earthquakes beneath the Bungo Channel, Southwest Japan, Geophysical Research Letters, 26 (21), 3237-3240, 1999.

Ide, S., D.R. Shelly, and G.C. Beroza, The mechanism of deep low frequency earthquakes: further evidence that deep non-volcanic tremor is generated by shear slip on the plate interface, Geophys. Res. Let, in review, 2007.

Ito, Y., K. Obara, K. Shiomi, S. Sekine, and H. Hirose, Slow Earthquakes Coincident with Episodic Tremors and Slow Slip Events, Sciencexpress, 10.1126 (science.1134454), 1-4, 2006.

Kao, H., S.J. Shan, H. Dragert, G. Rogers, J.F. Cassidy, and K. Ramachandran, A wide depth distribution of seismic tremors along the northern Cascadia margin, Nature, 436 (7052), 841-844, 2005.

Kawasaki, I., Y. Asai, Y. Tamura, T. Sagiya, N. Mikami, Y. Okada, M. Sakata, and M. Kasahara, The 1992 Sanriku-Oki, Japan, ultra-slow earthquake, Journal of Physics of the Earth, 43 (2), 105-116, 1995.

Kostoglodov, V., S.K. Singh, A. Santiago, S.I. Franco, K.M. Larson, A.R. Lowry, and R. Bilham, A large silent earthquake in the Guerrero seismic gap, Mexico, Geophysical Research Letters, 30 (15), 1807, 2003.

Larson, K.M., A.R. Lowry, V. Kostoglodov, W. Hutton, O. Sanchez, K. Hudnut, and G. Suarez, Crustal Deformation measurements in Guerrero, Mexico, JGR Journal of Geophysical Research B, 109 (b04409), doi:10.1029/2003JB002843, 2004.

Lowry, A.R., K.M. Larson, V. Kostoglodov, and R. Bilham, Transient fault slip in Guerrero, southern Mexico, Geophysical Research Letters, 28 (19), 3753-3756, 2001

McCausland, W., S. Malone, and D. Johnson, Temporal and spatial occurrence of deep non-volcanic tremor: From Washington to northern California, Geophysical Research Letters, 32 (24), 2005.

Miller, M.M., T.I. Melbourne, D.J. Johnson, and W.Q. Sumner, Periodic Slow Earthquakes from the Cascadia Subduction Zone, Science, 295, 2423, 2002.

Obara, K., Nonvolcanic deep tremor associated with subduction in Southwest Japan, Science, 296 (5573), 1679-1681, 2002.

Ohta, Y., J.T. Freymueller, S. Hreinsdottir, and H. Suito, A large slow slip event and the depth of the seismogenic zone in the south central Alaska subduction zone, Earth and Planetary Science Letters, 247 (1-2), 108-116, 2006.

Ozawa, S., M. Murakami, M. Kaidzu, T. Tada, T. Sagiya, Y. Hatanaka, H. Yarai, and T. Nishimura, Detection and monitoring of ongoing aseismic slip in the Tokai region, central Japan, Science, 298 (5595), 1009-1012, 2002.

Ozawa, S., M. Murakami, and T. Tada, Time-dependent inversion study of the slow thrust event in the Nankai Trough subduction zone, southwestern Japan, Journal of Geophysical Research, B, Solid Earth and Planets, 106 (1), 787-802, 2001.

Rogers, G., and H. Dragert, Episodic tremor and slip: The chatter of slow earthquakes, Science, 300 (1942-1944), 2003.

Royle, G.T., A.J. Calvert, and H. Kao, Observations of non-volcanic tremor during the northern Cascadia slow-slip event in February 2002, Geophysical Research Letters, 33 (18), 2006.

Shelly, D.R., G.C. Beroza, S. Ide, and S. Nakamula, Low-frequency earthquakes in Shikoku, Japan, and their relationship to episodic tremor and slip, Nature, 442 (7099), 188-191, 2006.

Szeliga, W., T. Melbourne, V.M. Santillan, and M.M. Miller, GPS constraints on 34 slow slip events in the Cascadia Subduction Zone, 1997-2005, Journal of Geophysical Research (in review), 2007

A FIRST GLIMPSE OF CRUSTAL STRUCTURE FROM USARRAY

Morgan Moschetti, Michael Ritzwoller • University of Colorado, Boulder
Thomas Owens, Philip Crotwell • University of South Carolina

The USArray Transportable Array (TA) is providing data that promise significant improvements in estimates of the crust and upper mantle structure across the United States. The expansion of the TA provides data from a densely-spaced, widely-distributed array that now spans California, Oregon, Washington, much of Nevada and Idaho, and western Montana, Utah, and Arizona.

Two of the most promising approaches to utilize the entire TA for earth structure studies are the analysis of ambient noise Rayleigh waves (see one-pagers by Lin et al. and Moschetti et al.) and the automated estimation of bulk crustal properties from teleseismic receiver functions (see one-pager by Owens and Crotwell). Individually, each illustrates the immediate capabilities of USArray in lithospheric structure studies. However, the true power of USArray will be in the hybrid analysis methods that are spawned by this community resource.

Here we describe initial work on one such method, the joint inversion of ambient noise Rayleigh wave surface wave tomography and receiver function results using TA data to generate a three-dimensional shear-wave velocity model of the crust and upper mantle in the western United States (US). The ambient noise method generates a large data set for surface wave analysis, with high path density and good azimuthal coverage across the western US. In conjunction with crustal property estimates automatically generated for TA stations and other broadband instruments in the western US by the EarthScope Automated Receiver Study (EARS) system, improved estimates of crustal velocity structure are being made. The resulting crustal thickness estimates correlate well with previous studies and geologic features. Application of the techniques to emerging data from the TA promises to improve the inversions and expand the region of inversion. Although the joint inversion of these methods remains under development, we present initial results that provide a glimpse at the potential of integrated analysis of TA data.

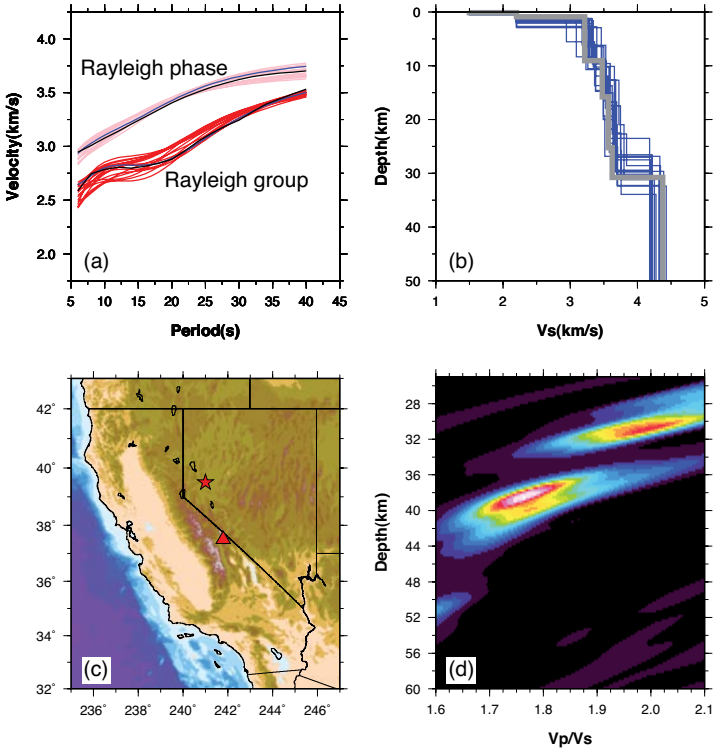

Figure 1: Background figures for the surface wave and receiver function inversions. Surface wave results are shown in (a) and (b) for the grid point (241.0, 39.5) identified in (c) with the star. The local dispersion curves are plotted in black in (a). All fitting phase and group dispersion curves are given in pink and red, respectively. The best-fitting dispersion curve is plotted in blue. The associated fitting velocity structures are presented as blue lines in (b), where the best-fitting model is plotted in gray. The receiver function results from EARS are for station S08C, plotted in (c) with a triangle, and are shown as a H-K plot in (d) with the warmer colors signifying preferable pairs of unknowns. This station returns an estimated crustal thickness of 38 km and a Vp/Vs ratio of 1.76.

Ambient noise surface wave tomography has been shown to provide accurate, high resolution surface wave dispersion maps at multiple spatial scales and over a broad period band. Surface wave data processing is described in detail by Bensen et al. (2007). Using data available from the TA and regional networks, we have cross-correlated records using up to 27 months of data from more than 300 stations to recover estimated vertical-component Green`s functions for all station-pair paths. An automated frequency-time analysis measures the Rayleigh wave group and phase velocity dispersion along each path from 6 to 40 sec period. From these measurements, standard tomographic methods (e.g., Barmin et al.) yield group (e.g., Moschetti et al., 2007) and phase (e.g., Lin et al., 2007) velocity maps for both Rayleigh and Love (Lin et al.) waves. These maps are then used to generate local dispersion curves that are the basis for inversion for the 3-D shear velocity structure of the crust and uppermost mantle. The local dispersion curves have been generated on a half-degree grid across the western US, but the preliminary results shown here are only for California and Nevada.

The surface wave inversion is based on a Monte-Carlo method, as illustrated in Figure 1. Rayleigh wave group and phase velocity curves for grid point (241.0 E, 39.5 N) are displayed in Figure 1a with the curves that acceptably fit these data. The models from which the fit curves are derived are displayed in Figure 1b. The Monte-Carlo method yields a best-fitting model and a spread of models at each depth and for each interface. The spread is interpreted as model uncertainty.

Crustal thickness estimates using the best-fitting model based on the ambient noise data alone are shownin Figure 2. These

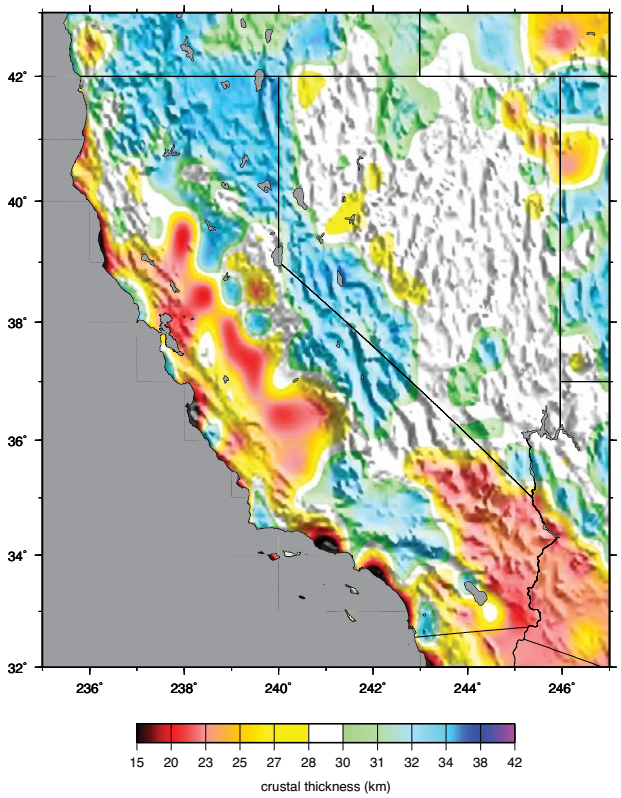

Figure 2: Results from the surface wave inversion for crustal thickness. The crustal thickness from the best-fitting model is shown at each node on a 0.5 degree grid.

Nevada. Crustal thickness estimates greater than 45km from EARS were considered anomalous and were not included. The results are broadly consistent with the inversion using surface wave data alone shown in Figure 2, but with smaller spatial variability. Thickened crust occurs in the Sierras and northeastern California and thinner crust is observed for the Mojave block and Salton Trough. Incontrast to the surface wave inversion, however, the crust beneath the Peninsular Ranges is uniformly thickened, and Nevada shows regions of both thinned and thickened crust.

Joint inversion of the receiver function and ambient noise surface wave data is able to benefit from the homogeneous coverage of the surface wave data and the higher local sensitivity of the receiver functions. Surface wave inversions alone are characterized by a trade-off between crustal thickness and the neighboring velocities in the deep crust and uppermost mantle. Receiver functions are assimilated into the surface wave inversion by simultaneously fitting the surface wave dispersion curves and the P-minus-S (P-S) time from the receiver function at each grid point. Where uncertainty estimates in the P-S time are available, we allow these values to vary within two standard deviations of the estimate. The P-S times are interpolated onto the half-degree grid and smoothed to provide a range of expected values at each grid point. The Monte-Carlo inversion returns an ensemble of one-dimensional velocity models at each grid point that fit both the dispersion curves and the P-S time within uncertainties.

At most grid nodes, the surface wave and receiver function data can be fit simultaneously. One aspect ofthe resulting 3-D model, results are broadly consistent with local geology. Broad regions of thickened crust are observed in the Sierra Nevada Mountains, the Transverse Ranges, and the Peninsular Ranges in southern-most California. Thinner crust is observed in the Great Valley and the northern California coastal ranges, throughout much of the Mojave block, and from the Salton Trough southwards. The crust in western Nevada abutting the Sierras is also thickened, but much of the state comprising the Basin and Range province contains crust of intermediate thickness.

Independent constraints on crustal thicknesses comes from receiver function analysis. EARS carries out automated receiver function analysis using data from multiple arrays, including the TA (www.seis.sc.edu/EARS; Crotwell and Owens, 2005). The automated processing of receiver functions by EARS for the TA data has resulted in crustal thickness estimates within much of the footprint of the TA. The use of a consistentanalysis method across all of the TA provides a uniform dataset for a joint inversion with the ambient noise results. A comparison of the crustal thickness estimates between Yan and Clayton (2006) and the results from EARS for forty-one common stations from the Caltech Regional Seismic Network shows a root-mean-squared difference of 3.41 km. The receiver function result for station S08C, processed by EARS, is given in Figure 1d.

Figure 3 presents the result of gridding and smoothing the receiver function estimates of crustal thicknesses across California and

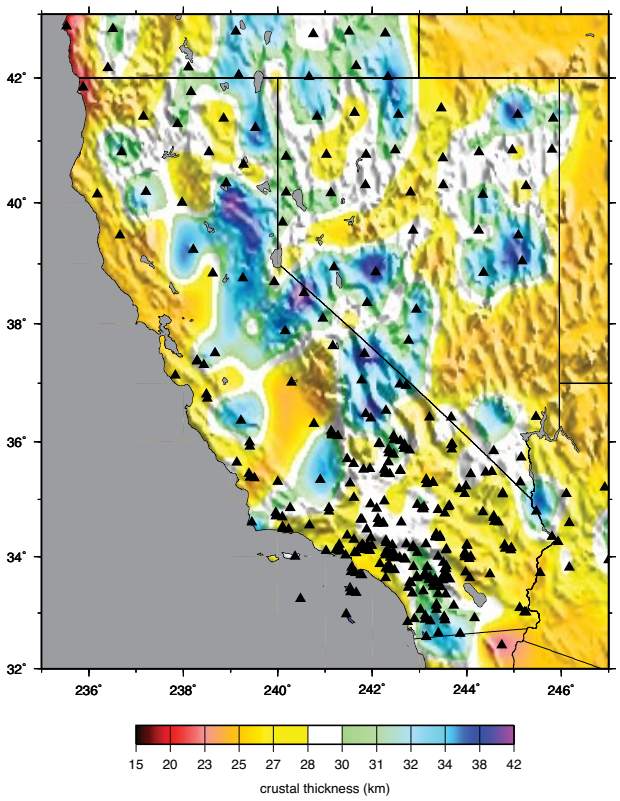

Figure 3: Gridded and smoothed crustal thickness results from the EARS receiver function analysis at TA and regional network stations, shown with black triangles. Receiver crustal thickness are interpolated between stations. Some of the results in southern California are taken from Yan and Clayton (2006).

crustal thickness, is shown in Figure 4, estimated from the joint surface wave and receiver function inversion. The joint inversion retains thickened crust in the Sierras, Northern California, the Southern Cascades, Peninsular Ranges, Transverse Ranges, and Southern Nevada. Thinner crust is observed in the Great Valley, Mojave block, Salton Trough, and Northern Nevada. In contrast to the surface wave inversion, the broad regions of crust thicker than 34 km in north and east California are not observed, but are replaced by crustal thicknesses varying from 30 to 42 km. The crust in northern Nevada is thinned by 1 to 3 km, and the crust in southern Nevada is both thinned and thickened in places. The Salton Trough region shows a significantly thinned crust (by 3 to 5 km) compared to the surface wave inversion. The Mojave block is slightly thickened relative to the surface wave inversion result. The lack of many receiver functions in the Great Valley leads to smoothed estimates of crustal thickness in that region.

As the TA expands across the US, additional station-pair paths and receiver function analyses will be added to the inversion data set. Longer paths between stations will facilitate the measurement of group and phase velocities at longer periods for surface waves which will provide improved constraints on deeper velocity structures, including crustal thicknesses. Incorporation of the automated receiver functions from EARS will continue to provide high local sensitivity to crustal thickness, which improves constraints onlocal crustal thickness and crustal velocity and also improves the resolution of smaller-scale features than those imaged by surface waves alone.

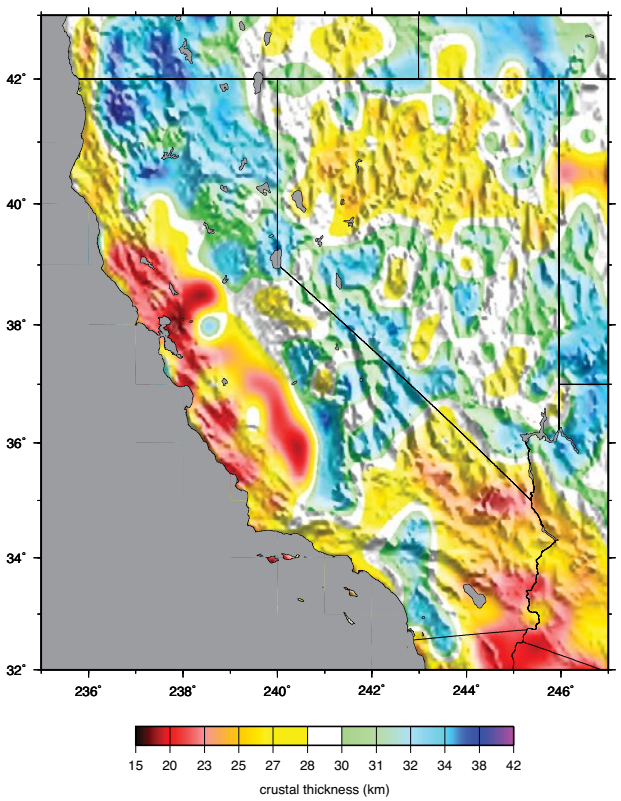

Figure 4: Results from the joint inversion of ambient noise surface wave dispersion curves and receiver function P-S times for crustal thickness.

Barmin, M.P., M.H. Ritzwoller, and A.L. Levshin, A fast and reliable method for surface wave tomography, Pure Appl. Geophys., 158(8), 1351 - 1375, 2001.

Bensen, G.D., M.H. Ritzwoller, M.P. Barmin, A.L. Levshin, F. Lin, M.P. Moschetti, N.M. Shapiro, and Y. Yang, Processing seismic ambient noise data to obtain reliable broad-band surface wave dispersion measurements, Geophys. J. Int., in press., 2007.

Crotwell, H.P. and T.J. Owens, Automated receiver function processing, Seis. Res. Lett., 76, 702-708, 2005.

Lin, F., M.P.Moschetti, and M.H. Ritzwoller, Surface wave tomography of the western United Stated from am bient seismic noise: Rayleigh and Love wave phase velocity maps, in preparation, 2007.

Moschetti, M.P., M.H. Ritzwoller, and N.M. Shapiro, Surface wave tomography of the western United Stated from ambient seismic noise: Rayleigh wave group velocity maps, submitted to Geophys. J. Int., 2007.

Yan, Z. and R.W. Clayton, Regional Mapping of the Crustal Structure in Southern California from Receiver Functions, submitted to J. Geophys. Res., 2006.

This research is funded by the EarthScope office of the National Science Foundation - NSF EAR-0450082. The EarthScope Automated Receiver Survey (EARS) is funded by the Earth Sciences Division of the National Science Foundation under grant EAR-0346113 to the University of South Carolina. MPM acknowledges a National Defense Science and Engineering Graduate Fellowship from the American Society for Engineering Education. The data are principally from the ANSS Backbone and the USArray Transportable Array and were obtained from the IRIS Data Management Center.

STRESS IN THE CRUST AND LITHOSPHERE: INSIGHT FROM EARTHSCOPE

Anne Sheehan • University of Colorado at Boulder
Paul Silver • Carnegie Institution of Washington, DTM

Stress is of major interest to Earth scientists because it can tell us about the forces driving deformation of the crust and lithosphere. With strain alone, we obtain a kinematic view of the Earth, whereas the inclusion of stress provides information on dynamics. Stress is related to strain (deformation) through a constitutive relation (rheology, viscosity). While stress and strain are the starting point of most seismology, structural geology, and continuum mechanics courses, the accurate determination of stress in the crust and lithosphere is a difficult problem. This is because stress can only rarely be measured directly, and is most often obtained by indirect means. Knowledge of lithospheric stress is essential to understand the forces driving both plate boundary and intraplate deformation, as well as the viscoelastic redistribution of stress that accompanies the earthquake cycle including both earthquake triggering, and postseismic deformation.

The collective Earthscope facility (SAFOD, PBO, and USArray) will provide important observations that can be used to better constrain stress in the crust and lithosphere. SAFOD is providing some of the first in situ measurements of stress and physical properties of a major fault zone. Well breakouts can be used to determine stress orientation, and the vertical variations of stress and strength in the vicinity of the borehole can be measured directly. Geodetic measurements using PBO will provide direct measurements of the strain field of western North America. The strain, combined with rheology, can then be used to estimate stress. The long-term deployment of PBO is essential to capture all phases of the earthquake cycle – preseismic, coseismic, and postseismic. The post-seismic signal can be used to estimate viscosity, which can then be used to estimate stress, given an observed strain rate. Studies of large earthquakes that occur within the PBO network should provide unprecedented coverage of the earthquake cycle. USArray data will be used to develop more appropriate structural models for use in stress-related studies. For example, accurate determinations of Moho depth combined with topographic and gravity data can be used to estimate lithospheric stress and to assess the relative contributions between body forces and plate boundary forces. Additional uses of USArray studies include studies of mantle seismic anisotropy, which can be related to strain in the lithosphere. Better estimates of lithospheric structure can give us a better handle on the body forces driving some of the deformation away from plate boundaries.

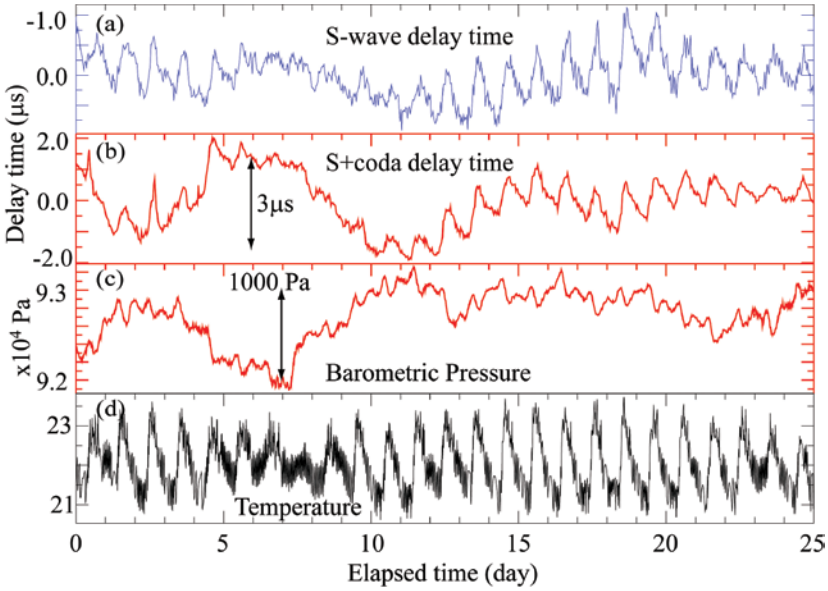

Figure 1: Delay times of S wave (a) and S+coda (b) are shown with variations in barometric pressure (c) and temperature (d). Notice the good negative correlation between the delay time and pressure.

Several broad problems related to crust and lithospheric stress that can be addressed with data from the collective Earthscope facility are outlined below. Further examples describing specific studies can be found in the collection of Earthscope 1-pagers.

1. The properties of active faults at depth can be addressed with the SAFOD project. SAFOD gives some of the first in situ measurements of active fault properties at seismogenic depth, as well as samples of fault material for further study in the lab. Understanding of fault friction is a critical parameter required to calculate changes in Coulomb stress (Freed and Lin, 1998). Information from SAFOD on constitutive properties of the active fault, composition and distribution of pore fluids along the fault zone, quantity and properties of fault gouge, and dimensions of the seismogenic zone, factor into studies of crustal stress and earthquake stress transfer.

2. Stress in the lithosphere can be explored using studies that link anisotropy to geodynamics and geodesy. The extent to which sublithospheric mantle flow couples to and stresses the base of the lithosphere is an open question. In many cases mantle anisotropy is used as a proxy for flow or deformation. These studies explore how flow affects plate motion and the transfer of stress to the lithosphere. For example, it is possible to estimate the magnitude and orientation of shear strain in the asthenosphere and to infer the orientation of the shear stress at the base of the lithosphere. This permits an assessment of the magnitude of stress by modeling the expected style of lithospheric deformation that would arise from the stress. Examples of this line of research include Silver and Holt (2002) and Becker et al. (2006a, 2006b).

Improved knowledge of seismic velocities and anisotropy from USArray will greatly increase our ability to correctly model lithospheric structure, such as the depth and topography of the Moho, vertical and lateral heterogeneities in lithospheric rigidity, and identification of the brittle/ductile transition. Better lithospheric structure provides stronger constraints on body forces, and the balance between body forces and plate boundary forces can be better understood. Many of these studies focus on the active tectonics of the western United States. The question of intraplate stress should not be overlooked, however. An important example is New Madrid. It is unclear whether New Madrid is a zone of weakness or a zone of strength (high stress). USArray in particular will provide observations that will lead to improved lithospheric structure constraints, which can be used in modeling of regional stress. During the 10-year deployment of USArray enough local earthquakes will be recorded and can be used to obtain stress estimates even where such events are relatively infrequent.

3. Since the 1992 Landers and Hector Mine earthquakes, much effort has been focused on understanding the extent to which earthquakes influence the behavior of nearby subsequent seismicity (Stein, 1999; Anderson and Chen, 2003; Steacy et al., 2005). The possibility of earthquakes triggering one another through changes in the regional stress field is called earthquake stress transfer. Given coseismic slip, the subsequent postseismic deformation can be used to infer rheology (Agnew et al., 2000), and therefore predict the redistribution of stress. Models that invoke postseismic viscoelastic stress transfer had particular success with linking the Hector Mine and Landers earthquakes (Pollitz and Sacks, 2002; Freed and Lin, 2001). In contrast, the 7-year delay between events has been hard to reconcile with a static coseismic stress change (Harris and Simpson, 200). The PBO deployment, especially where dense arrays of strainmeters and GPS receivers are placed in regions of high seismicity, will be able to observe both coseismic and postseismic deformation that are vital to constrain models of fault slip and transient processes that control the evolution of stress and strain in the lithosphere.

4. The long-term and high resolution observations possible with Earthscope provide and outstanding opportunity to study temporal variations in seismic velocity, slip rates, and seismic scatterers. Snieder (2002) uses 'coda wave interferometry' to study temporal variations in seismic coda, which can be related to stress changes. Much of this work has included lab and ultrasonic studies, the Earthscope facility, particularly SAFOD, will provide an important field site for this research. Taira et al. (this document, Volume III) examine the temporal decay of seismic scatterers after the Parkfield earthquake of 2004, which they interpret as due to postseismic stress relaxation. Niu et al. (2003) study repeating earthquakes in the Parkfield region, and see changes in S-wave code with time associated with the well-documented aseismic transient. Their results are interpreted in terms of stress-induced changes in fluid filled cracks.

Agnew, D., S. Owen, G. Anderson, L. Hearn, and B. Hager, A GPS cluster in the eastern Mojave Desert: Studying rheology with postseismic transients, in Proceedings of the second Plate Boundary Observatory workshop, 2-15 – 2-17, 2000.

Anderson, G., and J. Chen, Geophysical Research Letters, 30, 1310, doi:10.1029/2002GL016724, 2003.

Becker, T. W., Chevrot, S., Schulte-Pelkum, V., and Blackman, D. K.:

Becker, T. W., Schulte-Pelkum, V., Blackman, D. K., Kellogg, J. B., and

Freed, A. M., and J. Lin, Time-dependent changes in failure stress following thrust earthquakes, J. Geophys. Res., 103, 24393-24409, 1998.

Freed, A. M., and J. Lin, Delayed triggering of the earthquake at Hector Mine, California in 1999 by viscoelastic stress transfer, Nature, 411, 180-183, 2001.

Harris, R. A., and R. W. Simpson, The 1999 Mw 7.1 Hector Mine, California, earthquake: A test of the stress shadow hypothesis, Bull. Seism. Soc. Am., 92, 1497-1512, DOI: 10.1785/0120000913, 2002.

Niu, F., P. G. Silver, R. M. Nadeau, and T. V. McEvilly, Stress-induced migration of seismic scatterers associated with the 1993 Parkfield aseismic transient, Nature, 426, 544-548, 2003.

Pollitz, F. F., and I. S. Sacks, Stress triggering of the 1999 Hector Mine Earthquake by transient deformation following the 1992 Landers earthquake, Bull. Seism. Soc. Am., 92, 1487-1496, 2002.

Silver, P. G., and W. E. Holt, The mantle flow field beneath western North America, Science, 295, 1054-1057, 2002.

Snieder, R., Coda wave interferometry and the equilibration of energy in elastic media, Phys. Rev. E 66, 046615, 2002.

IMAGING DEEP STRUCTURE IN THE UPPER MANTLE UNDER NORTH AMERICA

Suzan van der Lee • Northwestern University
Barbara Romanowicz • University of California, Berkeley

One of the main scientific goals of USArray is to provide an unprecedented density of seismic recordings that will help us gain a better understanding of the deep structure of continents, and in particular address fundamental questions, such as: How does lithospheric thickness vary with geological age? How is the lithosphere coupled to the underlying convecting mantle? Does a low velocity asthenospheric layer exist under stable and in particular cratonic areas? Among these questions, there are some long standing controversies, for example whether a thick tectosphere translates coherently with the continent, or whether SKS splitting originates from fossil anisotropy frozen in the lithosphere or anisotropy in the asthenosphere induced by present day plate motions.

Tomographic models of upper mantle structure under North America consistently show that 3-D seismic velocity is correlated with surface tectonics down to 200 km depth. In fact, a striking difference between the low-velocity tectonically active western region and the high-velocity stable central and eastern shields is observed (Figure 1), emphasizing the high degree to which simplified surface geology correlates with mantle structure hundreds of km deep. High heat flow values suggest that the negative velocity perturbations in the western US represent young hot upper mantle material, perhaps exceeding 1500 oC. East of the Rocky Mountain Front, tomographic models show a large area of fast isotropic V_S. This anomaly represents the lithospheric root of the North American craton and extends to about 250 km depth in the oldest part of the continent. At 250 km depth, recent models find a low velocity anomaly beneath the Appalachians, parts of which have been observed previously in both V_p and V_s models. The anomaly may be due to intrusion of asthenosphere into the edge of the continental keel or it could indicate the presence of water, brought into the mantle by past subduction. The 3-D structure changes character at depths greater than 200-250 km, and the large velocity perturbations (dln V_S > 4%) observed in the uppermost mantle give way to anomalies not exceeding ~2%

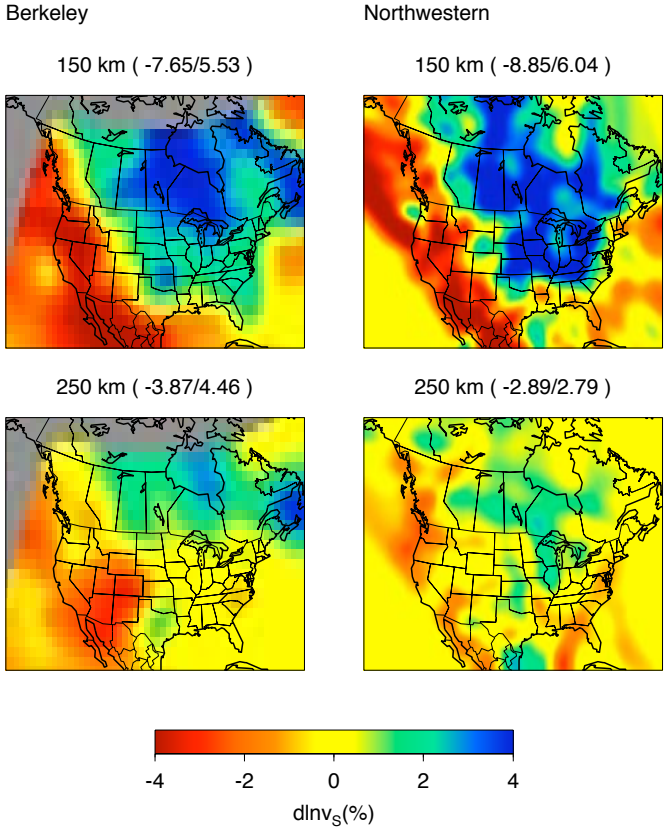

Figure 1: Maps of isotropic S-velocity distribution at 150 and 250 km for two recent models: Marone et al. (in revision) and Bedle and Van der Lee (in preparation). These two models are based on almost completely independent data sets, one of which (BL) includes some of the first USArray data. The two models were obtained using different methodologies, one of which (MGR) corrects for anisotropy and lateral heterogeneity of sensitivity kernels. The two imaging efforts have in common that both fundamental-mode and higher-mode surface waves are modeled. Despite differences in data sets and modeling methods, the models show a remarkable overall resemblance. However, they differ at some scales relevant to the fundamental science as discussed in the text. A completed USArray will help resolve features at these scales (see Figure 4).

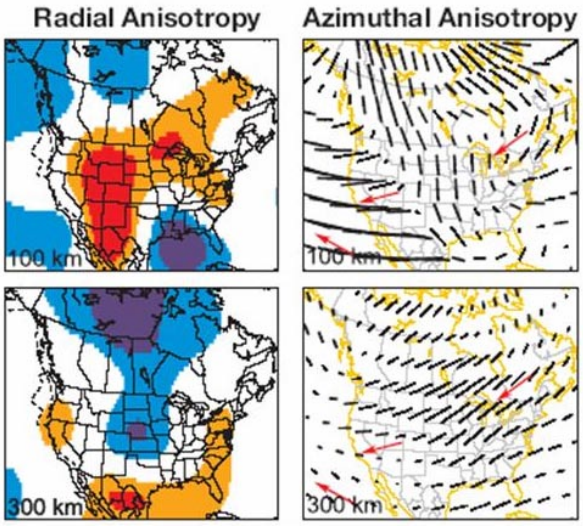

Figure 2: Preliminary results based on existing stations in North America, including isotropic velocities, radial and azimuthal anisotropy, indicate the presence of significant lateral variations in upper mantle structure across the continent down to asthenospheric depths. Left: radial anisotropy distribution at depths of 100 and 300 km (Marone et al., 2007). Blue indicates $\Delta\xi > 0$, where ξ is the anisotropic parameter $\xi = (v_{SH}/v_{SV})^2$ to which surface waves are primarily sensitive; ξ is shown with respect to the PREM model which is anisotropic down to 200 km. Right: azimuthal anisotropy at the same depth. The black lines indicate the direction and size of the fast axis of anisotropy, and the red arrows, that of absolute plate motion (after Marone and Romanowicz, in revision).

throughout the continent. The deep upper mantle is characterized by the presence of fast material beneath western North America, which is likely related to subducted lithosphere: the Juan de Fuca plate in the north and the extinct Farallon plate in the south. While existing models show very similar large scale features, especially in the uppermost mantle, some disagreements remain in important details, such as the precise location of the subducted trailing fragments of the Farallon Plate and whether they can be distinguished from the deep continental root. Finer scale resolution would thus also help address such questions as: what is the cause of the low velocities beneath the western, central, and eastern US and how does this material interact with the lithosphere above it?

Beyond gaining spatial and depth resolution on the distribution of isotropic seismic velocities under the North American continent, the high quality, dense coverage of the USArray's planned Transportable (TA) and Flexible (FA) arrays will provide the opportunity to map in greater detail two important components of structure: the distribution of anisotropy, which informs us on past and present day flow, and the lateral variations of major discontinuities, such as the lithosphere-asthenosphere boundary (LAB), the 400 and 660 km discontinuities and, possibly, other significant isotropic or anisotropic structural horizons within the lithosphere or below, which inform us on the thermo-chemical nature of 3D structure and its relation to surface features.

As shown in a recent study based on pre-USarray data, the resolution of anisotropic structure is best addressed using a combination of surface wave (fundamental and overtone) data and SKS splitting measurements (Figure 2). These two types of data have different resolution properties: SKS measurements do not have much depth resolution, but provide information on azimuthal anisotropy at the local scale under each station. Surface waves, on the other hand, have much poorer lateral resolution, but better depth resolution. They also provide information on radial anisotropy. At shallow depths (~100 km), the origin of the observed anisotropy must be lithospheric under the stable continent, but asthenospheric in tectonically active and oceanic areas. Deeper, this widespread anomaly disappears beneath the oceans/active areas and its presence is mainly restricted to the cratonic part of the North American continent (Figure 2). At 250 300 km depth, lateral variations in isotropic velocity have faded out, but persisting radial anisotropy with $v_{SH}>v_{SV}$ suggests an asthenospheric origin. The anisotropic structure is consistent with horizontal shear flow causing the preferred alignment of anisotropic minerals and confirms the results obtained under cratons at the global scale. The distribution of azimuthal anisotropy under the North American continent further confirms the presence of two distinct depth domains under the central and eastern part of the continent, with different directions of the fast axis, roughly consistent with the depth domains imaged in isotropic Vs and radial anisotropy. This direction is nearly parallel to the absolute plate at depths greater than 250km, while at shallow depths (~100 km), it is oriented more north-south (Figure 2). In contrast, under the western US, the direction of anisotropy is sub-parallel to the absolute plate motion even at shallow depths.

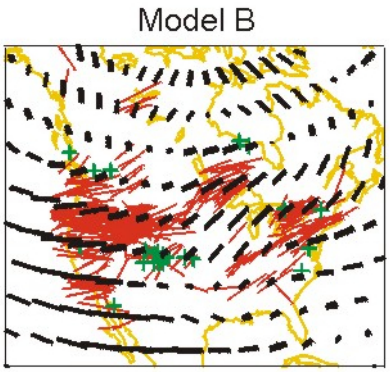

Figure 3: Available collection of SKS splitting measurements (pre USArray) from the literature. The fast axis direction and amplitude is shown in red (reliable measurements) and green (measurements do not resolve a consistent splitting direction). Note the very poor distribution in the central and southern US. Black lines indicate the fast axis direction and amplitude of splitting predicted from a model of radial and azimuthal anisotropy constructed using long period surface waveforms and SKS splitting data (Figure 2).

These and other results thus indicate the presence of two distinct anisotropy domains under the stable part of the continent, differing both in isotropic velocity and in the character of anisotropy. One, at shallower depth, is most likely associated with the lithosphere, while the other, at depths greater than 250 km, is associated with the asthenosphere. The boundary between these two domains, although not precisely mapped, varies laterally, following the surface tectonic and geological structure. The resolution obtained is, however, limited by the available distribution of shear wave splitting data, especially east of the Rocky Mountain Front (Figure 3.). Much more detailed and robust lateral variations of anisotropy could be obtained with the higher and more uniform distribution of planned USArray stations for at least two reasons: one is, simply, a more uniform and dense dataset of surface wave and shear wave splitting measurements, the other is a better control of the trade-offs between isotropic and anisotropic structure. USArray will provide comparable data coverage for the central and eastern US as for the western US, thus providing the unique opportunity to more precisely determine the depth of origin of anisotropic signal and to minimize trade-offs between isotropic and anisotropic structure. Potential bias in isotropic velocity models has been estimated for example by using pre-USArray regional coverage by S and surface wave trains from broadband seismogram for a distribution of anisotropy similar to that in Figure 2. The estimated bias is very small compared to isotropic S-velocity anomalies imaged from the same data and vanishes if the anisotropy is concentrated in the deeper layers. The bias also vanishes if the wave path coverage is improved to be near-uniform, such as through USArray. USArray will thus not only allow anisotropic structure to be resolved with necessary accuracy, it also will prevent anisotropy from biasing isotropic models, thus providing better maps of thermal and compositional heterogeneity on the one hand, and mantle flow or structural alignment, on the other.

To demonstrate the resolving power of USArray for isotropic structure, we show results of two resolution tests. One test uses the actual data coverage from the first USArray data collected and the other test uses hypothetical data expected from the

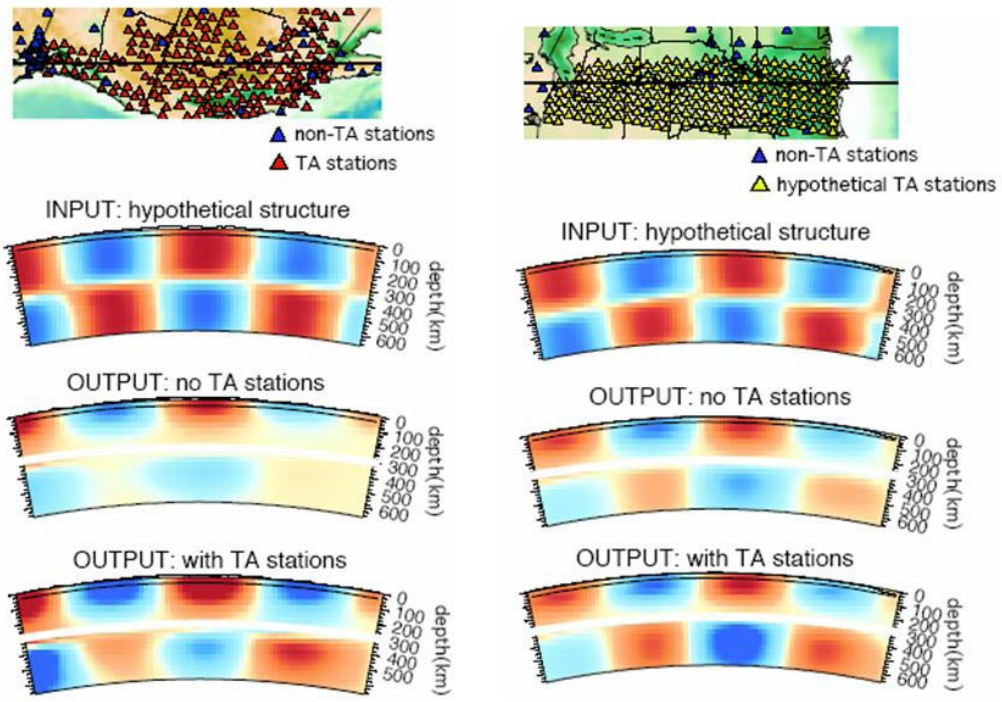

Figure 4: Resolution tests for hypothetical checkerboard-style isotropic velocity structure. The left column shows test results for the western US, using the actual data coverage of the very first stage of USArray's Transportable Array (TA). The right column shows test results for the central US, using hypothetical data coverage of the planned lodging of the TA there. Regularization in tomographic inversions underestimates the strength of anomalies. Here we show how TA data help alleviate this problem. The factor of underestimation is less at shallow depths, hence we use a different color scale for the top ~300 and the bottom ~300 km. However the color scale is the same between the "OUTPUT" cross section with and without USArray data. USArray clearly improves the resolution of relatively small-scale features in the both the top and bottom of the upper mantle.

period that USArray stations will populate states in the Midwest. Both tests illustrate the significant improvement in resolving power that USArray stations bring (Figure 4). With this improved resolving power, USArray will also, for example, provide relevant evidence to matters such as whether or not the mantle beneath the New-Madrid seismic zone has lower or similar seismic velocities as the surrounding mantle and whether or not there is a correlation between mantle structure and intraplate seismic activity.

Methods have also been developed to detect and characterize scattering horizons in the lithosphere and below using teleseismic S to P and P to S converted phases. Application to the few existing permanent broadband stations in the eastern US showed the presence of a westward dipping discontinuity at depths of 87-105 km which was identified as the bottom of the lithosphere. Recently, Sp imaging in the western US revealed an lithosphere-asthenosphere boundary at depths of 60-95. The sharpness and strength of the associated velocity gradient has important implications for its origin, in particular whether it is thermal or compositional, and how it relates to the possible presence of volatiles in the continental asthenosphere. Mapping more precisely, at the continental scale, lateral variations in the depth of the lithosphere-asthenosphere boundary, as well as its nature (velocity contrast and gradient, anisotropic character) will shed important light on lithosphere/asthenosphere dynamics as well as the compositional nature of this boundary under continents, in the context of "tectosphere" models. This can only be achieved with a denser and more uniform distribution of stations over the entire width of the North American continent, such as is planned with USArray. Other discontinuities have been observed within the lithosphere. USArray will provide data that will tell us whether such features occur over laterally extensive areas of North America.

In addition, a variety of discontinuities in the mid-upper mantle have been found within North America and globally, for example the discontinuity often called the Lehmann at depths of around 200 km. This discontinuity is sometimes seen preferentially under stable continents, sometimes not, and its nature and significance is the subject of debate. Evidence has been suggested of discontinuities at somewhat greater depths, which are sometimes called the "X" discontinuity. The mantle transition zone discontinuities at nominal depths of 410 and 660 km have been observed across North America at a wide variety of scales. The lateral variations of their topography and their thickness help quantify thermal/compositional variations. Eventually, one of the goals of USArray deployments is to provide dense enough spatial sampling by broadband data in order to combine industry-style imaging techniques for reflectors and tomography to obtain high resolution maps of the main horizons in the north American crust and upper mantle. Even with the 70 km station spacing of the Transportable Array, unaliased images of mantle interfaces using methods that involve forms of wave-field back propagation.

In summary, addressing many fundamental geophysical questions related to the dynamics of the north American continent requires a high resolution comparison of deep structure in the western, central and eastern US, using a variety of seismological imaging methods. For this, it is essential that USArray completes its TA and FA deployments across the central and eastern US.

This work was partially supported by NSF awards EAR-0345481 (BR) and EAR-0346200 (SvdL). We thank IRIS for providing high quality data on which the preliminary work described here is based.

STRENGTH, STRUCTURE AND RHEOLOGY OF FAULTS

Mark Zoback • Stanford University
Steve Roecker • Rensselaer Polytechnic Institute
Fred Chester • Texas A&M University

Most of what we now know about the structure, composition and deformation mechanisms of crustal faults has been learned from geological and geophysical investigations at the Earth's surface and laboratory tests on materials presumed to be representative of active faults at depth. Field observations of exhumed faults have shaped our understanding of the geometrical complexity, spatial heterogeneity in physical properties, and deformation mechanisms operating at different crustal levels (Figure1). Although these studies continue to provide important information, they are limited because some important processes are poorly recorded in rock, exhumed faults provide only a cumulative record of deformation that masks temporal variations, near-surface processes may alter the record from depth, and it is difficult to know if exhumed fault structure reflects seismic or aseismic behavior.

Over the past several decades, integration of field, laboratory and theoretical work has been successful in improving our understanding of the mechanical and hydrological behavior of faults but has also posed a suite of intriguing questions about the structure and properties of active faults at depth. Advances in geophysical techniques, notably seismic tomography, have also been successful in imaging the crustal structure of major fault zones on a km scale. Nonetheless, it is currently impossible to differentiate between—or even adequately constrain—the numerous conceptual models of active faults proposed over the years. For this reason, the Earth science community is left in the untenable position of having no generally accepted paradigm for the structure, properties or mechanical behavior of faults at depth. One of the primary causes for this dilemma is the difficulty of directly observing environmental conditions (e.g., stress and pore fluid pressure), physical properties, and deformation mechanisms along faults at depth associated with aseismic creep and the earthquake cycle.

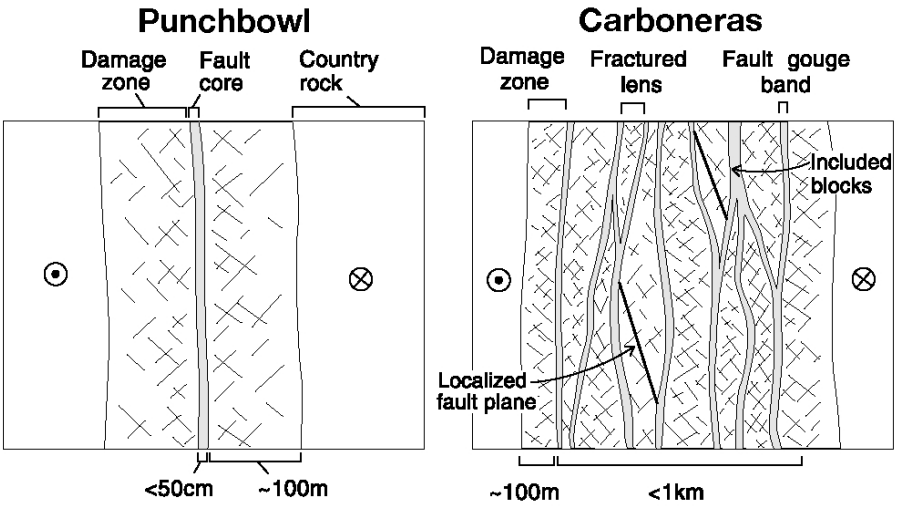

After Faulkner et al., 2003

Figure 1: Conceptual models for the structure of large-displacement faults; end-member structure of fault zones represented by the Punchbowl and San Gabriel faults with a single fault core centrally located within a damage zone and the Carboneras fault with multiple, anastamozing gouge layers isolating lenses of fractured rock within a damage zone. Fault cores are sites of large shear strain and usually consists of foliated cataclasite or microbreccia containing layers of gouge or ultracataclasite and mesoscopic slip surfaces (e.g., Chester et al., 2004; Chester et al., 2005).Faulkner et al. [2003] noted the presence of localized slip surfaces in the damaged rock of the Carboneras fault, and hypothesized that these represent paleoseismic slip surfaces. They suggest that the Carboneras fault structure is consistent with macroscopic aseismic creep with embedded microseismic slip and may be a good analog to the SAFZ near SAFOD.

SAFOD provides a unique opportunity to directly sample fault rocks and fluids, measure in-situ physical properties, and monitor chemo-mechanical processes within an active plate-bounding fault zone. Through drilling, we can recover fault zone materials for laboratory analysis of fluid and rock chemistry, microstructural state, and constitutive properties; measure the state of in-situ stress and pore pressure across the fault zone; and study time-dependent processes along both creeping and seismogenic fault segments. Equally important, downhole measurements and sampling in SAFOD allow calibration of surface-based geophysical images of the crustal volume containing the San Andreas Fault against rock types, geologic structure, and physical properties actually encountered during drilling (Figure 2).

SAFOD allows us to address a number of first-order questions related to fault mechanics.

- *What is the static and dynamic strength of active segments of the San Andreas fault?* How does the stress state change across fault zones, with depth, and with time? What are the friction constitutive properties of highly sheared, fine grained fault rocks at realistic in-situ conditions of stress, fluid pressure, temperature, strain rate and pore fluid chemistry? Are faults weakened by static or transient fluid pressurization in fault zones?
- *What controls the stability of fault slip?* Why do some fault segments creep? Are fault surfaces defined by background microearthquakes and creep the same? What determines the depth of the shallow seismic-to-aseismic transition? What

do mineralogical, geochemical and microstructural analyses reveal about the nature and extent of water-rock interaction, processes of fault weakening and strength recovery? How does strain communication occur within fault zones over different time scales?

- *What are the physical properties of fault-zone materials and country rock?* How do physical properties from core samples and downhole measurements compare with properties (e.g., seismic velocity and electrical resistiviy) inferred from surface geophysical observations? What are the dilational, thermoelastic and fluid-transport properties of fault and country rocks and how might they interact to promote either slip stabilization or transient over-pressurization during faulting?
- *What is the architecture of the fault?* How is it segmented? How deep do surficial low velocity zones along the fault extend into the Earth? How does fault structure affect fluid flow? What processes control the localization of slip and strain? Would active slip surfaces be recognizable through core analysis and downhole measurements in the absence of seismicity and/or creep?

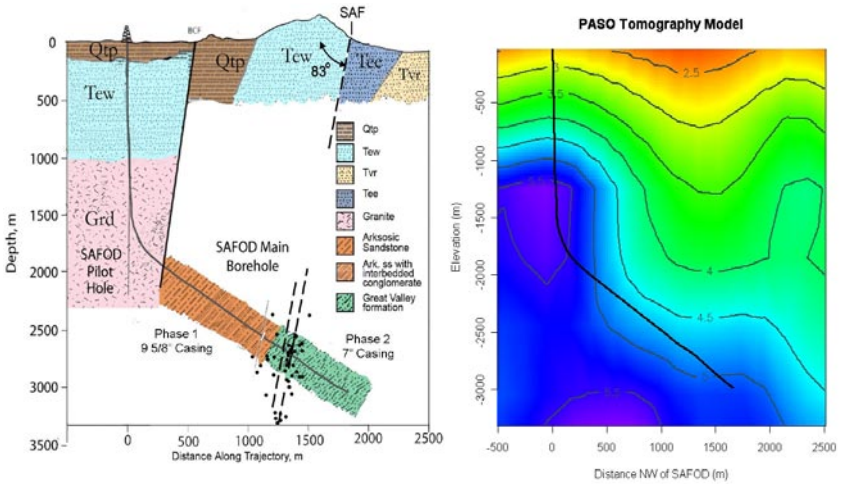

Figure 2: Comparison of geological and geophysical cross sections through SAFOD. Left figure shows the geologic model derived from surface mapping and analysis of drill cuttings and well logs. The position of the SAFOD main borehole and pilot hole are shown as well as the location of major fault traces encountered during drilling and as inferred by projecting microearthquake locations onto the section. Right figure shows a cross section of a 3-D velocity model obtained by Roecker et al. (2006) from the EarthScope Transportable Array (Parkfield Area Seismic Observatory) and other data sources.

Over the past several decades, there has been considerable controversy over the levels of shear stress required to drive slip along active faults, both along major plate-bounding faults and along relatively small displacement faults in plate interiors. Figure 3 shows representative in situ stress measurements in relatively deep wells and boreholes from a variety of faulting regimes. These data, in conjunction with information on the attitude of nearby active faults, indicate fault strengths in intraplate areas that are comparable to those predicted by Coulomb theory and laboratory derived coefficients of friction between 0.6 and 1.0.

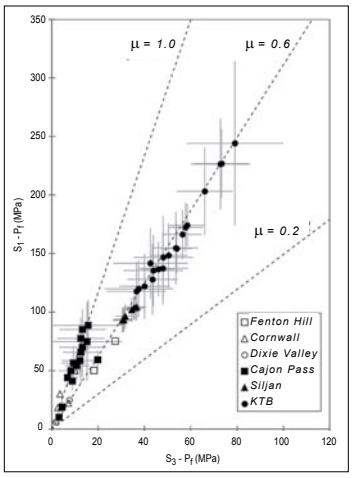

Figure 3: Stress measurements in deep boreholes indicate high crustal strength in accordance with Coulomb faulting theory with laboratory-determined coefficients of friction between 0.6 and 1.0 and hydrostatic pore pressure, which is observed in each borehole (after Townend and Zoback, 2000). It should be noted that the uncertainties in these measurements are likely significantly smaller than the conservative values shown here.

In contrast, a substantial (and growing) body of evidence indicates that earthquake slip along major plate-bounding faults, including the San Andreas, occurs at much low levels of shear stress than shown in Figure 3. Our inability to reconcile conflicting evidence of the strength of faults is sometimes referred to as the San Andreas Stress/Heat Flow Paradox. In the context of the San Andreas, there are two principal lines of evidence that the fault has low frictional strength – observations of heat flow and in situ stress. A large number of heat flow measurements adjacent to the San Andreas Fault place an upper bound on the amount of frictionally generated heat, which implies that shear stress resisting motion along the fault is approximately five times less than shown in Figure 3. Numerous stress measurements along the San Andreas Fault throughout California show that the direction of maximum horizontal compression is at a very high angle to the fault, indicating that right-lateral strike slip motion on the San Andreas Fault occurs in response to low levels of shear stress.

SAFOD provides the unique opportunity to directly measure the state of stress acting within and adjacent to the San Andreas Fault at depth. Horizontal differential stress magnitudes measured in the SAFOD pilot hole at a distance of 1.8 km from the surface trace of the fault were found to be very high, but the orientation of maximum horizontal stress indicates low levels of shear stress resolved onto the San Andreas Fault itself. Shear-wave anisotropy measurements in the inclined portion of the SAFOD main hole crossing the fault zone, as well as fracture patterns in spot cores recovered close to the fault at depth, further indicate that the direction of maximum horizontal compression remains nearly perpendicular to the fault to within a few hundred meters of the active fault trace. In addition, heat flow measurements (to 3 km depth) in SAFOD and the SAFOD pilot hole show no evidence of frictionally-generated heat.

The concept that plate bounding faults like the San Andreas are anomalously weak faults imbedded in an otherwise strong fractured and faulted crust has fundamental implications to geodynamic processes and earthquake hazard. As the weakness of plate boundaries (relative to plate interiors) is a fundamental aspect of plate tectonics, how and why plate boundary faults lose their strength is the basis for understanding why plate boundaries form, how they evolve with time, and how deformation is partitioned along them. The profound weakness of faults at subduction zones, continental and oceanic rifts, and transform margins likely places a major constraint on the global behavior of the lithospheric plates.

The remarkable long-term weakness of plate boundary faults may also be related to the mechanical processes responsible for the occurrence of large and great earthquakes. For seismogenic faults, the low average strength may result from dynamic weakening processes, such as thermal pore-fluid pressurization, that are promoted by large slip magnitudes during earthquakes and favor continued rupture propagation. In this case the characteristics of earthquake rupture and radiated energy likely depend on a multitude of processes that are different for nucleation, transitions to dynamic weakening during propagation, rupture arrest, and interseismic strength recovery. In contrast, in aseismic (creeping) faults the low long-term strength must arise from operation of quasi-static flow processes, presumably activated by mechanical and chemical fluid-rock interactions.

The mechanics of earthquake slip on weak faults has great significance to earthquake hazard assessment and mitigation. Through improved understanding of the roles of fluid pressure, intrinsic rock friction, chemical reactions and the physical state of active fault zones in earthquake generation, it will be possible to construct more realistic numerical models of earthquakes on fault systems spanning multiple earthquake cycles. These models will also allow for improved prediction of earthquake effects and fault interactions, including stress transfer and earthquake triggering, radiated energy directivity and strong ground motion following large earthquakes, and fault segmentation and will provide a deterministic basis for seismic hazard forecasting over a range of time scales.

Drilling and downhole measurements in active fault zones, together with laboratory studies of their rheological properties and framework geophysical studies of the crust that contains them provide critical data to test hypotheses arising from seismologic observations, laboratory rock deformation experiments and geological observations of exhumed fault zones. Drilling provides the only direct means of measuring pore pressure, stress, permeability and other important parameters within and near an active fault zone at depth. It is also the only way to collect fluid and rock samples from the fault zone and wall rocks at seismogenic depths for laboratory investigations. SAFOD is providing the unique opportunity to integrate in-situ sampling, downhole measurements and long-term monitoring of an active fault zone that is so critically needed to test and refine the broad range of current theoretical models for faulting and seismogenesis.

Chester, F. M., J. S. Chester, D. L. Kirschner, S. E. Schultz, and J. P. Evans (2004) Structure of large-displacement, strike slip faults in the brittle continental crust, in Rheology and deformation of the lithosphere at continental margins, Karner, G. D., B. Taylor, N. W. Driscoll, and D. L. Kohlstedt (eds.), Columbia Univ. Press, New York

Chester, J. S., Chester, F.M., Kronenberg, A.K., Fracture surface energy of the Punchbowl fault, San Andreas system, Nature, 437, 133-135, 2005.

Continental scientific drilling, A decade of progress and challenges for the future (2007) Harms, U., C Koeberl, and M.D. Zoback, eds., Springer, Berlin, ISBN-13 978-3-540-68777-1.

Faulkner, D. C., Lewis, A. C., Rutter, E. H., On the internal structure and mechanics of large strike-slip fault zones; field observations of the Carboneras Fault in southeastern Spain, Tectonophysics. 367, 235-251. 2003.

Hickman, S. (1991), Stress in the lithosphere and the strength of active faults, U.S. Nat. Rep. Int. Union Geod. Geophys. 1987-1990. Rev. Geophys., 29, 759-775

Hickman, S., M. D. Zoback and W. L. Ellsworth (2004), Introduction to special section: Preparing for the San Andreas Fault Observatory at Depth. Geophys. Res. Letters,. 31, L12S01, doi: 10.1029/20040GL20688

Hickman, S. and M. D. Zoback (2004), Stress measurements in the SAFOD pilot hole: implications for the frictional strength of the San Andreas fault. Geophysical Research Letters, 31, L15S12

Kanamori, H. (1980), State of stress in the Earth's lithosphere, in Physics of the Earth's Interior. Soc. Italiana di Fisica, Bologna, Italy, p. 531-554

Lachenbruch, A. H., and A. McGarr (1990), Stress and heat flow, in The San Andreas Fault System, California. R. E. Wallace (ed.), pp. 261-277, U.S. Geol. Surv. Prof. Paper 1515

Mount, V. S., and J. Suppe (1992), Present-day stress orientations adjacent to active strike-slip faults: California and Sumatra. J. Geophys. Res., 97, 11995-12013

Rice, J. R. (1992), Fault stress states, pore pressure distributions, and the weakness of the San Andreas fault. Fault Mechanics and Transport Properties of Rocks, B. Evans and T.-F. Wong (eds.), pp. 475-503, Academic, San Diego, Calif

Rice, J. R. and M. Cocco, Seismic fault rheology and earthquake dynamics, in The Dynamics of Fault Zones, ed. M. R. Handy, Dahlem Workshop (Berlin, January 2005) Report 95, The MIT Press, Cambridge, MA, USA, publication expected 2006-07.

Roecker, S., C. Thurber, D.K. McPhee (2004), Joint inversion of gravity and arrival time data from Parkfield: new constraints on the structure and hypocenter locations near the SAFOD drill site, Geophys. Res. Lett., 31, DOI 10.1029/2003GL019396.

Roecker, S., C. Thurber, K. Roberts and L. Powell (2006), Refining the image of the San Andreas Fault near Parkfield, California using a finite difference travel time computation technique, Tectonophysics, 426, 189-205.

Scholz, C. H. (2006), The strength of the San Andreas Fault: a critical analysis, in Earthquakes, radiated energy and the physics of faulting, R.E. Abercrombie, A. McGarr, G. Di Toro, and H. Kanamori (eds.), Geophysical Monograph 170, Amer. Geophys, U., Washington, D.C., 301-311.

Saffer, D. M., B. A. Bekins and S. Hickman (2003), Topographically driven groundwater flow and the San Andreas heat flow paradox revisited. J. Geophys. Res 108 (B5), ETG 12-1

Sleep, N. H., and M. L. Blanpied (1994), Ductile creep and compaction: A mechanism for transiently increasing fluid pressure in mostly sealed fault zones. Pure Appl. Geophys., 143, 9-40

Townend, J. (2006), What do faults feel? Observational constraints on the stresses acting on seismogenic faults, in Earthquakes, radiated energy and the physics of faulting, R.E. Abercrombie, A. McGarr, G. Di Toro, and H. Kanamori (eds.), Geophysical Monograph 170, Amer. Geophys, U., Washington, D.C., 313-327.

Townend, J. and M. D. Zoback (2000), How faulting keeps the crust strong. Geology, 28, 399-402

Zoback, M. D. (2000), Strength of the San Andreas. Nature, 405, 31-32

Zoback, M. D. and eight others (2003), Determination of stress orientation and magnitude in deep wells. Int'l. Jour. Rock Mech., 40, 1049-1076

Funding from the NSF is gratefully acknowledged by the authors.

One-Page Essays

The following section is comprised of about 100 one-page summaries of research projects that make use of EarthScope data, or that have been carried out on an exploratory scale using similar data, using new methods that promise to dramatically increase our understanding of Earth structure and processes when applied on a continental scale. These project summaries offer a taste of EarthScope science that will be accomplished as the facility is completed, new experimental avenues are explored and advanced analytical techniques evolve.

CONVECTIVE INTERACTIONS IN THE MANTLE BENEATH THE PACIFIC NORTHWEST: THE FATE OF THE JUAN DE FUCA PLATE

Richard Allen, Mei Xue • University of California, Berkeley

Beneath the Pacific Northwest remanents of the Farallon plate continue to subduct beneath the North American continent. While the subducting slab has been imaged extending to the transition zone beneath British Columbia, previous studies suggest that the maximum imaged depth decreases to the south, reaching ~400 km beneath northern Washington, ~300km beneath southern Washington, and perhaps only ~150km beneath Oregon. To the east of the Cascadia subduction system lies the Yellowstone hotspot track. The origins of this track can be traced back to the voluminous basaltic outpourings of the Columbia River Basalts around 17 Ma. If the Columbia River Basalts are the result of a large melting anomaly rising through the mantle to the base of the North America continent, the anomaly would need to punch through the subducting Farallon slab. We image the subducting Juan de Fuca slab beneath Oregon using teleseismic body-wave travel-time tomography and the stations of the OATS deployment across Oregon, combined with data from regional seismic networks and the EarthScope Transportable Array. The 3D compressional and shear-velocity models show the high velocity slab extending to a depth of ~400km with a dip of ~50°, slightly shallower than the observed dip to the north which ranges from 60 to 65°. Resolution tests show that the dataset used would resolve the slab to greater depths if it was present in the mantle, suggesting that the slab ends abruptly at 400 km depth. GPS observations constraining global plate motion models provide an estimate of the convergence rate of the Juan de Fuca plate with respect to North America allowing us to trace the current location of the bottom edge of the imaged slab back to its location at 17 Ma when the source of the Columbia River Basalts reached the surface. We estimate that the bottom of the imaged slab would have been at the trench at 17 Ma. One explanation for the observed lower end of the slab is therefore that an upwelling responsible for the voluminous basaltic outpouring caused the Farallon slab to disintegrate around 17 Ma leaving a hole or gap in the slab at depths greater than the 400 km maximum depth extent that we observe today.

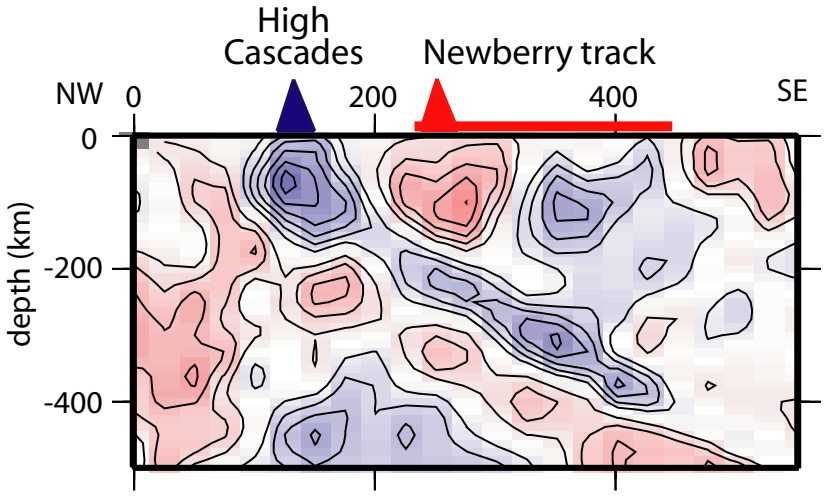

Vertical cross-section through the 3D S-velocity model beneath Oregon showing the high-velocity (blue) Juan de Fuca slab diving down into the mantle with a dip of 50°.

Waite, G.P., R.B. Smith R.M. Allen, (2006) Vp and Vs structure of the Yellowstone hot spot from teleseismic tomography: Evidence for an upper-mantle plume J. Geophys. Res. 111, B04303, doi:10.1029/2005JB003867.

Xue, M. and R.M. Allen (2006) Origin of the Newberry Hotspot Track: Evidence from shear-wave splitting. Earth Planet. Sci. Lett. 244, 315-322, doi:10.1016/j.epsl.2006.01.066.

Xue, M and R.M. Allen (2006) The Fate of the Juan de Fuca Plate. Eos Trans. AGU, 87(52), Fall Meet. Suppl., Abstract S51D-06.

This work was supported by NSF EAR-0539987.

A GROUND VELOCITY MAP FOR THE BASIN AND RANGE BASED ON INSAR

Falk Amelung, Noel Gourmelen • University of Miami

The Basin and Range Province in the western U.S. accommodates 25% of the relative plate motion between the North American and the Pacific plates. The accumulated deformation is occasionally released in earthquakes with magnitude larger than 7, which are among the largest earthquakes on the North American continent. The major unresolved science issue is where active deformation is occurring and what driving mechanisms are responsible for this deformation. Space geodetic measurements based on GPS indicate that only the Western Basin and Range is under active deformation and that the remainder behaves as a rigid plate. This finding is consistent with the location of historic earthquakes. Between 1916 and 1954, a sequence of six earthquakes with magnitude larger than 7 occurred in the Central Nevada Seismic Belt. As part of the National Science Foundation`s EarthScope project, UNAVCO is installing a network of ~100 new continuous GPS stations in the Basin and Range to better quantify tectonic deformation in this region. These GPS stations are part of the EarthScope Plate Boundary Observatory, PBO. The project includes the acquisition of a space geodetic dataset to optimally address important issues about Basin and Range geodynamics. UNAVCO is in the process of acquiring several thousand scenes from the European Space Agency`s ENVISAT and ERS satellite missions to complement the GPS measurements using synthetic aperture radar (SAR) interferometry.

This project is funded by the National Science Foundation and supported by UNAVCO as part of GeoEarthScope.

PROPOSED SAR ACQUISITION ACROSS THE BASIN & RANGE

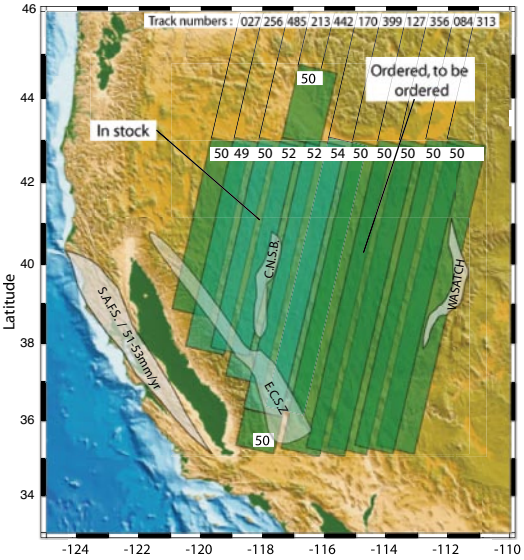

Acquisition plan for the Basin&Range. ~6000 SAR data from the satellites ERS1&2 are archived at the European Space Agency for the period 1992-2002. This is unique opportunnity to produce a large scale InSAR deformation map of the Basin&Range and help the PBO site selection process. In between WINSAR and our effort, more than 2000 SAR data have already been acquired and are being processed (see side figures). The SAR data coverage encompasses the Eastern California Shear Zone, the Walker lane, the Central Nevada Seismic belt and the Wasatch actively deforming areas of the Basin&Range. We also discovered a intensive surface deformation related to mining activities that can potentially affect the permanent GPS sites installed or in the process of being installed by PBO.

CENTRAL NEVADA SEISMIC BELT DEFORMATION

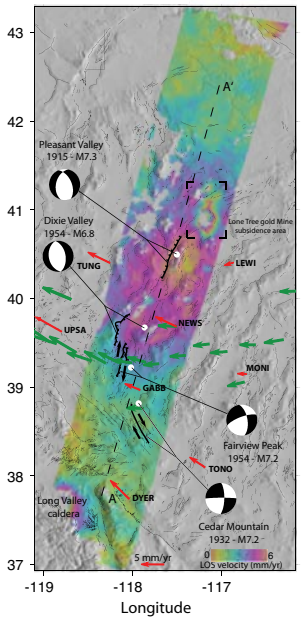

1992-2000 LOS velocity map for the area of the 1915-1954 Nevada earthquakes together with epicenter (blank circles), focal mechanisms (spheres), and surface ruptures. Green arrows, campaign GPS velocities (7); red arrows, BARGEN permanent GPS velocities and site names (9). Gourmelen&Amelung, Science, 2005

SUBSIDENCE AND PBO GPS SITES SELECTION

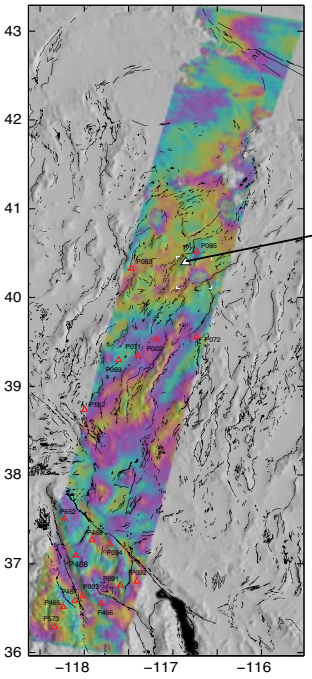

TIME SERIES OF DEFORMATION

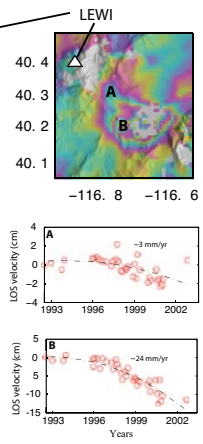

Single interferogram for the PBO site selection process. The planned PBO GPS sites (red triangles) are susceptible to suffer from anthropogenic activities (mining, agricultural land). We processed a consequent number of interferograms through Nevada and reported man made related subsidence that could possibly affect PBO GPS sites. The right column shows a time series for one of the subsidence area (Crescent Valley) which might reach the permanent BARGEN site LEWI.

EXPLORING THE SEISMIC WAVEFIELD WITH THE TRANSPORTABLE ARRAY

Charles Ammon • Pennsylvania State University

The uniqueness of USArray's large aperture, broadband Transportable Array (TA) has a number obvious characteristics for mapping details in lithospheric structure across the country, and for focused studies of a number of select deep earth structures. The TA also affords new opportunities to view a much more complete sample of the seismic wavefield from local and distant earthquakes. The simpler aspects of the wavefield can be used in education, to illuminate such fundamental wave-propagation concepts as directionality and phase velocity and to provide dynamic animations of seismic waves traveling across large tracts of the continent [Ammon, 2007]. For the more complex parts of the wavefield, the TA offers insight into the interaction of seismic waves with Earth's heterogeneity. The vertical component of the S wave in this distance range includes complicated interactions of the free-surface S-to-P wave conversions that reverberate post-critically off the crust-mantle transition (the incident S-wave phase velocity is approximately 8 km/s) [e.g. Langston and Baag, 1985; Zandt and Randall, 1985]. For this particular event, embedded within the vertical component S-wave coda is a less coherent wave that appears to propagate from west to east with a phase velocity of approximately 3.5 km/s. Whether the wave is related to trapped post-critical S-wave energy, interaction with the Gorda Slab, or S-to-Rayleigh wave scattering near the ocean-continent transition remains unknown at present. But the off-azimuth observation may partly explain the difficulty that seismologists have had modeling these complicated part of the seismic wavefield. As the large-aperture, densely sampled TA records additional seismic wavefields, we will gain the insight needed to begin modeling the rich complexity of these observations and tp begin extracting the information contained in these nearly-uniformly sampled seismic ground motions from the TA.

Ammon, C. J., (2007) TA Seismic Wavefield Animations - PSU, http://eqseis.geosc.psu.edu/~cammon/QA/ .
Langston, C. A., and C.-E. Baag (1985), The validity of ray theory approximations for the computation of teleseismic SV waves, Bull. Seismol. Soc. Am., 75, 1719-1727.
Zandt, G., and G. E. Randall (1985), Observations of shear-coupled P-waves, Geophys. Res. Letters, 12, 565-568.

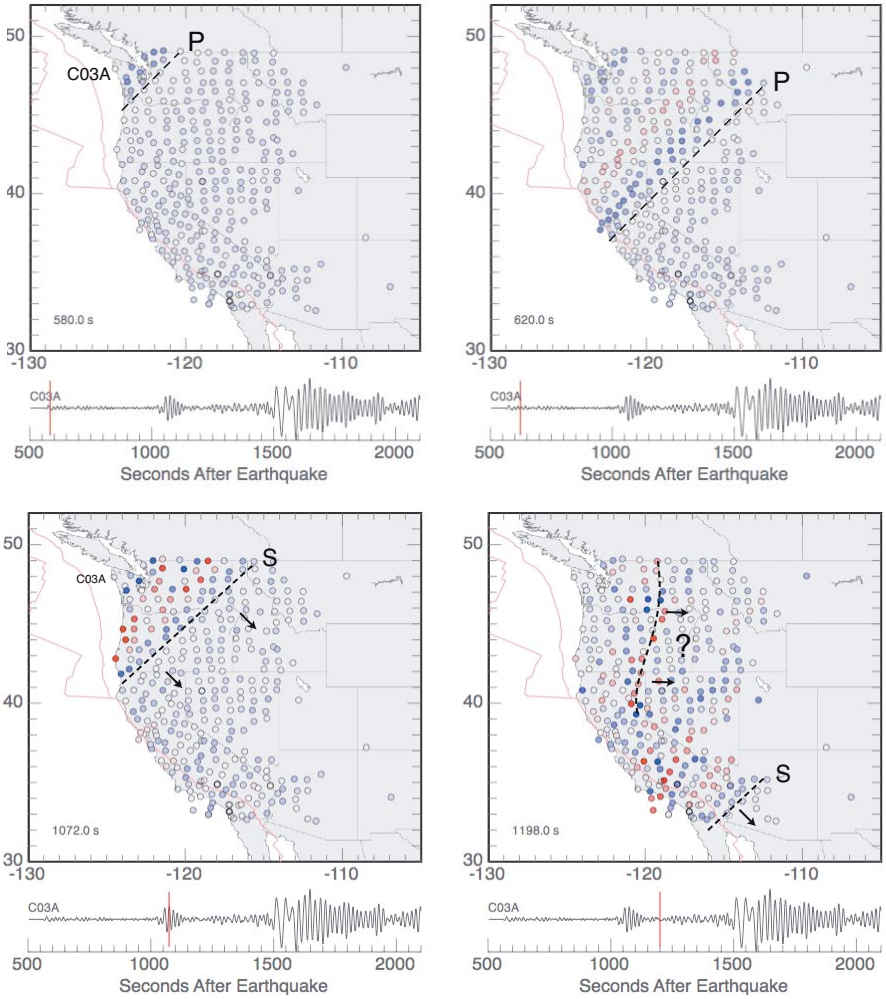

Above: P-wave propagation across EarthScope's Transportable Array. Stations are represented by circles and the color of the circle (red for positive, blue for negative) indicates the ground motion amplitude at a particular time slice. Each image shows the gain-equalized filtered (15-300s period) vertical velocity seismogram amplitude at a particular time following the 13 January, 2007 Kuril Islands earthquake. Seismogram at the bottom shows the velocity seismogram for the closest station (C03A). Dashed lines show the P-wave front at each time which can be used to illustrate the concept of wave phase velocity.

Left: Snapshots of vertical-component S wave and S-wave coda propagation across the western United States. Dashed lines show the wave fronts at two times around the S-arrival. The S wave propagates across the array as a mostly planar front. An unusual, complicated wave in the S-wave coda appears to propagate from west to east with a phase velocity of approximately 3.5 km/s.

ISOLATING SMALL, DISTANT SEISMIC EVENT SIGNALS WITH THE TRANSPORTABLE ARRAY

Charles Ammon • Pennsylvania State University
Thorne Lay • University of California, Santa Cruz

We used the EarthScope-USArray Transportable Array (TA) seismic stations to isolate the P-waveform from the 09 October, 2006 North Korean nuclear test [Ammon and Lay, 2007]. Seismic signals from the explosion were well recorded on regional stations in northeast Asia and on a network of seismic arrays operated around the globe for the detecting explosion sources. Although the design of the TA is optimized for probing the lithospheric structure of North America and seismic events within or near the array, the large number of stations and the broad array aperture and high-quality of the seismic installations allows application of the facility to the study of small, distant seismic events. Our example demonstrates the TA's small event detection capabilities – extracting nanometer-level signals from the distant explosion (USGS mb ~ 4.2). We observed the signal in the 1-4 Hz signal band directly on about 45 seismic stations located over a broad region of the array, but commonly inland, away from the seismically noisy coast. To include more stations in the array stacking procedure we used station delays from a deep, but nearby earthquake that occurred beneath the Japan (East) Sea, about one month earlier than the nuclear test. We measured the time shifts from the impulsive deeper event and shifted the TA signals from the North Korean explosion by the same time (these delays account for near-station earth structure and station elevation differences). The resulting stack is quite clean with a sub-nanometer noise level. Using more accurate shifts can increase the extracted signal coherency. Using 35 of the cleanest stations that can be aligned by picking the largest positive peak amplitude produces a more coherent signal alignment and isolation. The peak signal amplitude is on the order of 1-2 nanometers (consistent with the event magnitude and distance). The ability to extract nanometer-level signals from teleseismic distances opens the possibility to use the TA to detect and to study events originating in the coda of large events, or earthquakes in remote regions, such as oceanic transforms and intermediate- and deep events in subducting slabs. Teleseismic body waves, in particular, that change relatively slowly over the large aperture of the TA allow extraction of the slowly-varying teleseismic body-wave signals – including the separation of direct waves P and S from reflected waves such as PcP, ScS, which could allow one to use distant events to study the onset characteristics of large earthquakes.

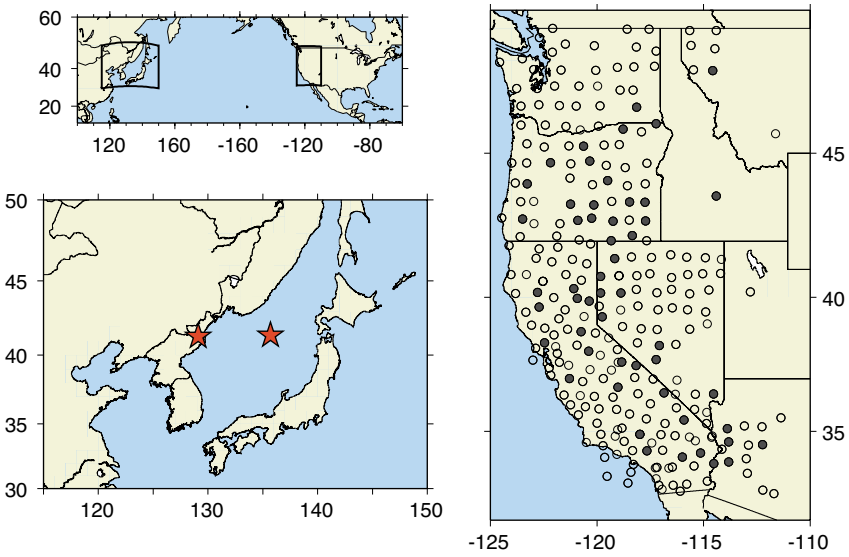

(Upper left) Event and station map locations. (Lower left) Locations of the North Korean nuclear test and a deep event beneath the Sea of Japan (East Sea). (Right) Locations of unavailable TA station signals (light gray circles), stations with usable, but low signal-to-noise records (dark unfilled circles), and stations with clear P wave arrivals for the North Korean test (filled circles).

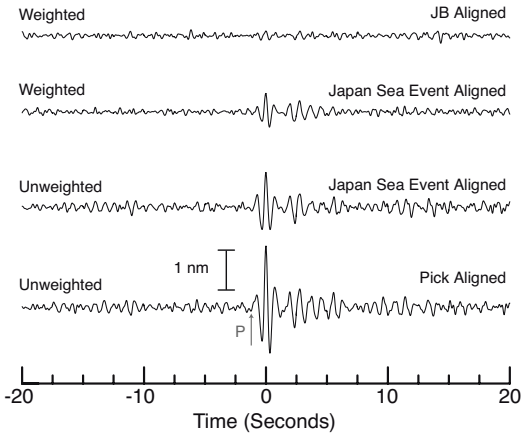

Linear stacks of P wave signals from TA stations for the North Korean event. All stacks are shown on the same amplitude scale – the weighted averages are scaled by the sum of the weights to produce displacements. The top trace is a stack of 172 signals aligned with only a standard travel time reference before averaging; the second trace from the top is the stack of the same 172 signals time-shifted using stations delays from the Sea of Japan event; the third stack is a stack of applying the Sea-of-Japan-event time corrections on the 36 high-quality signals in Figure 2; the bottom trace is a stack of the same 36 signals aligned by picking the peak arrival time directly. The top two stacks were computed using signal weights equal to the inverse of the signal's RMS amplitude; the lower two stacks were constructed using observed ground displacements. The first, emergent upward polarity, indicated by the arrow labeled P, is the compressional first arrival.

Ammon, C. J. and T. Lay (2007), EOS, Trans. Am. Geophys. Union,. 88, 37-38.

This work was supported in part by the U.S. National Science Foundation under grants EAR-0125595 and EAR-0453884 (TL) and the U.S. Geological Survey under award number 05HQGR0174 (CJA). The maps were generated using GMT package and we also used SAC2000 (Lawrence Livermore National Laboratory) and Robert B. Herrmann's GSAC seismogram analysis tool.

USING USARRAY DATA TO TOMOGRAPHICALLY IMAGE THE UPPER MANTLE

Heather Bedle, Suzan van der Lee • Northwestern University

The overall 3-D structure of the upper mantle beneath the Western United States can be inferred from S and Rayleigh wave trains from regional earthquakes. USArray's Transportable Array (TA) stations provide a wealth of such wave train data. In this study we have included some of the very first TA data that is now available in our tomographic imaging efforts. And we find that the addition of these TA data to the more traditional North American data set has significant effects on the resolution with which we can image the upper mantle structure. We perform resolution tests to determine how well synthetic velocity structures can be retrieved with TA versus the more traditional raypath coverage, similar to that which existed before the deployment of TA stations. The figure shows that while our traditional imaging tends to underestimate the strength of velocity anomalies, the inclusion of data from USArray seismic stations greatly improves the tomographic model's resolution and associated estimates of anomaly strength in the Western US. The TA data not only allow us to image smaller features, but also allow us to better image deeper structure, such as seismic anomalies in the transition zone. One of our preliminary tomographic models shows that the lithosphere in the western United States has a near-negligible presence in the mantle, which is dominated by very low velocities. The model implies that the top 100 km of the mantle is at least ~360 m/s slower than the reference 4.5 km/s. These extremely low velocities, which characterize much of the western US, extend beneath Mexico and the Gulf of California. Our model also shows outlines of high-velocity anomalies in the transition zone, which have previously been interpreted as subducted trailing fragments of the Farallon Plate [Van der Lee and Nolet, 1997], and are now coming into clearer view, thanks to USArray data. It appears as if the transition zone is heterogeneously populated with such fragments of subducted lithosphere but still more USArray data are necessary to outline individual fragments. Such data would also help us image details in and below the low-velocity zone, which could help its interpretation in terms of a temperature and composition.

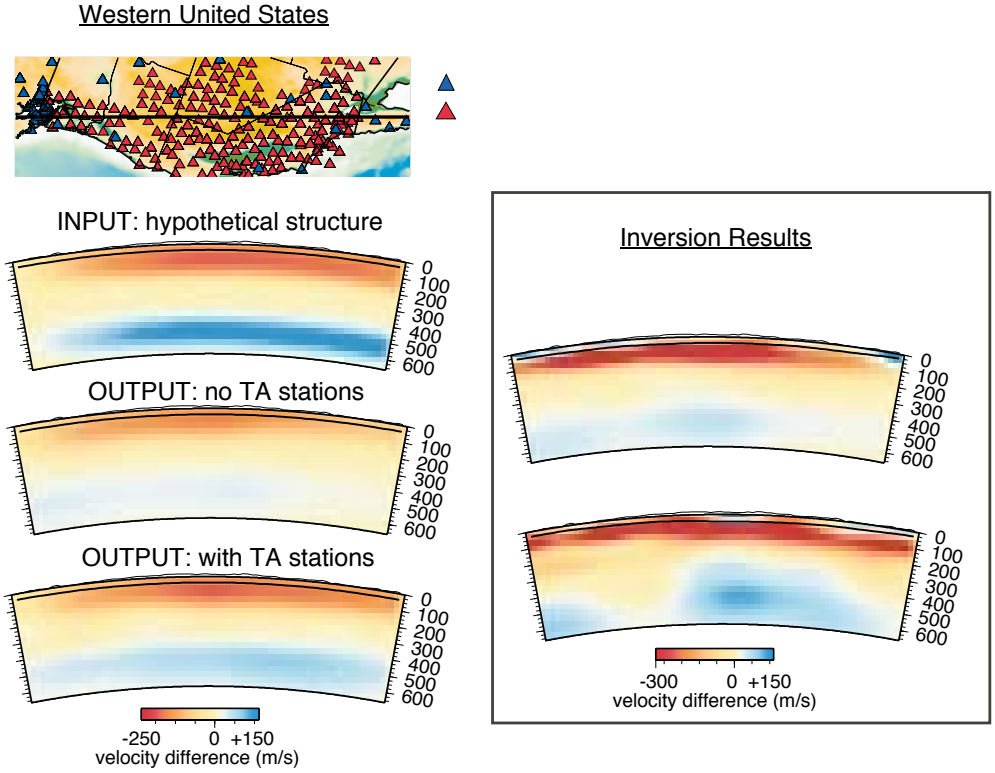

Tomographic results demonstrating the improvement in the resolution of S-velocity structure with the addition of USArray's Transportable Array. Shown are map views of the western US area transected. The input shows the hypothetical synthetic velocity structure, which was inverted for, while the output shows how well the input structure would be resolved in the case of i) that no Transportable Array seismic stations were included, and ii) Transportable Array stations were included. Also shown are the actual inversion results for velocity structure for the same profile.

Van der Lee, S. and G. Nolet, (1997), Seismic image of the subducted trailing fragments of the Farallon plate, Nature, 386, 266–269

We are grateful to NSF for supporting this work under award EAR-0346200.

UPPER MANTLE SEISMIC VELOCITY STRUCTURE IN THE GREAT BASIN

Caroline Beghein, Matthew Fouch • Arizona State University
Arthur Snoke • Virginia Polytechnic Institute and State University

The relationship between lithospheric and asthenospheric processes is still poorly understood in the western United States, and fundamental questions remain concerning the influence of a subducting slab on the dynamics of upper mantle flow. Imaging upper mantle structure, detecting the presence of seismic anisotropy, and how it varies with depth in the mantle are key elements to answer these questions. We determine seismic velocity variations in the upper mantle beneath the Great Basin to improve our understanding of the interactions between lithosphere and asthenosphere. In this study, we utilize surface wave dispersion data to image the upper mantle because of their good vertical sensitivity to bulk Earth structure. We employ a traditional two-station method [e.g., Larson et al., 2006] to generate Rayleigh wave dispersion curves between 20 and 170s using USArray seismic stations. The large number of broadband seismic stations from USArray enables excellent lateral and good azimuthal coverage of the region.

We apply the Neighborhood Algorithm (NA) forward modeling approach to the measured dispersion curves in order to model shear-wave velocities in the upper mantle. This approach allows us to determine quantitative model uncertainties and parameter trade-offs, which are essential to interpret seismological results, and it enables us to include a priori constraints such as the Moho depth based on independent estimates from receiver functions. Three events produced high quality Rayleigh wave dispersion curves for about 70 station pairs with interstation distances between 200 and 400km. For each event, the phase velocity dispersion curves were first combined into an average dispersion curve and a standard deviation was calculated. The dispersion curves obtained for paths aligned in the N-S and NW-SE directions are very similar and they differ from the data corresponding to SW-NE paths. We applied the NA to each average dispersion curve to obtain three shear-wave velocity profiles across the Great Basin. In our initial work, we choose a layered parameterization, including one layer in the crust and five layers below the Moho. We allow variations in the Moho depth and in shear-wave velocities within fixed boundaries. Our forward models show an increase in Vs in the crust compared to model TNA [Grand and Helmberger, 1984] for all three averaged datasets. Between 60 and 100km, we do not find any change in Vs with respect to model TNA. At greater depths, the results change with the azimuth. A well-resolved reduction in Vs (about 0.2km/s) with respect to model TNA is found between 60 and 100km depth for the NW-SE and N-S paths but not for SW-NE paths, which can be explained by model TNA at those depths. At larger depths (100-150km) SW-NE profiles clearly display shear-wave velocities lower than in model TNA by about 0.5km/s. The seismic wave velocities are less well constrained at those depths for other azimuths. Our results are consistent with a shear-wave velocity profile containing a small velocity jump across the Moho. Our models can be explained by the presence of a thin lithosphere down to about 60km with no well-defined azimuthal anisotropy, and an azimuthally anisotropic upper asthenosphere with a fast SW-NE direction between 60 and 100km depth. At this stage, we cannot rule out the presence of lateral heterogeneities to explain this azimuthal dependence, but the existence of azimuthal anisotropy is consistent with recent results from shear-wave splitting analyses for the northern part of the Great Basin [West and Fouch, in prep., 2007].

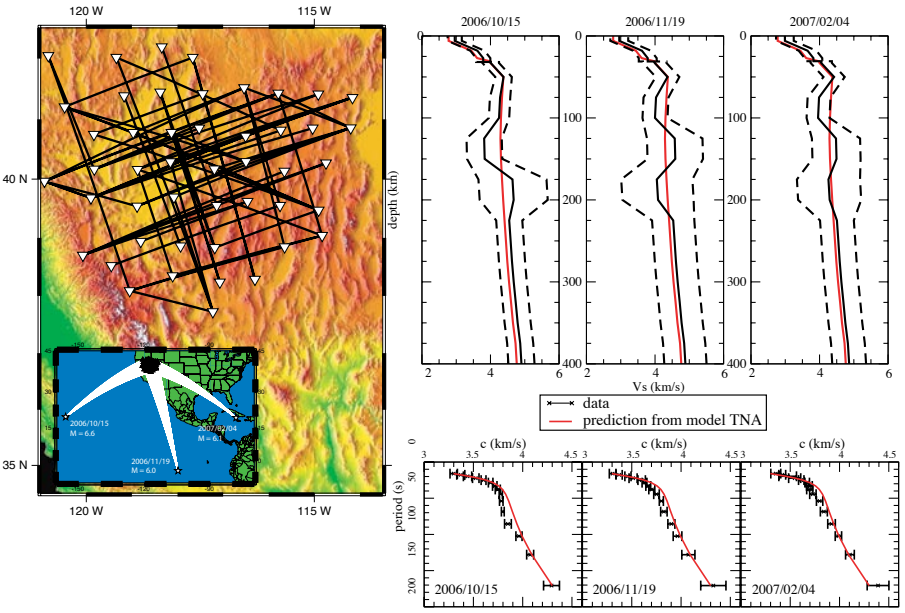

Results of interstation surface wave dispersion analyses for shear wave velocity structure across the Great Basin. [Top left panel] Interstation raypaths for selected stations in this study. All data come from USArray Transportable Array stations. Inset shows raypaths from three example events from different backazimuths. [Bottom right panel] Rayleigh wave phase velocity dispersion curves for selected events. Black lines denote phase velocities and associated errors for measured period ranges. Red line shows predicted disperson curve for TNA velocity model (see text). [Top right panel] Ranges of acceptable models determined by NA analysis for each event dispersion curve. Resolution for these models is best in the uppermost 100 km of the model. Results show azimuthal variations with reduced velocities for event backazimuths from the SSE and ESE, consistent with azimuthal anisotropy results from shear wave splitting analyses for this region.

This work has been supported by NSF-EarthScope CAREER grant EAR-0548288 [MJF].

THE EPISODIC TREMOR AND SLIP 2005 (ETS05) GPS CAMPAIGN, CASCADIA SUBDUCTION ZONE

R.A. Bennett • University of Arizona
S. Thompson, S. Hreinsdóttir, D. Johnson • Washington and Univ. Puget Sound

We deployed 29 GPS units to capture the 2005 Cascadia Episodic Tremor and Slip (ETS05) event. This experiment represents the first large-scale EarthScope-supported campaign GPS system deployment. The project was conducted with extensive UNAVCO facility and PBO field- and archiving-support. The 29 Topcon GB1000-based systems, designed to be entirely self-supported, were configured in semi- permanent mode on temporary monuments, designed to comply with Olympic National Park requirements. The systems and data were retrieved in October with support from UNAVCO. We are in the process of installing permanent markers that can be used for annual semi-continuous measurement. Four of these have been built as of July 2006, and several additional sites have been permitted as of September 2006. The ETS05 experiment was a success; data retrieval rate was near 90% and time series from this network clearly record transient displacements associate with the slow slip event. Results from station 0L28 at Hurricane Ridge are shown below on the right as an example.

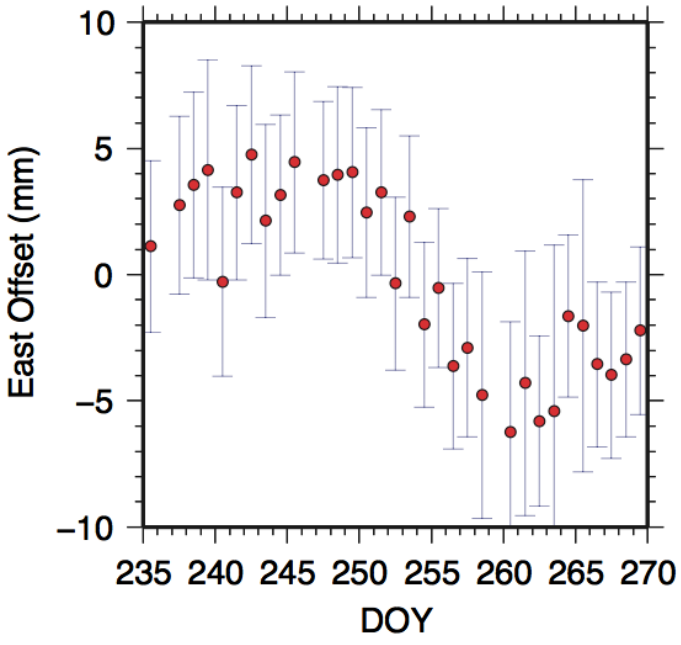

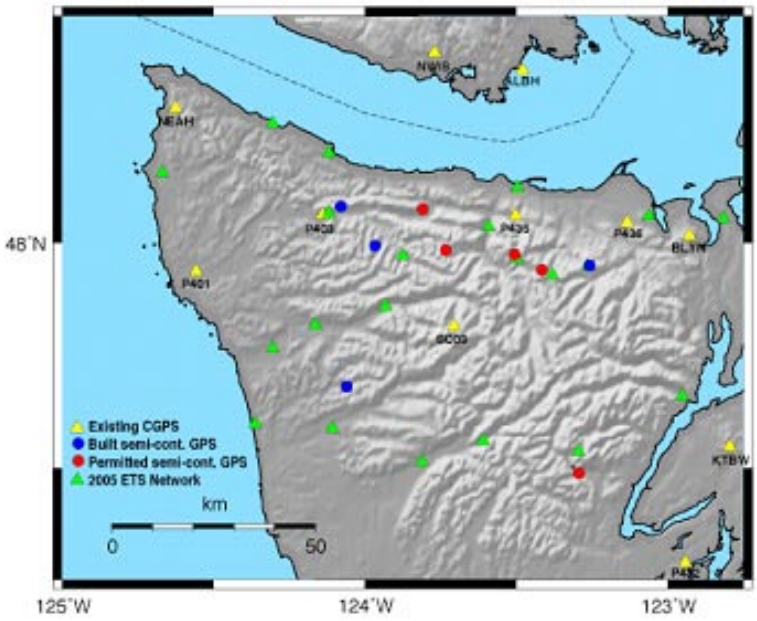

BROAD-BAND AMBIENT NOISE SURFACE WAVE TOMOGRAPHY ACROSS NORTH AMERICA USING EARTHSCOPE/USARRAY DATA

Gregory Bensen, Michael Ritzwoller • University of Colorado at Boulder
Nikolai Shapiro • Laboratoire de Sismologie, CNRS, Paris, France

We have extended ambient noise tomography from periods of 8 to 100 sec on the scale of the continental United States. Cross-correlations were computed from up to two years of continuous ambient noise data recorded at nearly 200 permanent and temporary stations. Many of these stations are part of USArray, including stations from the Transportable Array and the ANSS backbone. The data set contains about 9,000 acceptable group and phase velocity measurements at any given period. The resulting dispersion maps provide new information about crustal and mantle structures underlying the continental United States. The data processing method has undergone extensive development and now provides reliable empirical Green functions in a variety of geologial settings for a broad range of periods [Bensen et al., 2007a]. The resulting paths on which the measurements are obtained are entirely contained within the continent. The repeatability of the measurements provides a natural method to assess errors. Measurements of Rayleigh wave group and phase speed curves are input into a inversion for the 2D tomographic maps at particular periods [Bensen et al., 2007b]. These dispersion maps possess sensitivity to characteristic depths depending on period, wave type and measurement type (Rayleigh/Love, group/phase). The spread of depth sensitivities makes direct interpretation difficult, but maps provide a useful intermediate step prior to inversion for the 3D shear velocities distribution that causes them. The Rayleigh wave group and phase speed maps from 8 to 100 seconds period correlate well with various types of geological features at depths less than 10 km to over 150 km. On the 12 sec map, sedimentary basins are evident as prominent low velocity anomalies. Presently, Love wave Green functions are being estimated and analyzed to develop similar group and phase speed maps. These four curves (Rayleigh wave group and phase speed, Love wave group and phase speed) form the basis for a joint inversion for the 3D shear velocity structure of the crust and uppermost mantle. Additionally, work is underway to understand the background noise distribution and level both to constrain the source of ambient noise and to assess how the distribution may affect the ambient noise measurements.

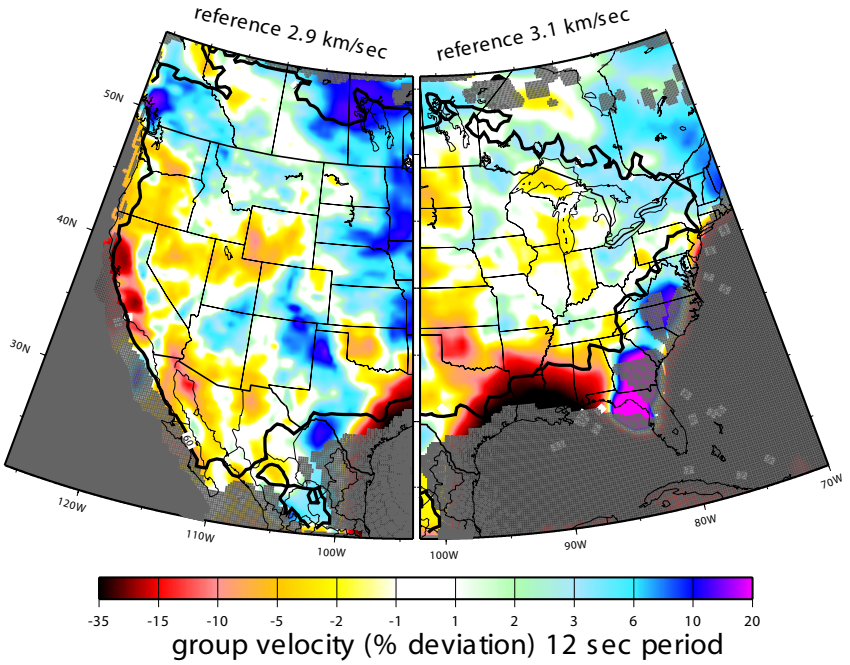

The figure shows the 12 second Rayleigh wave group speed map developed from ambient noise tomography using EarthScope USArray data and other data obtained primarily from the IRIS DMS. The black contour encloses the region with spatial resolution of 120 km or better. Regions with resolution worse than 400 km are shaded grey. At this period, low velocity anomalies coincide with thick sediments or high crustal heat flow.

Bensen, G.D., M.H. Ritzwoller, M.P. Barmin, A.L. Levshin, F. Lin, M.P. Moschetti, N.M. Shapiro, and Y. Yang, Processing seismic ambient noise data to obtain reliable broad-band surface wave dispersion measurements, Geophys. J. Int., in press, 2007a.

Bensen, G D, McCoy, C, Ritzwoller, M H, Levshin, A L, Barmin, M P, Shapiro, N M. (2006), Rayleigh wave tomography using ambient noise cross-correlations: long period applications in the United States., manuscript in preparation, 2007b.

The data used in this research were downloaded from the IRIS Data Management Center (DMC) and the Canadian National Data Center (CNDC). This research was supported by the US Department of Energy, DE-FC52-2005NA26607, and two grants from the US National Science Foundation, EAR-0450082 and EAR-0408228 (GEON project support for Bensen).

FUNDAMENTAL STUDIES OF EARTHQUAKE AND STRUCTURE PROPERTIES BASED ON DATA ASSOCIATED WITH THE SAFOD FACILITY

Yehuda Ben-Zion • University of Southern California

The data recorded in and around the SAFOD facility provide fundamental opportunities for clarifying key aspects of earthquake and fault properties that can not be resolved with standard data. Key earthquake studies include derivation of source properties from P and S records containing very high frequencies, examination of potential scaling between various signals in the early waveforms and final event size, reliable estimates of the energy partition during earthquakes between seismic radiation and dissipative mechanisms, and reliable analysis of slip histories of seismic events. Key structure studies involve reliable imaging of the internal architecture of the San Andreas fault zone with signals indicative of material discontinuity interfaces and damaged rocks. These include scattering, anisotropy, non-linearity, and guided head and trapped waves. Systematic analysis of such signals in several large fault zones, based on standard surface data, suggest that trapped S waves are generated typically by ~100 m wide layers that extend only to ~3-4 km depth and are characterized by 30-50% velocity reduction and strong attenuation [e.g., Ben-Zion et al., 2003]. The trapping structures appear to be surrounded by broader anisotropic and scattering zones limited primarily also to the shallow crust. Results associated with anisotropy and scattering around the North Anatolian fault using repeating earthquake clusters do not show precursory temporal evolution [Peng and Ben-Zion, 2005, 2006]. The anisotropy results show small co-seismic changes, while the scattering results show larger co-seismic changes and post-seismic logarithmic recovery. The temporal changes probably reflect evolution of properties in the top few hundred m of the crust. Systematic analyses of head waves along several sections of the San Andreas fault reveal material interfaces that extend to the bottom of the seismogenic zone [e.g. Lewis et al., 2007]. Joint arrival time inversions of direct and fault zone head waves imply velocity contrasts of 20% or more in the top 3 km and lower contrasts of 5-15% in the deeper section. In several places, analyses of trapped and head waves indicate that the shallow damaged layers are asymmetric across the fault. The observed damage asymmetry may reflect preferred propagation direction of earthquake ruptures. These, and almost all the available results on earthquake source properties, provide blurred versions of the true structures and processes. Data recorded in and around the SAFOD borehole will lead to results that reflect better the true earthquake and structure properties.

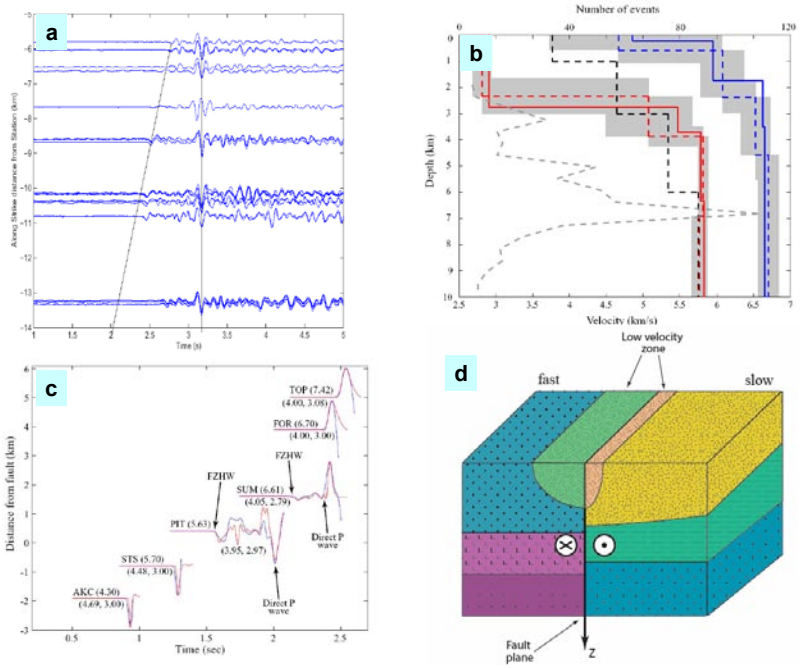

(a) Vertical component P waveforms at NCSN station BHR northeast of the SAF south of Hollister with direct body wave (vertical line) and first arriving fault zone head wave (diagonal line). (b) Inversion results of P wave velocity contrast across the SAF versus depth from arrival times of head and direct waves. The solid red and blue lines are the best-fitting velocity profiles for the slow and fast sides of the fault, respectively, out of 10 inversion runs. The dashed red and blue lines are the average depth and velocity of each layer from the 10 inversions, and the grey shaded area around the mean represent the standard deviation of the depth and velocity of that layer. The dashed black line is the initial velocity and depth model used in the inversion. The dashed gray line and horizontal axis on top give the number of events as a function of depth. (c) Example of synthetic waveform fits (red) for observed seismograms (blue) for stations on the fast and slow sides of the SAF. Some of the direct P and head wave arrivals are indicated by arrows with corresponding labels. The average P wave velocities in km/s of the crustal block used to generate the synthetic seismograms are given in parenthesis under the waveforms. (d) A schematic diagram of the inferred velocity structure of the SAF south of Hollister, consisting of two layered quarter-spaces, joined along a sharp material interface, and a shallow asymmetric low velocity zone around the fault. See Lewis et al. (2007) for details.

Ben-Zion, Y., Z. Peng, D. Okaya, L. Seeber, J. G. Armbruster, N. Ozer, A. J. Michael, S. Baris and M. Aktar, A shallow fault zone structure illuminated by trapped waves in the Karadere-Duzce branch of the North Anatolian Fault, western Turkey, Geophys. J. Int., 152, 699-717, 2003.

Lewis, M.A, Y. Ben-Zion and J. McGuire, Imaging the deep structure of the San Andreas Fault south of Hollister with joint analysis of fault-zone head and direct P arrivals, Geophys. J. Int., in press, 2007.

Peng, Z. and Y. Ben-Zion, Spatio-temporal variations of crustal anisotropy from similar events in aftershocks of the 1999 M7.4 Izmit and M7.1 Düzce, Turkey, earthquake sequences, Geophys. J. Int., 160(3), 1027-1043, doi: 10.1111/j.1365-246X.2005.0256

Peng, Z. and Y. Ben-Zion, Temporal changes of shallow seismic velocity around the Karadere-Duzce branch of the north Anatolian fault and strong ground motion, Pure Appl. Geophys., 163, 567-600, DOI 10.1007/s00024-005-0034-6, 2006.

The discussed studies were supported by the NSF, USGS and SCEC. The results were obtained in collaboration with Zhigang Peng, Michael Lewis, Jeff McGuire and others. The employed data were recorded by Nano Seeber, John Armbruster, Frank Vernon, Cliff Thurber and others.

THE EARTHQUAKE ENERGY BALANCE

Gregory Beroza • Stanford University

When a fault starts to slip, slowly accumulated strain energy is suddenly converted to different forms. The fracture energy, Ec, is the component needed to initiate shear failure. As slip continues, frictional energy, Ef, is dissipated in the form of heat. The seismic energy, Es, is the component radiated in the form of seismic waves. This radiated energy is broadband, with most of it radiated above the earthquake "corner" frequency, which makes it difficult to measure. An earthquake energy balance can be expressed using a simple equality involving the change in potential energy, ΔEp, and the other energy terms:

$$Es + \Delta Ep + Ec + Ef = 0$$

Constraints on the energy balance may come from magnitude dependence of the Es. In particular, if the fracture energy is only an important part of the energy budget for small earthquakes, then larger earthquakes should radiate waves more efficiently.

There is a lot of scatter in the measurements, but representative values of Es/M0, suggest a representative value of ~ 5×10^{-5} for many earthquakes. Some studies find Es/M0 increases with earthquake size [Kanamori and Heaton, 2000], while others suggest it does not [Ide and Beroza, 2001]. Thus, whether Es/M0 scales with earthquake size is a remains an important open question.

Es/M0 vs. M0 from various studies [Ide and Beroza, 2001]. Open symbols show original measurements. filled symbols show values once seismic energy possibly missing due to limited bandwidth is restored. Gray triangles show areas where earthquakes are excluded from two studies due to limited bandwidth. No clear break in scaling is apparent.

Two elements of the Earthscope project, the PBO borehole seismometers and SAFOD, have the potential to help resolve this debate. Borehole observations of earthquakes yield measurements of small earthquake processes that are relatively uncontaminated by propagation effects [Abercrombie, 1995]. Even borehole recordings can be affected by unmodeled propagation effects [Ide et al., 2003], but the SAFOD project, by making observations in the extremely near field of micro-earthquakes, will allow seismic energy measurements that are free from the propagation effects that cloud compilations such as those shown in the figure above. Moreover, direct measurements of temperature, pore pressure, and strain will help constrain the different components that control the earthquake energy balance.

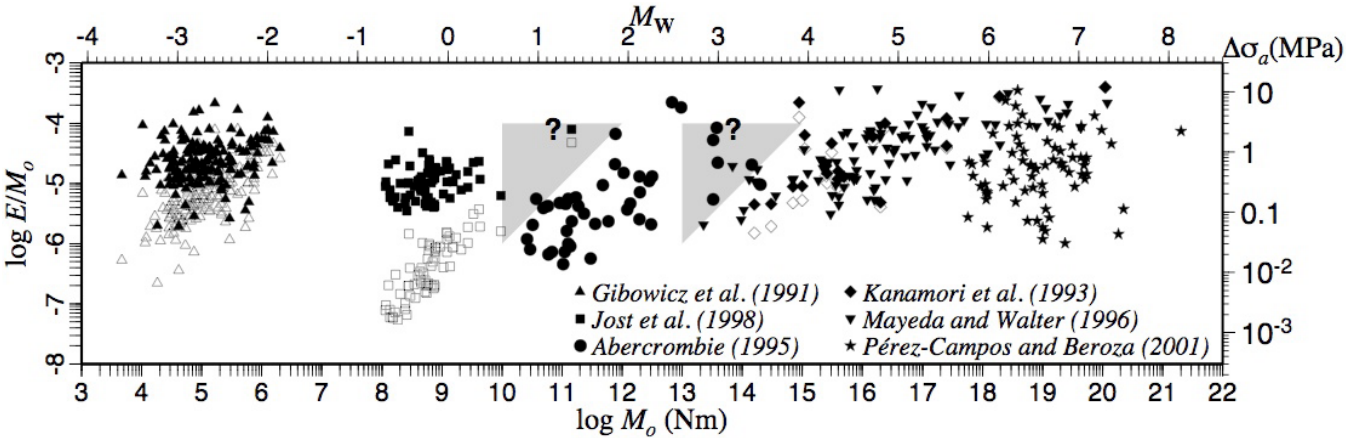

Es/M0 vs. M0 from various studies (Ide and Beroza, 2001). Open symbols show original measurements. filled symbols show values once seismic energy possibly missing due to limited bandwidth is restored. Gray triangles show areas where earthquakes are excluded from two studies due to limited bandwidth. No clear break in scaling is apparent.

Abercrombie, R. E., Earthquake source scaling relationships from -1 to 5 ML, using seismograms recorded at 2.5 km depth, J. Geophys. Res., 100, 24015-24036, 1995.

Ide, S., and G. C. Beroza, Does apparent stress vary with earthquake size? Geophys. Res. Lett., 28, 3349-3352.

Ide, S., G. C. Beroza, S. G. Prejean, and W. L. Ellsworth, Apparent break in earthquake scaling due to path and site effects in deep borehole recordings, J. Geophys. Res., 108, 10.1029/2001JB001617, 2003.

Kanamori, H., and T. H. Heaton, Microscopic and macroscopic physics of earthquakes, Geophyiscs and the Complexity of Earthquakes, Geophysical Monograph 120, American Geophysical Union, 147-163, 2000.

This research was supported by NSF grant EAR-0208499.

HIGH RESOLUTION MAPPING OF THE SOUTHERN SAN ANDREAS FAULT SYSTEM USING AIRBOURNE LASER SWATH MAPPING

Mike Bevis • Ohio State University
Ken Hudnut • U.S. Geological Survey

NCALM and UNAVCO supported the NSF-funded B4 project led by Ohio State University and the USGS. This project used Airborne Laser Swath Mapping (ALSM), also known as LIDAR, to produce very high resolution digital elevation models (DEMs) of the near-field of the southern and central San Andreas fault system, including the San Jacinto fault. B4's laser point clouds can support DEMs with a horizontal resolution of 0.25-0.5 meters, and provide vertical accuracy approaching 10 cm. The total length of the faults imaged by B4 exceeds 1,200 km. This survey differed from previous ALSM surveys by using far more GPS control on the ground, in order to understand and mitigate the height errors associated with GPS positioning of the aircraft. UNAVCO fielded 15 GPS systems and an engineer to make this 'GPS Heavy' approach possible.

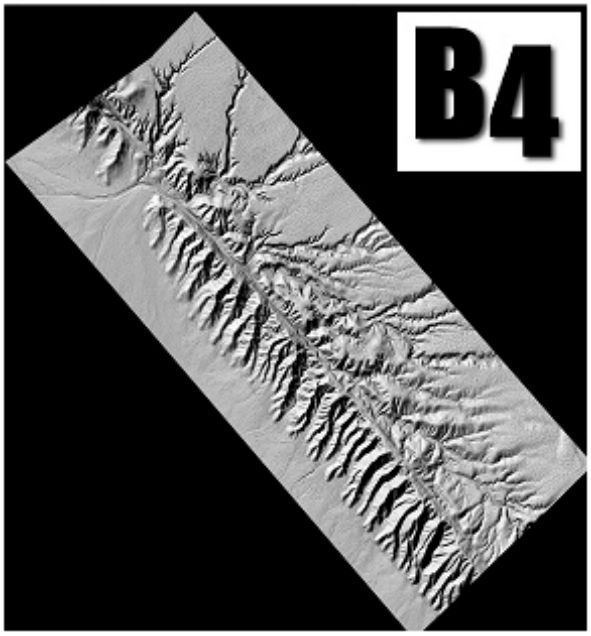

The primary motivation of the B4 project was to image the fault before the next 'Big One' occurs (hence 'B4'), so that by performing a second survey immediately following a great earthquake, it will be possible to capture the near-field deformation with unprecedented accuracy and thereby help resolve several long standing problems in earthquake source physics. The secondary motivation was to support a wide range of applications (in structural geology, geomorphology, paleoseismology, etc.) that require only the present day morphology, but captured with very high resolution. Accordingly, the B4 project has an open data policy, and is structured as an 'open collaboration.' For example, the LIDAR point clouds and customized DEMs are being distributed by the GEON web portal at Arizona State University, and DEMs are also being made available in a Google Earth and Fledermaus formats by Scripps Institute of Oceanography. As of 2/2007, B4 data are being used by at least one dozen university research groups, and by the USGS, as well as by professional geologists involved in fault zone mapping to ensure safe development of housing tracts along these faults, as regulated by the State of California. FEMA has expressed interest in using the B4 DEMs for flood plain mapping and modeling.

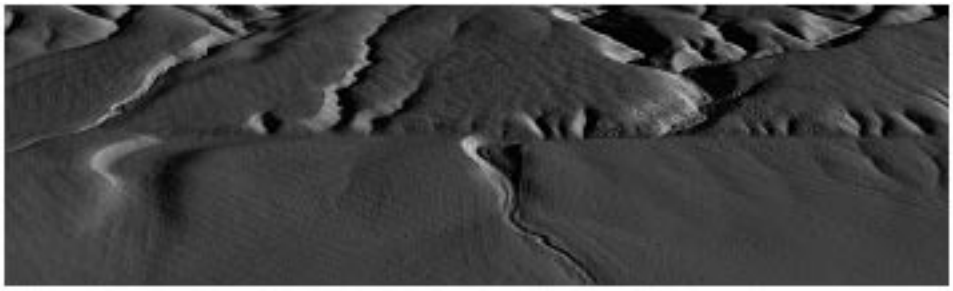

Oblique view of Wallace Creek, the classic San Andreas slip rate site in central California, as imaged by the B4 Project and gridded at 0.25 m resolution. The 1857 Fort Tejon earthquake (MW 7.9) produced the most recent ~9 m of slip at this location. Note the offset stream channels.

The section of the San Andreas fault in the Carrizo Plain (below) is perhaps the best-studied fault in the world; the site is a superb 'laboratory' for understanding fault behavior in great earthquakes. During the recent sesquicentennial commemoration of the 1857 event, the Southern California Earthquake Center (SCEC) which is supported by NSF and USGS, announced formation of its new special project, the Southern San Andreas Fault Evaluation (SoSAFE) Project. The first scientific workshop of the SoSAFE group initiated a large-scale team effort that will make systematic use of the B4 data by paleoseismologists along the entire southern San Andreas and San Jacinto (throughout the B4 coverage area). The SoSAFE Project will furthermore link with NSF`s GeoEarthScope and its funding of geochronological support, using radiocarbon and other new dating facilities and methods to better define the past 2000 years of earthquake history, as well as slip rates along the fault system. This information is expected to enhance our ability to forecast the occurrence of future destructive earthquakes along the fault system.

OBSERVING SEISMIC WAVES USING HIGH-RATE GPS: THE 2002 DENALI FAULT EARTHQUAKE

Andria Bilich, Kristine M. Larson • University of Colorado at Boulder

Recent advances in GPS receiver technology and increased data storage capabilities enable sampling and archiving of GPS data at higher rates than the traditional 30 second or lower rates; 1-Hz data are increasingly available through institutions such as UNAVCO and the EarthScope Plate Boundary Observatory. These new GPS data rates are sensitive to short-period motions such as the passage of seismic waves [e.g. Larson et al. 2003], serving as a natural complement to traditional seismometry where instruments may clip during strong accelerations.

Noise reduction via sidereal and spatial filtering has been shown to effectively increase the signal to noise ratio of GPS positioning by reducing repeating errors. Sidereal filtering [Choi et al., 2004] removes site-specific errors by capitalizing upon the day-to-day repeatability of multipath geometry and satellite orbit distribution. Position solutions for time periods without displacements are used to model these errors, which are then subtracted from the date of interest. Recent work by Larson et al. [2006a, 2006b] has established the theory behind and improved the effectiveness of modified sidereal filtering. Similarly, spatial filtering models errors common to all stations in a network [Wdowinski et al., 1997]; these common-mode errors include reference station errors from the least-squares solution.

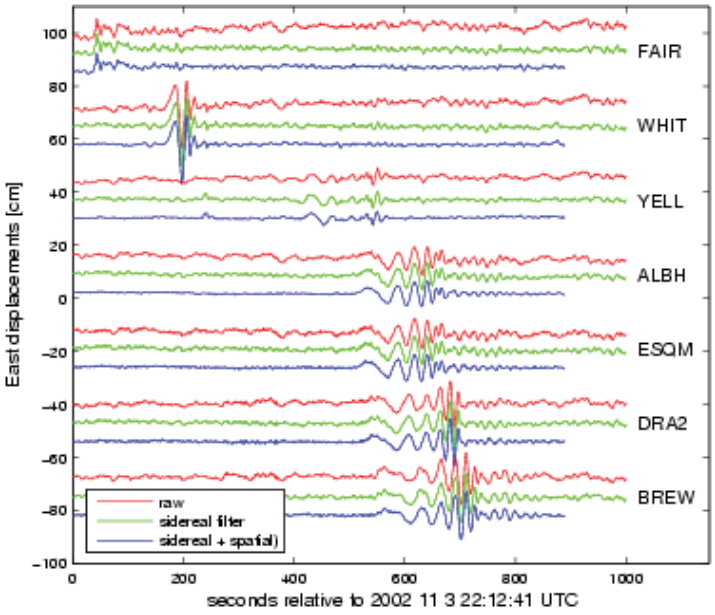

Examples of seismic waveforms derived from 1-Hz GPS positions. The raw positions (red) are contrasted with the positions after sidereal (green) and sidereal plus spatial filtering (blue). Stations are ordered by increasing distance from the epicenter, where time zero equals the origin time of the Denali Fault event.

Applying these high-rate GPS analysis techniques to recent datasets has enabled accurate determination of displacements due to seismic waves. As an example, the 3 November 2002 Denali Fault earthquake, a large-magnitude (M=7.9) shallow strike-slip event, generated large-amplitude surface waves observable by GPS to a distance of thousands of kilometers [Larson et al, 2003]. A network of 26 1-Hz GPS stations that observed surface wave displacements due to the Denali Fault event was assembled [Bilich et al., 2004; Bilich, 2006]. Implementing sidereal and spatial filtering on this dataset resulted in a 30-50% reduction in noise, depending on the component, and revealed low-noise GPS seismograms with clear waveforms at stations experiencing several centimeters of displacement and greater.

Bilich, A., K. Larson, P. Axelrad, C. Choi, Techniques for reducing spatially-correlated errors in high-rate GPS, EOS Trans. AGU, 85(47), Fall Meet. Suppl., Abstract G53A-0110, 2004.

Bilich, A, "Improving the precision and accuracy of geodetic GPS: Applications to multipath and seismology," University of Colorado, Ph.D. Dissertation, expected summer 2006.

Choi, K., A. Bilich, K. M. Larson and P. Axelrad. Modified sidereal filtering: Implications for high-rate GPS positioning, Geophysical Research Letters, 31(22), doi:10.1029/2004GL021621, 2004.

Larson, K., P. Bodin and J. Gomberg, Using 1-Hz GPS data to measure deformations caused by the Denali fault earthquake, Science, 300, 1421-1424, 2003.

This research was sponsored by NSF grants on multipath (EAR-0003943) and high-rate GPS (EAR-0337206), a NSF graduate student research fellowship (AB), and a CU Faculty Fellowship (KL).

COLLABORATIVE RESEARCH: LOW TEMPERATURE THERMOCHRONOLOGY ON THE SAN ANDREAS FAULT OBSERVATORY AT DEPTH (SAFOD).

Ann Blythe • University of Southern California
Ken Farley • California Institute of Technology
Roland Burgmann • University of California, Berkeley

Apatite fission track and (U-Th)/He analyses are being used to study the long-term thermal history of the SAFOD pilot and main holes, in order to: (1) constrain the geothermal gradient as a function of time near the SAF, (2) infer the exhumation history of the Salinian block in Central California, and (3) assess the feasibility of imaging frictional heat from individual earthquakes on the SAFOD borehole. In our initial study of the pilot hole [Blythe et al., 2004], 15 apatite fission-track and 5 (U-Th)/He analyses were obtained. Fission track ages ranged from ~60 Ma at the surface to ~ 3 Ma at the base of the hole; (U-Th)/He ages at the base of the hole were ~1 Ma. Thermal models indicated that there was an early phase of slow cooling in this region from ~80 until 31 Ma, followed by reheating from ~ 31 Ma to ~8 to 4 Ma, probably as the result of subsidence and burial by 2 km of sediments, and finally, cooling caused by ~1 km of Coast Range exhumation beginning at ~8 to 4 Ma. We are currently working on obtaining new data on samples collected from the main hole to a depth of 2700 m; these new samples promise to further our understanding of the behavior of the San Andreas fault at depth.

Blythe, A.E., d'Alessio, M., and Bürgmann, R., 2004, Constraining the exhumation and burial history of the SAFOD pilot hole with fission track and (U-Th)/He thermochronometry, Geophysical Research Letters, v. 13, L15S16, doi:10.1029/2003GL019407.

Matt d'Alessio collaborated on this project. Lindsay Hedges assisted us with laboratory analyses. This work was funded by NSF (EAR-0207306, EAR-0207388, and EAR-0345563).

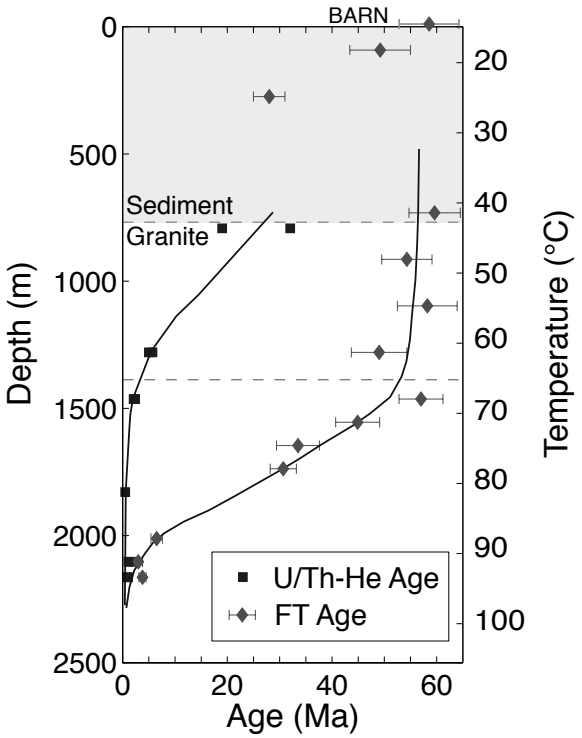

Apatite fission track and (U-Th)/He ages from the SAFOD pilot hole plotted with respect to sample depth and temperature.

SEISMIC-ASEISMIC DEFORMATION REVEALED BY MICROSTRUCTURES OF THE SAN ANDREAS FAULT ROCKS

Anne-Marie Boullier, Jean-Pierre Gratier, François Renard • Université Joseph Fourier - CNRS, France
Muriel Andreani • Université Montpellier 2, France

Microstructures in fault rocks may be interpreted in terms of high strain-rate (seismic) or low strain-rate (aseismic) deformation mechanisms and, therefore, may be tentatively correlated to different stages of the seismic cycle. Pore fluids are generally present and may also induce some slip-weakening processes during rupture propagation. Alternatively, these fluids enhance aseismic processes such as compaction, pressure solution creep, crack healing or sealing, that are responsible for permeability variations, fluid pressure build-up, and fault strength recovery between successive earthquakes. We have performed SEM and TEM observations on serpentinite gouges collected on outcrops along the Santa Ynez San Andreas fault system). They have revealed that their schistosity corresponds to serpentine fibres and forms by continuous syntectonic fiber growth implying a slow mass transfer process. We thus propose that a dissolution-diffusion-crystallization process explains the formation of this schistosity. This deformation mechanism could accommodate the aseismic creep of some fault segments where serpentinites are present.

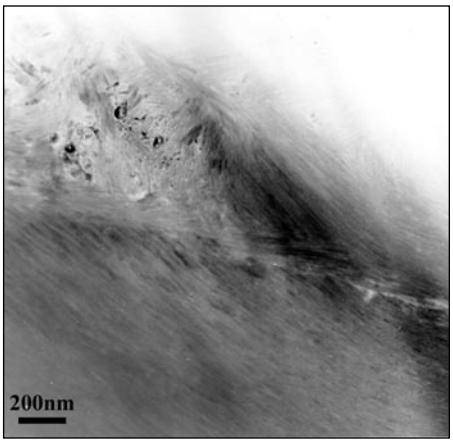

Serpentine has been recognized in cuttings collected from Phase 2 of SAFOD drilling using X-ray diffraction. Using SEM on these cuttings, we observed fibrous serpentine minerals (chrysotile) similar to those from outcropping serpentinite gouges and, therefore, suggest that aseismic creep may have occurred on the San Andreas fault and may have considerable influence on the fault frictional behavior. To model the decrease in permeability and the build-up of fluid pressure during the seismic cycle, one needs to i) characterize the fluid origins and pathways in the fault, ii) understand deformation textures, iii) measure the size of the closed system, and iv) acquire experimental data on kinetics of fluid/minerals interactions under stress (that we are currently performing). In the SAFOD program (cuttings and forthcoming core samples), we propose to characterize i) the textures induced by the aseismic deformation leading to permeability decrease and fault strength recovery, ii) the co-seismic fluid redistribution and fluid-rock interactions by combining microstructural and geochemical studies. These measurements on the borehole samples, coupled with geophysical records, and pressure solution experiments, will be integrated in master models (rate and state laws) of the permeability and strength evolution of faults during the seismic cycle and during an earthquake.

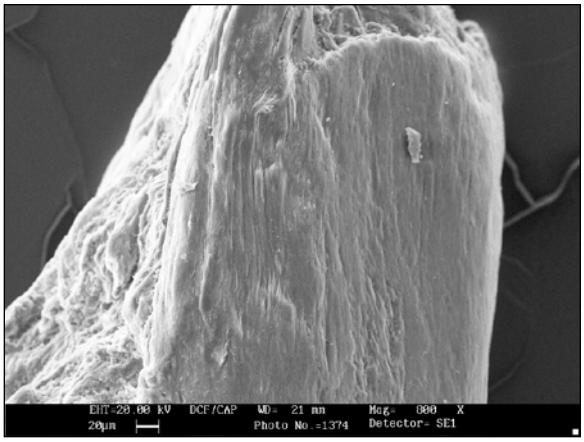

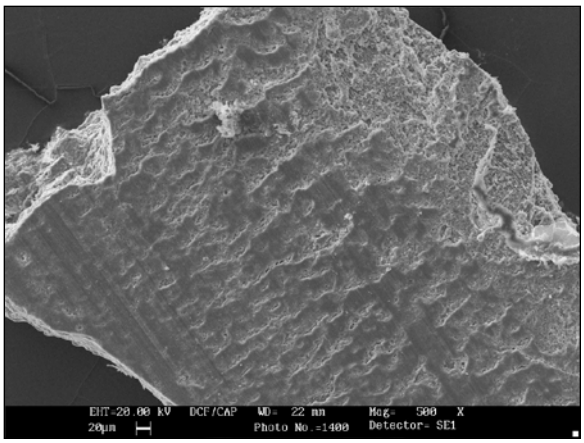

Top: TEM image of a "pressure-shadow" of a clast made of chrysotile and polygonal serpentine included within the schistosity charaterized by long and parallel chrysotile fibres in a serpentinite gouge outcropping in the Santa Ynez.

Middle: SEM image of a SAFOD cutting (10900ft) showing chrysotile fibers, similar to those of the top figure.

Bottom: SEM image of a SAFOD cutting (10900ft) showing frictional striations on clay minerals.

Andreani, M., A.-M. Boullier and J.-P. Gratier (2005). Development of schistosity in a Californian serpentinite gouge. J. Struct. Geol. 27, 2256-2267.

Gratier, J.-P., P. Favreau and F. Renard (2003). Modelling fluid transfer along California faults when integrating pressure solution crack sealing and compaction processes. J. Geophys. Res. 108, 28-52.

Pili, E., F. Poitrasson and J.-P. Gratier (2002). Carbon-oxygen isotope and trace element constraints on how fluids percolate faulted limestones from the San Andreas Fault system: partitioning of fluid sources and pathways. Chem. Geol. 190, 231-250.

Solum J.G., S.H. Hickman, D.A. Lockner, D.E. Moore, B. van der Pluijm, A.M. Schleicher and J.P. Evans (2006) Mineralogical characterization of protolith and fault rocks from the SAFOD Main Hole. Geophys. Res. Lett. 33, L21314, doi:10.1029/2006GL027285.

We thank S.H. Hickman, J.G. Solum, D.E. Moore, M. Rymer, F.M. Chester, B. van de Pluijm, and J.P. Evans for their help. These studies are financed by the French CNRS and the Observatory of Grenoble (OSUG).

CONTRIBUTIONS OF EARTHSCOPE TO EARTHQUAKE HAZARD ASSESSMENT IN NORTHERN CALIFORNIA

Tom Brocher, Bill Ellsworth, Steve Hickman, Diane Moore • U.S. Geological Survey

We briefly describe some of the ways each of the three components of EarthScope (PBO, SAFOD, US Array) as well as GeoEarthScope contribute to earthquake hazard assessment in Northern California. First, SAFOD and US Array have directly contributed to the development and testing of regional 3D seismic velocity models for Northern California used to calculate strong ground motions for scenario earthquakes. Compressional- and shear-wave velocity logging of Salinian granitic rocks and sedimentary rocks in the SAFOD pilot and main boreholes provided important constraints on empirical Vp/Vs relations that were used to convert geology-based Vp models to Vs models. Arrival times between US Array stations in Northern California, determined from correlations of the ambient background noise, are being used to calibrate the accuracy of the regional 3D seismic velocity model for Northern California. Eventually, regional shear-wave velocity models developed from the US Array recordings of ambient noise may prove useful in calibrating regional geology-based velocity models outside of the Bay Area where the geology model is highly simplified. Second, identification of talc in cuttings from the SAFOD borehole, near the active trace of the San Andreas fault, suggests that its presence or absence may play an important role in the creeping and locking behavior of faults in the San Francisco Bay Area. Third, data from PBO continuous GPS sites are incorporated into our automated processing system as the stations come online. This station densification improves our ability to monitor deformation in Northern California. We are developing strategies for including PBO strainmeter data in routine monitoring as well. The continuous GPS data provide a strong framework of regional measurements which permit us to conduct focused survey-mode GPS observations in order to refine our understanding of Northern California deformation and fault slip rates, for example along the Bartlett Springs fault. Fourth, GeoEarthScope is acquiring 1400 square km of LIDAR data mainly along 1 km wide swaths centered on many of the major strike-slip faults in Northern California. As part of this effort, a consortium of other agencies and corporations will fund collection of an additional 220 sq. km of LIDAR data. These LIDAR swaths are designed to produce images of the fault zones that will help better locate and define active traces within these fault zones, identify new places suitable for paleoseismic excavations across fault strands, and provide baseline imagery prior to the next major earthquake with surface fault rupture.

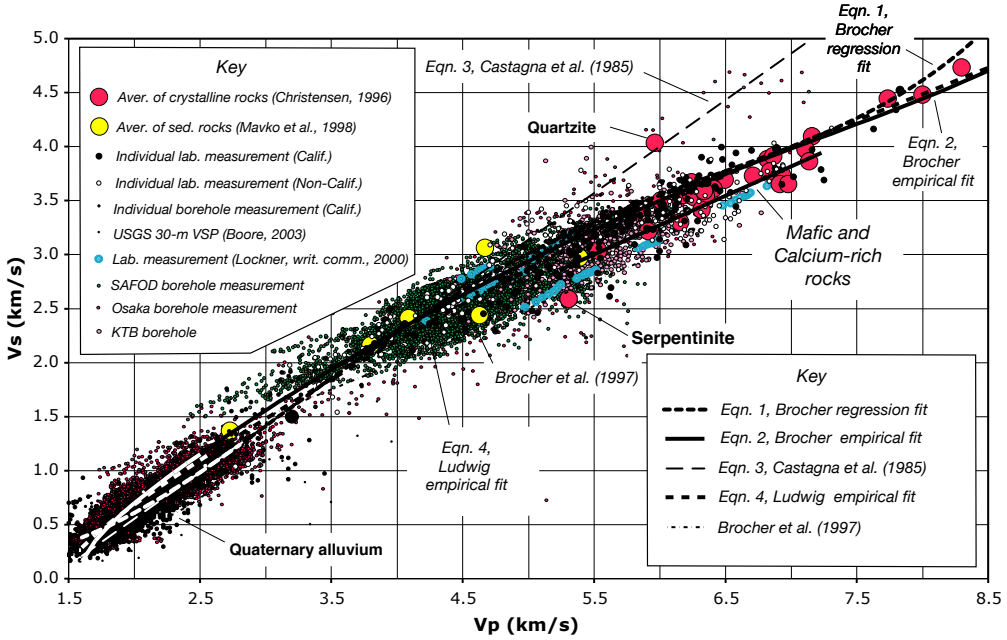

Compilation of compressional (Vp) and shear-wave (Vs) velocity measurements showing SAFOD Main Hole measurements in small green dots. Empirical regression lines relating Vp and Vs from Brocher (2005) are also shown. Figure from Brocher and Wentworth (2007).

Brocher, T. M., 2005, Empirical relations between elastic wavespeeds and density in the Earth's crust, Bull. Seism. Soc. Am., 95, 2081-2092.

Brocher, T.M., and C.M. Wentworth, 2007, Elastic wavespeeds in Quaternary alluvium in the Santa Clara Valley, California, Geol Soc. Am. Special Publication, R. Williams and R. Hansen, ed., in press.

We thank the PBO, SAFOD, US Array as well as GeoEarthScope for their contributions to earthquake hazard assessment in Northern California.

LONG-TERM MEASUREMENTS IN THE SAFOD BOREHOLE

Emily Brodsky • University of California, Santa Cruz

The accumulation of stress during an earthquake cycle is relatively well-understood, but the evolution of strength on a fault is almost unmeasured. Both factors are critical to the initiation of earthquakes and there is reason to believe both vary with time on a major fault. The SAFOD borehole provides an unprecedented opportunity to acquire long-term measurements at depth on an active fault of the key proxies for strength: seismic velocity, pore pressure changes and temperature.

Recent measurements have shown that seismic velocity decreases after a major earthquake and then recovers [Li et al., 2000; Li and Vidale, 2001; Vidale and Li, 2003].. These velocity changes have been interpreted as tracking the evolution of pore pressure or microcracking damage. In both cases, the velocity changes are inferred to measure the strength of the fault. However, it is unclear how relevant the surficial measurements are to seismogenic depths. Soils and other shallow structures might easily be creating the observed effects. Therefore, it is critical to obtain repeated measurements of seismic velocity at depth on a fault. The combination of the repeating earthquakes in Parkfield and the borehole seismometers provide a near-perfect configuration for this type of experiment. Seismic velocity changes are expected to be very slow in the interseismic period (<0.1% per year), thus it is important to obtain at least 10 years of measurements.

Another proxy for damage is permeability as measured by downhole pressure transducers. In a heavily fractured region, like a fault damage zone, permeability is controlled by the fractures and hence measurements of permeability evolution can be used to track healing. Recent work on 20 years of data from Pinon Flat Geophysical observatory showed that permeability evolves with time and is appreciably increased by the seismic waves from regional earthquakes [Elkhoury et al., 2006]. In Figure 1, the phase lag of water level relative to the known solid earth tide is used to measure permeability over time. The closer the phase lag is to zero, the higher the permeability of the system. A similar method modified for the packed intervals could be used to continuously measure permeability in SAFOD.

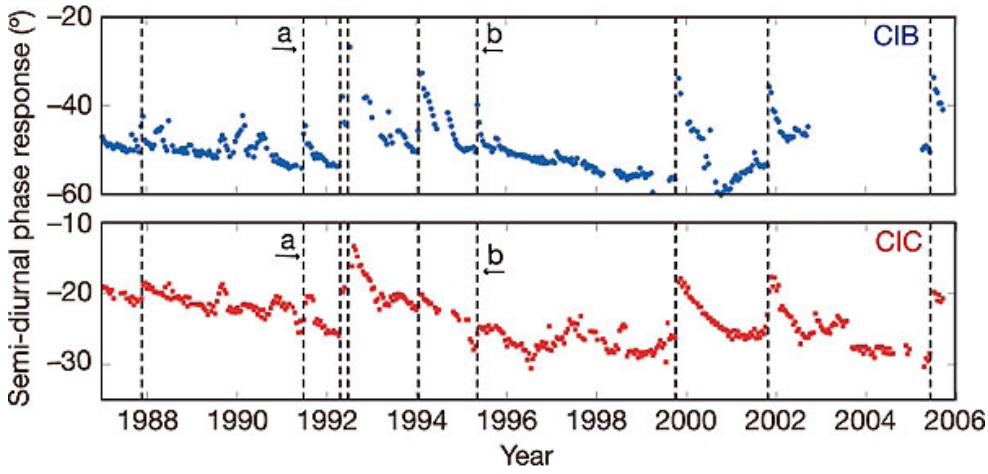

The third, and perhaps most widely recognized, proxy for strength is heat flow. The San Andreas is widely believed to be weak because of a lack of a heat flow anomaly over the fault[Lachenbruch & Sass, 1980]. Recent earthquakes have reawakened an interest in downhole temperature measurements as a way to infer friction on faults [Ma et al., 2006; Kano et al. 2006]. The recent results have been handicapped by a lack of long-term repeated measurements. The act of drilling significantly perturbs the temperature field around a borehole. Thus, it is important to repeatedly measure a temperature profile in order to track its evolution back to its natural, stable shape. The usual rule-of-thumb for wait times is six times the drilling time. The prolonged drilling activity in the SAFOD borehole will necessitate waiting over 12 years until we can be certain of the measurements.

The SAFOD borehole provides an opportunity to pin down the evolution of fault strength which is a key component of the earthquake cycle. Targeted use of the existing facilities with appropriate maintenance can yield major results through repeated seismic velocity, permeability and temperature measurements over the next 10 to 15 years.

Elkhoury, J., E. E. Brodsky, and D. C. Agnew, Seismic waves increase permeability, Nature, 441 , 1135–1138, 2006.

Kano, Y., J. Mori, R. Fujio, H. Ito, T. Yanagidani, S. Nakao, and K. F. Ma, Heat signature on the Chelungpu fault associated with the 1999 Chi-Chi, Taiwan earthquake, Geophys. Res. Let., 33 , 473–476, 2006.

Lachenbruch, A. H., and J. H. Sass, Heat flow and energetics of the San Andreas fault zone, J. Geophys. Res., 85 , 6185–6222, 1980.

Li, Y.-G., and J. Vidale, Healing of the shallow fault zone from 1994–1998 after the 1992 M7.5 Landers, California earthquake, Geophys. Res. Let., pp. 2999–3002, 2001.

Li, Y.-G., G. Vidale, K. Aki, and F. Xu, Depth-dependent structure of the Landers fault zone from trapped waves generated by aftershocks, J. Geophys. Res., 105 , 6237–6254, 2000.

Ma, K. F., et al., Slip zone and energetics of a large earthquake from the Taiwan Chelungpu-fault Drilling Project, Nature, 444 , 473–476, 2006.

Vidale, J. E., and Y.-G. Li, Damage to the shallow Landers fault from the nearby Hector Mine earthquake, Nature, 421 , 524–526, 2003.

DEFORMATION OF THE NORTH AMERICAN PLATE INTERIOR FROM A DECADE OF CONTINUOUS GPS MEASUREMENTS

E. Calais • Purdue University
C. DeMets • University of Wisconsin

Large earthquakes within stable plate interiors (e.g., 1811-1812 New Madrid events in the Mississippi valley) are direct evidence that significant amounts of elastic strain can accumulate far from plate boundary faults, where the vast majority of seismic energy is released. Because significant intraplate earthquakes are infrequent and strain rates in continental interiors are so low, neither the rates nor pattern of intraplate strain are well constrained, as is also the case for the mechanism(s) responsible for strain accumulation and release on faults inside plates. Using more than 300 continuous GPS stations in the central and eastern U.S. and Canada spanning 1993-2005, we find that surface deformation in the North American plate interior is best fit by a rigid rotation of North America with respect to ITRF2000 plus a component of strain qualitatively consistent with that expected from Glacial Isostatic Adjustment (GIA). After correcting for the North American plate motion, residual horizontal velocities show a north-to-south deformation gradient of ~1 mm/yr, mostly localized between 1000 and 2200 km from the GIA center, corresponding to strain rates of about 10^{-9} yr^{-1}. At distances farther than 2100 km from the GIA center, horizontal residual velocities are random with no evidence for regions of elevated strain rates. In particular, we find no detectable residual motion at the 95% confidence level in the New Madrid Seismic Zone, where the average weighted misfit of 0.7 mm/yr is the same as the weighted misfit of our rigid plate model. Vertical velocities show (1) a maximum uplift rate of 10 mm/yr at the assumed GIA center, (2) a hinge line located 1500 km from that center, and (3) a subsidence rate up to 1.4 mm/yr in the forebulge, with a maximum located about 2000 km from the GIA center. Our results have the potential to better constrain GIA models and contribute to a better definition of stable North America for tectonic and geodetic applications.

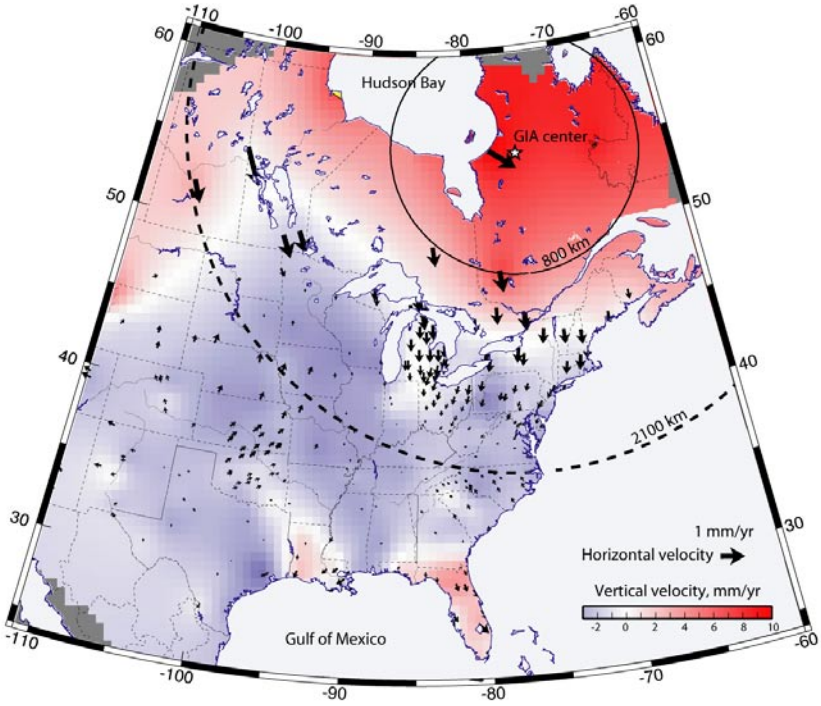

Spatially averaged residual velocities calculated using a nearest neighbor scheme with a search radius of 800 km. The dashed circle has a radius of 2100 km and is centered on the GIA uplift (star). A solid circle with a 800 km radius is shown to illustrate the search radius dimension. Background: Interpolated vertical velocities. Black squares show site locations. The red dashed line correspond to zero velocity (hinge line). The interpolation scheme uses an adjustable tension continuous curvature surface gridding algorithm with a tension factor of 0.9.

Calais, E., G. Mattioli, C. DeMets, J.M. Nocquet, S. Stein, A. Newman,
Calais, E., J.Y. Han, C. DeMets, and J. M. Nocquet, Deformation

This research was supported by USGS/NEHRP Award 03HQGR0001.

USING EARTHSCOPE DATA FOR ENVIRONMENTAL STUDIES

Philip Carpenter • Northern Illinois University

EarthScope data obtained with the transportable seismic network and flexible array, when combined with data from the ANSS/NSN, have the potential to image velocity structure of the upper crust with resolutions as small as 100s to 10s of meters. The flexible array, in particular, offers the opportunity to image the upper crust at resolutions relevant to some types of groundwater, environmental and engineering studies. For example, in the Chicago area, P-wave velocity variations could be used to map dewatered portions of shallow bedrock aquifers in areas of heavy groundwater usage. Analysis of shear-wave splitting, or birefringence, could help delineate fractures in the upper 1-2 km that affect regional groundwater flow and recharge. Such fracture zones are presently obscured by 50-100 m of glacial drift. Shear-wave velocity structure of the uppermost parts of the crust is an essential parameter for accurate site-specific seismic hazard assessment and seismic design of critical facilities.

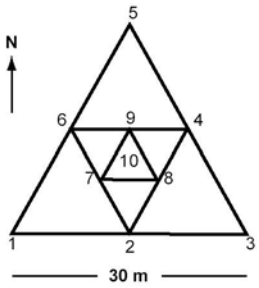

Array for seismic noise surveys, after Okada (2003). Okada's f-k method may be used to determine the direction of seismic waves migration and the layered structure of a site.

Seismic noise from industrial operations, railroads, airports and expressways is also of concern to facilities requiring a vibration-free environment. We recently investigated ambient ground motion in the suburban Chicago area for the preliminary International Linear Collider (ILC) site selection study, funded by the Fermi National Accelerator Laboratory [Higuera and Carpenter, 2004]. As a part of this study, we used data from the EarthScope-enhanced ANSS/NSN station at Jewell Farm, WI, (JFWS), as well as other seismic stations in the suburban Chicago area and north-central Illinois. Absolute values of ground displacement (or velocity), and associated amplitude (or power) spectra were computed using the Seismic Analysis Code 2000 (SAC2000), free to IRIS members. Distinctive seismic noise peaks were identified among the different sites, regardless of the background noise level. These included peaks in the 0.14-0.2 Hz range, probably corresponding to traditional oceanic microseismic noise, and noise peaks that probably correspond to resonant frequencies of the various sites, as detailed in Higuera and Carpenter [2004]. To investigate local ground motion in more detail, noise from was recorded using local arrays of geophones. Power spectra from arrays reveal a number of peaks in the 10-100 Hz range, reflecting cultural sources (trains, vehicles, mechanical equipment) and wind. We are presently processing the data from the arrays to identify directions of ambient noise propagation for each energy peak.

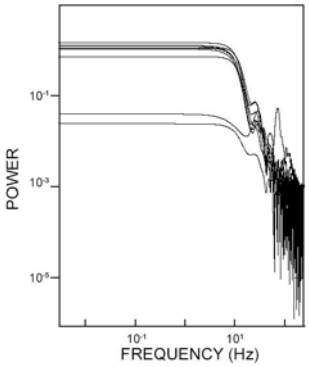

Power spectra for geophone waveforms.

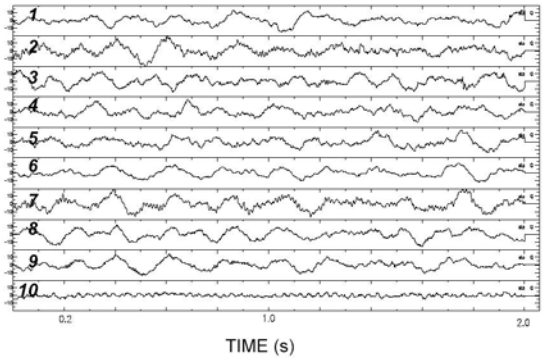

Waveforms from an array consisting of 4.5 Hz horizontal geophones. Numbers in the left correspond to the position of the geophone in the array.

Higuera-Diaz, I.C. and Carpenter, P.J. (2004). Frequency content of ambient seismic noise in north-central Illinois (abstract): Eos: Trans. Amer. Geophys. Un., v. 25, no. 47, S13C-1074.
Okada, H. (2003). The microtremor survey method: translated from Japanese by K. Suto, Geophysical Monograph Series, 12, Society of Exploration Geophysicists, Tulsa, 135 p.

Support for this work was provided by the Fermi National Accelerator Laboratory.

CONTEMPORARY DEFORMATION OF THE WASATCH FAULT, UTAH, FROM GPS MEASUREMENTS WITH IMPLICATIONS FOR INTER-SEISMIC FAULT BEHAVIOR AND EARTHQUAKE HAZARD

Wu-Lung Chang, Robert B. Smith • University of Utah

Developed over the past decade, high precision GPS data were acquired by eight University of Utah continuous stations and seven campaign surveys between 1992 and 2003 to evaluate horizontal velocity field of the Wasatch Front area [Chang et al., 2006]. Observations across a 65-km wide area centered on the Wasatch fault indicates a horizontal extension rate of 1.6 ± 0.4 mm/yr nearly perpendicular to the fault, which accommodates ~50% of the crustal deformation across the ~200 km-wide eastern Basin-Range. Analysis of the spatial variation of the strain-rate field reveals that the strain accumulation is concentrated near the Wasatch fault, which suggests an abrupt transition in the horizontal deformation at the fault between the eastern Basin-Range and the Rocky Mountains.

Using the horizontal deformation results from the continuous and campaign GPS survey, we have calculated nonlinear inversions on fault geometry, locking depth, and loading rates. Results suggest that a dislocation dipping 27° and creeping at 7 mm/yr from depths of 9-20 km, which corresponds to the interseismic loading part of the Wasatch fault, is our favorite model based on the current GPS data. Note that this loading rate is notably higher than the ~1 to 2 mm/yr rate derived from the paleoseismic data.

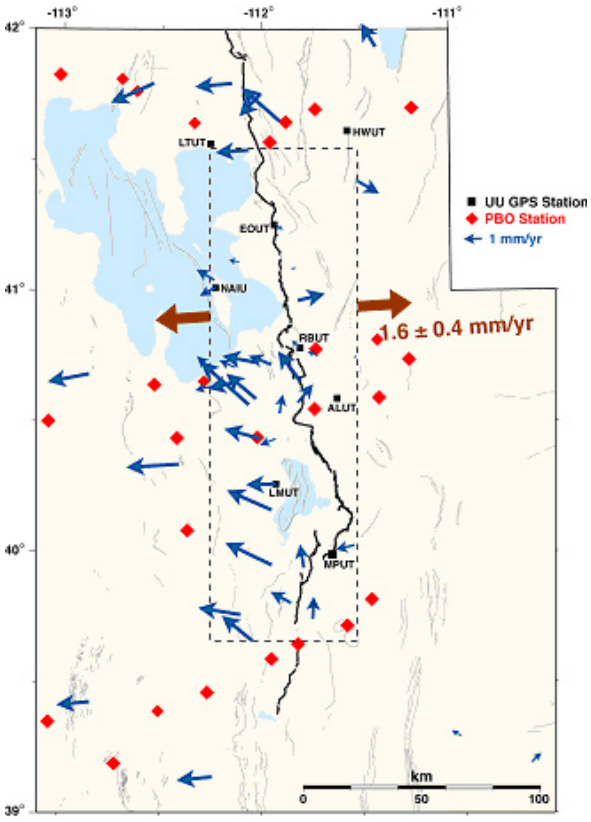

Wasatch Front horizontal velocity field from continuous and campaign GPS observations. PBO stations are shown by red diamonds.

To consider along-strike variations of the fault behavior, moreover, a dual-dislocation model that reflects the changes in strikes of the surface trace of the Wasatch fault better explains the variations of the velocity field near the fault. The improved results of using two fault segments to model the Wasatch Front horizontal velocity field suggest that multi-dislocation models with geometry similar to the fault surface traces may be plausible to describe the interseismic behavior of the Wasatch fault.

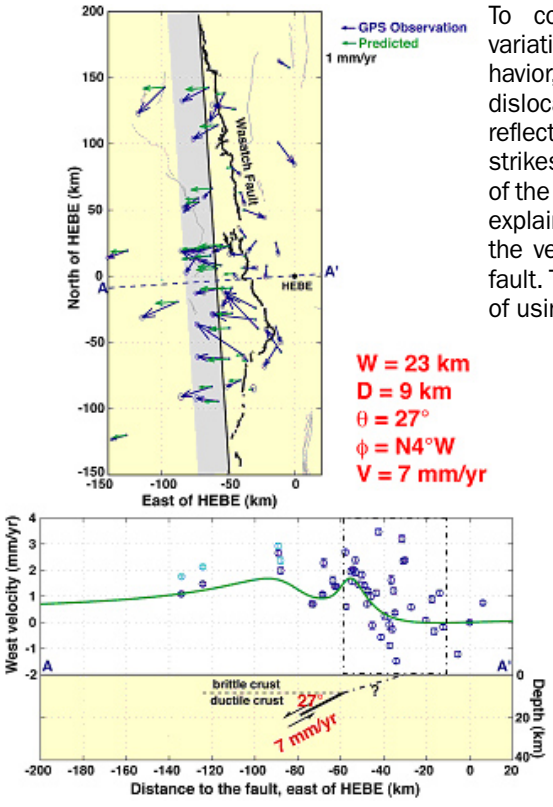

Single-dislocation model for interseismic loading of the Wasatch fault.

To examine the physics of normal faults in a broad area of regional intra-plate deformation, the EarthScope PBO has established three profiles of GPS stations across the eastern Basin Range including parts the northern (I-84 corridor), central (I-80 corridor) and southernmost (central to southern Utah) Wasatch fault. Data from these 27 (21 currently operating) stations greatly benefit studies of the interseismic loading of the Wasatch normal fault.

Chang, W. L. and R. B. Smith, 2002, Integrated earthquake hazard analysis of the Wasatch Front, Utah, Bull. Seism. Soc. Am., 92, 1904-1922.

Chang, W. L. and R. B. Smith, 2006, Contemporary deformation of the Wasatch Fault, Utah, from GPS measurements with implications for inter-seismic fault behavior and earthquake hazard: observations and kinematic analysis, J. Geophys. Res., 111, B11405, doi:10.1029/2006JB004326.

This research was supported by USGS grant # 1434-HQ-96-GR-02746.

ACCELERATED UPLIFT OF THE YELLOWSTONE CALDERA, 2004-2006, FROM GPS AND INSAR OBSERVATIONS

Wu-Lung Chang, Robert B. Smith, Chuck Wicks, Christine M. Puskas • University of Utah

Geodetic techniques have been employed to monitor the crustal motion of Yellowstone beginning with the precise leveling of benchmarks installed in 1923. Since 1997, the University of Utah has installed six permanent GPS stations inside Yellowstone National Park for continuously monitoring the ground deformation associated with seismic, volcanic, and hydrothermal activities. Starting in mid-2004, the GPS network recorded an episode of unprecedented uplift of the Yellowstone caldera concomitant with subsidence of the northeast caldera area including Norris Geyser Basin. The deformation continues into 2007, with nearly constant inflation rates of ~6 cm/yr and 4 cm/yr at the Sour Creek and Mallard Lake resurgent domes, respectively. These rates are up to three times faster than preceding caldera uplift rate from 1923 and 1984. The horizontal velocities, in addition, are 7 to 21 mm/yr outward from both domes. Meanwhile, Norris Geyser Basin experienced subsidence at ~4 cm/yr that is two times higher than the 1996-2002 uplift rate.

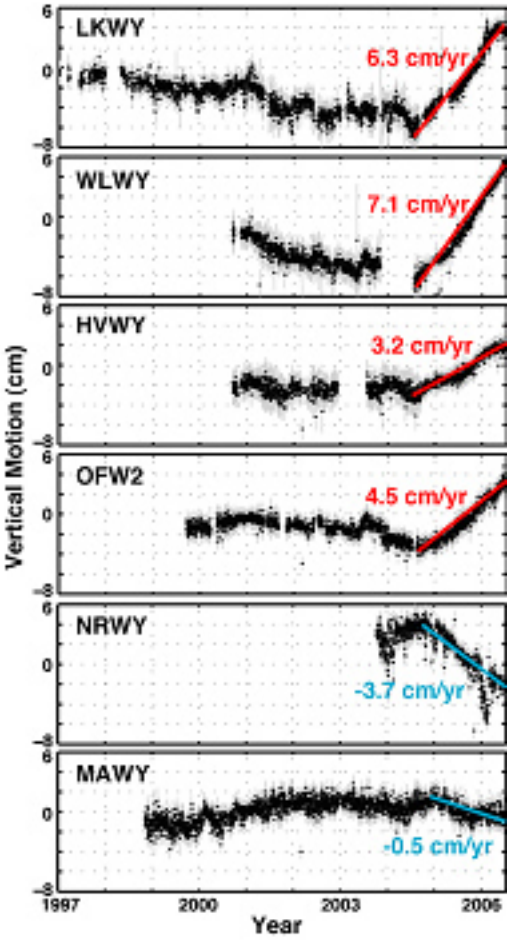

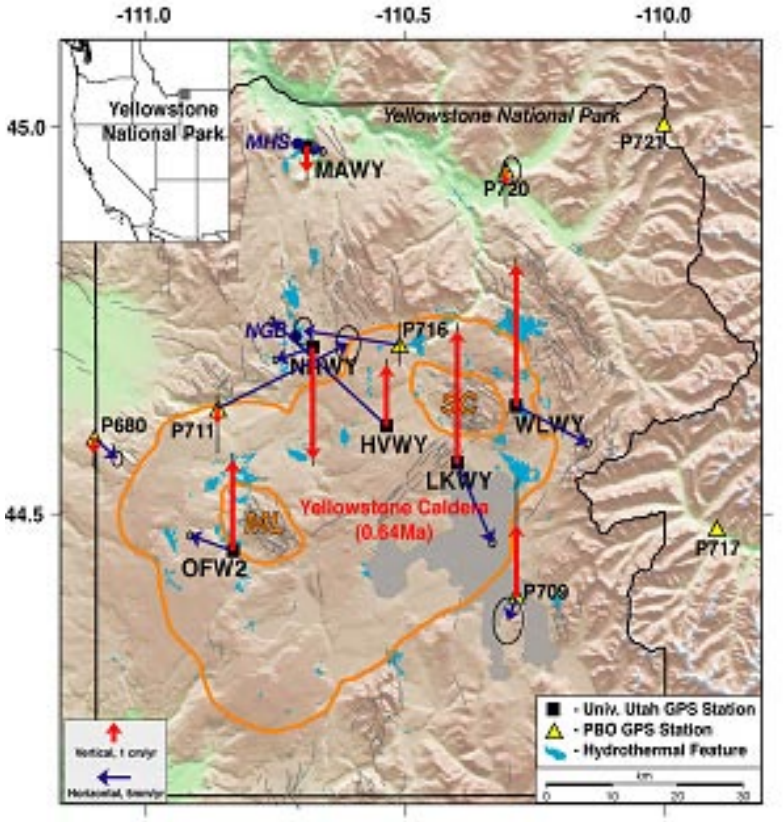

Incorporating GPS data from the University of Utah and five new PBO stations, we evaluated source models by inverting the GPS and InSAR data for the geometry and expansion (contraction) of dislocations in an elastic half-space [Chang et al., 2007]. The results indicate two horizontal sill-like structures ~8 km beneath the caldera with a total volumetric expansion rate of 0.11 km^3/yr, and a northwest-dipping tabular body 16 km beneath the Norris Geyser Basin with a volumetric contraction rate of 0.018 km^3/yr. Incorporating seismic, hydrothermal, and geochemical evidence, we propose that a new intrusion of magma into the mid-crustal or pressurization of a deep hydrothermal system likely caused the uplift within the Yellowstone caldera. The Norris subsidence, in contrast, may be induced by the crystallization and contraction of crustal magmatic bodies and the associated loss of dissolved fluid and gas to shallow fault and hydrothermal systems.

Chang, W., R.B. Smith, C. Wicks, C. Puskas, and J. Farrell, 2007, Accelerated uplift and source modeling of the Yellowstone caldera, 2004-2007, From GPS and InSAR observations, in preparation.

This research was supported by NSF Grants #0314298, #9725431, and #9316289.

SAFOD DATA & COMPUTER SIMULATIONS TO CLARIFY EARTHQUAKE PHYSICS

Ting Chen, Nadia Lapusta • California Institute of Technology

Repeating earthquakes occur on a number of creeping faults including Parkfield. A conclusive physical model of their occurrence would be of great importance to understanding the physics of earthquake processes and fault slip in general. In part, such model would help to determine the proper relation between the repeat time and the average creeping rate of the fault, as the repeat time is often used to infer the fault creeping rate.

Before detailed SAFOD data, the most intriguing observation about repeating earthquakes had been the scaling of their repeat time T with their seismic moment $M^{0.17}$ [Nadeau and Johnson, 1998]. The scaling is abnormal compared to other earthquakes that have $T \propto M^{1/3}$. This typical scaling also results from a simple conceptual model in which earthquakes are treated as circular ruptures with stress drop independent of the seismic moment and slip that is proportional to the repeat time. Several explanations for this discrepancy have been proposed, including dependence of stress drop on seismic moment, with much higher stress drops for small events [Nadeau and Johnson, 1998], and occurrence of repeating earthquakes at a border between large locked and creeping patches [Sammis and Rice, 2001]. However, recent studies based on SAFOD data indicate that stress drops fall into the typical range, and there is no evidence for a large locked asperity. Beeler et al. [2001] considered a fixed-area patch governed by a conceptual law that incorporated strain-hardening and showed that aseismic slip on the patch can explain the observed scaling relation.

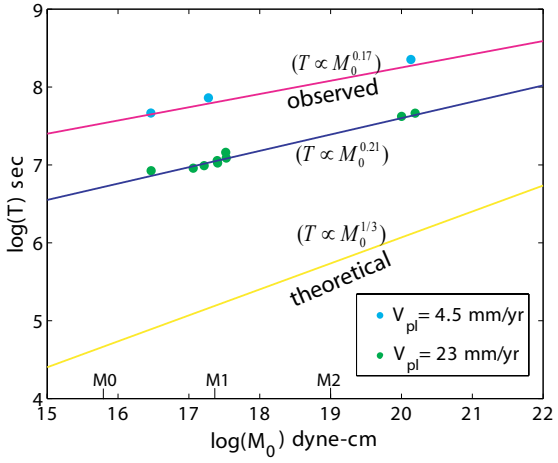

Repeat time vs. seismic moment. Dots show the results of our simulations; two sets of dots correspond to two creeping rates. For each set of dots, all model parameters are held constant except for the size of the rate-weakening patch. The top line shows the observed scaling, the bottom line show the typical scaling. Our models produce the observed scaling; slower plate rate reproduces repeat times better.

Our studies show that a simple model based on laboratory-derived rate and state friction laws provides a physical basis for the idea of Beeler et al. [2001] and results in repeating earthquakes that have the observed scaling. In the model, a small patch with rate-weakening friction is surrounded by a much larger region with rate-strengthening friction. Our simulations use the 3D methodology of Liu and Lapusta [AGU, 2006] and fully resolve all aspects of seismic and aseismic behavior of the fault, including inertial effects during seismic slip. In simulations, the rate-strengthening region accumulates slip through stable sliding with the imposed plate rate. Small enough rate-weakening patches also accumulate slip through stable, if slightly perturbed, sliding. Rate-weakening patches only slightly larger than theoretical estimates of nucleation sizes accumulate a lot of slip aseismically but also produce repeating earthquakes. Stress drops for the simulated earthquakes are in the typical range.

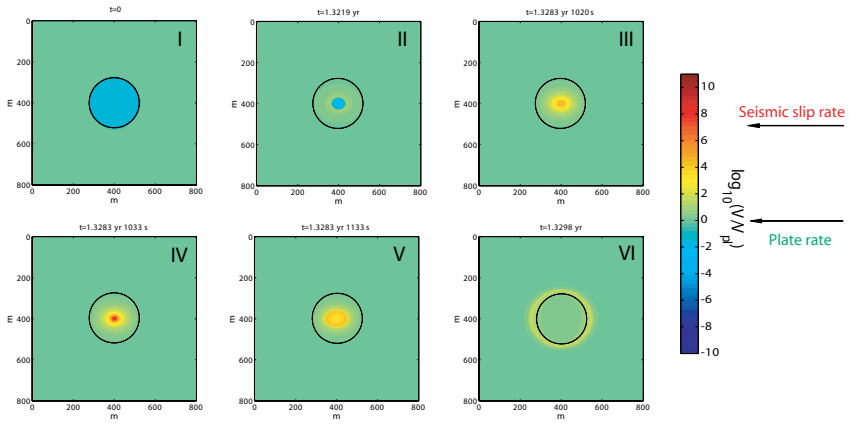

Simulation example, snapshots of slip rate on the fault. (I) Initial conditions: the patch is locked (significantly below creeping rate). (II) Creep enters the rate-weakening patch. (III) Slip in the patch accelerates. (IV) Slip rates reach seismic values in the middle of the patch. Note that the extent of seismic slip is much smaller than the diameter of the patch. (V) Post-seismic slip occurs in the patch. (VI) Postseismic slip enters the rate-strengthening region.

Beeler, N. M., D. L. Lockner, and S. H. Hickman, 2001. A Simple Stick-Slip and Creep-Slip Model for Repeating Earthquakes and its Implication for Microearthquakes at Parkfield, Bull. Seism. Soc. Am. 91, 1797–1804.

Chen, T., and N. Lapusta, 2006. Scaling of Seismic Moment with Recurrence Interval for Small Repeating Earthquakes Simulated on Rate-and-State Faults, Eos Trans. AGU 87 (52), Fall Meet. Suppl., Abstract S23C-0187.

Liu, Y., and N. Lapusta, 2006. Three-Dimensional Elastodynamic Simulations of Seismic and Aseismic Slip History of a Planar Strike-Slip Fault, Eos Trans. AGU 87 (52), Fall Meet. Suppl., Abstract S34A-07.

Nadeau, R. M. and L. R. Johnson, 1998. Seismological studies at Parkfield VI: Moment release rates and estimates of source parameters for small repeating earthquakes, Bull. Seism. Soc. Am. 88, 790-814.

This study is funded by NSF and USGS. The numerical simulations for this research are performed on Caltech Division of Geological and Planetary Sciences Dell cluster.

INFLUENCE OF STRUCTURE AND COMPOSITION OF THE SAN ANDREAS FAULT ZONE ON ASEISMIC AND SEISMIC SLIP PROCESSES AT SAFOD

Judith S. Chester, Frederick M. Chester • Texas A&M University

We are mapping the mesoscopic structure and lithology of the SAFOD core, characterizing microstructures, mineral reactions, and fluid-rock interactions, performing mesoscopic and microscopic fabric analyses of fractures to delimit average orientations of principal stresses relative to the fault and to place constraints on long-term strength of the fault zone, characterizing the reduction in grain size and formation of new fracture surfaces in seismically active portions of the fault zone to place constraints on the energy budget of seismic events, and exploring the frictional behavior of fault rocks at coseismic slip rates.

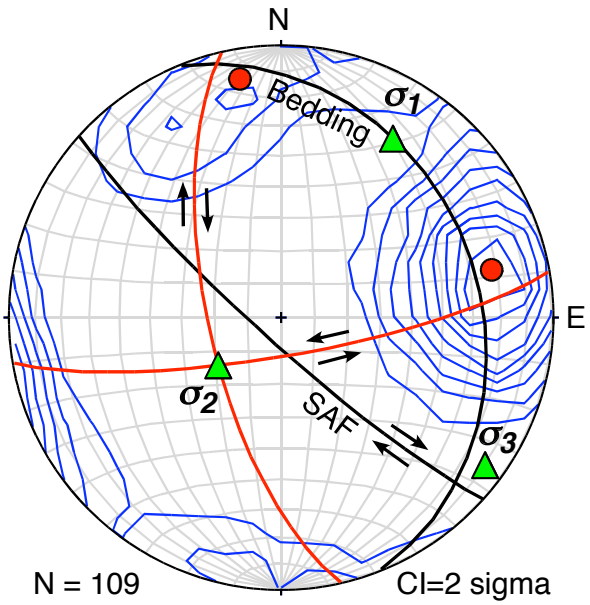

Shear fracture orientations and inferred principal paleostress directions for the lower, Phase 1 SAFOD core sample at 3056-3067 m MD adjacent to the SAFZ. Lower hemisphere, equal area projection with North at top. Black great circles show bedding and San Andreas fault plane. Kamb contour of poles to shear fractures. Shears define a conjugate set, and best fit poles and planes in red with sense of shear indicated. Inferred paleostress directions are indicated by green triangles, and are consistent with strike slip faulting and maximum principal compression axis at 80 degrees to the San Andreas fault.

We have compared estimates of paleostress from the upper portion of the seismogenic zone, inferred from mesoscale fracture fabrics in the spot cores, to measurements of the current in situ stress at the same location, adjacent to seismogenic patches of the main fault. We show that mesoscale fractures in core recovered from 3055.6-3067.2 m suggest that principal paleostress directions were nearly parallel and perpendicular to the fault. Fractures define a conjugate pattern consistent with strike-slip faulting and a maximum principal compressive paleostress at 80 degrees to the fault plane. The similarity between the current stress and paleostress states supports the suggestion that the fault has been weak on average over geologic time. In addition we have shown that the main fault (3067 m MD) captured during Phase 1 spot coring is likely a member of the left-lateral fault set, and not a candidate for the Southwest Trace of the San Andreas fault as previously suggested.

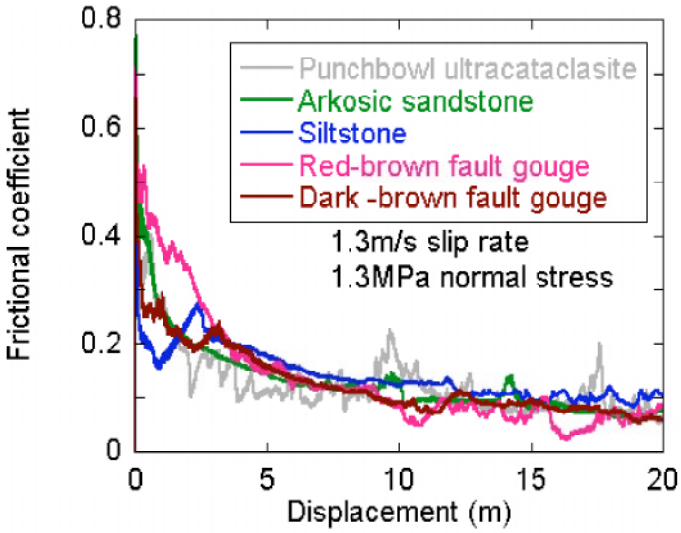

Representative results of high-speed friction experiments on fault-rock samples from the shear zone at 3067 m MD at SAFOD compared to that for the Punchbowl fault ultracataclasite. Al fault-rock types display a dramatic reduction of friction to coefficients less 0.1 at the coseismic slip rates. The initial friction and critical slip distance for weakening varies with rock type.

From our high speed friction work we have shown that when rocks from the 3067 m MD fault are sheared at 1.3 m/s and normal stresses of 0.3, 0.6, and 1.3 MPa that the coefficient of sliding friction decreases from an initial value of approximately 0.5 to less than 0.1 within tens of meters of displacement. The friction coefficient at steady state is similar overall, but the transient weakening behavior is variable, which is interpreted to reflect initial microstructural state and mineralogy of the fault-rocks. All results indicate that frictional strength is strongly related to friction heating.

Almeida, R., Chester, J.S., Chester, F.M., Fracture Fabric and Paleostress along the San Andreas Fault at SAFOD, to be submitted to Geophysical Research Letters, 2007.
Almeida, R., Chester, J., Chester, F., Kirschner, D., Waller, T., and Moore, D., Mesoscale Structure and Lithology of the SAFOD Phase I and II Core Samples, Eos Trans. AGU, 86(52), T21A-0454, 2005.
Chester, J. S., Kitajima, H., Shimamoto, T., and Chester, F. M., Dynamic weakening of ultracataclasite during rotary shear at seismic slip rates, EOS Trans. AGU, T21B-0472, 86(52), 2005.
Kitajima, H., Chester, J.S., Chester, F.M., and Shimamoto, T., Dynamic Weakening at Seismic Slip rates Demonstrated for Fault-Rocks From SAFOD Core and Punchbowl Fault, Eos Trans. AGU, 87(52), S41D-04, 2006.

Collaborators: James P. Evans (USU) and David Kirschner (SLU), Hiroko Kitajima (TAMU), Toshihiko Shimamoto (Kyoto Univ.), Rafael Almeida (TAMU). Funding: Chester, J.S. and Chester, F.M., Collaborative Research: Structural-Petrologic Characterization of the San Andreas Fault Zone in the SAFOD Drill Holes, NSF-0454525. Chester, J.S., Investigation of Weakening Mechanisms in High-speed Experimental and Natural Slip-surfaces, NSF/SCEC-0106924.

PHYSICAL PROPERTIES OF SAFOD ROCKS

Nikolas Christensen, Herb Wang • University of Wisconsin, Madison

A fundamental part of establishing rigorous constraints on structure models and fault mechanics of the San Andreas fault zone rests in understanding the physical properties of rocks from the SAFOD borehole and the country rock sampled from outcrop. Once sufficient numbers of samples are obtained by drilling and detailed mapping has been conducted in the vicinity of the drillhole, we plan a major investigation of physical properties of SAFOD rocks. Our study is designed to link the geological observations with the geophysical studies in the vicinity of the drill site. It will consist of five major physical property measurements: (1) Compressional wave velocities, (2) shear wave velocities, (3) differential strain analysis, (4) poroelastic constants, and (5) density. Components (1), (2) and (5) will complement existing surface-based geophysical surveys and downhole measurements that produce seismic velocity and density images. Component (3) will provide information about microcrack populations, which are both present in situ and induced from drilling damage or stress relief when core is removed to the surface. Component (4) will characterize the properties of the San Andreas fault zone for hydromechanical modeling, which is key to understanding patterns of seismicity influenced by pore pressure changes. The combined set of measurements provides constraints on the geologic and lithologic composition, the physical state of the rock, and the presence, location, and pressure of fluids in the rock. Compressional and shear velocities will be measured in specimens from the borehole and from outcrop at sufficient confining pressures (200 to 600 MPa) to eliminate the influence of drilling and sampling produced microcracks on velocities. With these measurements, Vp/Vs values and elastic constants can be determined and compared with field generated velocity cross-sections. Shear-wave splitting will be analyzed as an indicator of anisotropy. Electron backscatter diffraction (EBSD) and petrofabric analyses will be performed to correlate mineral orientation with seismic anisotropy. The effects on velocities of varying confining pressure and effective pressure of the cores will be studied to better understand the importance of pore pressure and its influence on velocity structure in the vicinity of the drillhole. Differential strain analysis (DSA) measurements have proven useful for delineating stress-relief microcracking effects in samples returned from deep drill holes and interpreting in situ stresses and paleostresses. Also, porosities and densities of the samples are routinely measured in our laboratories. Finally, complete sets of poroelastic constant measurements will be made on the samples as a function of confining and pore pressure to help understand fault mechanics and water level changes associated with fault slip. The poroelastic coefficients, together with the permeability, allow prediction of fluid flow following stress changes.

Pressure vessel capable of measuring velocities as functions of confining pressure, pore pressure,temperature and frequency.

In summary, this research will address key questions about fault strength and crustal lithology by providing rock laboratory measurements at crustal pressures for interpretation of geophysical data in the vicinities of fault zones. The physical property measurements, in combination with geophysical surveys in the vicinity of SAFOD, drilling results, and downhole logging, will provide valuable information on the composition, fabric and structure of the crust adjacent to the drillhole.

ANISOTROPY IN THE SHALLOW CRUST OBSERVED AROUND THE SAN ANDREAS FAULT BEFORE AND AFTER THE 2004 MW6 PARKFIELD EARTHQUAKE

Elizabeth Cochran • University of California, Riverside
Yong-Gang Li • University of Southern California
John Vidale • University of Washington

Local seismic arrays were deployed at two locations along the San Andreas Fault (SAF) near Parkfield, California before and after the 2004 Mw6 Parkfield earthquake. Using local earthquakes we determine the anisotropic field within 1-2 km of the main trace of the SAF at the two array locations separated by 12 km. The initial array, near the SAFOD site, was deployed for six weeks in Oct.-Nov., 2003 and the second array, located near the town of Parkfield, was deployed for 3 months following the 28 September, 2004 Mw6 Parkfield earthquake. We examine crustal shear-wave anisotropy to investigate lateral and possible temporal variation in anisotropy related to the San Andreas fault [Cochran et al., 2006].

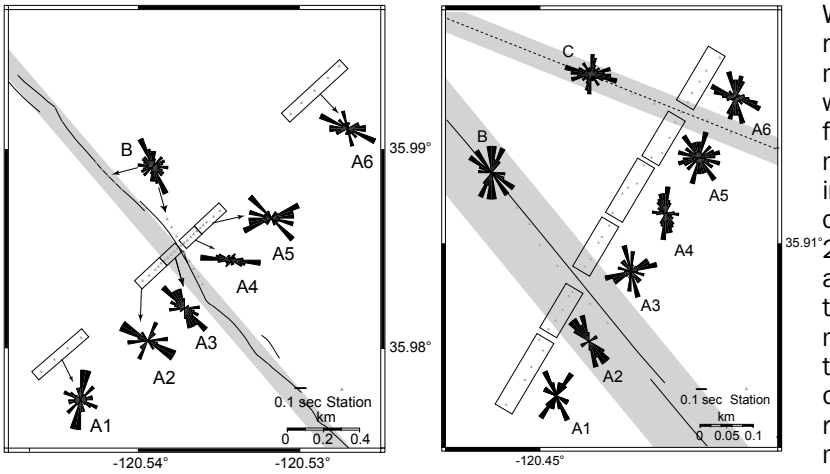

a) Rose diagrams giving a polar histogram of the fast orientations from 2003. Fast directions are grouped by station location. Groups A[1-6] are splitting measurements from the cross fault array and Group B is results from the along fault array. Grey rectangle shows the reduced velocity fault zone as determined by Li et al. [2006]. Plotted fault trace is mapping by Rymer et al. [2006]. b) Rose diagrams giving a polar histogram of the fast orientations from 2004 Fast directions grouped by station location. Groups A[1-6] are splitting orientations from the cross fault array. Group B are the fast orientations from the along fault array on the main trace of the SAF. Group C are those from along the northern branch of the SAF approximate location shown by a dotted line.

We find the fast shear-wave polarization direction nearly fault-parallel (N40°W) for stations on the main fault trace and within 100 m to the southwest of the SAF at both array locations. These fault-parallel measurements span the 100 -150 m wide zone of pervasive cracking and damage interpreted from fault zone trapped waves associated with the main fault core [Li et al., 2004; 2006]. Outside of this zone, the fast orientations are scattered with some preference for orientations near N10°E, roughly parallel to the regional maximum horizontal compressive stress direction. In addition, fast directions are preferentially oriented parallel to a northern branch of the SAF recorded on stations in the 2004 Parkfield deployment. The measured anisotropy field is likely due to a combination of stress-aligned microcracks away from the fault and shear fabric within the highly evolved fault core. A recent study by Boness and Zoback [2004] detailed the anisotropic structure observed at SAFOD Pilot Hole stations and suggest that the anisotropy observed in the drillhole is also likely due to both aligned microcracks and localized shear fabric. We estimate the density of microcracks from the measured delay times and find apparent crack densities are approximately 3%, with large scatter. Most of these data lay outside of the main damage zone so this estimate gives the local, but not fault core, crack density. The data suggest weak depth dependence to the measured delay times for source depths between 2 and 7 km. Below 7 km source depth, the delay times do not correlate with depth suggesting higher confining pressure force the microcracks to close. No coseismic variation in the anisotropic parameters is observed suggesting little to no influence on measured splitting due to the 2004 Mw6 Parkfield earthquake. However, the pre- and post- mainshock data presented here are from arrays separated by 12 km limiting our sensitivity to small temporal changes in anisotropy.

Boness, N.L. and M.D. Zoback, Stress-induced seismic velocity anisotropy and physical properties in the SAFOD Pilot Hole in Parkfield, CA, Geophys. Res. Lett., 31, L15S17, doi:10.1029/2003GL019020, 2004.

Cochran, E.S., Y.-G. Li, J.E. Vidale, Anisotropy in the shallow crust observed around the San Andreas Fault before and after the 2004 Mw6 Parkfield earthquake, Bull. Seismol. Soc. Am., 96, S364-S375, 2006.

Li, Y-G., J.E. Vidale, E.S. Cochran, Low-velocity damaged structure of the San Andreas Fault at Parkfield from fault zone trapped waves, Geophys. Res, Lett. 31, L12S06, doi:10.1029/2003GL019044, 2004.

Li, Y.-G., P. Chen, E.S. Cochran, J.E. Vidale, and T. Burdette, Seismic Evidence for Rock Damage and Healing on the San Andreas Fault Associated with the 2004 Mw6 Parkfield Earthquake, Bull. Seismol. Soc. Am., 96, S349-S363, 2006.

Many thanks to Z. Peng for the use of his automated splitting code and to SAFOD PIs S. Hickman, W. Ellsworth, and M. Zoback. This study was supported by NSF/EarthScope Grant EAR-0342277 and the Southern California Earthquake Center. SCEC is funded by NSF Cooperative Agreement EAR-0106924 and USGS Cooperative Agreement 02HQAG0008.

EPISODIC TREMOR AND SLIP LOCATIONS USING EARTHSCOPE DATA

Kenneth Creager, Aaron Wech, Stephen Malone • University of Washington

Every 14 months the Pacific Northwest experiences slip on a fault that is the equivalent of a magnitude 6.5 earthquake. While a typical earthquake of this magnitude, happens in less than 10 seconds, the duration of these Episodic Tremor and Slip (ETS) events is two or more weeks. The EarthScope Facility will allow us to probe the last two ETS events in unprecedented detail. To locate tremor, we select a 15-minute time window, band-pass filter from 2-6 Hz, calculate the envelope function and low-pass filter to 0.1 Hz. All pairs of envelope functions are cross correlated. For each point in a spatial grid the differential S-wave travel time for each station pair is calculated. The cross-correlation values at those differential times are determined and summed over all the station pairs. The tremor source is estimated to be at the location that provides the best weighted sum of cross correlations. Using this method we have located 150 tremor bursts, approximately evenly spaced in time, for the September 2005 and January 2007 ETS events in northern Washington and southern Vancouver Island. The locations of tremor for these two episodes are quite similar, although the migration pattern is very different. The 2005 sequence initiated just south of the San Juan Islands, migrated 50 km to the SW towards Port Angeles, then bifurcated heading simultaneously NW and SE. On the other hand, the 2007 episode started in the southern Puget Sound region and headed linearly NW at a nearly constant rate of about 10 km/day ending at southern Vancouver Island. This method locates epicenters of typical earthquakes to within a few km, but errors in depths can be 10 or more km. Similarly, the tremor appears to be robustly located in epicenter, but not in depth. Data from the EarthScope Transportable Array, PBO borehole seismometers and the Pacific Northwest Seismograph Network are currently used in the locations. Data for the 2007 ETS recorded on the 62 stations of the EarthScope Flexible-Array CAFE experiment are being retrieved from the field as this report is being written. An important, unresolved question is whether the tremor is occurring on the plate interface or distributed in depth from the plate interface up into the continental crust. These stations, which include 3 small-aperture arrays designed specifically for elucidating tremor should allow us to determine the tremor depths. We also deployed 11 EarthScope seismometers in an array near Port Angeles that captured the September, 2005 event. During the week or so that the tremor was within 40 km of the array, the polarization of particle motion was aligned with the direction of plate motion, which is predicted if the tremor was caused by slip on the plate boundary.

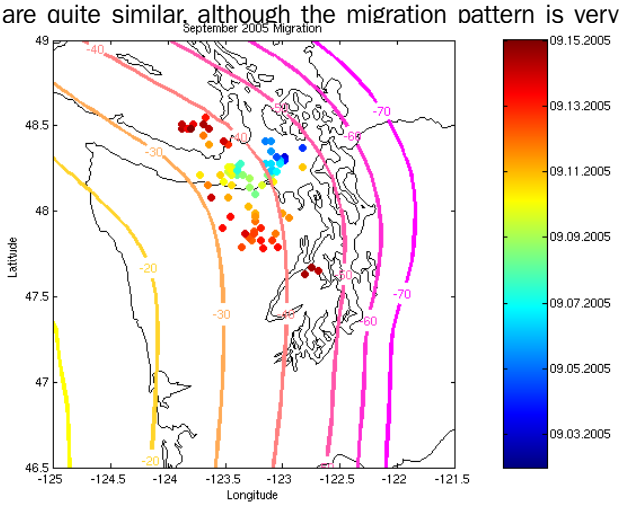

Map showing locations of deep tremor bursts (dots) color coded by date from September 2 through September 15, 2005. Contours indicate depth (km) to the subducting plate interface. Tremor continued until the end of September, but we have not yet located the later events.

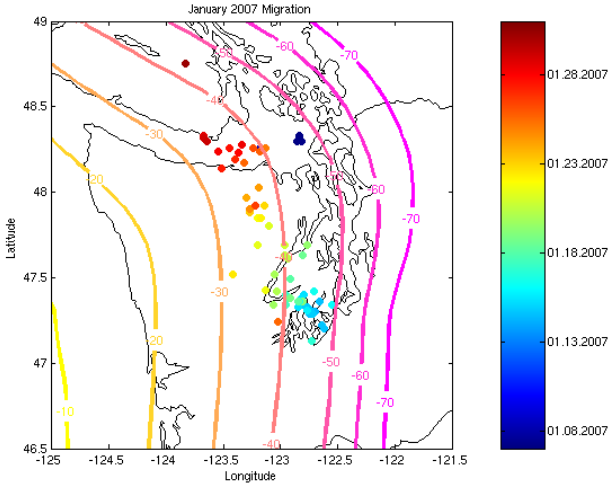

Map showing locations of tremor bursts for the January, 2007 ETS.

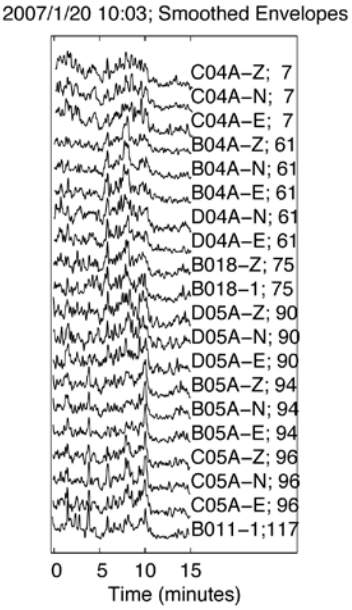

Examples of 15-minute envelope functions from EarthScope Transportable Array and PBO borehole seismometers that are used to locate one of the tremor bursts. Envelopes are aligned on the relative predicted time assuming a shear-wavespeed model. Labels indicate station name, sensor orientation and epicentral distance (km).

TRANSIENT MOTIONS IN THE BASIN AND RANGE FROM BARGEN GPS DATA

J. L. Davis, E. Malikowski • Harvard-Smithsonian Center for Astrophysics
B.P. Wernicke, K. Mahan • California Institute of Technology

We have been examining transient motions on a range of spatial and temporal scales using the Basin and Range Geodetic Network (BARGEN). The network currently consists of 70 GPS sites installed at various times beginning in 1996. The accuracy of the velocities for the longer-running sites is ~0.2 mm/yr [Davis et al., 2004]. Comparison of the present-day geodetic rates across the Wasatch fault with geologic displacement rates over the last few kyr, ~100 kyr, and 10 Myr implies that measurements of strain accumulation and strain release may be strongly timescale-dependent [Friedrich et al., 2003]. If, however, local strain accumulation and release are influenced by the viscoelastic diffusion of stress, then we might expect a significant difference between displacement rates inferred from geologic evidence and geodesy. Elósegui et al. [2004] showed that transient deformation at GPS sites near Great Salt Lake is caused by crustal loading associated with lake-level changes. In addition to seasonal variations, the level of Great Salt Lake between 1996–2002 had a slow variation of ~1.5 m that caused a loading signature of ±1.5 mm radial and ±0.7 mm horizontal in the GPS time series. Large-scale transients have also been identified. Sites of the northern transects of BARGEN located generally to the west of 146° W longitude display an eastward velocity change in late 1999 [Davis et al., 2006]. The change in velocity for these sites, and the constant velocities for sites in the east, are evident from the time series. The velocity changes may be evidence for an episodically creeping detachment horizon ~500 km wide at or near the base of the crust in the western part of the network.

Davis, J. L., R. A. Bennett, and B. P. Wernicke, Assessment of GPS velocity accuracy for the Basin and Range Geodetic Network (BARGEN), Geophys. Res. Lett., 30, 1411, doi:10.1029/2003 GL016961, 2003.

Davis, J. L., B. P. Wernicke, S. Bisnath, N. A. Niemi, and P. Elósegui, Subcontinental-scale crustal velocity changes along the Pacific–North America plate boundary, Nature, 441, doi:10.1038/nature04781, 2006.

Elósegui, P., J. L. Davis, J. X. Mitrovica, R. A. Bennett, and B. P. Wernicke, Crustal loading near Great Salt Lake, Utah, Geophys. Res. Lett., 30, 1111, doi:10.1029/2002GL016579, 2003.

Friedrich, A. M., B. P. Wernicke, N. A. Niemi, R. A. Bennett, and J. L. Davis, Comparison of geodetic and geologic data from the Wasatch region, Utah, and implications for the spectral character of Earth deformation at periods of 10 to 10 million years, J. Geophys. Res., 108, 2199, doi:10.1029/2001JB000682, 2003.

Supported by the National Science Foundation, the Department of Energy, and the Caltech Tectonics Observatory.

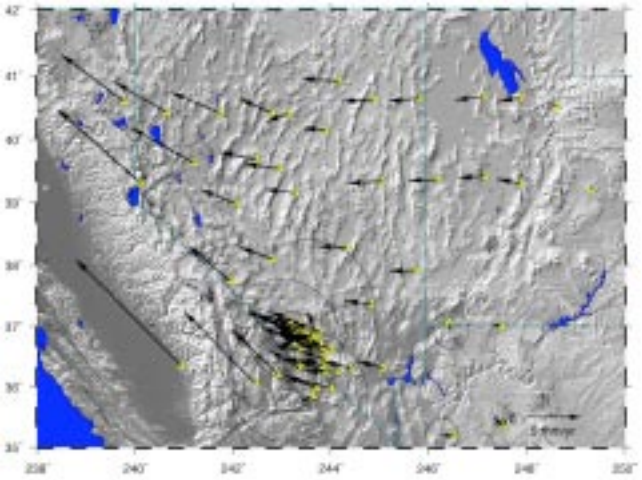

Velocity solution for the BARGEN network as of Sept. 2006.

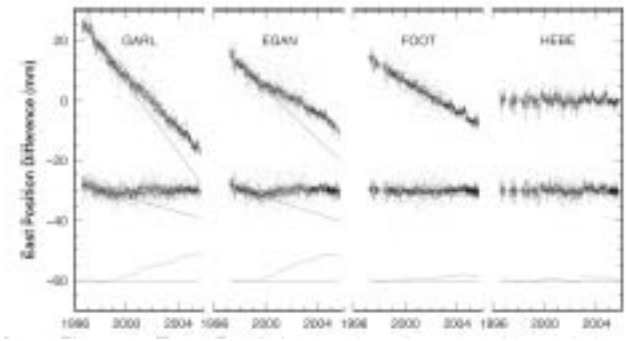

Top: "Raw" time series of east position relative to North America. The straight line is the best-fit straight line using position estimates from the first 2.5 years. Middle: Residuals of the raw time series from a best-fit model consisting of a straight line and time-variable seasonal terms. Bottom: Smoothed residuals relative to the 2.5 yr fit. The final time series indicates deviation from temporally linear motion. Site w. longitudes: GARL, 119° 21'; EGAN, 114° 56'; FOOT, 113° 48'; HEBE, 111° 22'. From Davis et al. [2006].

USING LIDAR DIGITAL TOPOGRAPHIC DATA TO DETERMINE FAULT SLIP RATES ALONG THE FISH LAKE VALLEY FAULT ZONE

James F. Dolan, Kurt L. Frankel • University of Southern California, Los Angeles

The Fish Lake Valley fault zone, together with its southern continuation in Death Valley (the Death Valley fault zone), is the largest and most continuous fault system in the eastern California shear zone (ECSZ). This Death Valley-Fish Lake Valley fault system (DV-FLVFZ) extends 310 km northward from its intersection with the Garlock fault . Both geologic and geodetic observations suggest the DV-FLVFZ accommodates the majority of deformation in the ECSZ north of the Garlock fault. In this study, we will address questions of the spatial and temporal constancy of seismic strain accumulation and release by determining long-term slip rates at time scales of 103 to 105 years from different locations on the DV-FLVFZ. Our recent acquisition of ~420 km2 (collected in a one-kilometer to four-kilometer-wide, along-strike swath) high-resolution (one-meter horizontal, 10- to 15-centimeter vertical) digital LiDAR topographic data will allow us to map deformed Pleistocene and Holocene landforms in unprecedented detail.

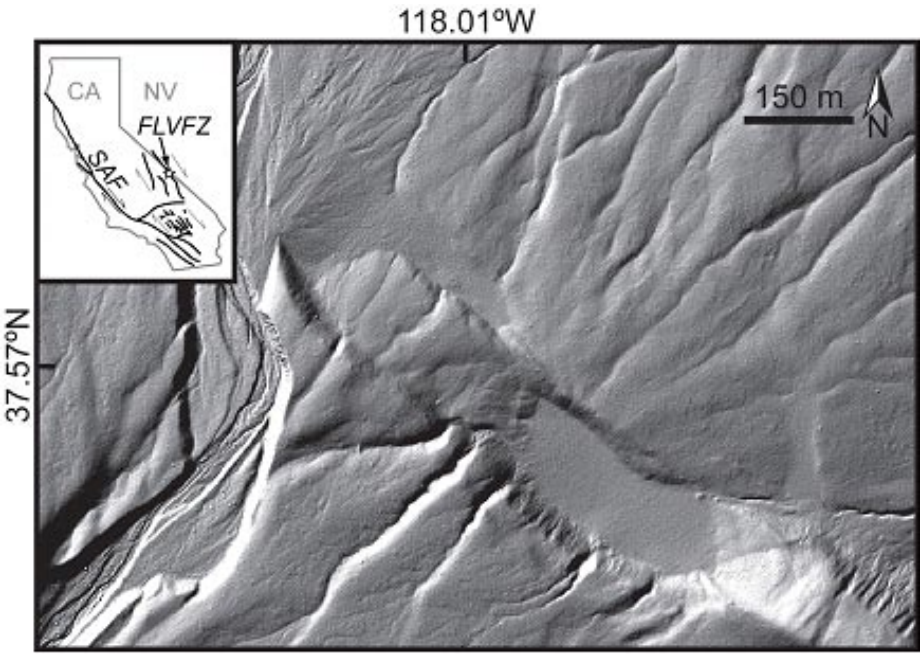

One-meter resolution LiDAR image of the Furnace Creek alluvial fan complex in central Fish Lake Valley, California. The alluvial fan is offset by the right-lateral Fish Lake Valley fault zone. The star on inset index map indicates the approximate location of the Furnace Creek site. FLVFZ = Fish Lake Valley fault zone. SAF = San Andreas fault. Modified from Frankel et al. [in prep].

Dating of these offset landforms by terrestrial cosmogenic nuclide (TCN) and optically stimulated luminescence (OSL) techniques will yield slip rates at a variety of time scales. The slip rates that we will generate by combining with TCN and OSL geochronology will fill in one of the last major missing pieces of the slip rate "puzzle" in the ECSZ. These data, in combination with published rates, will also provide a synoptic view of the cumulative slip rates of the major faults of the ECSZ north of the Garlock fault. Comparison of these longer-term rate data with short-term geodetic data will allow us to determine whether or not strain storage and release have been spatially and temporally constant along this part of the Pacific-North America plate boundary during Holocene to late Pleistocene time.

This investigation was supported through the EarthScope GeoEarthScope program.

RESOLVING SUBTLE EPISODES OF TREMOR AND SLIP

H. Dragert • Geological Survey of Canada

Examination of the past 12 years of seismic and continuous GPS data for northwestern Washington and southern Vancouver Island has shown that this part of the Cascadia subduction zone is marked by clearly recognizable, repeated episodes of deep plate slip and seismic tremors, called Episodic Tremor and Slip (ETS). For this part of the Cascadia margin, these prolonged ETS episodes last anywhere from a week to a month and, over the past 12 years, have occurred fairly regularly with a recurrence interval of 14.5 +/- 1.2 months. Shorter, more sporadic episodes of seismic tremor have been observed at other times throughout northern Cascadia, but corresponding crustal displacements have not been well resolved with GPS, leaving unanswered the question of whether the identical phenomenon is taking place for these more random tremor events. Data from PBO borehole strainmeters (BSM) recently installed under the EarthScope Project may provide the answer. A recent four-day episode of seismic tremor in central Vancouver Island resulted in ill-defined surface displacements at the closest continuous GPS stations. However, strain data from the BSM (B012) at Ucluelet, located on the west coast of central Vancouver Island, are consistent with an episode of slip on the deeper subducting plate interface to the northeast of this site, the region where the tremors were observed. Simple elastic dislocation models with

Area of tremor occurrence on Vancouver Island from November 9 to 12, 2006. The shaded region in central Vancouver Island indicates the primary area of tremor activity for this four-day period. The location of the B012 strainmeter is indicated by the red circle. Blue squares mark the location of nearby continuous GPS stations, none of which showed significant displacements coincident with tremor activity.

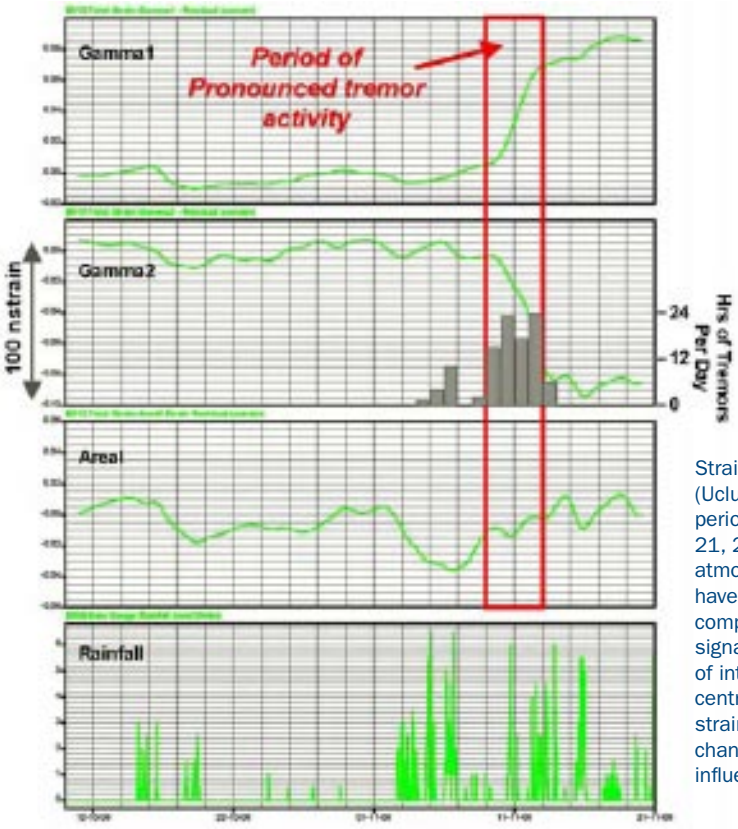

Strain components at B012 (Ucluelet, Vancouver Island) for the period of October 10 to November 21, 2006. Linear trends and atmospheric pressure signals have been removed. Shear strain components show a significant signal associated with a period of intense tremor activity in central Vancouver Island. Areal strain variations show a smaller change and appear to be strongly influenced by rainfall.

2 to 3 cm of slip constrained to the subducting plate interface can replicate the observed strain signal as well as the limited surface displacements. These results suggest that BSM data may prove critical in identifying more subtle slip events and that sporadic, shorter episodes of tremor can be associated with slip on smaller asperities. Establishing the locations, size distribution, and recurrence patterns for the slip asperities is critical for understanding the processes involved in ETS and the relationship of ETS to regional earthquakes.

STRUCTURAL AND PETROLOGIC ANALYSES OF THE SAN ANDREAS FAULT IN THE SAFOD REGION

James Evans, Kelly Bradbury, Sarah Draper • Utah State University

We examine the lithology and structure of the fault zone complex encountered by the SAFOD borehole. We use drill cutting samples, sidewall cores, whole core samples, and wireline log data to constrain the subsurface geology at SAFOD, and, to develop a cm to 100's m scale understanding of the deformation and fluid-rock interactions that have occurred in the fault zone. We make extensive use of rock samples, and curation is critical for their use in the future. We use petrography of cuttings and core, X-Ray diffraction analysis, electric log image data, and borehole geophysical data to determine the nature of the fault zone at depth.. We [Bradbury et al., in review] identify lithological assemblages and infer the presenceof at least five major fault zones intersected by the borehole. Draper [2007] shows that the arkosic section is a deformed fault-bound block between the modern strand of the San Andreas fault and the Buzzard Canyon fault to the southwest with at least ten intraformational faults and two major block-bounding faults. Zircon fission-track cooling ages indicate a maximum age of earliest Paleocene for the arkoses. We suggest, based on the cooling history, petrography, and geophysical properties that these rocks are equivlent to a sequence of Eocene rocks derived from a fan complex shed off the Salinian block in the Paleocene-Eocene [Nilsen and Clarke, 1975; Nilsen, 1984, 1987] and that the SAF has most of the slip in the area. The entire zone between the Buzzard Canyon and San Andreas (senso stricto) faults at depth appear to contain a series of southwest-dipping faults and damage zones that bound blocks with a variety of bedding and fracture orientations. In detail the seismic velocities, which appear to depend at least in part on the presence of fracture zones and faults, are highly variable. Each of the larger faults zones have different characteristics. Continuing work will examine: 1) petrographic and microstructural analyses of sidewall cores; and 2) structure and composition of the deepest portions of the borehole; and 3) analysis of Vp and Vs data and its correlation with the presence of faults. Review of the sidewall cores in comparison to our results from cuttings analyses may substantiate our previous interpretations and allow for further understanding of deformation processes active at seismogenic depths. Further insights from core across the fault zone will require careful sample handling and curation, Examining the relationships between the borehole geophysical data and the lithologic data will further constrain the structure and composition of the borehole, and geochemical, microstructural, and isotopic studies of the cored intervals will allow us to examine the deformation mechanisms within the fault zone, and allow us to evaluate the fluid-rock interactions active at seismogenic depths.

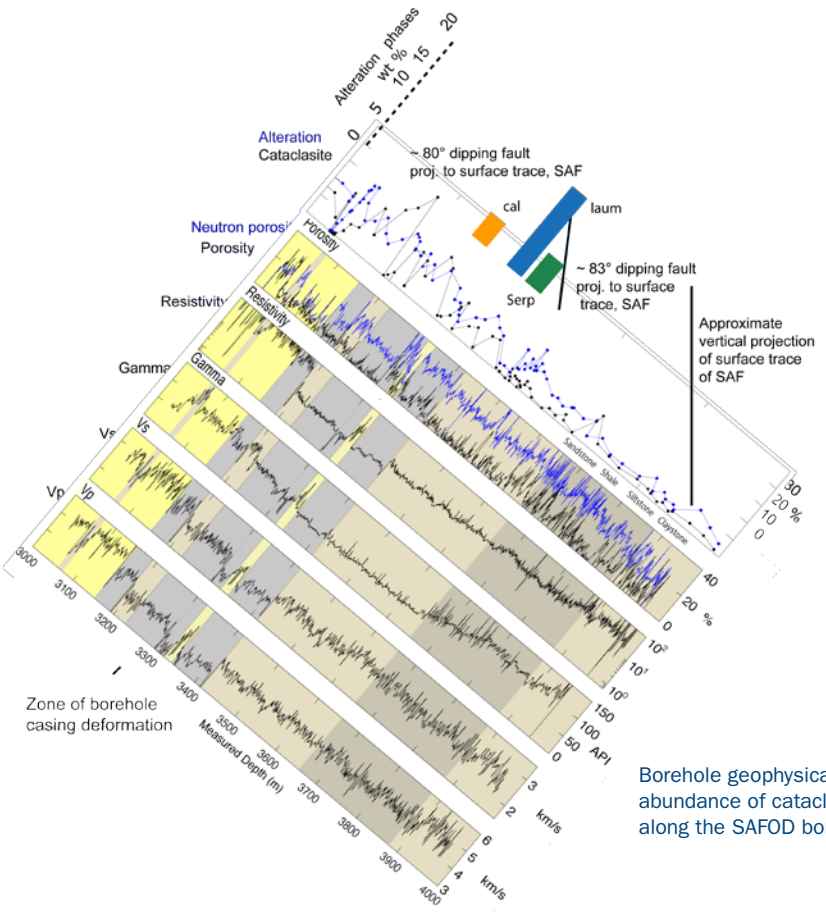

Borehole geophysical logs plotted with the abundance of cataclasite and alteration, along the SAFOD borehole trajectory.

Bradbury, K.K., Barton, D.C., Solum, J.G., Draper, S.D., Evans, J.P., in review, Mineralogic and textural analyses of drill cuttings from the San Andreas Observatory at Depth [SAFOD] boreholes: Initial interpretations of fault zone composition and constraints on geologic models: submitted to Geosphere, 2006.

Solum, J.G., Hickman, S.H., Lockner, D.A., Moore, D.E., van der Pluijm, B.A., Schleicher, A.M., and Evans, J.P., 2006, Mineralogical characterization of protolith and fault rocks from the SAFOD main hole: Geophysical Research Letters, v. 33, doi: 10.1029/

Funding from a National Science Foundation grant EAR-0454527 to Evans, a DOSECC grant to Draper, and a SCEC grant to Evans. We thank collaborators Judi and Fred Chester, David Kirschner, John Garver, John Solum, and undergraduates Corey Barton, Kelly Mitchell, Tamara Jeppson, and Kellen Springer for data acquisition and analysis.

MEASURING THE FLUID FLOW AND ELASTIC PROPERTIES OF CORE COLLECTED FROM SAFOD

Daniel Faulkner • University of Liverpool, UK
Ernest Rutter • University of Manchester, UK

Our recent research efforts have concentrated on measuring the permeability of fault zones to identify whether they may act as long term seals, leading to elevated pore fluid pressures and mechanical weakening [Faulkner and Rutter, 2000; 2001; 2003]. We have investigated the effect of temperature and stress on the permeability and permeability anisotropy of phyllosilicate-rich fault gouges from a major, well-exposed fault zone in Spain, as a precursor to applying the same methodology to SAFOD core. We have also gained experience in handling and preparing highly friable fault zone rocks. We have shown that the permeability anisotropy of phyllosilicate-rich gouge can vary by up to three orders of magnitude [Faulkner and Rutter, 2000]. This, and the very low permeability perpendicular to the fault zone (10-21 m^2) indicates that this material will perform as an effective seal [Faulkner and Rutter, 2001]. We have also made measurements that indicate that temperature plays an important role [Faulkner and Rutter, 2003]. Increasing temperature in the shallow crust may lead to enhanced fluid flow (increased permeability), whereas at deeper crustal levels, temperature will steadily reduce the permeability of these types of fault materials. Elastic properties of fault materials Recent research [Faulkner et al., 2006] has suggested that fracture damage surrounding fault zones will affect the elastic properties of the rock, leading to modification of the stress state in the close vicinity (~200m) of large faults. Stress modification, in particular stress rotation, is necessary to allow high pore fluid weakening of non-optimally oriented faults, such as the San Andreas fault is believed to be. Models can be tested by laboratory measurements of the elastic properties of rocks surrounding the fault zone that are being collected as part of the SAFOD programme. The SAFOD borehole, its instrumentation and the core sample materials that will have been collected by the end of the 2007 phase represent a uniquely important scientific resource that will enable many of the most significant questions, that have been outstanding for many years, to be answered. A great many investigations will be carried out by a large number of scientists, but this will only be possible if the sample materials acquired at such great effort are properly cared for over an extended time period, and with minimal wastage in their subsequent use.

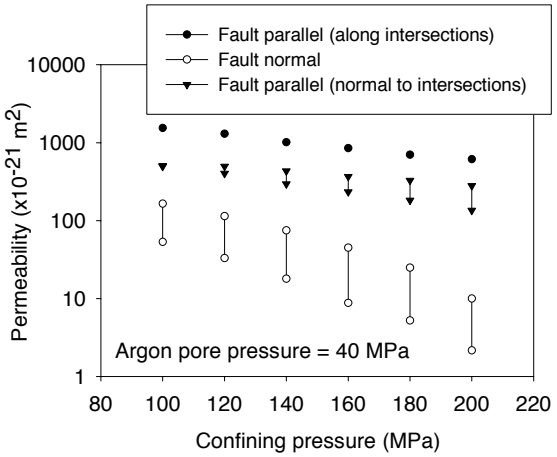

Permeability anisotropy as a function of effective pressure of natural phyllosilicate-rich fault gouge using argon as the pore fluid.

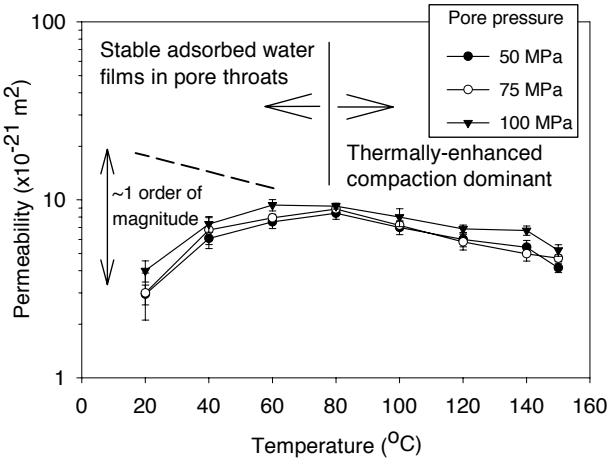

The effect of temperature on the permeability of natural phyllosilicate-bearing fault gouge. Confining pressure was 200MPa for all measurements.

Faulkner, D.R. and Rutter, E.H. 2000. Comparisons of water and argon permeability in natural clay-bearing fault gouges under high pressure at 20degC. Journal of Geophysical Research 105, 16415-16426.

Faulkner, D.R. and Rutter, E.H. 2001. Can the maintenance of overpressured fluids in large strike-slip fault zones explain their apparent weakness? Geology 29, 503-506.

Faulkner, D.R. and Rutter, E.H. 2003. The effect of temperature, nature of the pore fluid, and sub-yield differential stress on the permeability of phyllosilicate-rich fault gouge. Journal of Geophysical Research 108, No. B5, 10.1029/2001JB001581.

Faulkner, D.R., Mitchell, T.M., Healy, D. and Heap, M.J. 2006. Slip on 'weak' faults by the rotation of regional stress in the fracture damage zone. Nature, 444, 922-925. doi:10.1038/nature05353.

Natural Environment Research Council (UK) grants: GR3/11184, NER/A/A/2000/00468 and NE/C001117/1. The Nuffield Foundation (UK).

FAULT SLIP RATES ON THE NORTHERN DEATH VALLEY FAULT ZONE: IMPLICATIONS FOR PACIFIC-NORTH AMERICA PLATE BOUNDARY DEFORMATION

Kurt L. Frankel, James F. Dolan • University of Southern California
Robert C. Finkel • Lawrence Livermore National Laboratory
Lewis A. Owen • University of Cincinnati

The exact slip rate of the northern Death Valley fault zone (NDVFZ) has long been one of the last major missing pieces of the kinematic puzzle in the eastern California shear zone (ECSZ). Published models of geodetic data suggest the NDVFZ is storing much, and perhaps almost all, of the Pacific-North American plate boundary strain in the ECSZ north of the Garlock fault. However, the scarcity of geochronologically defined long-term slip rates has made it difficult to determine whether strain storage and release have been constant along this part of the plate boundary. Here, we present the first geochronologically determined geologic fault slip rate along the NDVFZ zone using high-resolution digital topographic data and cosmogenic nuclide surface exposure ages.

We have acquired 46 square kilometers of airborne laser swath mapping data (ALSM or LiDAR) from two locations along the NDVFZ. We are in the process of obtaining an additional ~400 square kilometers along the remainder of the northern Death Valley and Fish Lake Valley fault zones. The scarcity of vegetation in the study area is ideal for acquisition of ALSM data to survey deformed geomorphic features because removal of data points related to returns from the top of plants does not reduce the point density of bare-earth shots, as it might in a heavily-canopied area. ALSM data facilitate the efficient identification, mapping, and analysis of tectonically active landscapes in unprecedented detail. We use ALSM data to determine late-Pleistocene to Holocene fault offset along the northern Death Valley fault system and illustrate the utility of these data for active tectonics research. Surveying of deformed geomorphic features and the construction of high-precision topographic maps, which would take days to weeks with traditional methods, are accomplished in minutes using ALSM data. Digital elevation models (DEMs) derived from the ALSM data can also be used to generate maps of surface slope, curvature, and roughness to reveal subtle topographic features, produce reconnaissance surficial geologic maps, and measure fault offset. In addition, the DEMs can be artificially illuminated from any azimuth and elevation to highlight previously unrecognizable structures.

The initial focus of our study has been the dextrally-offset Red Wall Canyon alluvial fan along the NDVFZ (see Figure 1). Analysis of ALSM data reveals 297 ± 9 m of right-lateral displacement on the fault system since the late Pleistocene. In situ cosmogenic 10Be geochronology was used to date the Red Wall Canyon alluvial fan and a second, correlative alluvial fan also offset by the fault. 10Be dates from large cobbles and boulders provide a maximum age of ~70 ka for the offset landforms. Two other research groups have collected cosmogenic 36Cl depth profiles at the Red Wall Canyon site. These data will be combined with our 10Be dates to provide a more precise age for the offset alluvial fan (Frankel et al., in prep). Dividing the offset measurement with the cosmogenic 10Be surface exposure age yields a late-Pleistocene to recent minimum fault slip rate of ~4.3 mm/yr. Summing this rate with previously published rates on the Owens Valley and Saline Valley-Hunter Mountain fault zones at similar latitudes suggests a total, preferred long-term geologic rate across the northern ECSZ of ~9 mm/yr. This rate is commensurate with short-term geodetic data in the northern half of the ECSZ and implies the apparent discrepancy between geologic and geodetic rate data observed in the Mojave section of the ECSZ does not extend north of the Garlock fault. We suggest the lack of agreement between geologic and geodetic rate data in the southern half of the ECSZ may therefore be the result of local structural complexities in the Pacific-North America plate boundary, such as the Big Bend of the San Andreas fault.

AUGUSTINE VOLCANO: PBO DATA

Jeff Freymueller • University of Alaska

PBO data recorded before and during the eruption of Augustine Volcano provided new insights into the magmatic plumbing system at Augustine volcano, as well as surprises that will require further research to understand. These results give an example of the future gains expected from measuring deformation at other PBO volcanoes.

The first sign of unrest at Augustine appeared in early summer 2005, with an increase in seismicity accompanied by a small inflation signal. Surprisingly, from the beginning the inflation signal indicated a source at shallow depth, roughly at sea level. Campaign GPS measurements over the 15 years prior to the eruption indicated no previous accumulation of magma at such shallow depth. The initial inflation source was small, detectable only by high-quality continuous GPS, and it may be that deformation associated with the rise of this small initial pod of magma was simply too small to record with GPS – strainmeters or tiltmeters such as those that PBO plans to install might have provided further important data about the initial rise of magma.

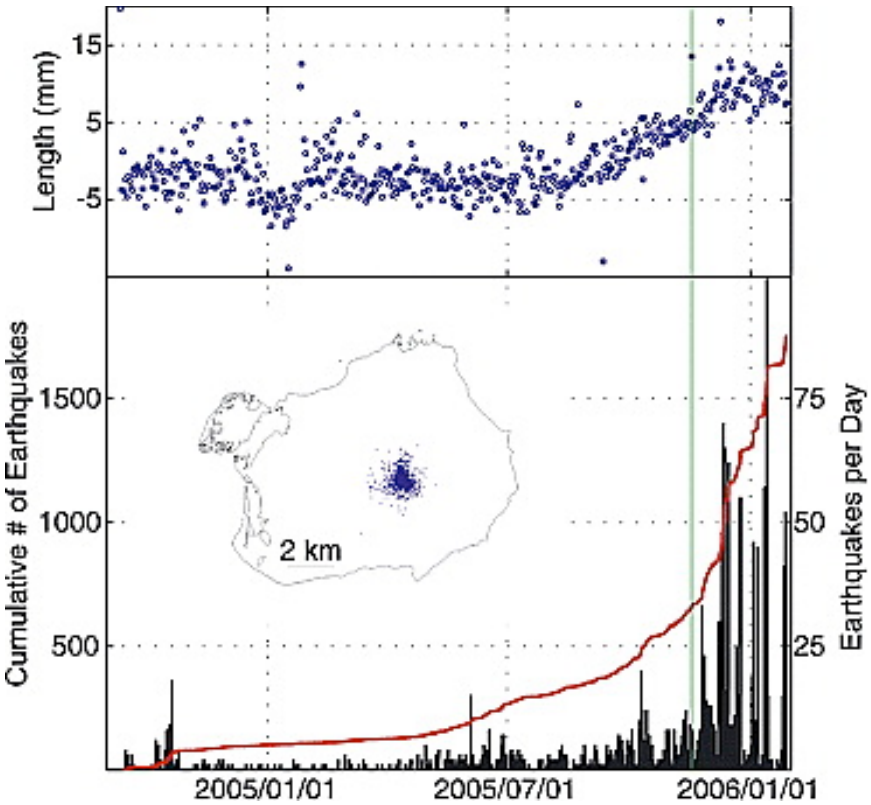

Time series of geodetic data and earthquake occurrence. (Top) The line length between GPS stations AV02 and AV03 as a function of time. (Bottom) A temporal histogram of located earthquakes, with the inset showing epicentral locations. The red line denotes the cumulative number of located earthquakes. The green vertical line marks November 17, 2005, the purported beginning of dike ascent. From Cervelli et al. [2006].

Once significant extrusion of magma began, about two weeks after the first major explosions, the surviving PBO sites recorded a deflation signal with a different spatial pattern than the inflation. Although only weakly constrained by PBO data because two sites were destroyed quickly, the deflation source clearly came from a significantly greater depth than the inflation source. Additional data from temporary sites deployed just before the volcano became too dangerous to visit helped constrain the source depth to mid-crustal depths. Together with the lack of pre-eruptive deformation prior to 2005, these observations lead to a model for the magma rise in which small leading pods ascended from mid-crustal depths, eventually reaching the surface. After there was a continuous magma column from the surface to mid-crustal depths, sustained extrusion began.

The destruction of some sites in the initial explosions and the first major pyroclastic flow also illustrated the need for redundancy in network design. Additional instrumentation installed on Augustine since the eruption addresses that need. The value of additional temporary continuous sites also suggests a future use for part of the PBO campaign instrument pool, as long as funding and approval for rapid response can be obtained.

Cervelli, P. F., T. Fournier, J. Freymueller, and J. A. Power (2006), Ground deformation associated with the precursory unrest and early phases of the January 2006 eruption of Augustine Volcano, Alaska, Geophys. Res. Lett., 33, L18304, doi:10.1029/2006GL027219.

DOES THE BERING PLATE EXIST?

Jeff Freymueller • University of Alaska
Mikhail Kogan • Columbia University

The boundary between the North American and Eurasian plates at the Mid-Atlantic Ridge is well known, but another and more diffuse boundary zone between the same two plates is found on the other side of the world, in eastern Siberia. A broad region from the Cherksiy Range in Siberia west to Alaska exhibits seismicity consistent with a rigid Bering Plate that moves independently of both Eurasia and North America. But does a rigid Bering Plate exist, and if so, what drives its motion? What are the implications for the tectonics of the broader region? These are the questions that motivate our ongoing NSF-funded study. We are carrying out GPS measurements of sites in Russia and Alaska to test the hypothesis. Most sites in Russia were newly established for this project, but in Alaska we have leveraged older data and have preliminary results.

We use data both from western Alaska and the Bering Sea islands, which may record Bering plate motion directly, and from the Aleutian arc, where site velocities record a superposition of translation of the arc (possibly as part of the Bering Plate) and elastic strain from the locked subduction zone . Separation of these two signals is possible where the observing network is sufficiently large, such as in the Andreanof Islands of the western Aleutians and parts of the Alaska Peninsula. In the Andreanof Islands, we find that the plate interface has both completely locked and completely creeping regions, and the locked region corresponds almost exactly to the combined rupture areas of the 1986 and 1996 M7.9 earthquakes. We also are investigating deformation associated with the 2006 M7.7 Koryak Highlands earthquake sequence.

This investigation will rely heavily on EarthScope PBO stations installed in western Alaska in the Aleutians.

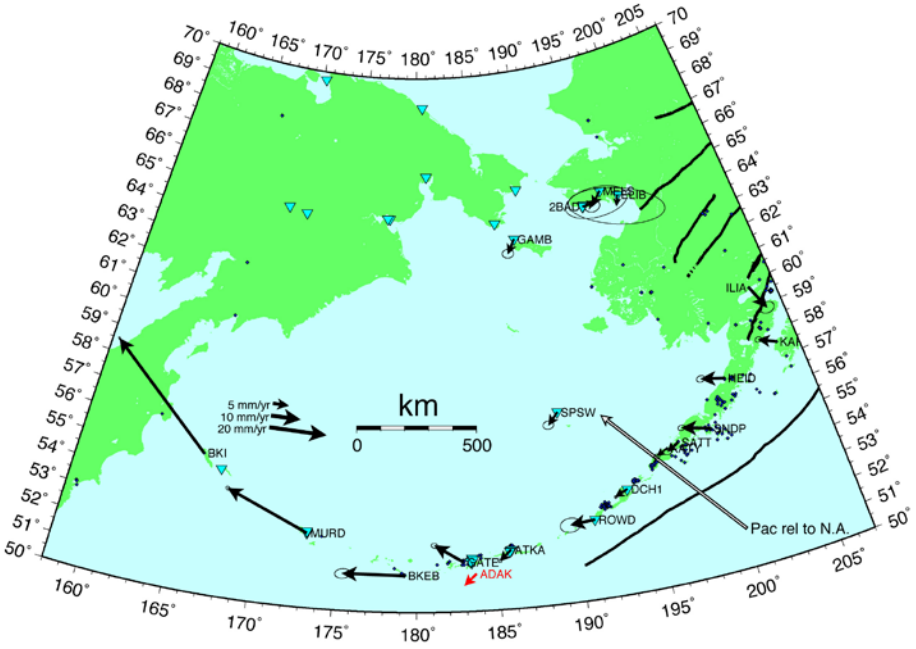

Velocities relative to North America for sites in the region of the hypothesized Bering Plate. Sites observed in this project are shown by blue triangles. The red vector is the velocity of the Aleutian arc crust at Adak inferred from modeling of elastic strain from the locked subduction zone.

PLATE COUPLING VARIATIONS IN THE 1964 ALASKA EARTHQUAKE RUPTURE ZONE

Jeff Freymueller • University of Alaska

The 1964 Alaska earthquake remains the second largest ever recorded, and slip in the earthquake was highly variable in space. Past studies have concluded that coseismic slip was concentrated in two large asperities, one beneath Prince William Sound and the eastern Kenai Peninsula (20-25 m average slip) and the second beneath and offshore of Kodiak Island (10-15 m average slip). Coseismic slip in the gap between them was much smaller, less than 5 meters. Previously, we found that horizontal site velocities measured today with GPS require the present distribution of locked and creeping regions on the plate interface to match the pattern of coseismic slip: the regions of high coseismic slip are locked today, while the region of low coseismic slip is creeping today.

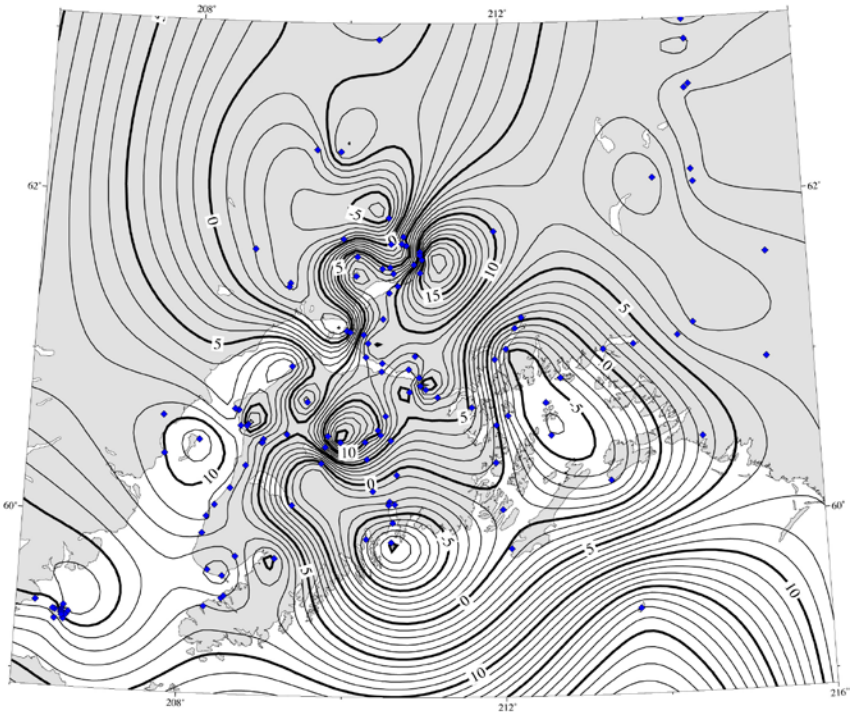

Contour map of vertical velocities in south-central Alaska based on data from 1992-present. Contours are in mm/yr. Small blue diamonds represent GPS sites, mostly campaign GPS surveys. UNAVCO supported this project through many equipment loans over the last decade.

Now, a careful reanalysis of the vertical GPS velocities shows that the Prince William Sound asperity actually consists of two distinct locked regions . GPS velocities show two separate subsidence regions, separated by a ridge of little subsidence. This suggests two distinct locked patches in the subsurface. The “ridge” of low vertical motions corresponds to the inferred edge of the subducted Yakutat block. The eastern subsidence bowl is centered on Prince William Sound, and we interpret it as being due to a locked region on the Yakutat-North America interface. The western patch is located beneath the Kenai Peninsula and we interpret it as being due to a locked region on the Pacific-North America interface.

This investigation was aided by EarthScope geodetic stations.

POSTSEISMIC DISPLACEMENTS FROM PBO SITES NEAR THE DENALI FAULT

Jeff Freymueller • University of Alaska

Large earthquakes offer rare opportunities to measure the response of the lithosphere and mantle to a sudden stress change; we must take full advantage of these opportunities to learn about the mechanical properties of Earth and move beyond kinematic descriptions of active tectonic processes.

Postseismic displacements from PBO sites near the Denali fault show a spatial and temporal evolution that cannot be explained by any single postseismic deformation mechanism [Freed et al., 2006a]. Far-field sites are dominated by deformation from power-law viscoelastic flow in the mantle, consistent with laboratory measurements of olivine rheology [Freed et al., 2006b]. Near-field sites show a significant contribution from afterslip (or possibly localized viscoelastic shear in the lower crust), and a small contribution from poroelastic rebound. While the need to include multiple deformation mechanisms in a successful model now seems clear, the relative contributions of the different mechanisms is less certain, and some important mechanical details remain in dispute. For example, Pollitz [2005] argued for a transient rheology for the mantle rather than a power-law rheology.

More work needs to be done on postseismic deformation models, and this work will require years of additional data. The optimal model is not yet fully constrained by the data. Models that fit the earliest data do not necessarily match the end of the time series, so additional data will be required to narrow down the range of possible mechanical models for the Alaskan lithosphere and mantle. In addition, all present models fit the vertical data poorly (not shown). Vertical displacements include a strong seasonal component, which can only be eliminated by careful modeling based on several years of data.

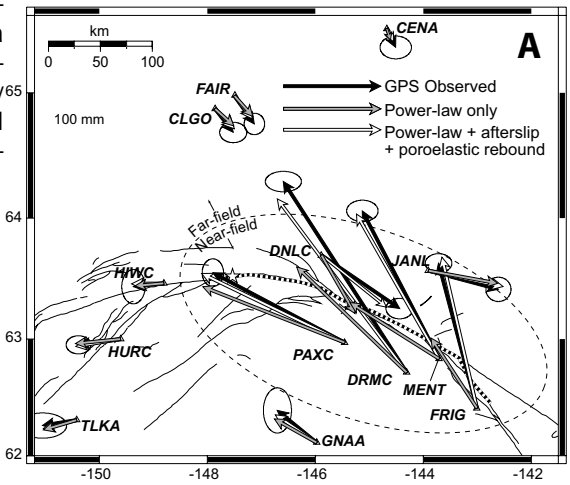

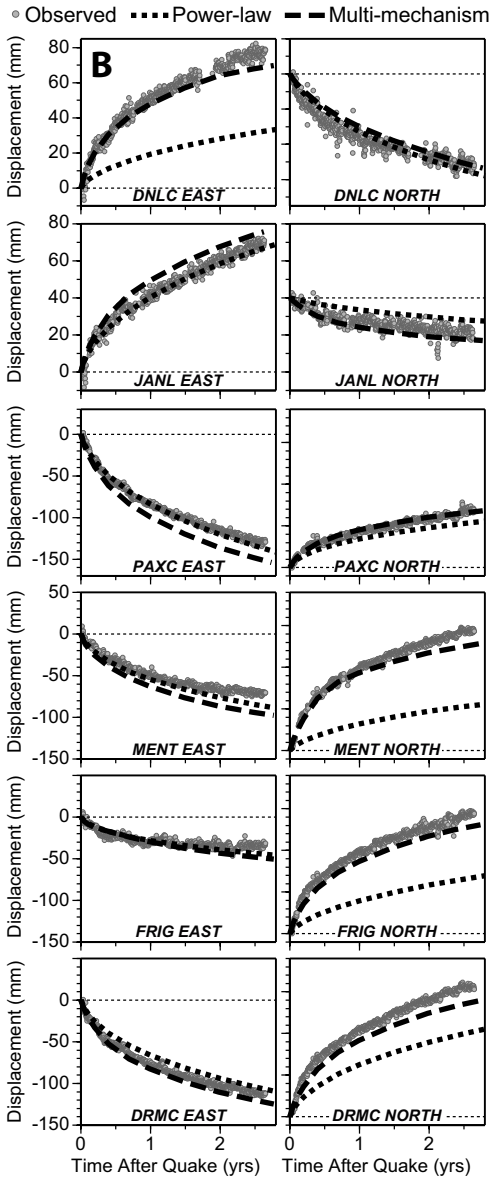

(A) Map view of Denali earthquake postseismic displacements, and model predictions calculated by viscoelastic flow due to power-law (n=3.5) flow and due to a combination of power-law flow, shallow afterslip, and poroelastic rebound. (B) Left columns: Comparison of observed GPS position time-series and displacements. Annual, semi-annual, and secular components have been removed from the observed time series. Right columns: Comparison of GPS observed velocity (based on a logarithmic fit to the data) and the power-law only and the combination model. Horizontal dashed lines indicate zero displacement/velocity. From Freed et al. [2006b].

Freed, A. M., R. Bürgmann, E. Calais, J. Freymueller, and S. Hreinsdóttir (2006a), Implications of Deformation Following the 2002 Denali, Alaska Earthquake for Postseismic Relaxation Processes and Lithospheric Rheology, J. Geophys. Res., doi:10.1029/2005JB003894.

Freed, A., R. Bürgmann, E. Calais, and J. Freymueller (2006b), Stress-dependent power-law flow in the upper mantle following the 2002 Denali, Alaska, earthquake, EPSL, 252, 481-489.

Pollitz, F. F. (2005), Transient rheology of the upper mantle beneath central Alaska inferred from the crustal velocity field following the 2002 Denali earthquake, J. Geophys. Res., 110, B08407, doi:10.1029/2005JB003672.

NORTHERN CALIFORNIA AIRBORNE LIDAR IMAGERY ACQUISITION FOR GEOEARTHSCOPE

K. Furlong, R. Bruhn, D. Burbank, J. Dolan • GeoEarthScope LiDAR Working Group

UNAVCO is coordinating a high resolution Airborne LiDAR survey of the San Andreas fault and other fault systems in northern California. This survey is the first of several major community-guided LiDAR imagery acquisition projects being conducted as part of GeoEarthScope. Approximately 70% of the total plate boundary motion is accommodated across a less-than-100-km-wide region in northern California. The nine counties that comprise the greater San Francisco Bay area, population approximately seven million, lie within this region, making this system of faults among the most important in the U.S. in terms of seismic hazard. Near the southern end of the region, at least half of the plate-boundary motion (25-30 mm/yr out of approximately 50 mm/yr) is concentrated along a single fault, the creeping section of the San Andreas Fault north of Parkfield. However, this situation changes dramatically north of the latitude of Hollister, where this single fault becomes a complex system of strike-slip and reverse faults that traverses the San Francisco Bay region, and continues northward to the latitude of the Mendocino Triple Junction. From the San Francisco Bay area northward to the subduction zone transition, most of the San Andreas motion is taken up by eight principle strike-slip faults: the San Andreas, San Gregorio, Hayward, Rodgers Creek, Maacama, Calaveras, Concord-Green Valley, and Bartlett Springs fault zones. In addition, a number of blind thrusts and reverse faults accommodate contractional motion in the region. The intense forest cover that blankets much of this region has hampered detailed study of these faults, making LiDAR data an especially useful tool. Imagery from this project will also connect with LiDAR imagery collected on the southern San Andreas fault as part of the "B4" project. Through this project and the B4 project, both supported by UNAVCO, the entire length of the San Andreas and other major fault systems in California will have been imaged with high resolution airborne LiDAR.

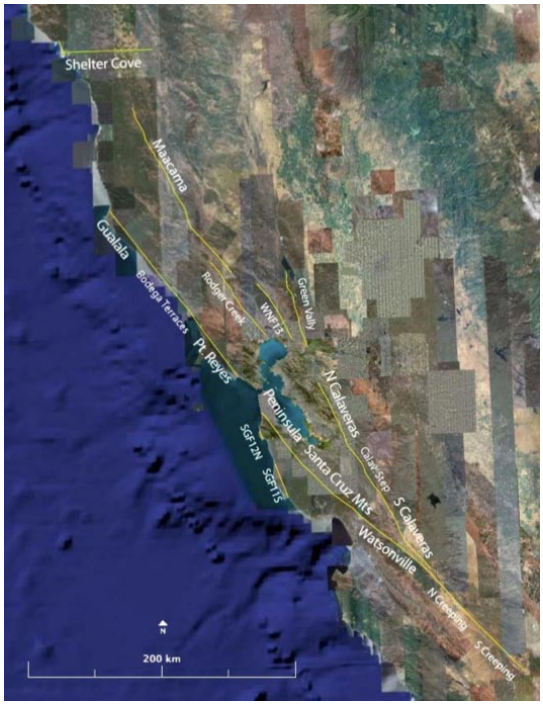

Map of northern California showing major targets for airborne LiDAR imagery acquisition for GeoEarthScope.

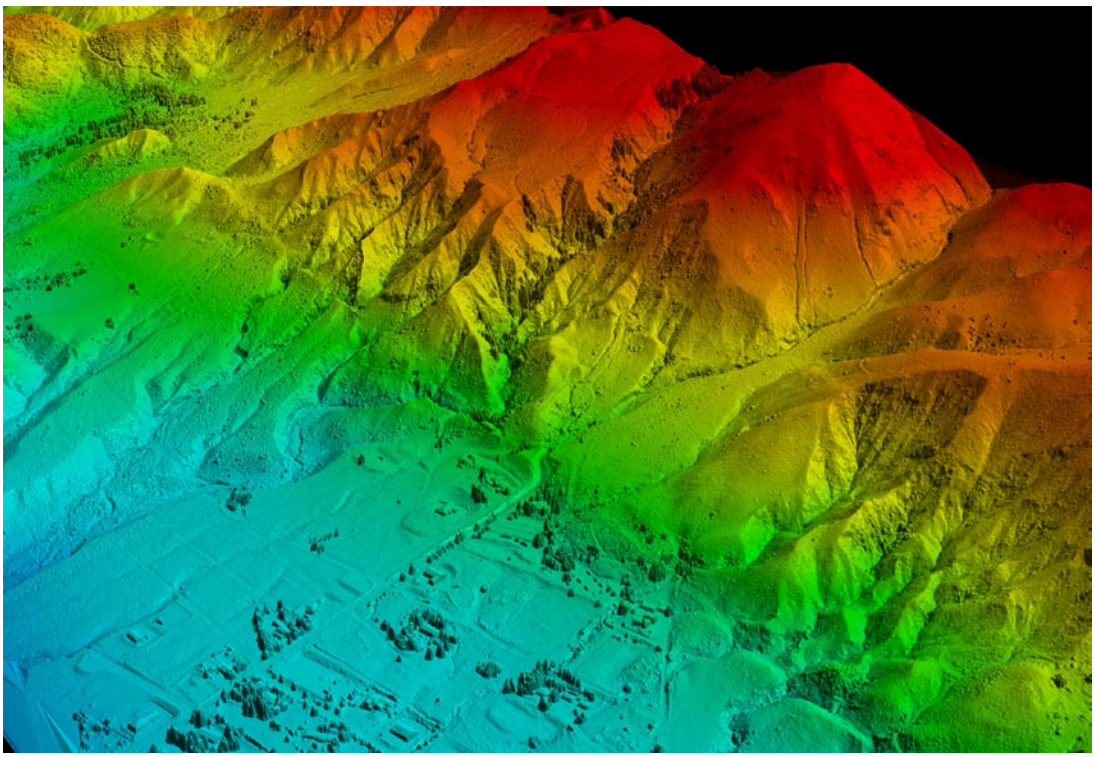

This airborne LiDAR image of the southern San Andreas fault was produced using data collected by the B4 project (image courtesy Ken Hudnut, USGS). Similar imagery of the northern San Andreas fault will be acquired as part of the GeoEarthScope northern California LiDAR project.

CONSTRAINING THE CRUSTAL CONVEYOR: EARTHSCOPE IMAGING OF MENDOCINO TRIPLE JUNCTION (MTJ) TECTONICS

Kevin P Furlong, Gavin P Hayes • Pennsylvania State University
Todd Williams • UNAVCO

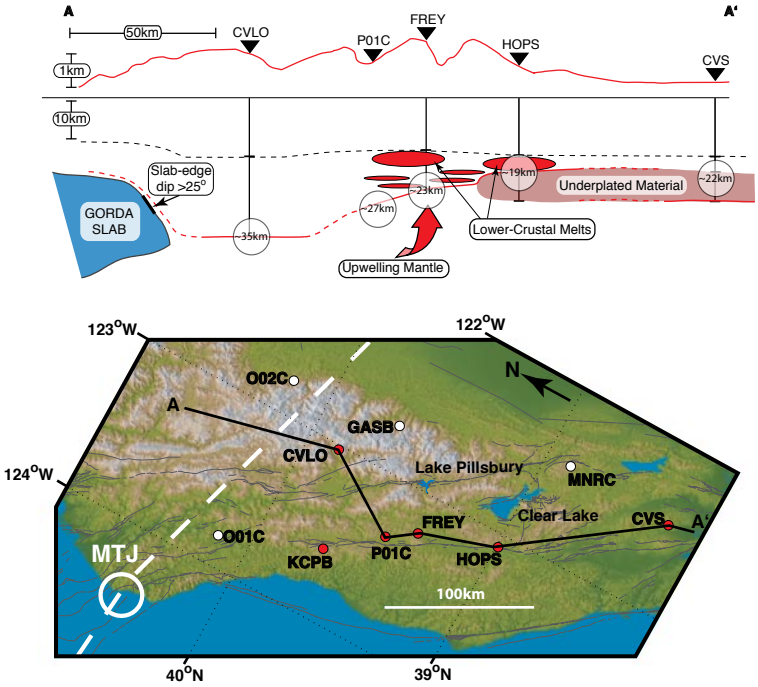

(a) Summary cartoon from Hayes & Furlong (2007), describing the variation in crustal structure across the Coast Ranges of northern California as inferred from receiver function analysis. (b) Map view of the cross-section path, and the locations of broad-band 3-component seismometers across the Coast Ranges. Several EarthScope TA stations are available for analyses (white dots on figure).

The general concept of faults developing and eventually coalescing into a primary plate boundary structure after MTJ passage serves as the framework for most tectonic and geodetic analyses of the fault system. What has been less well understood or quantified is specifically how the fault systems form, what drives fault localization, and how does the concomitant crustal evolution play a role in the plate boundary development. In the Mendocino Crustal Conveyor (MCC) model, Furlong and Govers [1999] proposed that crustal deformation, transient crustal thickening and thinning, and the associated topographic, heat flow, and seismic character of the crust are a consequence of viscous coupling within the evolving slab window. This model matched the general patterns of crustal structure and kinematics available in the pre-EarthScope era, but the spatial distribution of data precluded placing quantitative constraints on the process. The crustal thickening at and north of the MTJ, predicted by MCC processes, is clearly seen in the Receiver Function (RF) determined crustal structure, and crustal velocity and GPS derived strain fields, [Hayes and Furlong, 2007; Williams et al., 2006]. The ~ E-W extent of MCC deformation is delineated by the GPS data and RF analysis to occur primarily through the core of the northern Coast Ranges – consistent with the topographic and fluvial evolution of the region [Lock et al, 2006]. Seismic observations and the GPS data imply that the upper crust is only a minor participant in the MCC crustal thinning that occurs approximately 200 km south of the MTJ (i.e. ~ 4-5 million years after MTJ passage) – placing key constraints on the rheologic evolution of the crust along the developing San Andreas fault system [Hayes and Furlong, 2007]. Development of the precursor faults to the San Andreas plate boundary structure appears to be driven by the combination of MCC crustal deformation and the development of localized shear within the MTJ-formed slab window.

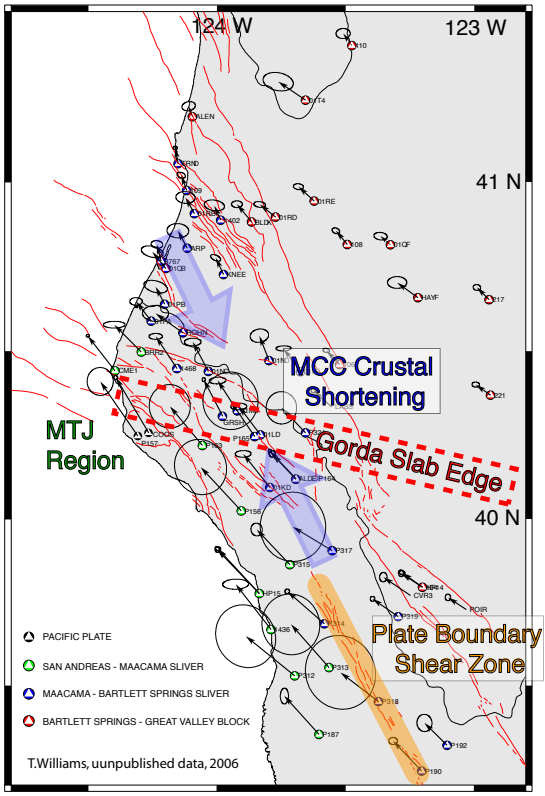

Crustal displacement field in vicinity of the Mendocino triple junction (MTJ). GPS velocity vectors are obtained from PBO CGPS and campaign data from Williams et al. (2006), USGS, and UCBerkeley.

Furlong, K.P., and Govers, R., 1999, Ephemeral Crustal Thickening at a Triple Junction: The Mendocino crustal conveyor, Geology v.27, pp. 127-130.

Hayes, G.P., and Furlong, K.P., 2007. Abrupt Changes in Crustal Structure Beneath the Coast Ranges of Northern California - Developing New Techniques in Recevier Function Analysis, Geophys. J. Int., in press.

Lock, J., Kelsey, H., Furlong, K.P, and Woolace, A., 2006, Late Neogene and Quaternary Landscape evolution of the northern California Coast Ranges: Evidence for Mendocino triple junction tectonics, Geol. Soc. Amer. Bull. v. 118, pp 1232-1246 doi: 10.1130/B25885.1

Williams, T.B, Kelsey, H.M., and Freymueller, J.T.,2006, GPS-derived strain in northwestern California: Termination of the San Andreas fault system and convergence of the Sierra Nevada–Great Valley block contribute to southern Cascadia forearc contraction, Tectonophysics v. 413, pp.171–184

Parts of this research were supported under USGS NEHRP funding to KPF. Discussions with Harvey Kelsey (HSU) have greatly added to this research.

MAPPING UPPER-MANTLE ANISOTROPY BENEATH THE WESTERN US: TOWARD AN INTEGRATED SEISMIC AND GEODYNAMIC ANALYSIS OF CRUST-MANTLE COUPLING

James Gaherty, Arthur Lerner-Lam • Columbia University
Li Zhao • Academia Sinica, Taiwan
Mousumi Roy • University of New Mexico

Surface deformation and plate-boundary evolution in the western US are likely driven by upper-mantle dynamics. The character of the tectonism is dependent not only on the forces driving the deformation, but also on the strength of the crust and mantle lithosphere that transmit those forces. Previous analyses of seismic anisotropy in the region imply that Pacific-North America plate boundary deformation penetrates into the mantle in northern California, while the crust and mantle are largely decoupled across the plate boundary in southern California. In this project, an integrated seismic-geodynamic analysis is being developed and applied to test and better quantify the coupling between crust and mantle across the plate boundary. From a seismological standpoint, we require a much more complete view of seismic anisotropy across the plate boundary. The Transportable Array provides, for the first time, recordings at sufficient spatial density to resolve 3D variations in anisotropy across the plate boundary. We measure and invert travel-times and amplitudes from recorded body and surface waves for anisotropic models using constraints provided by numerical calculation of upper mantle flow and fabric development across the Pacific-NA plate boundary. These numerical models simulate upper-mantle flow beneath the plate boundary using a viscous fluid subject to surface and basal kinematic boundary conditions, testing a variety of viscosity structures and rheologies (Newtonian vs. non-Newtonian). While the models are simple representations of the plate-boundary environment, the boundary conditions that drive them are derived from surface geologic and kinematic data, including surface deformation data from the Plate Boundary Observatory. Using existing theories of olivine fabric development, these kinematic flow models can be mapped into expected olivine LPO and hence anisotropy structure across the plate boundary. We will merge the expected flow-fabric-anisotropy from numerical models into the seismic inversions using a Gaussian-Bayesian formalism. This will allow us to explicitly assess the degree to which particular deformation scenarios are acceptable to the seismic data.

This three-year project initiated in Spring 2006, and is supported by grants from the NSF EarthScope program to CU and UNM. Post-doctoral Scientists Po Chen (LDEO) and Joya Tétreault (UNM) are participating in the analyses.

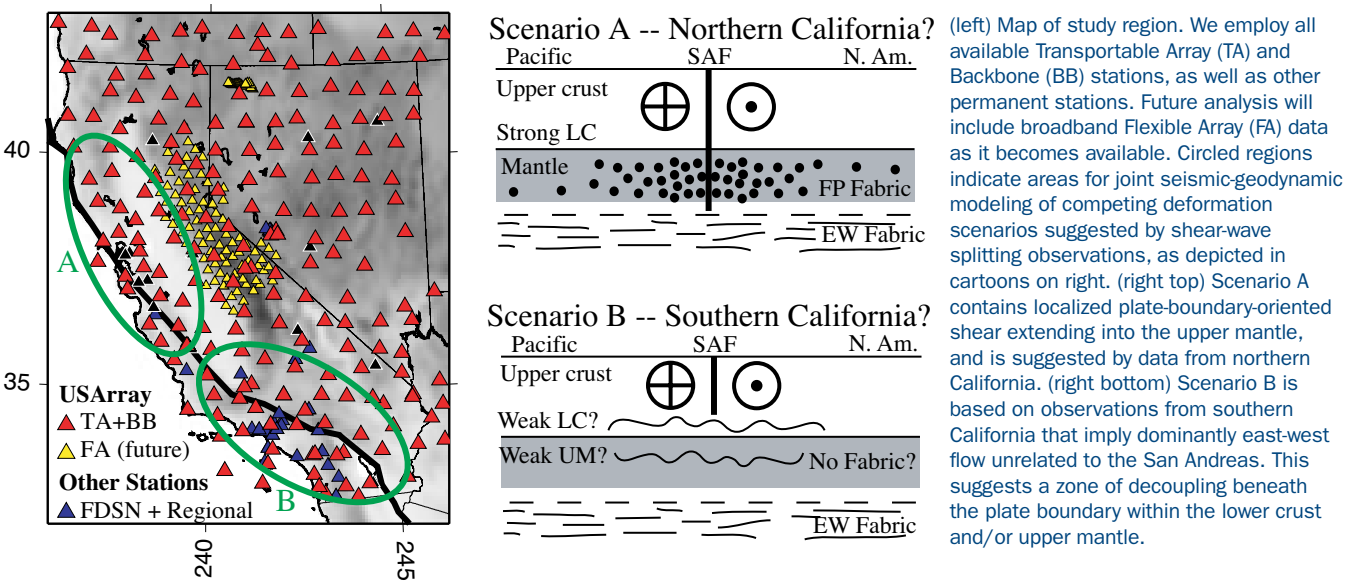

(left) Map of study region. We employ all available Transportable Array (TA) and Backbone (BB) stations, as well as other permanent stations. Future analysis will include broadband Flexible Array (FA) data as it becomes available. Circled regions indicate areas for joint seismic-geodynamic modeling of competing deformation scenarios suggested by shear-wave splitting observations, as depicted in cartoons on right. (right top) Scenario A contains localized plate-boundary-oriented shear extending into the upper mantle, and is suggested by data from northern California. (right bottom) Scenario B is based on observations from southern California that imply dominantly east-west flow unrelated to the San Andreas. This suggests a zone of decoupling beneath the plate boundary within the lower crust and/or upper mantle.

LINEAMENTS IN CENTRAL-EASTERN OREGON

Gary Egbert • Oregon State University
Randy Mackie • GSY-USA, Inc.
Shane Ingate • IRIS
Dean Livelybrooks • University of Oregon

In late 2006, IRIS conducted a project for site selection, permitting, installation and operation of 30 EarthScope MT sites in Oregon. Oregon was chosen because of the number of USArray FA and Continental Dynamics experiments being conducted by Humphreys, Fouch, James and Creager, and a high-density EMSOC/MT profile by Bedrosian that would provide the best possible synergy between EarthScope seismic and magnetotelluric data and science. Scientifically, Oregon combines a range of tectonic provinces including an active subduction zone to the west, active volcanism along the N-S spine of the Cascades in the center of the State and extending to the E-SE, high volcanic flood plains, and in the extreme SE, Basin and Range. A very preliminary 3-D inversion of the data was performed without testing the data, hypothesis testing, modeling experiments, or conducting distortion analysis. This truncated process of inversion served to identify individual data or sites that were generally problematic for purposes of producing smooth models and, thus, informs future efforts for more detailed inversions. The inversion shows a plan view at a depth of 30 km, along with a profile from NW to SE, with the 30 MT sites shown. The vertical exaggeration on the profile is 1:1, and extends to approximately 700 km depth. The Klamath-Blue Mountain Lineament (KBML) is seen as a conductor trending NE-SW. The KBML is a major crustal feature that shows in regional gravity and geological data that marks the southeast margin of the Columbia Embayment. Its correlation with the northwestern boundaries of the

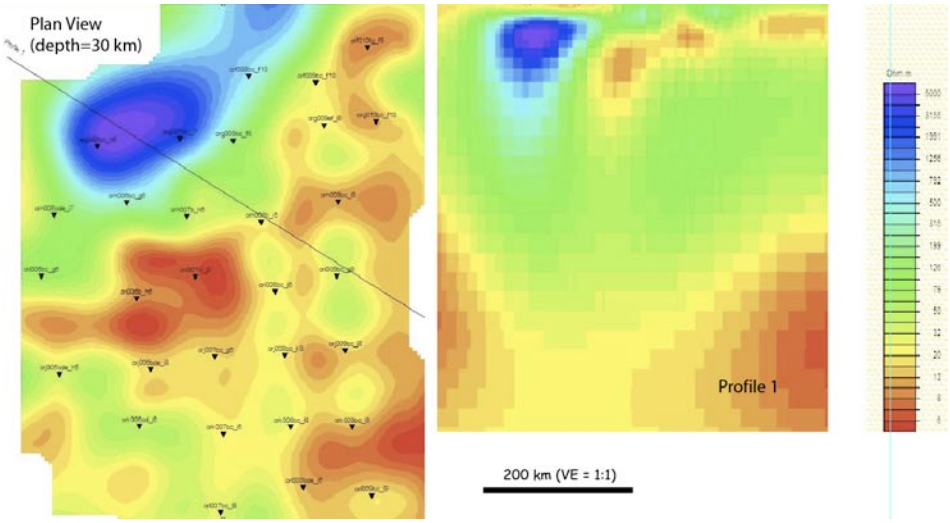

Plan view of inversion for conductivity at 30 km depth, with 30 MT sites superimposed, and NW to SE profile.

Klamath and Blue Mountain provinces suggests that these are continuous beneath the Cascade volcanic arc. The lineament may represent a pre-Tertiary strike-slip continental margin which, from paleomagnetic evidence, later rotated clockwise into its present position. The local enhancement of conductivity beneath sites ORI006 and ORI007 is interesting, and appears to lie between the John Day Basin and Harney Basin at depth, the latter an east-west extension of the Oregon-Idaho graben, both filled with Miocene flood basalts.

Robin P. Riddihough, Carol Finn, and Richard Couch, Klamath-Blue Mountain Lineament, Oregon Geology; June 1986; v. 14; no. 6; p. 528-531
D. I. Gough, D. M. McKirdy, D. V. Woods, H. Geiger Conductive structures and tectonics beneath the EMSLAB land array, JGR V94 No. B10 14,099–14,110, 1989
Hooper, P.R., Camp, V.E., Reidel, S.P., and Ross, M.R., accepted 2007, The origin of the Columbia River flood basalt province: plume versus nonplume models: in (Foulger, G.R. and Jurdy, D.M. (eds), Plates, Plumes and Planetary Processes, GSA Special Paper 430.

The authors wish to thank other members of the EarthScope MT Working Group (A. Schultz, R. Evans, P. Wannamaker, K. Mickus, S. Park and M. Unsworth), and also J. Booker and EMSOC for the loan of 10 long-period MT systems.

USARRAY IMAGES FOUNDERING LITHOSPHERE

Hersh Gilbert • Purdue University
George Zandt • University of Arizona
Craig Jones • University of Colorado at Boulder
Tom Owens • University of South Carolina

Combining seismic seismic data from the Transportable Array and FlexArray (SNEP) components of USArray in eastern California, we have identified a region where the mantle lithosphere appears to be currently being removed from beneath the Sierra Nevada batholith. Seismic observations from USArray stations around the Sierra Nevada exhibit differences in the crustal structure between the eastern and western portions of the mountain range. These observations appear consistent with models of lithospheric removal initiating along the eastern margin of the batholith and progressing to its western edge. As our understanding of processes related to the removal of mantle lithosphere improves the important roll played by lithospheric removal in continental deformation becomes increasingly apparent. Along the central portion of the western foothills of the Sierra, small earthquakes occur deep within the crust. These events may result from stresses associated with the lithospheric removal process. This work has been submitted for publication in Eos.

Yang, Y. and D.W. Forsyth (2006), Rayleigh wave phase velocities, small-scale convection,and azimuthal anisotropy beneath southern California, J. Geophys. Res., 111, B07306, doi:10.1029/2005JB004180.

The EarthScope program of the National Science Foundation supports this research under grants EAR-0454524, EAR-0454535, and EAR-0454554.

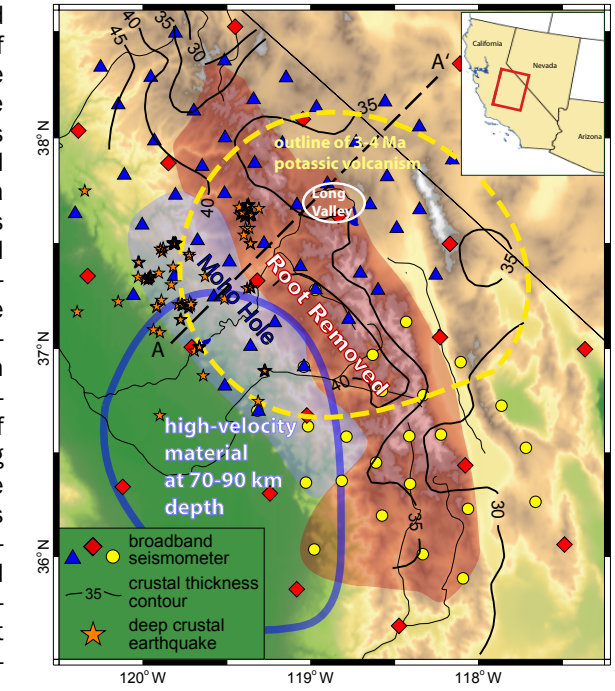

Topographic map of the Sierra Nevada indicating locations of seismic stations in the region of SNEP (blue triangles), the EarthScope/USArray Transportable Array (red diamonds), and the 1997 Sierran Paradox PASSCAL Experiment (yellow circles) are indicated. Crustal thickness variations, ranging from 30 to 45 km, are indicated as black contours, the region of postulated root removal (light red shading), and non-reflective Moho ("Moho Hole"; lavender shading) based on receiver functions, are indicated. High S-wave velocity anomaly in depth interval of 70-90 km is outlined with thick blue line and is from surface wave tomography by Yang and Forsyth [2006]. Deep crustal earthquakes, spatially and perhaps causally related to lower crustal delamination are shown by orange stars.

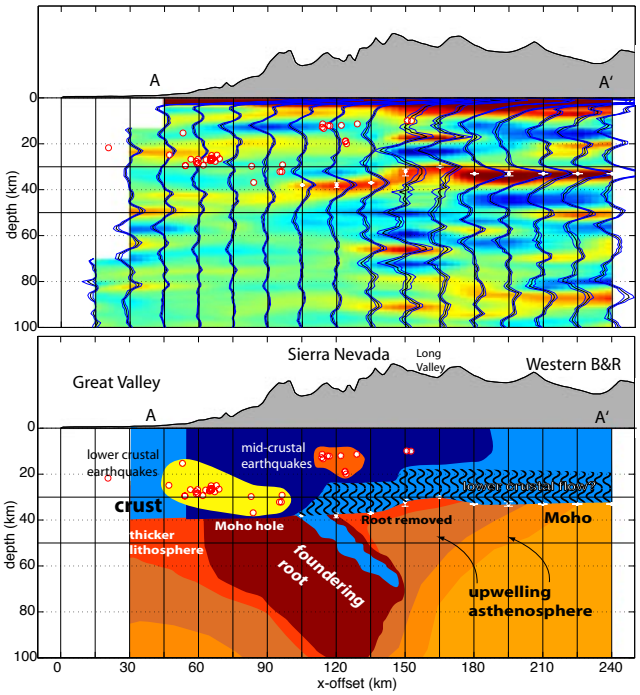

Topographic map of the Sierra Nevada indicating locations of seismic stations in the region of SNEP (blue triangles), the EarthScope/USArray Transportable Array (red diamonds), and the 1997 Sierran Paradox PASSCAL Experiment (yellow circles) are indicated. Crustal thickness variations, ranging from 30 to 45 km, are indicated as black contours, the region of postulated root removal (light red shading), and non-reflective Moho ("Moho Hole"; lavender shading) based on receiver functions, are indicated. High S-wave velocity anomaly in depth interval of 70-90 km is outlined with thick blue line and is from surface wave tomography by Yang and Forsyth [2006]. Deep crustal earthquakes, spatially and perhaps causally related to lower crustal delamination are shown by orange stars.

LABORATORY STUDIES OF THE FRICTIONAL BEHAVIOR OF MATERIALS CORED FROM THE SAN ANDREAS FAULT

David Goldsby • Brown University

We are measuring the frictional properties of samples obtained by SAFOD drilling into the San Andreas Fault (SAF) zone. Fundamental scientific questions that drive our experimental program include: 1) Why is the apparent magnitude of the resisting shear stress on the SAF so small?, 2) Why do some parts of the fault slip quietly via fault creep and others only in great earthquakes?, and 3) Does shearing occur over a broad zone of fault gouge or on one or more localized slip surfaces, and what are the implications of localization for fault stability?

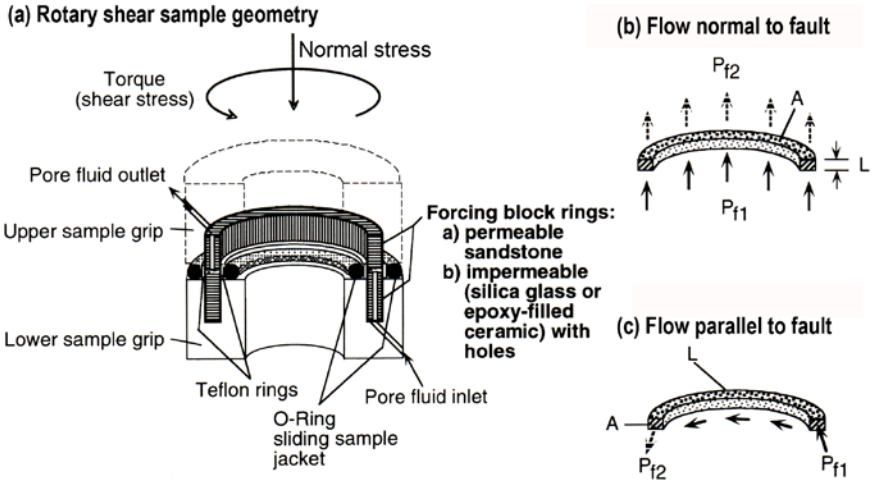

Cutaway views of the specimen assembly for the rotary-shear high-pressure apparatus. An experimental fault with or without simulated gouge lies between the upper and lower forcing block rings. The pore fluid pressure system is isolated from the gas confining pressure system by two Teflon rings and two O-rings inside and outside of the forcing block rings. Fluid permeability perpendicular and parallel to the fault is measured with permeable and impermeable forcing blocks, respectively. The flow direction (arrows), area (A), path length (L) and inlet and outlet pore pressures (Pf1 and Pf2) for permeability measurements are shown in (b) and (c).

Regarding 1), the most important physical property that affects the shear strength of the fault is the coefficient of friction of the rocks in the fault zone. We are measuring the frictional properties of SAFOD samples in large-slip experiments employing in situ velocities, pore pressures, and effective stresses (and, in the near future, temperatures). Regarding 2), SAFOD will core through creeping sections and through one or more spots that move in repeating earthquakes in Phase 3. Microstructural analyses of fault zone materials recovered from both the creeping sections and the repeating seismic patches, coupled with laboratory studies of their frictional properties, may provide important clues about which factors yield seismic and aseismic slip. Laboratory studies by us [e.g. Tullis and Weeks, 1986] and others, as well as theoretical studies, suggest that the velocity dependence of friction may be the most important factor affecting the stability of slip. Finally, regarding 3), the extent to which deformation is localized within the fault zone, and associated implications for fault stability and frictional velocity dependence [Scruggs and Tullis, 1998], are fundamental issues of fault mechanics that careful study of SAFOD drilling logs, together with observations and experiments on recovered core materials, can answer.

We are currently measuring the frictional properties of SAFOD samples obtained in Phase 1 drilling in our high-pressure rotary-shear apparatus. Tests are being conducted on both dry samples and samples with elevated pore-fluid pressures. Experiments in the near future will allow us to heat the samples to in situ temperatures. These experiments will serve as "proofs-of-concept" for future experiments on samples recovered from multilateral fault-crossing boreholes in Phase 3 drilling in the summer of 2007. Of particular interest is how the velocity dependence of slip for Phase 3 fault zone samples varies with the degree of slip localization at large shear strains. While our primary interest is in frictional properties, our tests will also measure the permeability of the samples. An important capability is that we can measure permeability both parallel and perpendicular to the sliding surface as a function of shear strain [Zhang and Tullis, 1998; Zhang et al., 1999]. Friction experiments will be coupled with microstructural analyses (thin sectioning, optical microscopy, SEM), in particular to correlate the friction velocity dependence with the degree of slip localization.

Tullis, T.E. and Weeks, J.D., Constitutive behavior and stability of frictional sliding of granite, PAGEOPH, 124, 383-414, 1986.

Scruggs, V.J. and Tullis, T.E., Correlation between velocity dependence of friction and strain localization in large displacement experiments on feldspar, muscovite, and biotite gouge, Tectonophys., 295, 15-40, 1998.

Zhang, S. and Tullis, T.E., The effect of fault slip on permeability and permeability anisotropy in quartz gouge, Tectonophys., 295, 41-52, 1998.

Zhang, S., Tullis, T.E. and Scruggs, V.J., Permeability anisotropy and pressure dependency of permeability in experimentally sheared gouge materials, J. Struct. Geol., 21, 795-806, 1999.

MICROSTRUCTURAL ANALYSES OF GOUGE FROM THE SAFOD BOREHOLE IN RELATION TO BRITTLE FAULT MECHANICS: A COLLABORATIVE STUDY

Jafar Hadizadeh • University of Louisville
Hassan Babaie • Georgia State University
Karen Mair • University of Oslo, Norway
Giulio Di Toro • University of Padova, Italy

This study uses microstructural characteristics determined from phase II and III core samples to test specific fault gouge evolution models. These working models are based on a large number of previous field and experimental studies of exhumed fault rocks, simulated fault gouge experiments, and numerical simulations of gouge deformation as well as theoretical considerations of brittle rock deformation and rock friction. The applied methodologies include quantitative microstructural analysis using electron microscopy, analytical techniques, customized image analysis and numerical simulations as well as sub-seismic velocity frictional sliding experiments on the SAFOD gouge samples. The results are available on the Worldwide Web, from several integrated databases and domain ontologies that are being developed and implemented specifically for this project. Although the main phase of our project awaits the result of phase III continuous coring, the preliminary research on some phase I and II core samples has been exciting and interesting.

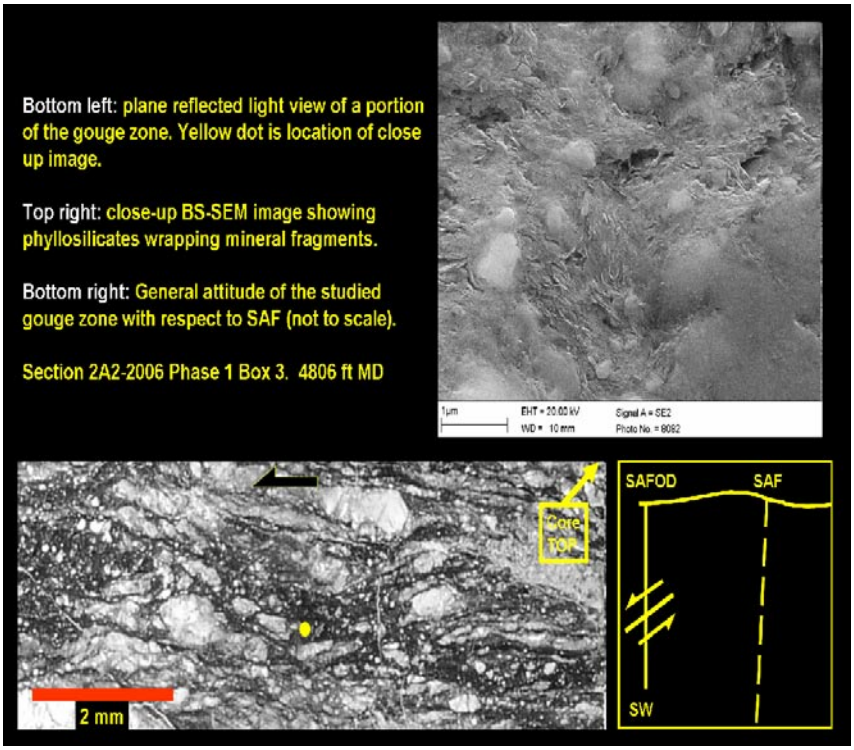

Foliated ultracataclasites in a minor gouge zone from SAFOD spot core at 1465m MD

We have been able to analyze the role of small gouge zones in the SAF damage zone. The microstructures of the studied gouge is compared to previously studied simulated and exhumed gouges, in which the development of similar microstructures had required only few tens of mm of shear displacement. The studied gouge is one of several zones with similar attributes that have been characterized or investigated by others in the SAFOD core samples to a measured depth of 3100m. The combined observations suggest that the studied gouge zone might have developed along preexisting suitably-oriented, and alteration-softened, fracture surfaces. This model is also consistent with previous findings that mesoscale fracture systems in fault damage zones act as fluid flow pathways and therefore are affected most by mineral alterations. Thus in addition to a network of fractures, a system of gouge zones with highly variable thickness and limited lateral extent might exist within the flower structure of the SAF at shallow depths giving the entire damage zone a beanbag-like deformability. We present evidence of repeated displacements along the studied gouge zone and discuss the mechanical implications of the proposed model for damage zone of mature fault zones such as the SAF system. These results will be presented at the upcoming EarthScope national meeting in Monterey, California. We are writing in support of funding for the long-term operations and maintenance of the EarthScope facilities.

Of particular interest to our project is the continuation of support for storage of SAFOD core collection, and administration and distribution of the SAFOD data products. We note that the current SAFOD-related research as well as efforts to be carried out in the future by various EarthScope Science projects, and the wider Earth Science community are most contingent upon the availability and flow of material samples and geophysical data from the SAFOD site after completion of the drilling phase in September 2007.

Babaie H., Oldow J. S., Babaei A., Richard S. M., Ave Lallemant H. G., and Watkinson A. J., 2005. Designing the structural geology ontology. In: Geoinformatics, edited by Sinha K., and Baru, C., Geol. Soc. Amer. Special Paper.

Di Toro G., Pennacchioni, G., Teza, G., 2004. Can pseudotachylytes be used to infer earthquake source parameters? An example of limitations in the study of exhumed faults. Tectonophys. 402, 3-20

Hadizadeh J. and Johnson W. K., 2003. Estimating local strain due to comminution in experimental cataclastic textures. J. Struct. Geol., 25, 1973-1979.

Mair K., Frye K.M. and Marone C., 2002. Influence of grain characteristics on the friction of granular shear zones, Journal of Geophysical Research, 107, (10), 2219, doi: 10.1029/2001JB000516.

J. Hadizadeh acknowledges funding support through National Science Foundation EarthScope Science-0545472

AN INTERACTIVE MAP TOOL FOR EARTHSCOPE EDUCATION AND OUTREACH

Michael Hamburger • Indiana University
Marianne Weingroff • Digital Library for Earth System Education/UCAR, Boulder
William Holt • State University of New York at Stony Brook
Lou Estey • UNAVCO

We have created a new, interactive, web-based map utility that can make EarthScope-related scientific results accessible to a large number and variety of users. The tool provides a user-friendly interface that allows users to access a variety of maps, satellite images, and geophysical data at a range of spatial scales. The EarthScope Voyager map tool allows users to interactively create a variety of geographic, geologic, and geodynamic maps of the EarthScope study area. The utility is built on the "Jules Verne Voyager" suite of map tools, developed by UNAVCO for the study of global-scale geodynamic processes. Users can choose from a variety of base maps (including satellite imagery, global topography, geoid, sea-floor age, strain rate and seismic hazard maps, and others), add a number of geographic and geophysical overlays (coastlines, political boundaries, rivers and lakes, earthquake and volcano locations, stress axes, etc.), and superimpose both observed and model velocity vectors representing a compilation of 5170 geodetic measurements from around the world. Users can select from 26 frames of reference, allowing a visual representation of both `absolute` plate motion (in a no-net rotation reference frame) and relative motion along all of the world`s plate boundaries. For the EarthScope Voyager, we include maps of proposed USArray and Plate Boundary Observatory sites and "Did You Know" educational modules, which provide examples of EarthScope-related scientific results linked to EarthScope study areas. Two versions of the tool are available: (1) a Java-based map tool "EarthScope Voyager", a server-based map creation system which allows users complete control over base maps, overlays, and map scale; and (2) "EarthScope Voyager, Jr.", an HTML-based system that uses pre-constructed GIF maps and overlays, allowing the system to rapidly create and display maps to

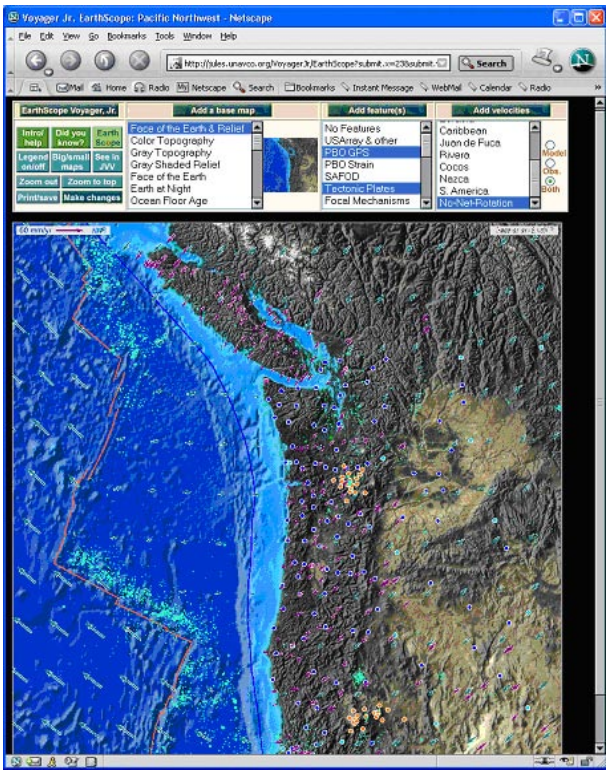

Image created using the EarthScope Voyager, Jr. map tool, showing proposed PBO sites (blue and orange circles for backbone and magmatic cluster sites, respectively), observed and modeled geodetic velocities (purple and blue vectors, respectively), seismicity and plate boundary locations, superimposed on a base map showing Face of the Earth imagery that combines satellite reflectance data with high resolution topographic and bathymetric data.

Image created using the new Jules Verne Voyager map interface, showing menu-based selection system and high resolution satellite image of the western U.S., with volcano locations superimposed.

a large number of users simultaneously. The tool allows users to zoom among at least four map scales. In addition, we have developed companion educational materials, on the "Exploring our Dynamic Planet" website, a JavaScript-based interface that incorporates explanatory material for the map tool and curricular activities that encourage users to explore Earth processes using the Voyager map tools. We have also created an entirely new user interface for the "Jules Verne Voyager" suite, which allows users to make 'maps on demand' using a new user-friendly menu interface. The map tool and associated educational materials can be viewed through the Jules Verne map portal http://jules.unavco.org.

This work was supported by NSF grant EAR-0346180.

COMPARING GEODETICALLY AND GEOLOGICALLY INFERRED DEFORMATION OF THE WALKER LANE, WESTERN BASIN AND RANGE

William C. Hammond, Corné Kreemer, Geoff Blewitt • University of Nevada, Reno

In the Basin and Range Province, the total crustal strain accumulation rate is a factor of 2 to 3 times larger than the strain release rate measured through geological investigation of fault slip rates. This apparent discrepancy is based on a comparison between a large national database of paleoseismic studies (the USGS Quaternary Fault and Fold database) and the total deformation rate inferred from the geodetic velocity field (Pancha, et al., 2006). One possible explanation is that the geologic database is incomplete in the sense that a significant number of crustal faults are missing or have slip rates that are estimated to be too low. Other possibilities are that 1) significant surface deformation occurs that is not localized onto faults, 2) the way we do the accounting of deformation rate is somehow flawed, 3) that geodetic deformation is anomalously enhanced by transient effects (Savage and Prescott, 1978, Pollitz, 1997, Hammond, et al., 2006), or 4) that the behavior of crustal blocks is time-variable over scales of thousands to millions of years, and we are currently in a time of anomalously

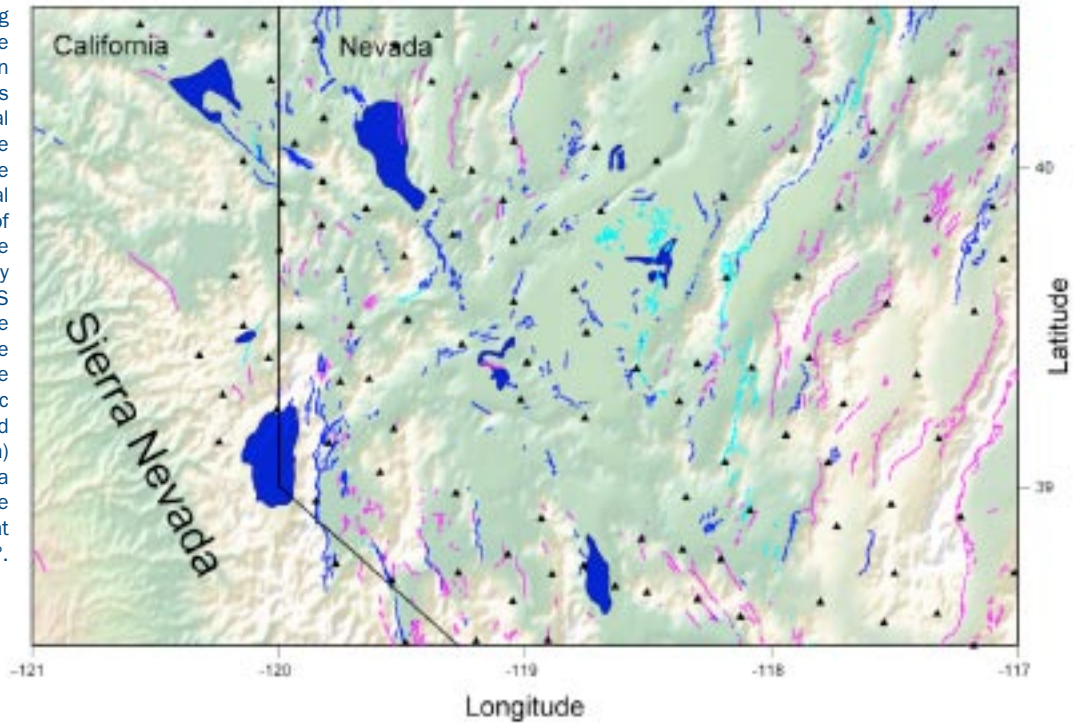

A complex pattern of faulting in the northern Walker Lane and westernmost Basin and Range accommodates ~10 mm/yr of regional transtension between the Sierra Nevada microplate and relatively rigid central Basin and Range (east of longitude -117°). We have established approximately 120 new semi-permanent GPS sites (black triangles) inside the region indicated by the box at left. Shown over the topography are the Historic (cyan), Holocene (blue) and late Pleistocene (magenta) faults. The California-Nevada state border is the black line passing through Lake Tahoe at longitude -120°, latitude 39°.

high deformation rate compared to the recent geologic past. We are attempting to resolve which of these issues is the cause by using a multi-faceted approach that includes three factors: 1) making detailed GPS measurements of Walker Lane crustal deformation, 2) developing improved block modeling algorithms to explore the spatial and temporal relationship between strain accumulation and release, and 3) developing viscoelastic models of the lithosphere to account for earthquake cycle effects on the geodetic velocity field.

Hammond, W.C., C. Kreemer G. Blewitt, 2006, Geodetic constraints on contemporary deformation in the northern Walker Lane: 3, Postseismic relaxation in the Central Nevada Seismic Belt, Late Cenozoic Structure and Evolution of the Great Basin – Sierra Nevada Transition, in review.

Pancha, A., J.G. Anderson C. Kreemer, 2006, Comparison of seismic and geodetic scalar moment rates across the Basin and Range province, Bull. Seismol. Soc. Am., 96, 11-32, doi:10.1785/0120040166.

Savage, J.C. W.H. Prescott, 1978, Asthenosphere readjustment and the earthquake cycle, J. Geophys. Res., 83, 3369-3376.

This work was supported by NSF Grant No. EAR-0610031.

GEOTHERMS, FLUIDS AND LITHOSPHERIC STRUCTURE OF THE GREAT BASIN–COLORADO PLATEAU TRANSITION ZONE, 38.5N LATITUDE

Derrick Hasterok, David S. Chapman • University of Utah
Phillip E. Wannamaker • Energy and Geoscience Insititute
William Doerner • Quantech Geoscience

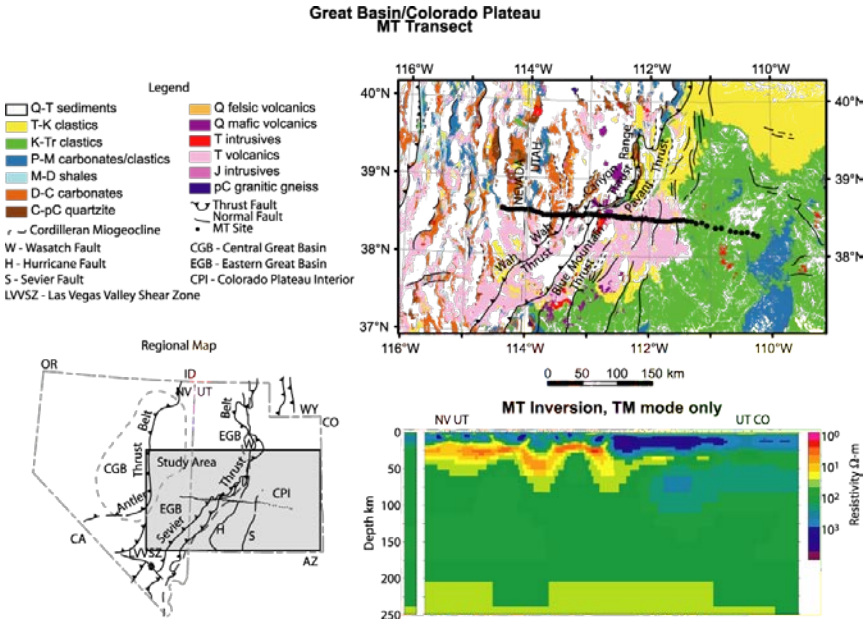

Surface geology and electrical structure of the Great Basin-Colorado Plateau.

The Colorado Plateau-Great Basin transition zone (TZ) in central Utah is a presently extending lithospheric block composed of previously stable Proterozoic lithosphere. TZ extension may be driven by high topography resulting from overthickening during the Laramide Orogeny and passive plate boundary forces similar to the Great Basin. However, high TZ topography may also indicate dynamic mantle upwelling and active processes acting within the TZ. We have collected 56 new broadband and 9 long-period MT sites to merge two existing MT lines for a combined length of 400 km (124 sites) covering the eastern Great Basin into the Colorado Plateau at a latitude of 38.5N. MT data show a highly conductive body that is semi-contiguous in the middle crust of the eastern Great Basin that rises to a shallow depth of <20 km beneath the TZ. This conductive layer appears to be connected to the surface by a series of symmetric rift related normal faults mapped at the surface. These normal faults may be acting as pathways for large scale fluid connection between the upper and lower crust. Using over 300 new heat production measurements made across the southwest, combined with existing heat flow data and MT measurements, we estimate the thermal structure and lithospheric thickness of the mantle along the MT profile. Temperatures within the asthenosphere appear to be near the current average mantle adiabat. Lithospheric thicknesses estimated from the thermal structure suggest a thick, 150 km, lithosphere beneath the resistive core of the Colorado Plateau and thin, 60 km, in the Great Basin. Geodynamic modeling using the new thermal constraints may reveal insight into the active/passive nature of the rift. Data collected by EarthScope will help provide a regional framework to constrain the 3-dimensional extent of the processes acting within the TZ.

REAL-TIME DATA FEEDS FROM THE PLATE BOUNDARY OBSERVATORY BOREHOLE INSTRUMENTS AT ANZA TO THE CALTECH/USGS SOUTHERN CALIFORNIA SEISMIC NETWORK

Egill Hauksson • Seismological Laboratory, Caltech

The Caltech/USGS Southern California Seismic Network (SCSN/CISN), which is also a part of the California Integrated Seismic Network (CISN), is now analyzing real-time feeds of seismic data from the EarthScope PBO borehole stations located near Anza in southern California.

We are using real-time ORB-to-ORB transfer of waveform data from the PBO in Boulder, Colorado to Caltech in Pasadena. The SCSN/CISN is processing both downhole and uphole seismometer channels as well as available strong motion channels.

The real-time data streams allow us to use these data for real-time high-precision hypocenter determination, sometimes referred to as double-difference methods. The automatic location of a sample event of M1.3 and the corresponding waveforms are shown in the figures.

Our goal is to push the science and improve our capabilities associating hypocenters with mapped faults using real-time data. In the past, such associations have required extensive research and relocation efforts.

Having these real-time data will also improve earthquake safety in southern California, because we will have more data sources and data from the near field of the most active fault (San Jacinto fault) in southern California.

This effort benefits the EarthScope PBO because the SCSN/CISN data analysts will check the data daily and be able to provide quality control feedback back to the PBO.

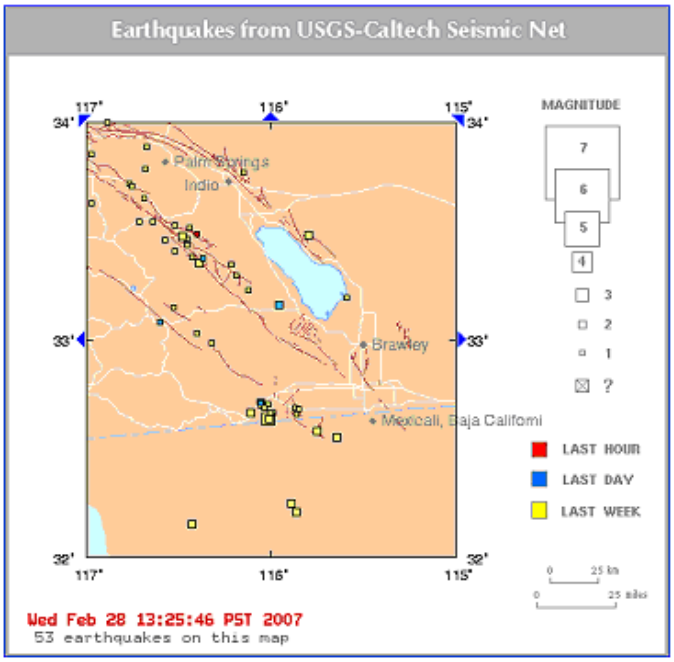

Real-time location of seismicity in the Anza region. Seismograms for the event, labeled with a red square, are shown in the figure below.

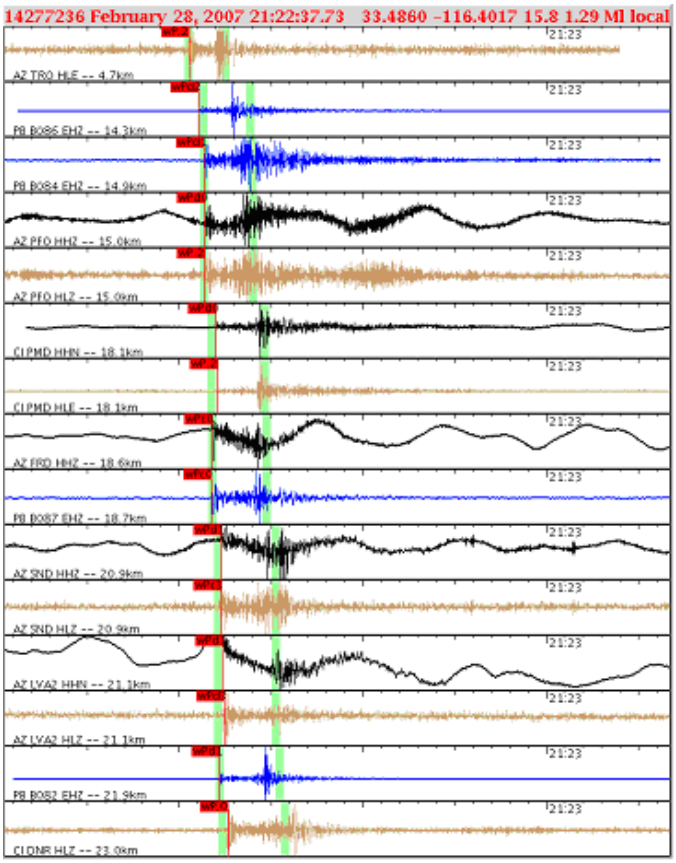

Seismograms from PB, AZ, and CI networks, processed in real-time at Caltech to determine earthquake location and magnitude. Waveforms are colored according to sensor type and channel name. The PBO stations B086, B084, B087, and B082 were used in the solution.

REAL-TIME DATA SHARING BETWEEN USARRAY AND THE CALTECH/USGS SOUTHERN CALIFORNIA SEISMIC NETWORK

Egill Hauksson • Seismological Laboratory, Caltech

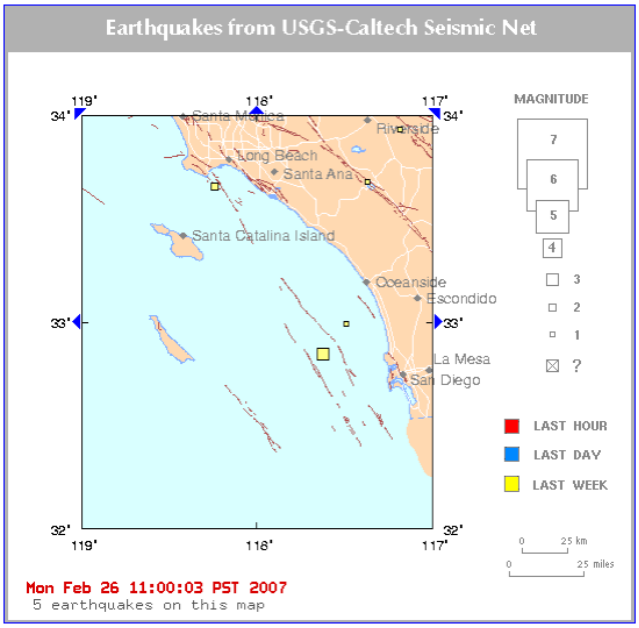

Map showing the location of the M3.11 earthquake, as a yellow square offshore from San Diego.

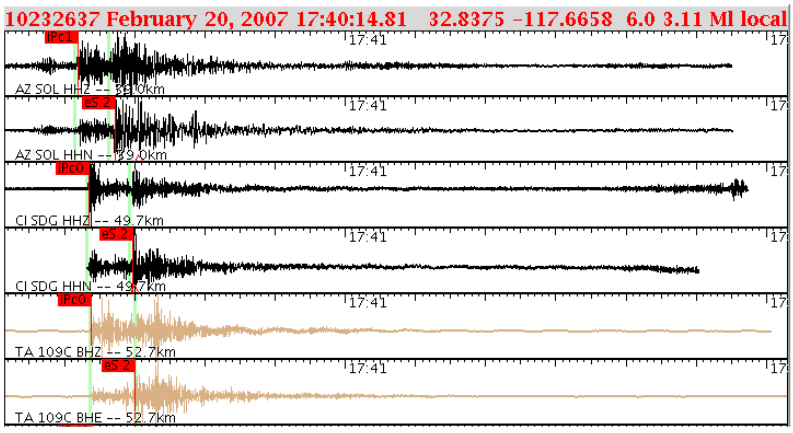

Seismograms from an earthquake located offshore from San Diego. Real-time data from the USArray station, TA.109C along with SCSN and Anza data were used to locate this event automatically.

The USArray and the Caltech/USGS Southern California Seismic Network (SCSN) share waveform data real-time. Waveforms from eight USArray stations are transmitted to Caltech for real-time processing, while waveform data from 41 SCSN stations are transmitted to the Array Network Facility (ANF) and are included in the USArray dataset.

The Caltech/USGS Pasadena collaboration with USArray is an opportunity to provide broadband data from the SCSN to a large segment of the seismological community. Similarly, the real-time availability of USArray data enables the SCSN to improve automated earthquake locations and moment tensors. About 600 phase picks were made on TA waveforms by the SCSN during 2006. In addition, the USArray data were used to constrain moment tensors for earthquakes of M>3.7 located along the edges of the SCSN. The inclusion of the USArray stations in the SCSN will allow us to establish the need for additional station coverage along the outer boundaries of the SCSN. Hence, this dual use of real-time data has benefited both USArray as well as the SCSN.

QUANTIFYING REGIONAL VELOCITY RATIO IN CALIFORNIA: USING SEISMIC DATA TO MAP SHALLOW STRUCTURE

Gavin Hayes, Kevin Furlong • Pennsylvania State University

For several decades, seismologists have used a variety of different methods to model the P-wave velocity structure of the Earth, and in particular, the Earth's crust. Modeling of the S-wave velocity field has been (and remains) more difficult, and as a result S-wave velocity structure is often directly related to P-wave models through empirical measurements of the velocity ratio in rocks. These velocity models are subsequently used in many different types of analyses, such as the calculation of strong ground motions in regional hazard maps, earthquake locations, and the inference of subsurface geology. In all cases, better estimates of S-wave velocity models lead to more accurate models of the parameters they are used to describe. This is of particular importance for estimates of shallow S-wave velocity structure, where we need improved models to aid in any predictive hazard analysis.

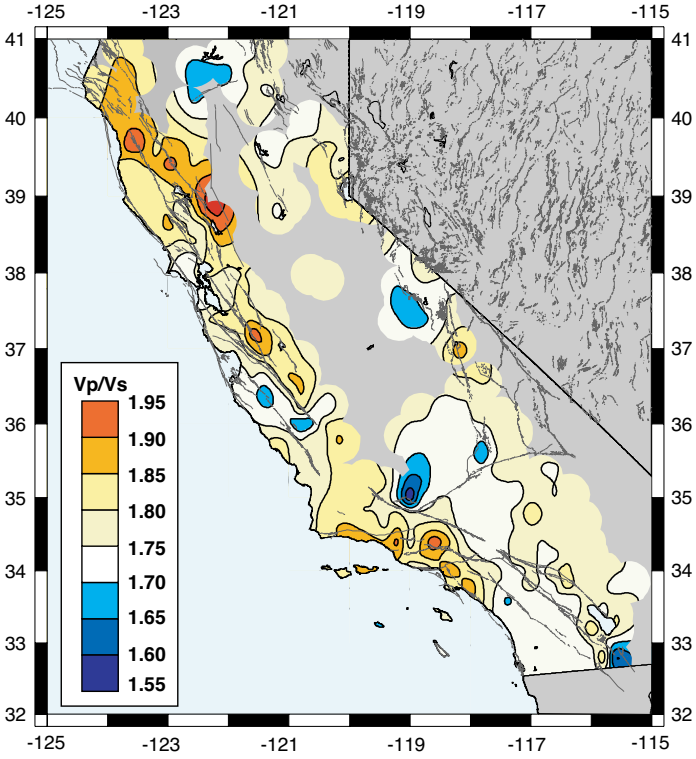

Velocity ratio map of California

Here, we develop a straightforward technique for computing apparent velocity ratio of both the bulk seismogenic crust and shallow crust throughout California based on P- and S-wave travel-times from earthquakes to the dense network of broadband and short-period stations across the state, significantly improved since the implementation of the EarthScope project. As the seismogenic zone is constrained to the shallow, brittlely deforming part of the crust, we can use these earthquake travel-times to estimate the apparent velocity ratio of that crust. Using this approach, we produce regional maps of Vp/Vs for all California, where station coverage is dense enough and rates of seismicity high enough to allow this type of analysis. We can also isolate the very shallow (generally aseismic) crustal section to construct a velocity ratio map of the near surface.

This method, which we call the Local Velocity Ratio Calculation (LVRC), provides a simple yet powerful way to analyze the velocity ratio of the crust on a regional basis. The model compares favorably to the SCEC three-dimensional velocity model, giving confidence in the robustness of the approach. Results may be related to geologic structure, used to infer parameters such as ground shaking susceptibility, and also to calibrate geology-based three-dimensional velocity models such as the USGS 3D model of northern California.

CHARACTERIZING TRANSIENT STRAIN RATE DEPARTURES FROM A LONG-TERM STRAIN RATE FIELD

Daniel Hernandez, William E. Holt • State University of New York at Stony Brook
A. John Haines • University of Cambridge, United Kingdom
Richard A. Bennett • University of Arizona

Continuous Global Positioning System (GPS) time series from the Southern California Integrated GPS Network (SCIGN) and the highly active margin along the western United States enables for high resolution, four-dimensional solutions of model velocities and strain rate field for southern California. SCIGN served as a nucleus for the upcoming EarthScope Plate Boundary Observatory (PBO) and the high sampling rate of the geodetic monuments is ideal for recognizing strain rate transients.

While SCIGN does provide temporally dense displacement time series, until the PBO is fully operational, it is spatially sparse in some regions. We use PA-NA motion as a velocity boundary condition in all solutions and using bi-cubic splines as basis functions. We interpolate GPS velocity fields for spatially continuous estimates of the velocity gradient tensor field for two-week data epochs, thereby deriving a time dependent evolution of the strain rate field [Holt et al., 2000]. Each epoch solution includes a model strain rate estimated from Quaternary fault data [Shen-Tu et al., 1999] and geodetic data, all of which are later compiled as movies to evaluate the time dependent evolution of interseismic strain rates.

This technique was applied to data spanning late 1999 through 2004 allowing us to recognize a first order strain rate transient following the October 1999 Hector Mine earthquake. Of particular interest are the strain rate corridor between Hector Mine and the San Andreas fault, a diminished strain rate along the Anza section of the San Jacinto fault, and the subsequent redistribution of strain rates along the San Jacinto fault [Fialko, 2006].

Holt, W. E., Chamot-Rooke, N., Le Pichon, X., Haines, A. J., Shen-Tu, B., and Ren, J., 2000, Velocity field in Asia inferred from Quaternary fault slip rates and Global Positioning System observation: Journal of Geophysical Research-Solid Earth, v.105, p. 19185 - 19209.

Shen-Tu, B., Holt, W. E., and Haines, A. J., 1999, Deformation kinematics in the Western United States determined from Quaternary fault slip rates and recent geodetic data: Journal of Geophysical Research, B, Solid Earth and Planets, v. 104, p. 28927 - 28956.

Fialko, Y., 2006, Interseismic strain accumulation and the earthquake potential on the southern San Andreas fault system: Nature, v. 441, p. 968 – 971.

This research was supported by EAR-06030000.

EARTHSCOPE AND TECTONICS STRESS ACROSS NORTH AMERICA

Robert Herrmann • Saint Louis University
Charles Ammon • Pennsylvania State University

For more than a decade, the dense seismic networks in California have enabled waveform-based analyses of moderate-to-small earthquakes in California and western Nevada [Romanowicz et al., 1993; Ichinose et al., 2003]. The seismogram modeling procedures have been well exercised and reliably automated in these regions. Similar magnitude activity in the much larger, but less active regions across North America have been investigated [Du et al, 2003], but in a less systematic way. Early work shows that these small events carry important information on the stress variations across the continent [e.g. Zoback 1992]. More recent event catalogs [Herrmann, 2007] map broad, subtle changes in stress across the eastern half of the continent such as the transition from reverse to strike-slip faulting in the northeast US and southeastern Canada, and the transition from strike-slip to normal faulting in the south and westward into the Great Plains. North American seismic network expansion that includes the Canadian National Network, the U.S. Geological Survey National Seismic Network (USNSN), and USArray's backbone (BB) and transportable arrays (TA) will allow us to improve our mapping of small-earthquake processes across the continent. Although the dense TA will migrate across the continent over only a decade, even small events to the east are well recorded by broadband seismic instruments over most of the continent. The relatively large aperture of the array provides a good azimuthal sampling important for accurate faulting geometry and source depth estimation for all events in the contiguous Unites States (US) (and much of southern Canada and northern Mexico). When integrated with the USNSN and backbone networks observations permit inversion of observed waveforms to estimate depth, moment magnitude and faulting geometry. Thus even while the TA is initially deployed in western North America, TA observations can help constrain processes occurring in the more stable regions of the continent. Further, as we develop methods to exploit shorter-period observations from close to smaller events (about two source depths), we may be able to lower the modeling magnitude threshold for events within the TA, and possibly double the number of events available to image stress variations across the continent. We have begun a systematic effort to examine the waveforms for each earthquake with reported magnitude greater than 3.5 in the contiguous United States, excluding California, which is well covered by the California Integrated Seismic Networks.

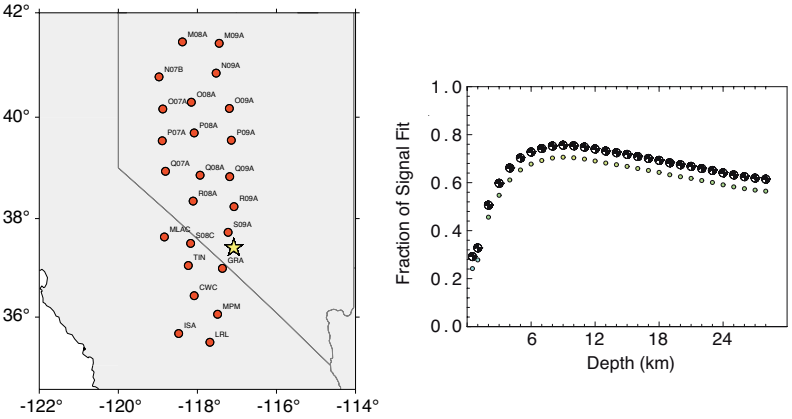

Modeling results for a small Mw 3.8 earthquake that occurred on 24 January, 2007 in central Nevada (37.41N 117.08W, 9 km). Dense azimuthal coverage at distance reliably constrains the faulting geometry and stations close to the source improve event depth resolution. The map shows the station locations used in waveform fitting; the depth versus fraction of signal fit chart shows the an optimal depth between 6 a 12 km. The faulting geometry is stable for the entire range of plausible depths.

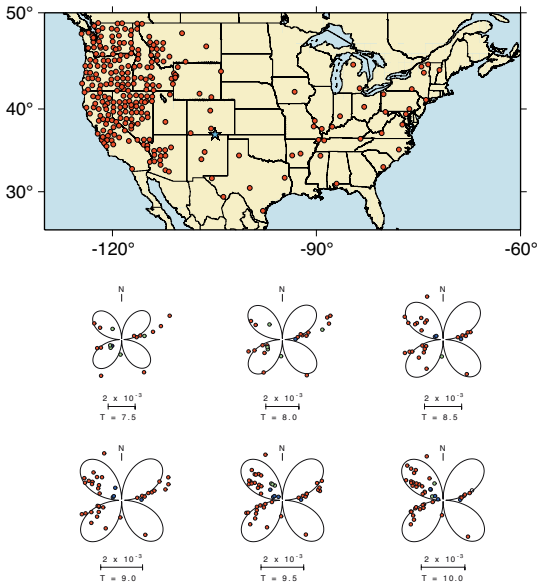

Modeling results for a small Mw 4.4 earthquake that occurred on 03 January, 2007 in southern Colorado (37.06N 104.90W, 2 km). Station locations are shown on the left and Love-wave spectral amplitudes are shown on the right. The TA and backbone networks station density allowed superb azimuthal coverage for spectral amplitude matching at short periods. Dense azimuthal coverage at distance reliably constrain the faulting geometry and allows us to extract short-period observations critical to resolving subtle depth differences for shallow earthquakes.

Herrmann, R. B., (2007) An online catalog of recent earthquake focal Mechanism estimations for events in Canada and the United States (outside California and Alaska) http://www.eas.slu.edu/Earthquake_Center/MECH.NA

Ichinose, G. A., J. G. Anderson, K. D. Smith, and Y. Zeng (2003), Source parameters of eastern California and western Nevada earthquakes from regional moment tensor inversion, Bull. Seismol. Soc. Am., 93, 61-84.

Romanowicz, B., D. Dreger, M. Pasyanos, and R. Uhrhammer (1993), Monitoring of strain release in central and northern California using Broadband data, Geophys. Res. Letters, 20, 1643-1646.

Zoback, M. L. (1992), Stress field constraints on intraplate seismicity in eastern North America, J. Geophys. Res., 97, 11,761-11782.

We thank the U.S. Geological Survey for their support of this research through award numbers 05HQGR0047, 05HQGR0174 and 06HQGR0166. Data processing was performed using the open-source Computer Programs in Seismology package. Maps were created using GMT (Wessel and Smith, 1995).

WALLOWA MOUNTAIN UPLIFT AND ERUPTION OF THE COLUMBIA RIVER FLOOD BASALTS: A GREEN'S FUNCTION DELAMINATION EVENT

Gene Humphreys • University of Oregon

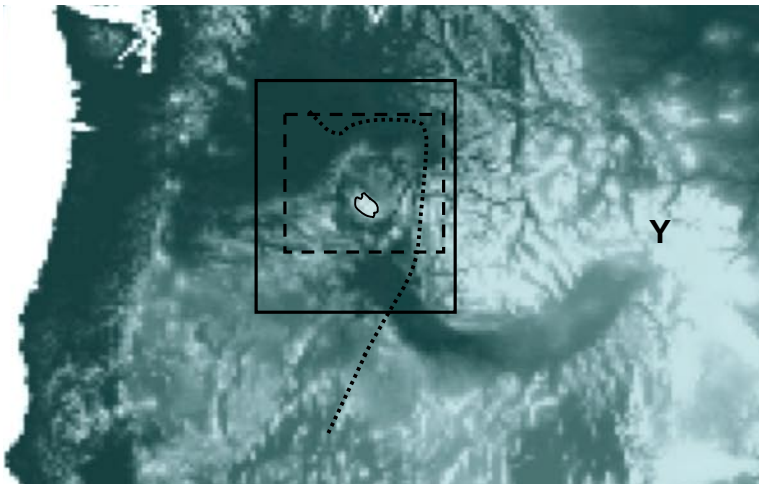

Pacific Northwest. Dotted line is western margin of Precambrian North America. Note bull's eye uplift pattern at western end of Snake River Plane, with Wallowa pluton (gray) at its center. Boxes refer to maps below. Y=Yellowstone.

Initial Yellowstone hotspot activity was dominated by Columbia River Basalt (CRB) flood eruptions from NE Oregon ~16 m.y. ago. Such eruptions commonly are attributed to plume head impact, although for Yellowstone, the CRB eruptions were far off track. Surface uplift following these eruptions created a bull's eye pattern. In this area of accreted oceanic arcs, the Wallowa pluton (age ~135 Ma) is the largest of what are relatively unusual granitic bodies, and it lies at the center of the bull's eye. Following CRB eruptions the pluton (and essentially only the pluton) was elevated ~2 km. We argue [Hales et al., 2005] that the fundamental cause of Wallowa Mountain uplift and CRB magmatism was delamination of the pluton's dense root (this delamination may have been triggered by pancaking plume). Delamination drives an asthenospheric return flow that generates mantle melting through decompression. Melt accumulates in a lower crustal magma chamber lying beneath the bull's eye area, itself underlain by the depleted mantle source area. Our EarthScope study of the Wallowa Mountain area will image the crust and mantle modifications created by the CRB event, and test the idea that this was a concentrated ("Green's function") delamination of the pluton root. Seismometers are currently deployed and data will be recovered and analyzed soon.

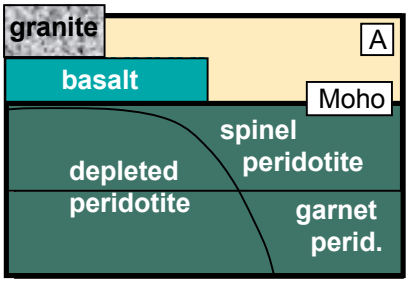

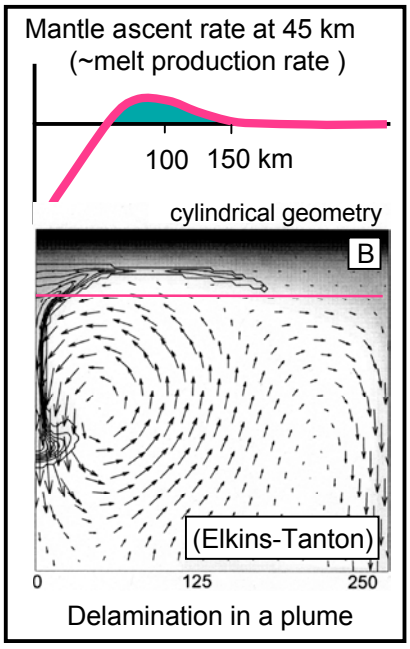

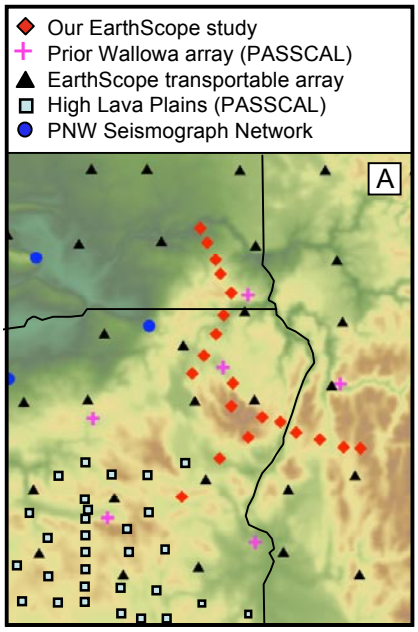

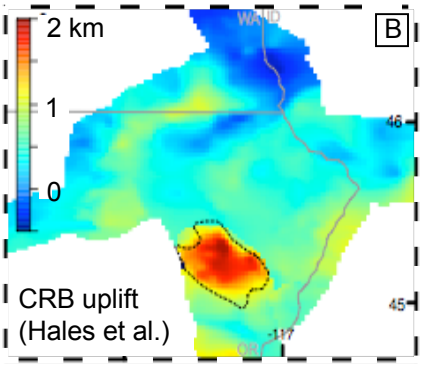

Hales, T.C., D. Abt, E. Humphreys, and J. Roering, A lithospheric instability origin for Columbia River flood basalts and Willowa Mountains uplift in northeast Oregon, Nature, 438, 842-845, 2005.

Partially supported by NSF award EAR-0511000. Equipment from the EarthScope facility.

Left: (A) Conceptual lithosphere structure, showing basalt magma chamber above depleted mantle and below the granitic Wallowa Pluton. (B) Delamination-driven flow model and expected melt production. The sinking of a dense pluton root would drive similar flow, causing melting around the sinking body.

Right: (A) Seismic arrays in study area. Red diamonds show our 20-station array, which crosses the bulls's eye margin at 3 locations, the Wallowa pluton, and the suture between accreted terrains and Precambrian North America.

USING LARGE APERTURE SEISMIC ARRAYS TO IMAGE THE RUPTURES OF THE NOVEMBER 15, 2006 AND JANUARY 13, 2007 KURIL EARTHQUAKES

Alexander Hutko • University of California, Santa Cruz

Back-projection of energy to grid points assumed to act like point sources at different times allows us to image the direction and propagation of recent Mw 8.1 and Mw 8.3 earthquakes in the Kuril Islands. We use high frequency P-waves recorded by USArray and other arrays across the globe with sufficient aperture to track the rupture front where high frequencies originate. Arrays with apertures of a few hundreds of kilometers and smaller do not span enough slowness and resulting images are grossly smeared along the great circle path. While energy from the rupture front away from the hypocenter arrives buried in the coda of the P wave, its moveout in time is unique and back-projects to a narrow region. In order to eliminate artifacts due to receiver side structure, station specific corrections based on residuals between predicted and observed first arrivals are applied. The travel time residuals are calculated by picking first arrivals for the January event. Corrections based on these residuals are also applied to the November event, whose first arrivals are very emergent and difficult to pick. Using the same corrections for these neighboring earthquakes adds confidence to interpretations of features unique to each earthquake.

Ishii, M., P. M. Shearer, H. Houston, & J. E. Vidale (2005), Extent, duration and speed of the 2004 Sumatra-Andaman earthquake imaged by the Hi-Net array, Nature, 435, 933-936.
Walker K., M. Ishii, and P.M. Shearer (2005), Rupture details of the 28 March 2005 Sumatra Mw 8.6 earthquake imaged with teleseismic P waves, Geophys. Res. Lett. 32, L24303, doi: 10.1029/2005GL024395.

This work is supported by NSF Grant EAR-0453884.

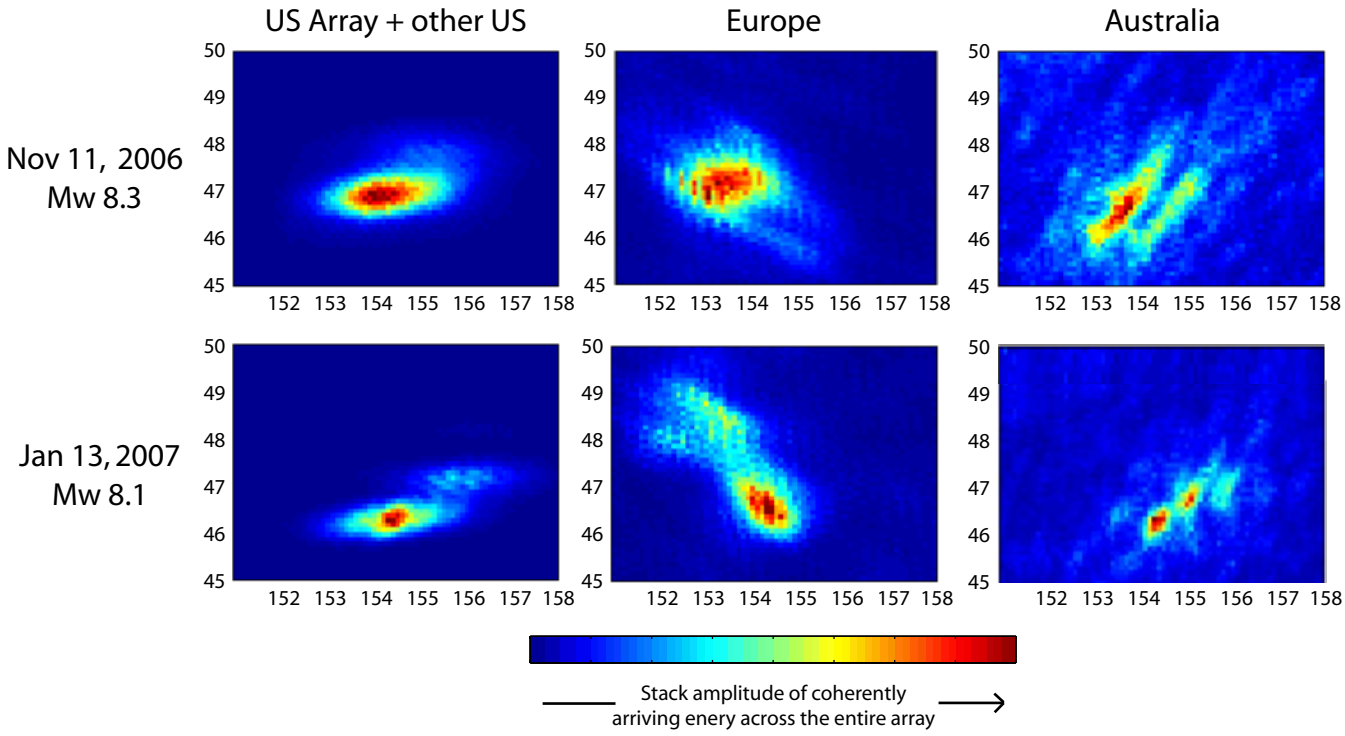

The figures show the distribution of high frequency energy radiated for the entire duration (~100 sec) of both earthquakes. Results are shown using data from different continents, each at a unique azimuth. All data were filtered from 0.8 to 2.0 Hz in order to focus on mapping coherent high frequency energy. Results at lower frequencies are smeared across too great of an area and appear as a bullseye. After the rupture spreads, the region radiating high frequency energy becomes too large and complicated to produce coherent arrivals across arrays. Only a small area around the hypocenter from the first few seconds of rupture, effectively a point source, is illuminated. 9th root stacking is applied to raise weak but coherent arrivals above the noise level. Hyper sensitivity to weak but coherent arrivals rather than semi-coherent large amplitudes limits the amount of smearing present. Results from Australian and European data for the November event are consistent with coseismic triggering on the outer rise where many aftershocks have been located. Results using USArray data for the January event show a secondary feature towards North America. It is difficult to distinguish between rupture propagation and an aftershock since the azimuth towards North America is along strike. Results from European stations show secondary features originating ~30 seconds after the main rupture initiation, but offset by at least 100 km to the Northwest, perpendicular to the strike of the fault. Given its large offset from the hypocenter, it is difficult to reconcile this as part of the main rupture and may be evidence for triggering of smaller earthquakes downdip. These intriguing observations may shed some light on earthquake triggering.

COPIOUS POSTSEISMIC SLIP FOLLOWING THE 2004 PARKFIELD EARTHQUAKE, CONSTRAINED BY GPS AND INSAR DATA

Ingrid Johanson • U.S. Geological Survey
Eric Fielding • Jet Propulsion Laboratory
Roland Bürgmann • University of California, Berkeley
Frederique Rolandone • Universite Pierre et Marie Curie, France

The September 28, 2004, Mw6.0 Parkfield earthquake was the long delayed fulfillment of the Parkfield Earthquake Prediction Experiment [Bakun and Lindh, 1985]. The years since the original prediction have seen the advent of space-based geodesy; both GPS and InSAR data can now be added to the wealth of information on this historic earthquake. We use these data to constrain a model of the coseismic and postseismic slip of the 2004 Parkfield earthquake. In Johanson et al. [2006], we examine the relationship between these two periods of the earthquake cycle, their relationship to aftershocks and the extent and importance of aseismic slip.

We invert eight interferograms jointly with campaign and continuous GPS data for slip in the coseismic and postseismic periods of the 2004 Parkfield earthquake. The two datasets complement each other, with the InSAR providing dense sampling of motion and the GPS providing more sparse, but three dimensional, measurements of ground motion. The model assumes exponential decay of the postseismic slip with a decay time constant of 0.087 years, determined from time series modeling of continuous GPS and creepmeter data.

Double-difference relocation of Parkfield aftershocks shows a prominent microseismicity streak at ~5 km depth [Thurber et al., 2006]. One interpretation of microseismicity streaks is that they occur at the boundaries of creeping and locked fault asperities [Nadeau et al., 1995]. The streak of aftershocks at 5 km depth occurs near the top of an area of high slip in Figure 1a, and could be interpreted as weakly bounding that asperity.

We find a geodetic moment magnitude of Mw6.2 for a 1-day coseismic model and Mw6.1 for the entire postseismic period. A comparison of the geodetic slip models with seismic moment estimates suggests that the coseismic moment release of the Parkfield earthquake is as little as 25% of the total. This finding underscores the importance of aseismic slip in the slip budget for the Parkfield segment.

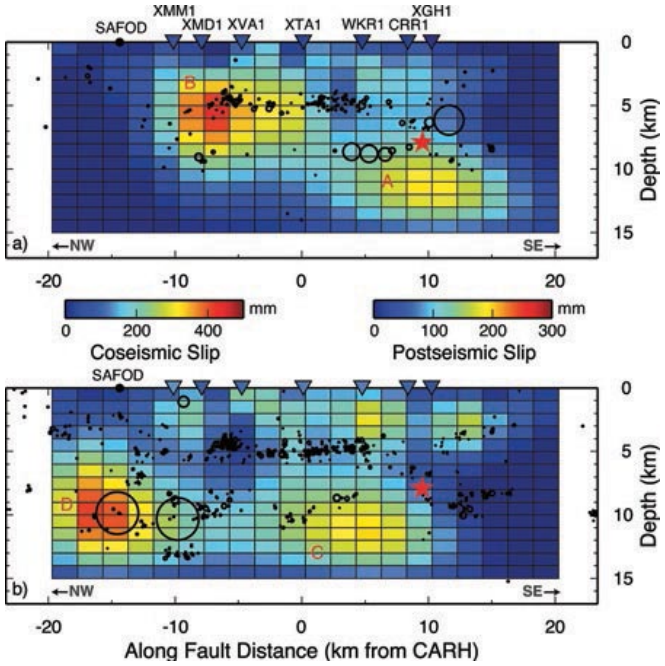

Results of inversion for a) Coseismic slip with one day of aftershocks.

b) Postseismic slip with aftershocks from September 29 through November 17. Red stars mark location of earthquake hypocenter. Triangles are color-coded creepmeter displacements roughly corresponding to the coseismic and postseismic periods.

Bakun, W. H., and A. G. Lindh (1985), The Parkfield, California, earthquake prediction experiment, Science, 229, 4714, 619-624.

Johanson, I. A., E. J. Fielding, F. Rolandone, R. Bürgmann (2006), Coseismic and postseismic slip of the 2004 Parkfield earthquake from space-geodetic data, B Seismol Soc Am., 96, 4b

Nadeau, R. M., W. Foxall, and T. V. McEvilly (1995), Clustering and periodic recurrence of microearthquakes on the San Andreas fault at Parkfield, California, Science, 267, 5197, 503-507.

Thurber, C., H. Zhang, F. Waldhauser, J. Hardebeck, A. Michael, and D. Eberhart-Phillips (2006), Three-Dimensional Compressional Wavespeed Model, Earthquake Relocations, and Focal Mechanisms for the Parkfield, California, Region, B Seismol Soc Am., 96, 4b

This research was supported by NSF Grant EAR-0337308 and the Southern California Earthquake Center (EAR-0106924).

EARLY TOMOGRAPHIC RESULT FROM THE BROADBAND FLEXARRAY DEPLOYMENT IN THE SIERRA NEVADA

Craig Jones • University of Colorado
Hersh Gilbert • Purdue University
George Zandt • University of Arizona
Tom Owens • University of South Carolina

The Sierra Nevada EarthScope (SNEP) experiment has been designed to understand the geodynamics of the Sierra Nevada and the significance of foundering of continental lithosphere in the evolution of the range. Foundering of lithosphere was inferred from earlier observations that included the petrology of xenoliths and geochemistry of basaltic eruptions. At one extreme, foundering could be responsible for much of the topography in the range and the development of the California Coast Ranges and accelerated motion of the Eastern California Shear Zone. At another extreme, the foundering might have only produced some unusual volcanism and minor uplift.

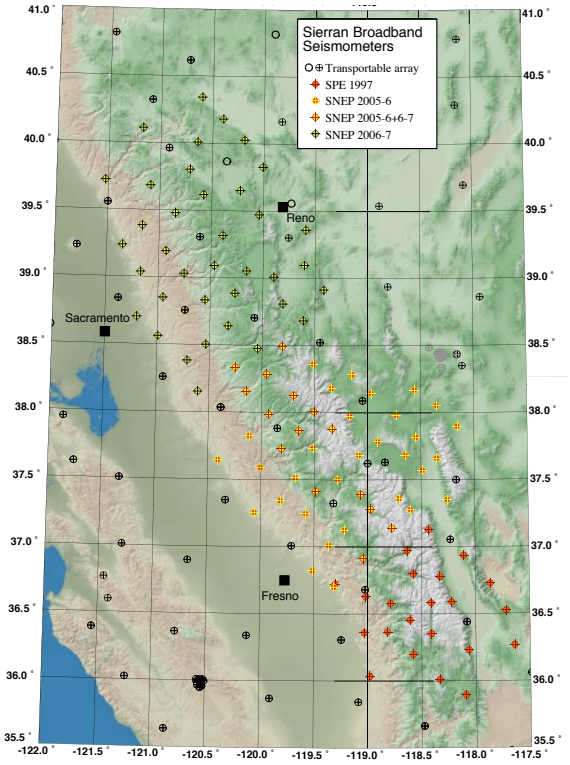

Map of SNEP seismometers, Transportable Array sites, and 1997 SPE seismometer sites on a topographic base.

Shown here are some results from the first phase of the 2005-7 SNEP deployment for teleseismic P-wave arrival times. This first phase of the deployment used 46 FlexArray broadband CMG3T seismometers in the central Sierra to densify the Transportable Array stations in the region. The second phase, underway at this writing, expands the network to the north. Most striking are the tightly focused early arrivals from events to the southeast; these are over 1 second earlier than stations only 50 km away. Events to the northwest show a much more distributed anomaly extending nearly to the Garlock Fault (as shown from earlier work). This clearly shows that the high wavespeed anomaly plunges to the southeast. Simple constraints from crossing rays in this dataset indicates that the base of the anomaly is above 300 km depth. This suggests that the material that was removed from the base of the Sierran crust is either still in the shallow mantle or has sunk well below 300 km depth. The strong confirmation of a southeast plunge presents an interesting challenge to geodynamic models of this foundering event.

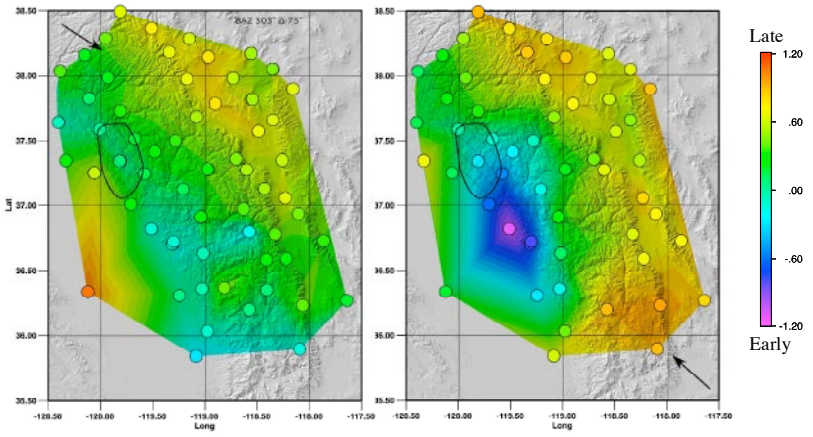

Maps of P-wave travel time residuals for 1997 SPE and 2005 SNEP deployments. Northwestern back-azimuths (left) show a broadly smeared area of early arrivals (light blue) in the southern foothills, but southeastern back-azimuths (right) reveal a compact area of profoundly early arrivals. Cross-hatched area has numerous deep (>20 km) earthquakes.

Ongoing work uses the Transportable Array to provide a wide aperture base for the more detailed tomography possible by combining the 1988 southern Sierran experiment, the 1997 Sierran Paradox experiment, the 2005-6 SNEP deployment in the central Sierra, and the 2006-7 SNEP deployment in the northern Sierra. This combination of experiments provides the first high-resolution, common baseline dataset to fully span the high-wavespeed anomaly under the southeastern Great Valley and adjacent Sierra Nevada.

Ian Bastow and IRIS intern Amanda Thomas picked and reduced many of the P arrivals shown here. NSF EarthScope grants 0454535 to Jones, 0454554 to Zandt and 0454554 to Owens support this experiment. Many others helped permit, deploy, and maintain these instruments.

EARTHQUAKE SOURCE PROPERTIES FROM NEAR-FIELD EARTHQUAKE MONITORING

Thomas Jordan, Yehuda Ben-Zion • University of Southern California
Ze'ev Reches • University of Oklahoma
Margaret Boettcher • U.S. Geological Survey

The main scientific objective of SAFOD is to further our understanding of earthquake and fault mechanics. This fundamental goal will only be achieved with long-term seismic monitoring in and around the SAFOD borehole. The lack of observed precursory signals before the 2004 Mw = 6.0 Parkfield earthquake [e.g. Johnston, et al, 2006] implies that the nucleation size of earthquakes is at most a few tens of meters, and that to detect related signals we will need instruments within the hypocentral region. Earthquake scaling relations have important implications for many aspects of earthquake physics and are directly related to seismic hazard analysis. Many authors have attempted to extend source parameter scaling to microseismic

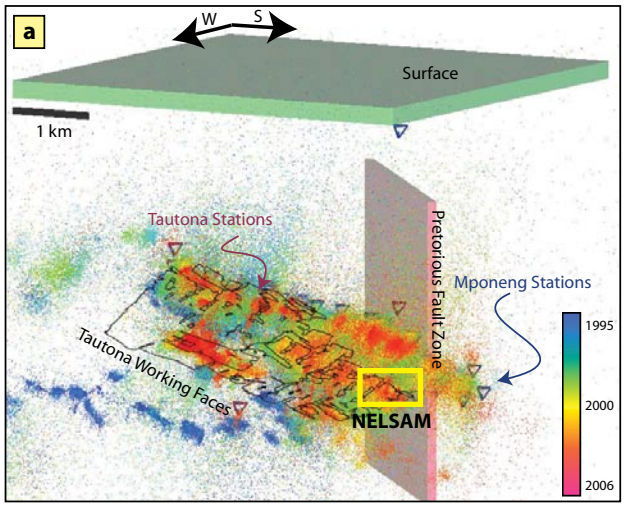

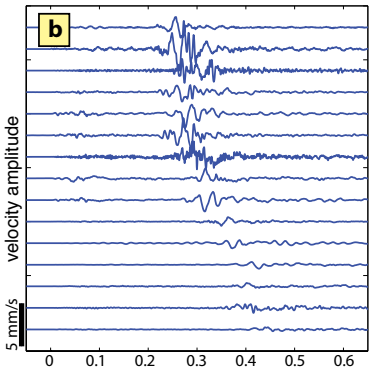

(a) Tautona Mine geometry including active mining stopes and tunnels (black lines), the ancient Pretorious Fault Zone, geophones in both Tautona and Mponeng mines, and ~500,000 events, recorded between 1995 and 2006 (dots colored according to time of occurrence, see the color scale). The yellow box marks the site of the NELSAM experiment. (b) Velocity seismograms from the largest amplitude component at each of 15 stations for the Dec. 12, 2004 MW = 2.2 earthquake. Approximately 40 MJ of radiated energy is calculated in the time-domain using signal out to 4 times the S-P time interval following the S wave, with a correction for distance-dependent attenuation.

events, leading to an on-going debate on whether or not there is a scale break between small and large earthquakes. Using near-source data, we can hopefully resolve the debate on earthquake scaling and determine if the wealth of data on small events can be utilized to understand the less frequent large events.

We are currently using data from the Natural Earthquake Laboratory in South African Mines (NELSAM) project, where we collect high-frequency (up to 12 kHz) seismic data at 3.6 km depth. We record earthquakes in the magnitude range -3.0 < Mw < 3.0 located meters to hundreds of meters from our seismometers. Using this dataset we are addressing critical issues concerning the earthquake source including (1) the scaling of source parameters such as apparent stress, stress drop, and rupture velocity with earthquake moment, (2) the possible scaling of seismic signals in the early waveform with the final event size, (3) the partitioning of energy between radiated seismic, frictional, and fracture energies, and (4) whether a minimum earthquake exists for a given tectonic environment.

While the NELSAM experiment has, and will continue to obtain, abundant high-quality data directly from the earthquake source region, ultimately the events recorded by NELSAM are mining-induced. Our Japanese collogues, working in a nearby South African mine, have made advances on similar topics [e.g. Yamada et al, 2005], but they too are investigating earthquake source processes of mining-induced seismicity, rather than natural tectonic events. In order to verify the applicability of our results to naturally occurring earthquakes, we need to compare our findings to high-quality seismic data from the hypocentral region an active tectonic fault, such as the San Andreas. The borehole data from the SAFOD array will provide an ideal dataset to observe the details of earthquake nucleation, rupture, and arrest within the seismogenic zone of a major plate-bounding and societally important fault.

Johnston, M.J.S., R.D. Borcherdt, A.T. Linde, and M.T. Gladwin, Continuous Borehole Strain and Pore Pressure in the Near Field of the 28 September 2004 M 6.0 Parkfield, California, Earthquake: Implications for Nucleation, Fault Response, Earthquake Predic

Yamada, T., J. J. Mori, S. Ide, H. Kawakata, Y. Iio, and H. Ogasawara, Radiation efficiency and apparent stress of small earthquakes in a South African gold mine, J. Geophys. Res., 110, B01305, doi:10.1029/2004JB003221, 2005.

Ide, S., G. C. Beroza, Does apparent stress vary with earthquake size?, Geophys. Res. Lett., 28(17), 3349-3352, 10.1029/2001GL013106, 2001.

Collaborators: Malcolm Johnston, Art McGarr, Michael Lewis, and Gerrie van Aswegen. Support: Natural Earthquake Laboratory in South African Mines, NSF.

RESULTS OF ELEMENTAL, STABLE ISOTOPE, ORGANIC MATTER, AND FISSION-TRACK ANALYSES OF SAFOD DRILL-HOLE CUTTINGS AND CORE MATERIAL

David Kirschner • Saint Louis University
Judith Chester • Texas A&M University
John Garver • Union College
Jim Evans • Utah State University

Geochemical analyses of cuttings and core material from the SAFOD drill hole provide important information on the subsurface geology and the fluid-rock interactions that have occurred in and adjacent to the fault zone. We have obtained an integrated geochemical data set from the main drill hole that includes elemental data for 120 cutting and core samples, stable isotope data for 100 vein and breccia samples, organic maturity data for 30 samples, and zircon fission-track data for 6 samples. In the elemental data set, there are 6 breaks/transitions in the abundance of individual elements: at 3197 m (potentially corresponding to the western fault-bounded margin of the SAF damage zone); at 1926 m (a granite-sandstone fault contact); at 3319 m (perhaps the most important fault contact within the core of the SAF zone); at 2570 (core of clay-rich shear zone?); at 3481 (near faulted contact between folded and non-folded sediments); and at 3078m (near clay-rich fault zone that was encountered at end of phase 1 coring).

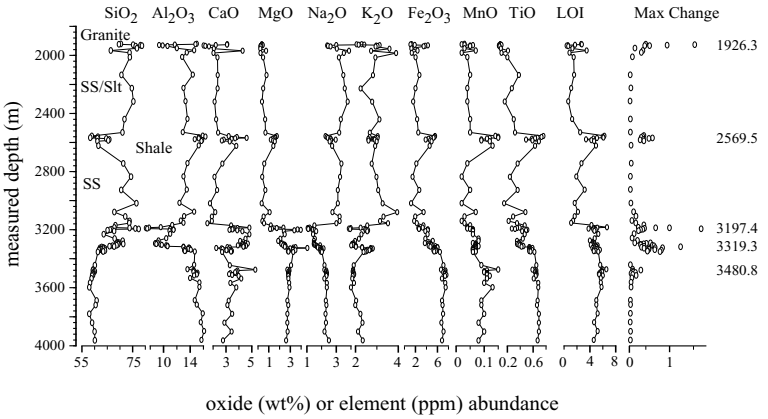

Elemental abundances in cuttings material from the SAFOD drill hole. Several distinctive breaks, which correspond to lithologic and/or faulted contacts, are evident in the data set.

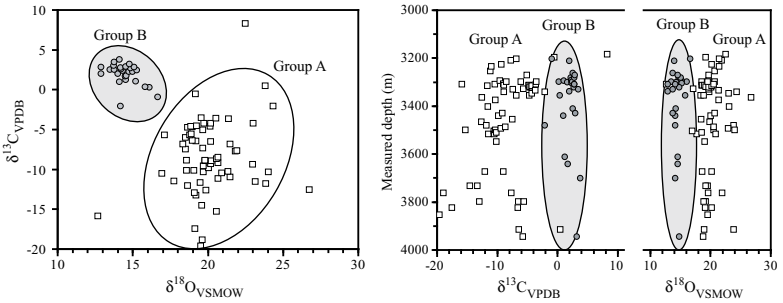

Isotopic data of carbonate veins and breccias from 3 to 4 km depth (MD) cluster into two groups (A and B) in d13C - d18O space. Although, veins from both groups are present in the cuttings below 3200 m (MD), half of the group B veins were from the 3260 to 3310 m interval, which corresponds with the highest abundance of carbonate in the sample cuttings.

In the stable isotope data , the carbon isotope values of the carbonate veins and cement vary significantly from +8 to negative 20 per mil; the oxygen isotope values vary from +26 to +12 per mil. The data can be separated into two groups, both of which are present on either side of the inferred SAF. The group with low carbon isotope values are consistent with the carbon having been derived from, or exchanged with, either 1) biogenically derived methane, 2) thermogenic methane at temperature greater than 180C rather than at their current down hole temperature of approximately 120C, or 3) dissolved carbon in groundwater that had been produced in the root zone of C3 plants. The latter hypothesis would be consistent with the carbon isotope data of soil gas in the Parkfield area [Lewicki et al., 2002]. In contrast, the other group of veins and breccias are in oxygen isotope equilibrium with the silicate-buffered formation water obtained from the drill hole and close to carbon isotope equilibrium with the thermogenic methane sampled in the drill hole. The total organic content (TOC) of the cuttings are below 1 percent by weight. The kerogen is considered to be “gas prone” on the basis of the TOC and Rock-Eval pyrolysis, hydrogen index, and oxygen index values. The vitrinite reflectance of 23 samples increase with depth from 0.70 at 3230 m to 0.95 at 3960 m. This increase in reflectance values is consistent with increasing temperature and organic maturation with depth. Although the data is limited, there is no significant offset in organic maturity across the inferred SAF zone. Six zircon fission-track dates range from 64 to 70 Ma, which are interpreted as cooling ages of the sediments’ source terranes. There is no discernable difference in dates across the inferred SAF zone. Zircons from approximately 15 other samples are in the process of being analyzed at this time.

Additional colloborators on this work include Fred Chester (Texas A & M) and John Solum (Sam Houston University). We also thank Stephen Hickman and Diane Moore of the U.S.G.S. for their contributions. This work has been funded by the National Science Foundation. NSF EAR-0454531 and NSF EAR-0346190

REFLECTION IMAGING THE 35°-DIPPING NORMAL FAULT THAT BOUNDS THE BASIN & RANGE PROVINCE

Simon Klemperer • Stanford University
Derek Lerch • Feather River College
Anne Egger • Stanford University
Joseph Colgan • U.S. Geological Survey

Surprise Valley, straddling the NV-CA-OR borders, is bounded to the west by the Warner Mountains forming the westernmost classic basin-range pair of the eponymous extensional province. The Surprise Valley fault (SVF) is an east-dipping, large-offset normal fault that developed isolated from other significant Basin-and-Range faulting by the essentially unfaulted Sheldon volcanic plateau to the south and east (and the Modoc Plateau to the west). Seemingly correlative Mio-Pliocene basalt flows and tuffaceous sediments east and west of Surprise Valley/Warner Range suggest continuous Pliocene basalt flows may have predated significant faulting, so that up to 5 km of offset (3 km strata exposed in the Warner Range, 2 km imaged by us) may have occurred on the SVF in 3 to 5 Myr (time-averaged slip-rate of 1-2 mm/yr). Large-magnitude Holocene rupture, modern seismicity, local geothermal activity and overpressured basin strata are all consistent with a high present-day slip rate. Our September 2004 EarthScope-supported seismic experiment across the northwestern margin of the Basin-and-Range province included a relatively high-resolution vibrator-source profile (20-m CMP spacing) from the surface trace of the SVF for 16 km east across Surprise Valley; a 300-km explosive-source seismic refraction survey including an 1100-kg shot-point on the east side of Surprise Valley recorded at 300-m spacing across the SVF, and complementary teleseismic recordings. Our explosive-source recording shows a reverse-moveout reflection projecting to the surface trace of the SVF that can best be modeled as from a fault plane dipping 30 to 45° east (dip depends on assumptions about near-surface velocities, 2±0.2 km/s) to a depth >7 km. The most significant reflector on our high-resolution reflection profile truncates intra-basin stratigraphic reflections, and has a migrated dip of 20°±2°. Our west-east 2-D profile has an oblique intersection with the strike of the SVF, but appropriate geometric correction for this obliquity steepens the true dip of the fault plane to only 35°±3°. We image a separate fault-splay above the main fault with a true dip of 30°±5°. Cenozoic volcanic strata uplifted in the Warner Range dip 20° to the west, documenting footwall-block rotation during the development of the SVF. Restoring this rotation, the orientation of the SVF at its formation becomes 55°±3°, compatible with normal fault geometries observed in laboratory experiments. However, trenching for paleoseismic studies constrains the near-surface dip of the active SVF to be ~65°, too steep to be the fault-plane geometry that produced the ~20°-dipping Cenozoic stratigraphy in the Warner Range. This active fault trace of the SVF is likely an extremely young feature in the Surprise Valley-Warner Range evolution, though it is not yet known whether it soles into, or cuts and offsets the less-favorable, now-shallow geometry (30°-35°) of the main SVF. Surprise Valley may provide the chance to study the process of abandonment of a major active low-angle fault in favor of a new high-angle fault.

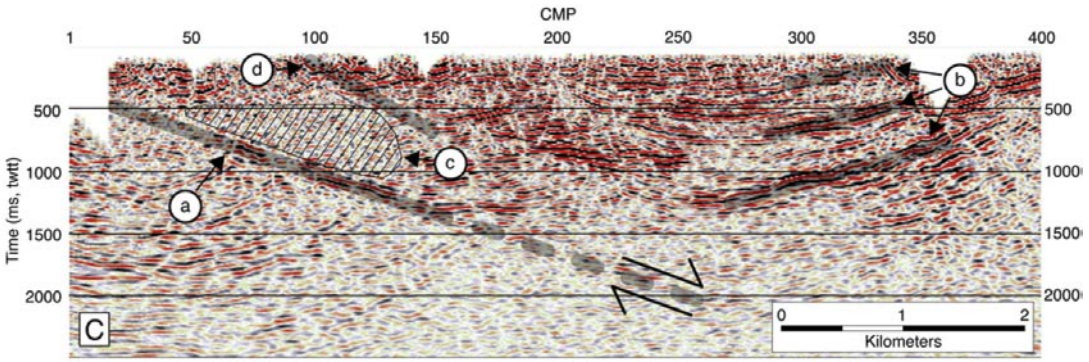

Migrated image of the Surprise Valley basin, with no vertical exaggeration based on basin-fill Vp=2 km/s. CMP spacing is 20 m. The SVF (a) forms a continuous, moderate–amplitude east-dipping reflection that bounds the western side of the basin. Prominent west-dipping reflections (b) on the eastern edge of Surprise Valley correspond to late Miocene to Pliocene (8–3Ma) volcanic strata. The reflection-free region (c) immediately above the SVF is interpreted as alluvium deposited along the range-front during footwall exhumation. West–dipping reflections near CDP100 appear to be truncated by a fault splay (d) above the SVF.

D. W. Lerch, S. L. Klemperer, A. E. Egger, J. P. Colgan, and E.L. Miller, Reflection profiling of active Basin and Range extension: Surprise Valley, CA, ms. in preparation for submission to Geology

Support for vibroseis profiling was provided by NSF-Geoenvironmental Engineering and Geohazard Mitigation grant 0444696; principal funding for the explosive-source profiling was provided by NSF-EarthScope grant 0346245 and by the Petroleum Research Fund of the American Chemical Society grant 39063-AC8. Field support and instruments were provided to all parts of the experiment by the PASSCAL Instrument Center.

CRUSTAL STRUCTURE OF THE NORTHWESTERN BASIN AND RANGE PROVINCE AND ITS TRANSITION TO UNEXTENDED VOLCANIC PLATEAUS

Simon Klemperer • Stanford University
Derek Lerch • Feather River College
Jonathan Glen, David Ponce • U.S. Geological Survey

The northwestern margin of the Basin and Range Province is characterized by a transition from low-magnitude (~20%) extension in northwestern Nevada to relatively unextended volcanic plateaus in northeastern California. Seismic-velocity and potential-field modeling provides new control on the Mesozoic-to-present tectonic evolution of this poorly understood portion of the U.S. Cordillera. We document ~20% crustal thinning associated with Basin and Range extension from a crustal thickness of ~37 km under northeastern California to ~31 km under northwestern Nevada that is consistent with the amount of extension recorded in the upper crust in northwestern Nevada, suggesting the crustal response to extension was relatively homogeneous over the entire crustal column. Our modeling also shows a well-defined, 80-km-wide zone of unusually low upper-crustal velocities (~5.9–6.1 km/s) that coincide with the surface location of sparse Cretaceous granites, locating the elusive northern extension of the Sierra Nevada batholith through northwestern Nevada for the first time in the subsurface. Combining geological and geophysical data, we reconstruct the late Cretaceous-to-present crustal evolution of this region, documenting an interplay between magmatic addition to the crust, erosional exhumation, sedimentation, and extension that has reversed the direction of crustal thinning from a west-facing continental margin to an east-facing interior basin margin over this time interval. Finally, we find no evidence in northwestern Nevada for unusually thick crust (>40 km) prior to Basin and Range extension.

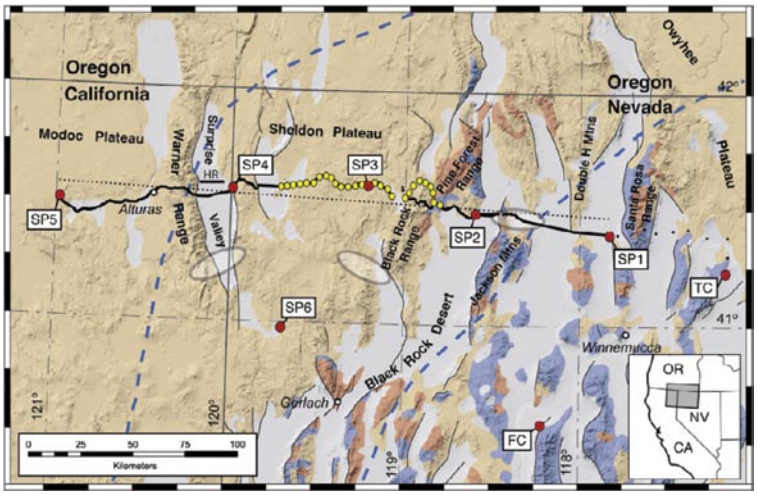

Experiment layout and geology: red circles: shotpoints and mine blasts; black circles: geophone locations; yellow circles: passive deployment. Blue dashed lines lines correspond to basement suggested to have >50% Cretaceous granitic material.

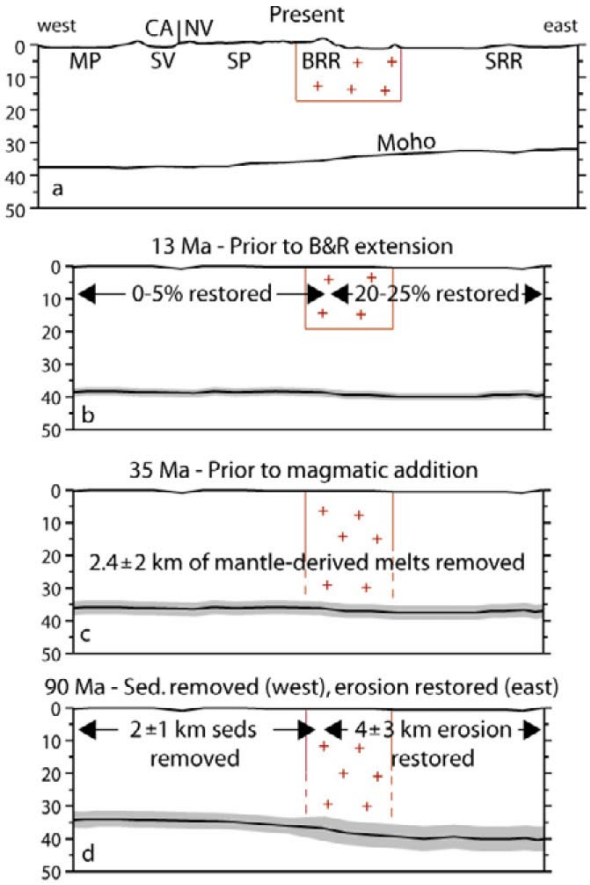

Inferred crustal evolution from late Cretaceous - present. (a) Present - day crustal structure with west-dipping Moho, lower- and mid crustal magmatic addition, and modern topography (MP=Modoc Plateau, SV=Surprise Valley, SP=Sheldon Plateau, BRR=Black Rock Range, SRR=Santa Rosa Range). Red crosses: region of low Vp inferred to mark location of the Sierra Nevada batholith. (b) Crustal structure before Basin and Range extension, with redeuced Moho topography. (c) Removing Cenozoic magmatic addition thins crust. (d) Restoring erosion (east) and removing sedimentation (west) produces an east - dipping Moho. Reconstruction uncertainty (RMS) is represented by the gray Moho outline. V.E.“2:1 topography is shown schematically.

Lerch, D.W., Klemperer, S.L., Glen, J.M.G., Ponce, D.A., Miller, E.L., and Miller, E.L. Crustal structure of the northwestern Basin and Range province and its transition to unextended volcanic plateaus. 2007. Geochemistry, Geophysics, Geosystems, v. 8, Q02011.

Principal funding for explosive-source profiling was provided by NSF-EarthScope grant 0346245 and by the Petroleum Research Fund of the American Chemical Society; support for vibroseis profiling was received from NSF-Geoenvironmental Engineering and Geohazard Mitigation grant 0444696; and funding for passive-source deployments came from Stanford University. Field support and instruments were provided to all parts of the experiment by the PASSCAL Instrument Center.

GEOLOGICAL INTERPRETATION OF MULTI-DIMENSIONAL GEOPHYSICAL MONITORING DATA BASED ON SELF-ORGANIZING MAPS

Christian Klose • Columbia University

Since geoscientific initiatives like EarthScope have been increasing with a number of monitoring projects, the amount of geophysical data is continuously accumulating over time. Thus, geoscientists are challenged to interpret large amounts of different geophysical parameters and many times simultaneously. Interpretation difficulties occur especially, when data, that need to be interpreted, are of arbitrary dimension. In tandem, interpretations (e.g., correlations) are very often based on single parameters that lead to ambiguous interpretation results.

This presentation describes the application of a statistical method, called Self-Organizing Maps (SOM), to classify and interpret multi-dimensional, non-linear, and highly noised geophysical data for prediction purposes of mechanically unstable geological regions and brittle deformation areas. Results of SOM-classifications can be represented as 2-dimensional images, called feature maps. These maps illustrate the complexity and demonstrate inter-relations between single parameters or clusters of the entire parameter space. SOM-images can be visually described and easily interpreted.

An application example is shown, based on a six geophysical parameters. Geophysical data were acquired by GFZ Potsdam and ETH Zurich from scanlines within tomographic images and seismograms as result from active seismic monitoring measurements in the 60 km long and up to 2000 m deep Gotthard base tunnel.

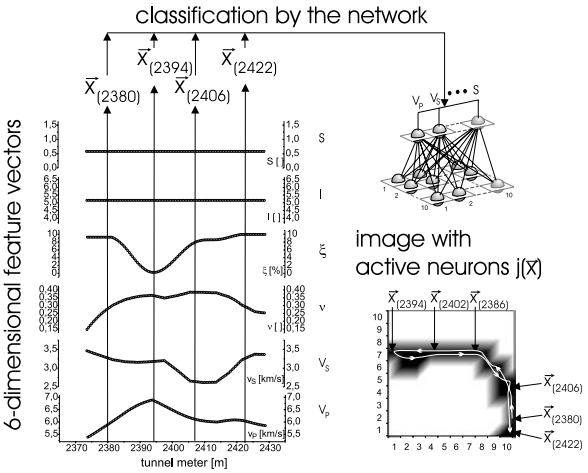

Classification scheme of a SOM neural network. 6-dimensional seismic feature vectors x were drawn along a seismic profile (here: profile 2360 - 2433 m). Several tunnel locations can be seen: 2380 m, (2386 m), 2394 m, (2402 m), 2406 m and 2422 m. Every x is presented to the SOM neural network. The classification is done, when a neuron in the Kohonen lattice is stimulated.

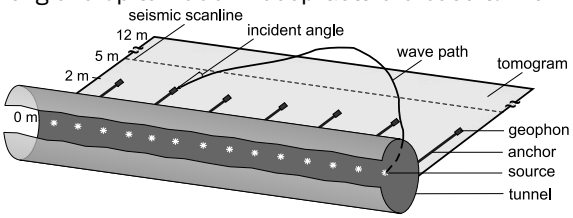

Schematic illustration of the installed geophysical measurement units (sources, receivers, and anchors) and of the tomographic imaging within the tunnel. A generated acoustic wave propagates in the interior of the rock and reaches a receiver with an incident angle that is only a few degrees from the idealized wave path.

The results demonstrate that it is possible to characterize geological rock mass properties from interpretations of multi-dimensional geophysical (seismic) in-situ data, when all seismic features are simultaneously used. Complicated distributions of parameters within the SOM-maps exemplify the complexity and non-linearity of the multi-dimensional parameter spaces. Hence, the overview of all features and all relationships can be retained for each interpretation. Visual interpretation results can be discussed among scientists and non-scientist as well as experts and non-experts. SOM-classifications are helpful for on-line predictions of unstable geological conditions in undiscovered rock mass regions (Figure 4). In conclusion, it is suggested that this interpretation method could be helpful for EarthScope monitoring projects, e.g., for the San Andreas Fault and Earth's upper mantel. (Reference: Klose, C.D. (2006) Self-Organising Maps for Geoscientific Data Analysis: Geological Interpretation of Multi-dimensional Geophysical Data, Computational Geosciences, 10(3), 1-13)

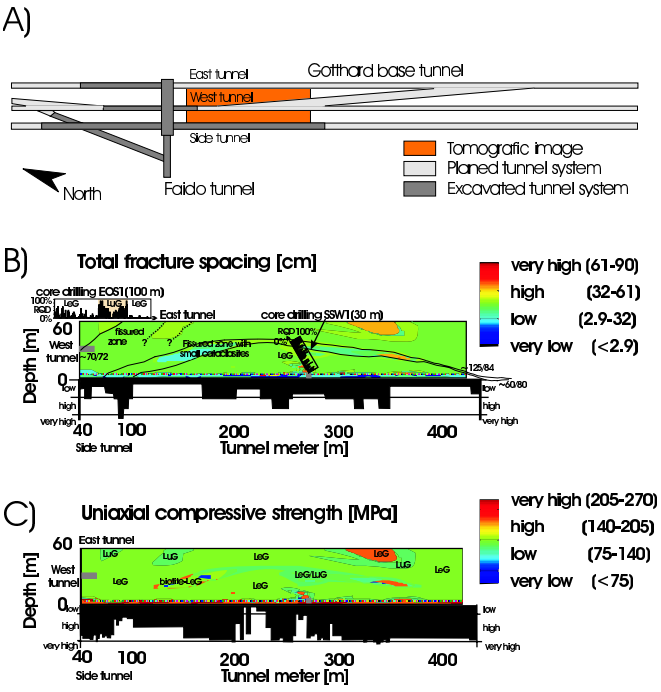

Interpretation results of a tomographic image (400x60 m2) in the Gotthard base tunnel (A). A SOM-network, trained with seismic data from the Faido adit, was applied to a new seismic data set in the Gotthard base tunnel. The total fracture spacing (B) and the uniaxial compressive strength (C) were predicted as class labels.

NOISE IN GPS MEASUREMENTS FROM SOUTHERN CALIFORNIA AND SOUTHERN

John Langbein • U.S. Geological Survey

Time series of position changes estimated from data from continuous GPS receivers spanning Southern California and Southern Nevada, including EarthScope PBO stations, are evaluated for noise models that characterize their temporal correlations. This paper extends the analysis of Williams et al. (2004) by using the methods of Langbein (2004). The time series range between 3.5 and 10 years in length. After adjusting these data for postseismic deformation, offsets, and annual and semi-annual periodicities, I find that no single type of noise model best represents these observations. Instead, about half of the time series have temporal correlations that are categorized as either flicker or random-walk noise. The remaining time series can be best categorized either a combination of flicker and random-walk, power law noise, first-order Gauss-Markov plus random-walk noise, or power law plus broad-band, seasonal noise. A variety of geodetic monuments are used in Southern California and Nevada, including deep-braced designs, cement pier, pins drilled in outcrop, and buildings. When I evaluate the noise for each time series in terms of estimating the standard error in velocity, I find that those sites located in Nevada having deep-braced monuments have the lowest noise. Sites located within regions of active pumping, both for ground water and oil, had the largest standard errors in velocity. In addition, even though regional filtering removed much of the common-mode signals in these time series, there remained a common-mode seasonal signal.

Langbein (2004), Noise in two-color EDM measurements revisited, JGR, v109 doi:10.1029/2003JB002819

Williams et al. (2004), Error analysis of continuous GPS position time series, JGR, v109

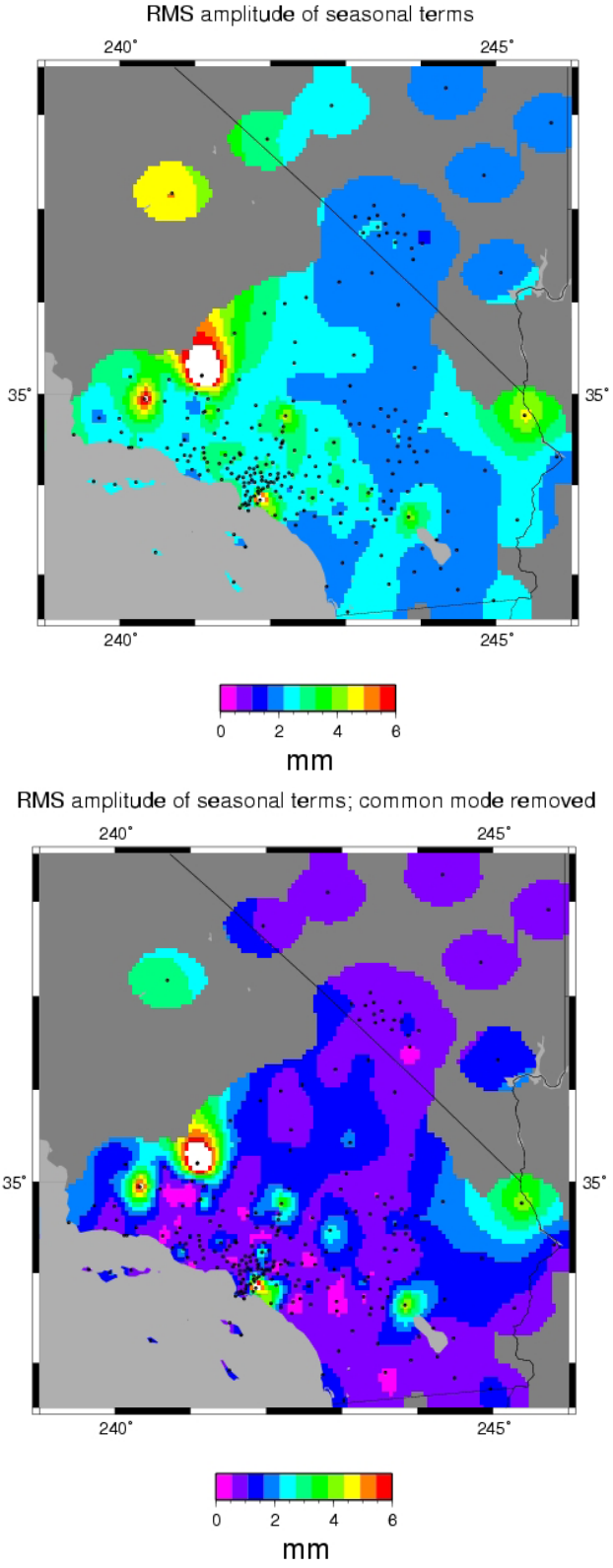

Estimate of RMS amplitude of seasonal noise from continuous GPS in Southern California and Nevada. Note that minimum amplitude is more than 1 mm. Dots show location of GPS sites. Estimate of residual RMS amplitude of seasonal noise from continuous GPS in Southern California and Nevada after removing common mode terms. Highest residual amplitudes are, in general, associated with anthropogenic sources.

TIDAL CALIBRATION OF PBO STRAINMETERS LOCATED IN THE PACIFIC NORTHWEST

John Langbein • U.S. Geological Survey

The Plate Boundary Observatory has installed a dozen Gladwin Tensor strainmeters in the coastal region between Vancouver Island and Oregon with the goal of measuring strain changes due to "episodic tremor and slip" (ETS) in the Cascadia subduction zone. Of those strainmeters, I have used the theoretical Earth tides with Ocean load adjustments (Agnew, 1999) to calibrate five strainmeters. The primary goal is to detect significant strain changes that can be attributed to tectonic activity. Each instrument consists of four extensometers. For each extensometer, all of the expected tidal amplitudes are estimated along with the response to changes in atmospheric pressure. At two sites located adjacent to inlets, the sensitivity of each extensometer to changes in ocean height due to the ocean tide are evaluated along with the standard tidal analysis; This become complicated since the local height change data needs to be filtered in two frequency bands; less than 18 hours and greater than 18 hours. Each band affects the instrument differently. Finally, the amplitude and phase of the M2 and O1 tidal constituents are compared against the theoretical tides of the tensor stain. I use method suggested by Hart el al. (1996) (their equation 13) where the theoretical tides are fit to the observed tides using standard least-squares. This is simply the "black-box" approach where there are no assumptions made concerning isotropic borehole deformation and topographic affects. After removing the affects of the grout curing, the background noise level of each tensor component is evaluated in terms of a power-law spectral density such that rate changes can be estimated with realistic estimates of their significance using the methods of Langbein (2004)

Hart et al., (1996), Tidal calibration of borehole strainmeters: Removing the effects of small-scale inhomogeneity, JGR, v101, p25,553–25,571.

Agnew (1999), SPOTL: Some programs for Ocean-Tide loading, http://igppweb.ucsd.edu/~agnew/spotlmain.html

Langbein (2004) Noise is two-color EDM measurements revisited, JGR v102, doi:10.1029/2003JB002819.

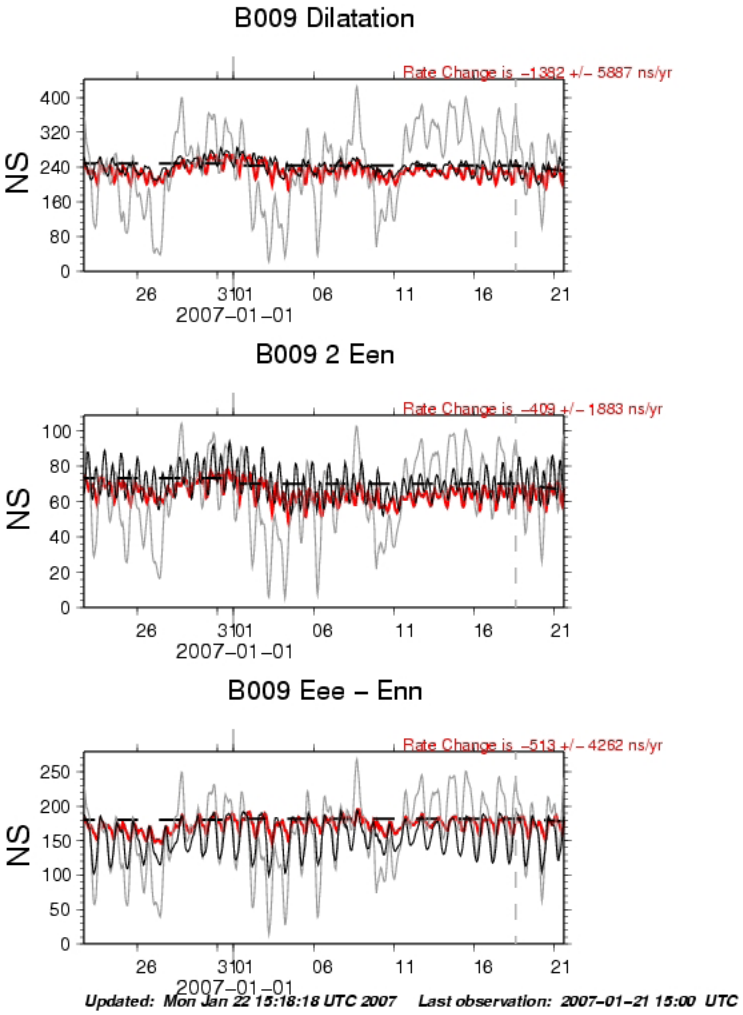

Example of reduction of borehole strainmeter data for site B009 which is located on Vancouver Island adjacent to Patricia Bay where tidal range is 3.8 meters. Grey are the raw data after the transforming the extensometer data into tensor quantities using tidal calibration. The black curve is the data after adjusting for changes in atmospheric pressure and the water level changes in Patricia Bay. Red represents the residual strain after removing the solid Earth tide and Ocean-load. The dashed line is a fit of linear trend over the 30 day interval and its rate change over the last 3 days; the rate change with its standard error is posted over each plot.

WAVE GRADIOMETRY FOR EARTHSCOPE

Charles Langston • University of Memphis

EarthScope facilities offer several opportunities for applying a new seismic technique, wave gradiometry, to the analysis of long-period waveforms recorded by USArray and PBO strain meter observatories. The spatial gradient of wave fields as a function of time and space over a gradiometer array gives information on horizontal slowness, geometrical spreading changes, azimuth, and radiation pattern changes of the wave field that, in principle, can be used to map heterogeneity in the lithosphere and mantle under North America. With an average station spacing of 70km, broadband stations of USArray can serve as gradiometer elements for the analysis of 100 s and longer period surface waves propagating across the continent and shorter period, but higher horizontal velocity teleseismic body wave phases. Maps of horizontal phase velocity, azimuth, and amplitude perturbations may yield empirical information on the location of major heterogeneity within the continent and provide a unique dataset for more detailed modeling of velocity structure. PBO strain meter observations in conjunction with a co-located broadband seismometer may also be used as a point "array" for analyzing the wave propagation of local, regional, and teleseismic events to yield additional constraints on event location and wave scattering. Such strain/seismic gradiometers may be useful in understanding the source of volcanic and deep fault tremor.

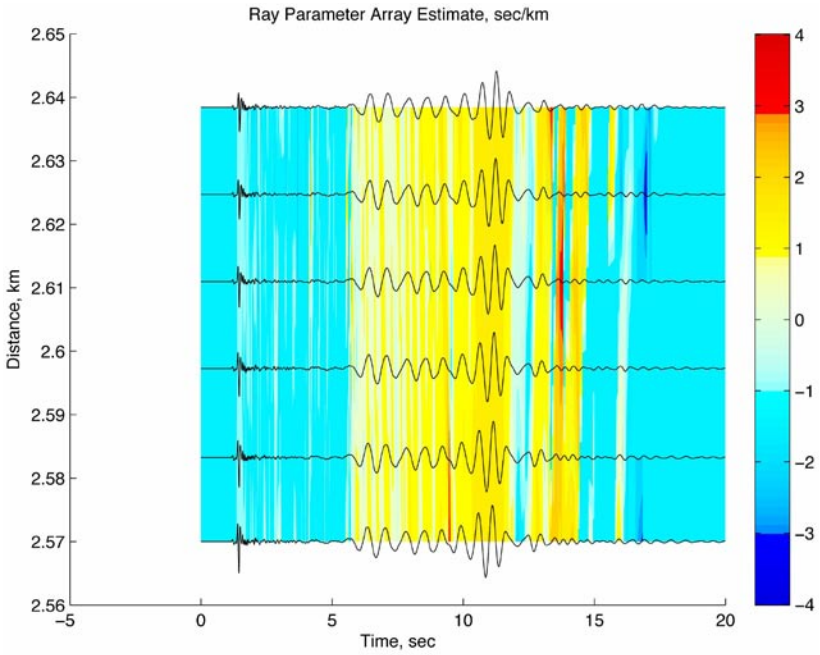

An example of mapping horizontal slowness as a function of time and space along a linear seismic gradiometer 105m in length. The source was a large explosion 2.5km distant. P and multimode Rayleigh waves are seen that propagate slowly across the array.

IS IT ALL WET? SEARCHING FOR HYDRATED MANTLE ROCK WITHIN CASCADIA MEGATHRUST.

Vadim Levin, Alex Nikulin • Rutgers University
Jeffrey Park • Yale University

One consequence of the "hydration" of mantle rocks adjacent to the subducting plate is a transformation of the original peridotite into serpentinite, a lighter, less stiff rock. Recently, we found evidence that a layer of serpentinite-rich rocks overlies the top of the subducted Juan de Fuca plate beneath central Oregon. The layer is not a part of the hydrated mantle wedge well-recognized in Cascadia (purple oval in the figure), but rather it is up-dip from the wedge corner. The layer is characterized by a high degree of anisotropy. Parameters of anisotropy are best explained by rock texture that would be formed by horizontal shearing in the north-south direction. The presence of a sheared serpentinite layer within the plate contact zone raises a number of important issues. Serpentinite is likely to promote sliding instead of rupture on the megathrust, and thus can act as a limiting factor on the maximum size of earthquakes. The orientation of inferred rock fabric we documented is difficult to explain in terms of subduction-related deformation, rather it is consistent with the northward motion of the Cascadia forearc relative to the stable North America. Overall, the issue of texture in rocks close to the plate interface is of great interest. The texture should be most closely related to the deformation, and hopefully diagnostic. By detecting and characterizing rock texture we should be able to learn about deformation causing it, and thus gain better insight into the sense of motion of rock bodies involved. We are investigating rock texture properties in the plate contact zone of the Cascadian forearc, using seismic data from existing permanent observatories, and from the transportable array nodes in the region. For the data from permanent seismic observatories in Cascadia we use existing anisotropy-aware receiver functions methodology that yields good results for individual sites. To date, in addition to Corvallis, OR, we observe seismic signature of the serpentinized layer at stations GNW (Green Mountain, WA) and DBO (Dodson Butte, OR). The signature is not obviously present at data-rich seismic stations LON and LTY in Northern Oregon. It is notable that all three sites showing a signature of the proposed serpentinite layer are ~40 km above the surface of the subducting Juan-de-Fuca plate. Sites where we cannot find the signature are further inland, and the slab surface beneath them is deeper. The transportable array data presents a challenge of "drinking from a fire-hose". We are experimenting with a number of variants of our receiver function technique that should facilitate efficient work with massive data flows.

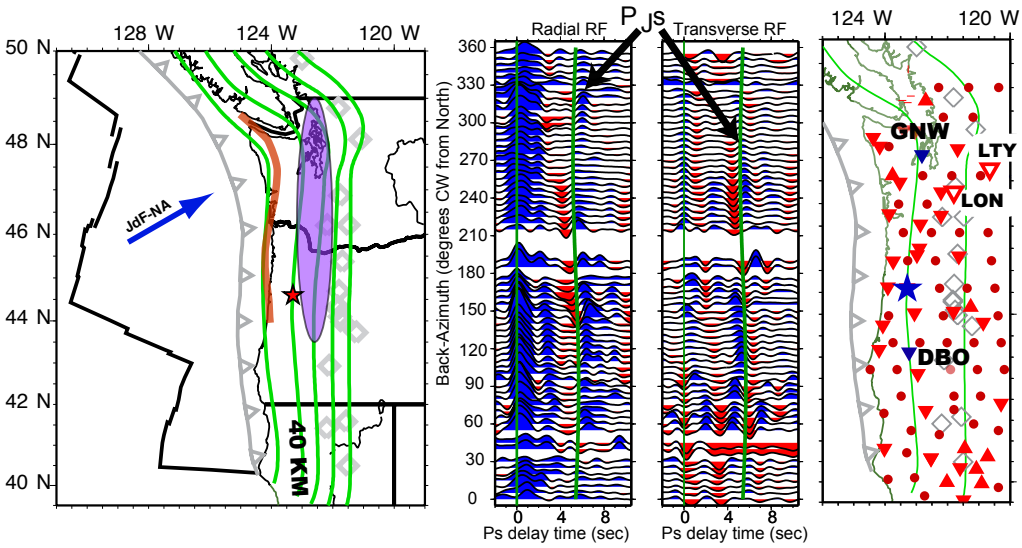

LEFT: A map of the Cascadia subduction zone shows volcanoes (grey diamonds) and contours of the subducting plate (green lines). Also shown are the location of the seismic station COR where the serpentinite layer has been identified (red star), the down-dip extent of the seismogenic zone based on thermal modeling and geodetics (orange line), and the region where the supra-slab mantle wedge is believed to contain significant amounts of serpentinite (purple oval). MIDDLE: Receiver functions computed from 602 earthquakes observed at Corvallis, OR. A straight green line marks the arrival time of the "parent" teleseimic P wave, the curved green line shows expected arrival time of the "daughter" P-to-S converted wave from an interface at 43 km, dipping 15 to the east. A clear two-sided phase seen on both sides of the curved green line is interpreted as evidence for the layer of sheared serpentinite above the Juan de Fuca slab. RIGHT: Existing permanent sites (triangles) for which data are available through IRIS DMC

Park, J., H. Yuan, and V. Levin, Subduction-zone anisotropy under Corvallis, Oregon: A serpentinite skidmark of trench-parallel terrane migration? Journal of Geophysical Research, 109, B10306, doi:10.1029/2003JB002718, 2004

THE LITHOSPHERE-ASTHENOSPHERE BOUNDARY BENEATH THE WESTERN UNITED STATES

Xueqing Li, Xiaohui Yuan and Rainer Kind • GeoForschungsZentrum Potsdam, Germany

The mechanical concept of a high viscosity lithosphere floating on a low viscosity asthenosphere is basic for plate tectonics. No sharp transition between both spheres is expected, which makes seismic high resolution observations difficult, especially since the asthenosphere is a seismic low velocity zone. The S receiver function technique has, however, shown in recent times to be a very good tool for high resolution mapping of the LAB. We applied this technique to seismic data in the western US and observed good signals from the LAB. A resulting map of the LAB depth is shown in Fig.1; seismic data along two profiles are shown in Fig.2 (LAB marked red). The lithosphere is 60-70 km thick and very clear south of the Mendocino Triple Junction; in the north it reaches 80-90 km and is less pronounced. A double low velocity zone is observed beneath the southern Sierra Nevada (Fig.2), perhaps indicating lithospheric delamination. These results have been obtained with pre-USArray seismic stations. The study will be repeated with USArray stations which will lead to much higher resolution.

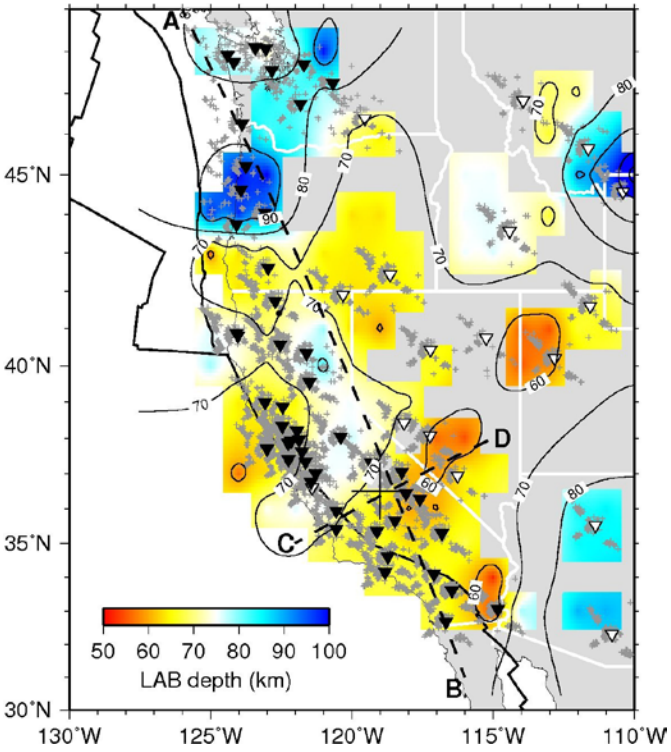

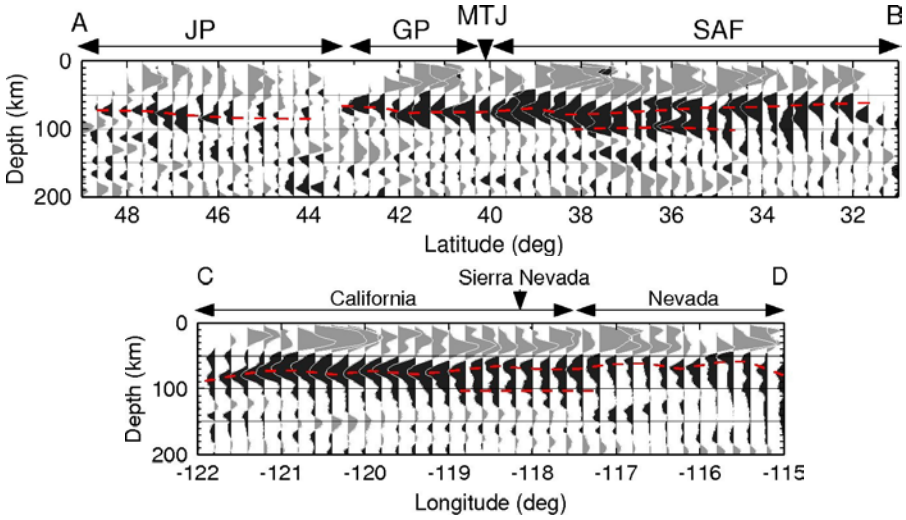

MONITOR PROPERTY VARIATIONS ON THE PARKFIELD SAN ANDREAS BY FAULT-ZONE TRAPPED WAVES

Yong-Gang Li • University of Southern California
Peter E. Malin • Duke University
Elizabeth S. Cochran • University of California, Riverside
John E. Vidale • University of Washington

The proposed project is a long-term effort to characterize and monitor spatio-temporal variations in fault zone property on the Parkfield San Andreas fault (SAF), using fault-zone trapped waves (FZTWs) for further understanding the origin and mechanisms of fault damage and healing as well as their influences on heterogeneities in stress-stain over multiple length and time scales in earthquake cycle. The spatial extent of fault weakness, and the loss and recouping of strength across the earthquake cycle are critical ingredients in understanding of fault mechanics.

We shall determine material properties of the fault core and damage zone and their variations with depth and along the strike. The FZTW data recorded in our previous experiments at Parkfield under EarthScope supports illuminate the fault-zone rock damage and healing at seismogenic depths associated with the 2004 M6 earthquake on the SAF. We interpret the low-velocity waveguide as being a zone of accumulated damage from recurrent major earthquakes, including the 2004 M6 earthquake.

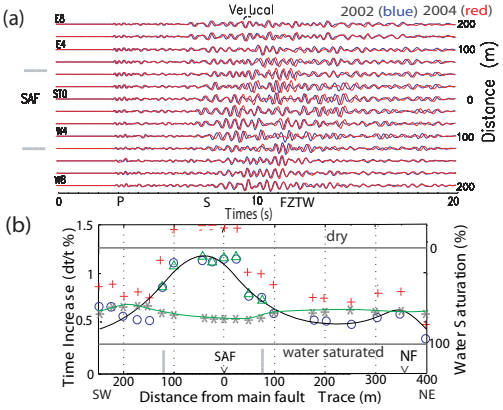

(a) Seismograms recorded at the cross-fault array for repeated shot PMM detonated within the SAF in 2002 and 2004. Fault-zone trapped waves (FZTW) are dominant at stations in the range of ~200 m marked by two bars. Waves traveled slower after the M6 Parkfield earthquake in 2004. (b) Traveltime increases for P-, S-, and trapped waves (red, blue, green circles) measured by cross-correlations of seismograms for the repeated shots, showing seismic velocity decreases caused by this M6 event. The solid curve is a polynomial fit to travel time increases of S waves in 2004, with greater changes in a ~200-m-wide zone denoted by a pair of vertical grey bars. Ratio of traveltime changes for P waves to S waves (green stars) indicates the degree of water saturation in cracks. Two horizontal light lines indicate the ratios predicted for a range of water percentage for Poisson solid.

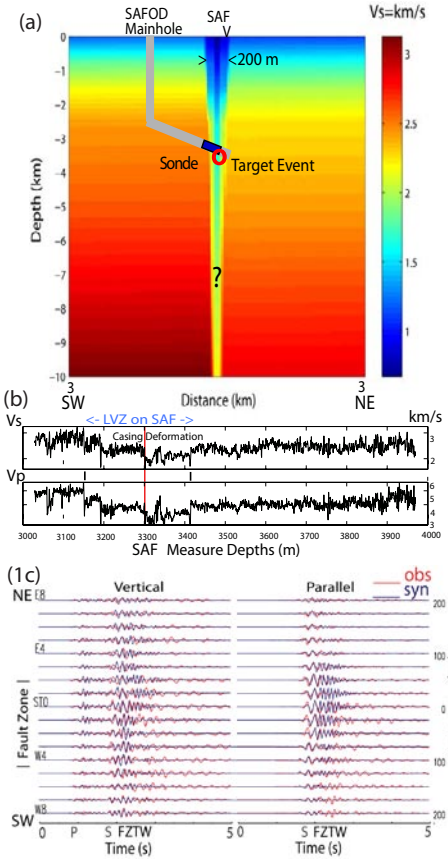

(a) Fault-normal depth section showing the S-wave velocity model for the SAFOD site, obtained from 3-D finite-difference fits to FZTWs generated by explosions and quakes at different depths. The model consists of a 30-m-wide fault core and a surrounding 100-200-m wide damage zone. (b) The width and velocity of the LVZ delineated by FZTWs as compared to SAFOD well logging at 3 km depth (Figure from Zoback et al., 2006). (c) Observed and 3-D finite-difference seismograms at borehole seismometers (Sonde) for the SAFOD drilling target event (red circle) using the velocity model in (a).

We have conducted several active and passive seismic experiments near the SAFOD site before and after the 2004 M6 Parkfield earthquake. These experiments indicate that the Parkfield low-velocity zone (LVZ) weakened co-seismically, and then healed back toward its pre-earthquake state over a period of several months to several years. Yet our data were too infrequent and coarse to completely resolve these matters. Instead, with the successful drilling and long-term instrumenting of the SAFOD mainhole and repeat seismic surveys as we did at Parkfield before, new information on this process should be forthcoming in the next cycle of the Parkfield earthquake engine. Results from our seismic fault-zone trapped waves characterization will be correlated to results from the SAFOD drilling, core studies, and many other studies at the Parkfield San Andreas fault.

Ellsworth, W. L., and P. Malin, A first observation of fault zone guided PSV-waves at SAFOD and its implications for fault characteristics, EOS, Transactions, American. Geophysics Union, 87, T23E-02, 154, 2006.

Hickman, S. H., M. D. Zoback, and W. L. Ellsworth, Structure and Composition of the San Andreas fault zone at Parkfield: Initial results from SAFOD Phase 1 and 2, EOS, Transactions, American. Geophysics Union, 86, 237, 2005.

Li, Y. G., J. E., Vidale, and S. E. Cochran, Low-velocity damaged structure of the San Andreas fault at Parkfield from fault-zone trapped waves, Geophy. Res. Lett., 31, L12S06, 2004.

Li, Y. G., P. Chen, E. S. Cochran, J. E., Vidale, and T. Burdette, Seismic evidence for rock damage and healing on the San Andreas fault associated with the 2004 M6 Parkfield earthquake, Special issue for Parkfield M6 earthquake, Bull. Seism. Soc. Am., 96, No.4, S349-363, doi:10.1785/0120050803, 2006.

We acknowledge the supports by NSF/EarthScope Grant EAR-0342277, USGS Grant NEHRP20060160, and partially by the SCEC. Special thanks to S. Hickman, W. Ellsworth and M. Zoback of SAFOD PIs for their coordination in our experiments at Parkfield, and collaborations of C. Thurber, S. Roecker, M. Rymer, R. Catchings, A. Snyder, R. Russell, L. Powell, B. Nadeau, N. Boness, D. McPhee, F. Niu and P. Chen in this study.

HIGH RESOLUTION AMBIENT NOISE SURFACE WAVE TOMOGRAPHY OF THE WESTERN UNITED STATES USING EARTHSCOPE USARRAY DATA: PHASE VELOCITY MAPS FOR RAYLEIGH AND LOVE WAVES

Fan-Chi Lin, Morgan P. Moschetti, Michael H. Ritzwoller • University of Colorado at Boulder

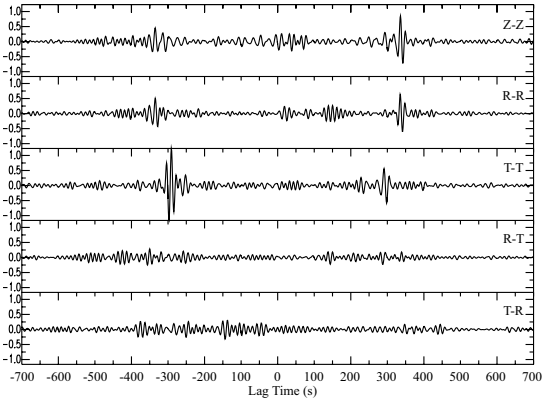

The 10-25 s bandpass filtered cross correlation functions observed between two USArray stations 116A (Eloy, Arizona) and R06C (Coleville, California).

Surface wave tomography based on the cross-correlation of long time sequences of ambient seismic noise is emerging rapidly as a new means to provide information about the crust and uppermost mantle homogeneously over large regions. Tomographic maps at both regional and continental scales show substantial correlation with well known geological features. The Transportable Array (TA) component of USArray, now with more than 300 stations distributed evenly across much of the Western US, provides a great opportunity to utilize ambient noise tomography to study the architecture of the structurally complex crust in this region. In earlier work, Moschetti et al. [2007] produced Rayleigh wave group velocity maps between 8 and 24 sec period in the region and the maps provide valuable information about the velocity structure of the Western US. We extend this study to measurements of phase velocities and to consideration of Love waves.

Perhaps surprisingly, estimated Green's functions for Love waves can also be measured by cross-correlating ambient noise. Using three-component ambient noise records from more than 250 stations of the TA observed from 1 Nov 2005 to 31 Oct 2006, we obtained estimated Green's functions for both Rayleigh and Love waves between each station-pair. In a typical example of a cross-correlation between different components for a single station-pair, the vertical-vertical (Z-Z) and radial-radial (R-R) cross-correlation clearly show the slower Rayleigh wave arrival compared to the faster Love wave signal found on the transverse-transverse cross-correlation. The ability to measure both Rayleigh wave and Love waves together is crucial to study radial anisotropy in the crust, which would be a potential indicator crustal deformation.

Phase velocity measurement on estimated Green's functions can also be obtained and, due to the smaller uncertainty, may be preferable to group velocity measurements. Valid phase velocity measurements for Rayleigh and Love waves at 12 sec period were made for more than 14,000 ray paths with a nearly evenly distributed path coverage, and this allows us to invert for high resolution tomography maps. Again, clear correlations between velocity anomalies and well know geological features, such as Sierra Nevada and Great Valley of California, can be seen.

Whether radial anisotropy of the crust is needed and can be inferred from these measurements is currently under study. The application of ambient noise tomography to data from the USArray provides great promise to improve the understanding of the crust across the entire US.

Moschetti, M.P., M.H. Ritzwoller, and N.M. Shapiro, Ambient noise tomography from the first two years of the USArray Transportable Array: Group speeds in the western US, submitted to Geophys. Res. Lett.

Lin,F., Moschetti, M.P., M.H. Ritzwoller, High resolution ambient noise surface wave tomography of the western United States using EarthScope USArray data: Phase velocity maps for Rayleigh and Love waves, in preparation.

This research is funded by the EarthScope office of the National Science Foundation - NSF EAR-0450082. The data are principally from the ANSS Backbone and the USArray Transportable Array and were obtained from the IRIS Data Management Center.

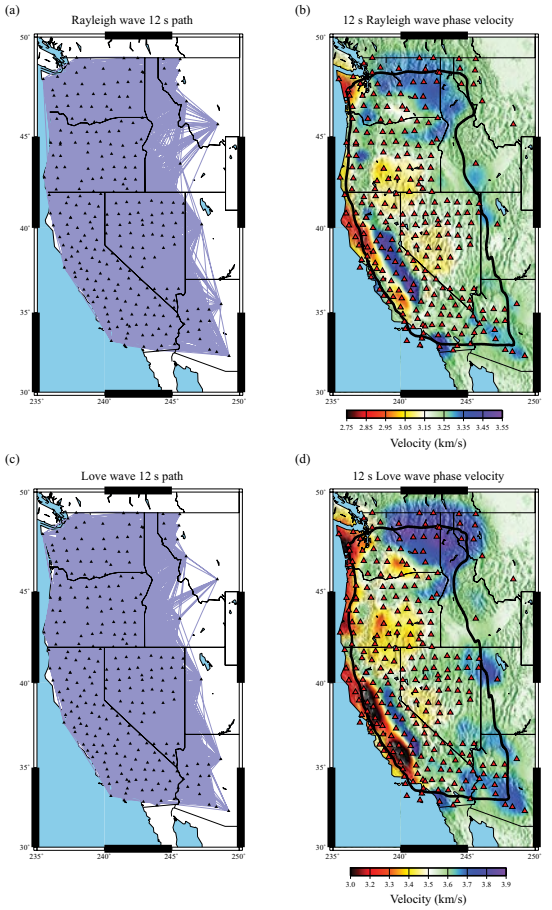

(a), (c) The path coverage for 12 s tomography inversion. (b), (d) The 12 s tomography maps with 100 km resolution contour shown in solid black curve.

DEFORMATION ASSOCIATED WITH ERUPTIVE ACTIVITY AT MOUNT ST. HELENS, WASHINGTON

Michael Lisowski, Larry Mastin, Daniel Dzurisin, Michael Poland • U.S. Geological Survey

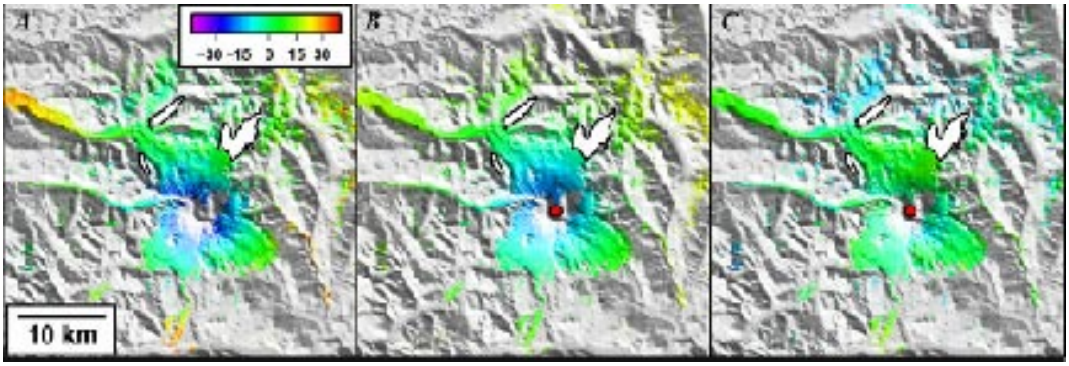

InSAR results from Mount St. Helens showing (A) observed, (B) modeled, and (C) residual deformation. Observed line-of-sight displacements are from a stack of 9 RADARSAT standard model 2 interferograms spanning 2004-2005. The model assumes a point source at 12 km depth with a volume loss of 27 × 106 m^3/yr.

On September 23, 2004, a seismic swarm marked the onset of eruptive activity at Mount St. Helens, Washington, after 18 years of quiescence. A few days later, an intensely deforming, uplifted welt was recognized in the southeast part of the crater, and a series of phreatic explosions lasting five days began on October 1, 2004. The USGS Cascades Volcano Observatory and Plate Boundary Observatory responded by deploying 18 continuous GPS stations on and around the flanks of the volcano, in addition to other stations elsewhere in the region. The network has measured remarkably little deformation. Prior to the eruption, only one continuous GPS station, JRO1, was operating, 8 km north of the volcano. JRO1 recorded about 2 cm of displacement towards the volcano during the first two weeks of the unrest. Between mid-October 2004 and the end of 2005, the GPS network detected only a few cm of deflation of the volcano. Deformation from Interferometric Synthetic Aperture Radar (InSAR) is similarly muted; a stack of 9 RADARSAT interferograms spanning 2004-2005 shows only about 2 cm of line-of-sight deflation centered on Mount St. Helens.

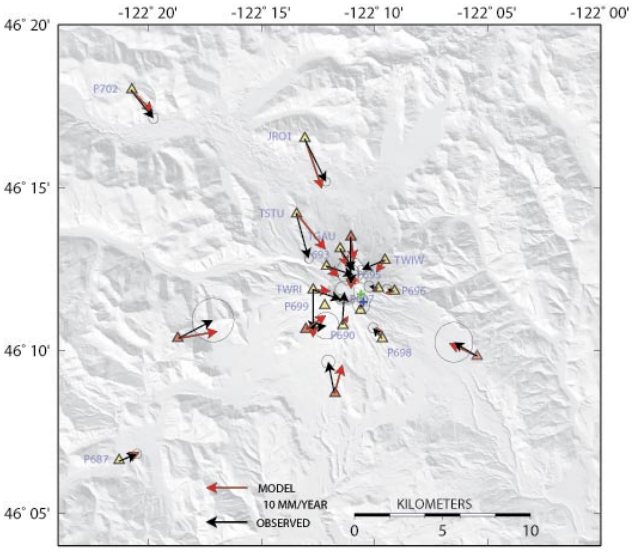

Average observed (black) and modeled (red) GPS displacements from Mount St. Helens between October 15, 2004 and December 31, 2005. The model assumes a vertical prolate ellipsoid between 6 and 12 km depth beneath the volcano with a volume loss of 20 × 106 m^3/yr.

Deformation from InSAR and GPS can be approximated by a volume loss of 20-30 × 10^6 m^3/yr at depths of 6 to 12 km (depending on the model geometry). Interestingly, during this time period at least 70 × 10^6 m^3/yr of lava was extruded. This discrepancy in volume does not necessarily imply recharge to the magma reservoir at depth. The difference can also be explained by the expansion of bubbles in the reservoir as volume is removed. Continued geodetic research at Mount St. Helens offers the chance to further investigate a variety of important issues in volcanology, including the relationship between erupted volume and modeled volume loss, the geometry and size of the magma reservoir, and the relationship between deformation rates and eruptive activity (e.g., explosive activity, effusion rate, magma chemistry, etc.).

FAULT SLIP IN C SHARP MINOR: FAULT SLIP RESONANCE AS A MECHANISM FOR SLOW SLIP

Anthony R. Lowry • Utah State University

GPS measurements in various different tectonic environments have recorded fault movements that are similar to earthquakes but much slower, occurring over timescales of ~1 week to ~1 year. These "slow slip events" have been observed in Japan, Cascadia, Mexico, Alaska, Hawaii, and New Zealand. The phenomenon is poorly understood, but several observations hint at the processes underlying slow slip. Modeling of GPS data and estimates of associated tremor location indicate that slip focuses near the transition from unstable ("stick-slip") to stable friction at the deep limit of the seismogenic zone. Perhaps most intriguingly, slow slip is quasi-periodic at several locations, with recurrence varying from 6 to 25 months depending on which fault (or even fault segment) is examined. Periodic slow fault slip may be a resonant response to climate-driven stress perturbations. Fault slip in southern Mexico recurs annually, and as shown in the figure, stress perturbations on the fault surface include an annual signal caused by surface hydrologic loading. The annual stress variation is only of order a few hundred Pa, which is a small fraction of the annual tectonic stress accumulation, so this stress would not be expected to produce a robust slip response unless the fault`s response to stress was somehow amplified at that period. Physical relations for rate- and state-dependent friction actually predict an amplified or "resonant" response at periods of order months to years, depending on frictional properties. Fault slip resonance helps to explain why slip events are periodic, why periods differ from place to place and why slip focuses near the base of the seismogenic zone. Resonant slip should initiate within the rupture zone of future great earthquakes, suggesting that slow slip may illuminate fault properties that control earthquake slip.

Lowry, A.R., Resonant slow fault slip in subduction zones forced by climatic load stress, Nature, 442(7104), doi:10.1038/nature05055, 2006.

Lowry, A.R., Resonant slow fault slip in response to climatic load stress, UNAVCO Science Workshop, Denver, Colorado, March 14-16 2006.

Lowry, A.R., Resonant slow fault slip in subduction zones forced by climatic load stress, Nature, 442(7104), doi:10.1038/nature05055, 2006.

Iglesias, A., S.K. Singh, A.R. Lowry, M. Santoyo, V. Kostoglodov, K.M. Larson, S.I. Franco-Sanchez, and T. Mikumo, The silent earthquake of 2002 in the Guerrero seismic gap, Mexico (Mw=7.4): inversion of slip on the plate interface and some implications, Geofisica Int., 43(3), 309-317, 2004.

This research was supported by NSF Grant EAR-0207820.

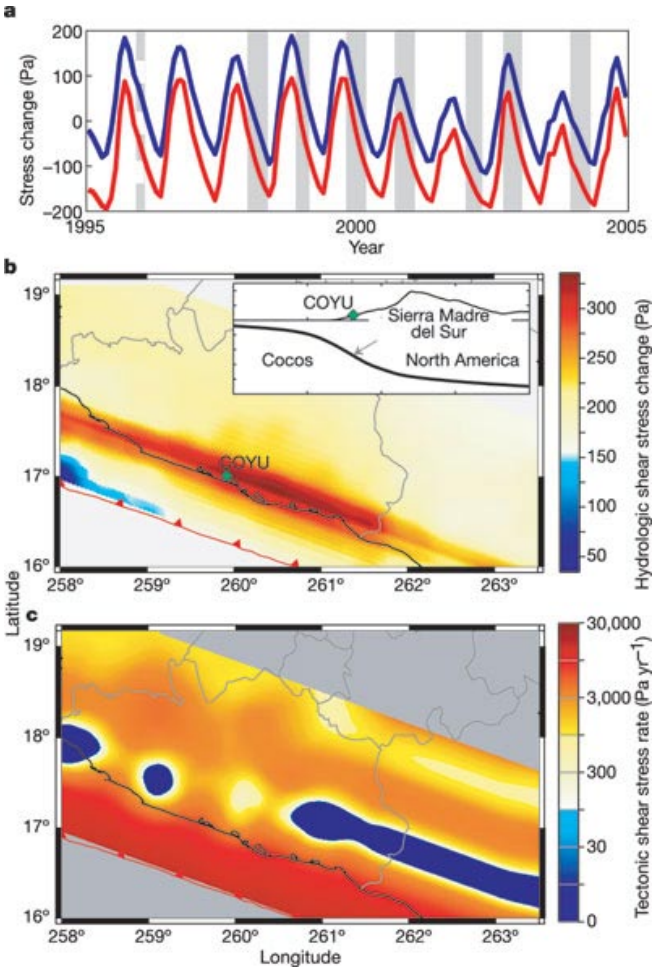

Stress variations on the plate boundary interface in southern Mexico. (A) Time series of normal stress (blue; positive indicates fault compression) and shear stress (red; positive favors thrust slip) at a point beneath GPS site COYU. Grey bars denote periods of deep slow slip; peak slip occurs at the center of the bar. (B) Map view of peak-to-peak shear stress perturbation, projected from the plate interface to the surface. Inset shows plate geometry and strike-averaged topography versus distance from the trench; arrow indicates location of time series sampled in A. (C) Rate of accumulation of tectonic shear stress.

LABORATORY STUDY OF THE MECHANICS AND PHYSICAL PROPERTIES OF THE SAN ANDREAS FAULT AND 3D SAFOD VOLUME

Chris Marone, Demian Saffer • Pennsylvania State University
Harold Tobin • University of Wisconsin, Madison

The principal goal of the SAFOD borehole is to gather critical data needed to understand fault mechanics and earthquakes. Through sampling, down-hole measurements, and long-term monitoring, the SAFOD experiment will provide data to test key hypotheses regarding long-term fault strength, earthquake nucleation, and fault slip behavior. However, the borehole itself will penetrate only a small part of the crustal volume surrounding the San Andreas Fault zone, and will sample only a subset of lithologies present in the subsurface. Although SAFOD will provide observations of the shallow seismogenic zone of a major plate bounding fault in unprecedented detail, additional characterization of rock properties for the 3-D volume containing SAFOD and the San Andreas Fault are also critical for addressing several outstanding questions in fault mechanics and earthquake physics. These include: 1) What causes spatial variability in fault slip behavior and seismicity? 2) Are elevated fluid pressures within the SAFOD 3-D volume plausible? 3) How are geophysical observations such as low velocity or resistivity linked to in situ conditions of stress and fluid pressure? 4) What do thermal data in the shallow subsurface tell us about the fault energy budget? We are carrying out a study of the processes and properties that affect mechanical behavior and transport properties of fault zones. The research involves laboratory measurements on SAFOD core samples and outcrop samples from the 3-D SAFOD volume. The data we collect will inform regional geologic, hydrologic, and thermal models. Our research is focused on the following objectives:

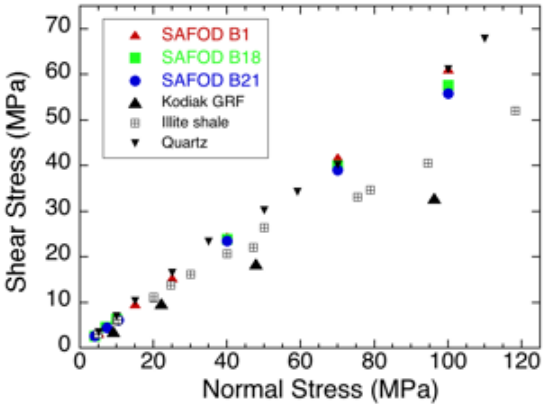

Coulomb failure data for phase 1 SAFOD core drilling and slabs of Kodiak, Ghost Rocks Formation. The frictional strength of SAFOD core is comparable to quartz powder.

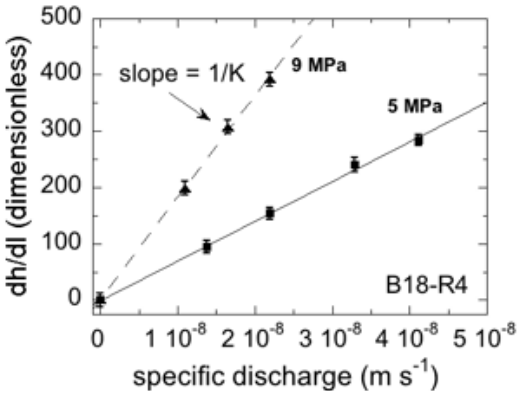

Coulomb failure data for phase 1 SAFOD core drilling and slabs of Kodiak, Ghost Rocks Formation. The frictional strength of SAFOD core is comparable to quartz powder.

- Determine the frictional strength and constitutive properties for SAFOD core material and host rock adjacent to the San Andreas Fault.
- Test the hypothesis that the upper stability transition from aseismic to seismic faulting is associated with a change in mineralogy of fault gouge and/or host rock.
- Develop experimental constraints necessary to test 1) the hypothesis that the San Andreas Fault is weak in an absolute and relative sense, and 2) models of long-term pore pressure generation and dynamic fault weakening.
- Provide constraints on processes relevant to the energy budget of faulting: including frictional heat generation, advective heat transport, and thermal refraction.
- Investigate the relationship between frictional strength (including healing and steady-state velocity dependence), seismic wave speed, and permeability.
- Investigate the stress and pore pressure dependence of P and S wave speeds and their anisotropies in fault zone and wall rock, to evaluate and improve seismic-attribute proxies for pore pressure, effective stress, frictional strength, fluid content, and other properties inferred from borehole log and surface seismic data.

To date, our preliminary results show that rocks from the SAFOD drill core and surrounding volume have relatively high frictional strengths, ~ 0.6 , and that permeability of the cemented sandstone ranges from 10^{17} to 10^{19} m^2. Ultimately, this research will provide an understanding of processes that govern the strength and stability of major faults, and will link fault rock properties to remotely sensed geophysical signatures, which is important for better assessment of earthquake hazard and for linking observations of fault behaviors with fundamental physical processes.

Funding for the SAFOD operation and planned stage 3 drilling is critical for the success of our research.

VELOCITY FIELD OF THE PACIFIC NORTHWEST

Rob McCaffrey • Rensselaer Polytechnic Institute
Robert W. King • Massachusetts Institute of Technology
Anthony Qamar • University of Washington

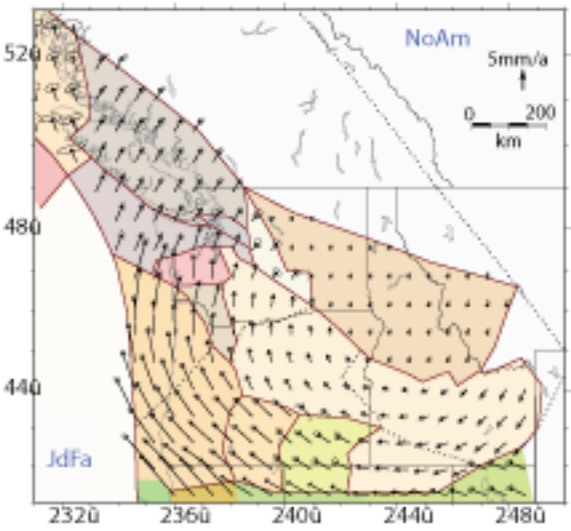

Block rotations estimated from GPS, slip vectors, and fault slip rates. Vectors are relative to North America.

We derived a surface velocity field for the Pacific Northwest utilizing continuous and survey mode GPS measurements made from 1992 through 2006. The velocity field reveals large-scale rotations of large parts of the region with superimposed strain rates from the Cascadia subduction zone and locked crustal faults. We modeled the velocity field simultaneously with fault slip rates, slip vectors, and other data. The predicted long-term velocity field is shown at left, locking on the Cascadia thrust is shown below. This region is a focus of EarthScope research on subduction zone processes and includes permanent GPS stations, borehole strainmeters, and campaign surveys.

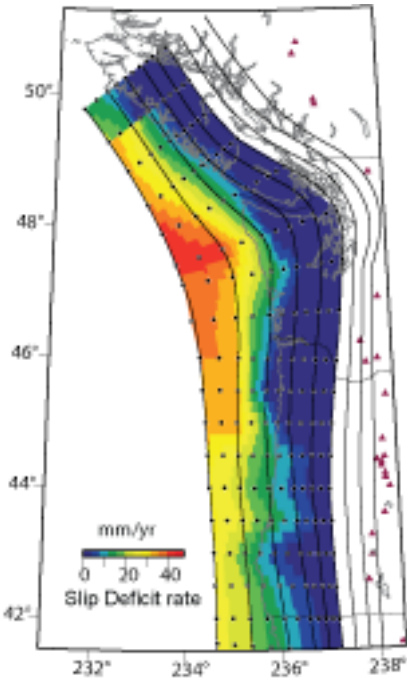

Plate locking model derived from GPS, uplift rates. Dots are node positions and curves are slab contours.

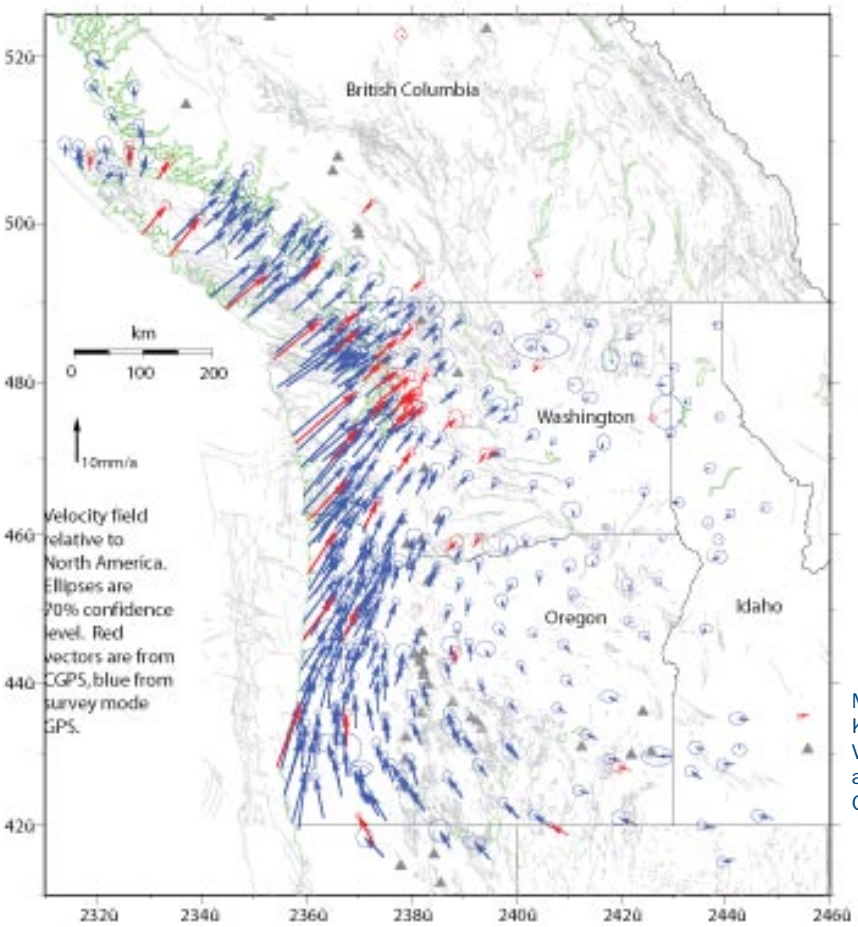

McCaffrey, R., A. I. Qamar, R. W. King, R. Wells, G. Khazaradze, C. A. Williams, C. W. Stevens, J. J. Vollick, and P. C. Zwick, Fault locking, Block Rotation and Crustal Deformation in the Pacific Northwest, Geophysical Journal International, in press, 2007.

SUBDUCTION TREMOR AND SLOW SLIP RECORDED IN JANUARY 2007 IN CASCADIA ON THE PLATE BOUNDARY OBSERVATORY (PBO) BOREHOLE NETWORK

Wendy McCausland, Evelyn Roeloffs • U.S. Geological Survey

The relationship between subduction tremor and slow slip events in Cascadia is being investigated using the PBO borehole strainmeters and seismometers. Though temporally correlated, it is not known whether the same source causes both the seismically-measured tremor and the geodetically-measured slow slip during tremor and slip events. During January 2007, a strain event is evident in 5-minute data on several of the strainmeters, and tremor is clearly visible on the borehole seismometers. The strain event first appears on strainmeter B018 (near Delphi, WA) on all components by January 19. The maximum E-W contraction was around January 25, and high strain-rates persisted throughout January. The strain changes began within days of the onset of strong tremor in the southern Puget Sound (as calculated by seismologists at the University of Washington). The strain event is evident on strainmeter B004 (northwestern Olympic Peninsula) by January 27, later than at B018 and consistent with the NNW migration of tremor epicenters (observed by scientists at the University of Washington). While the tremor signals are not yet evident on the 20-Hz strainmeter data, we are investigating the threshold of seismic event detection on the strainmeters in the frequency band of the tremor (1-6Hz).

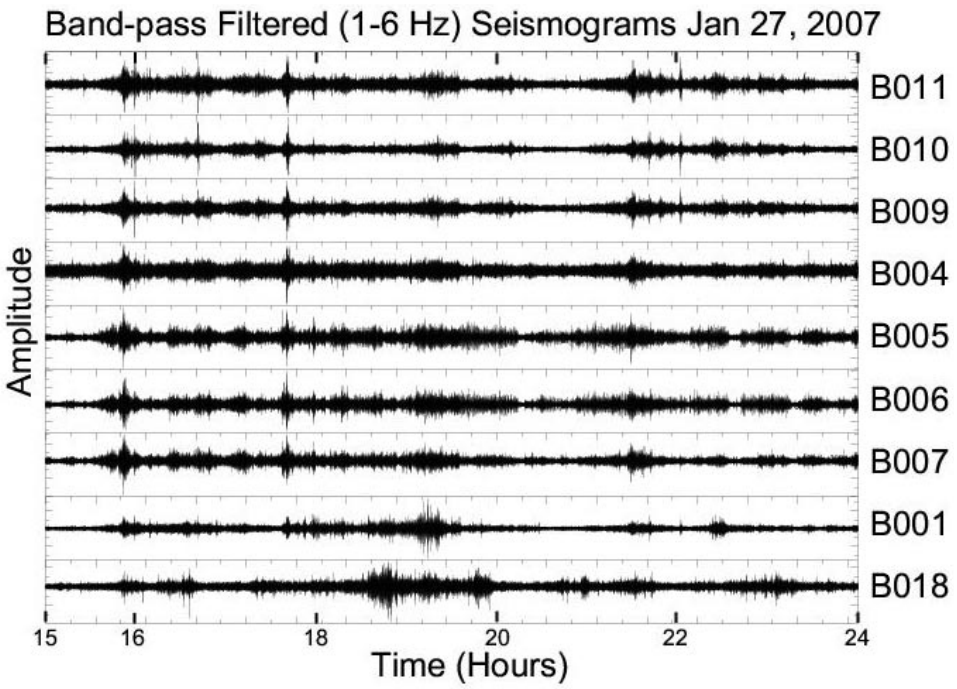

Nine hours of band-passed (1-6 Hz) tremor signals from January 27, 2007 on one of the horizontal components (EH1) of the borehole seismometers. Stations are ordered roughly north (top) to south (bottom). Bursts of tremor are evident on stations located on the southern end of Vancouver Island (B009, B010, and B011), northern Olympic Peninsula (B004, B005, B006, B007, and B001) and in the southern Puget Sound (B018).

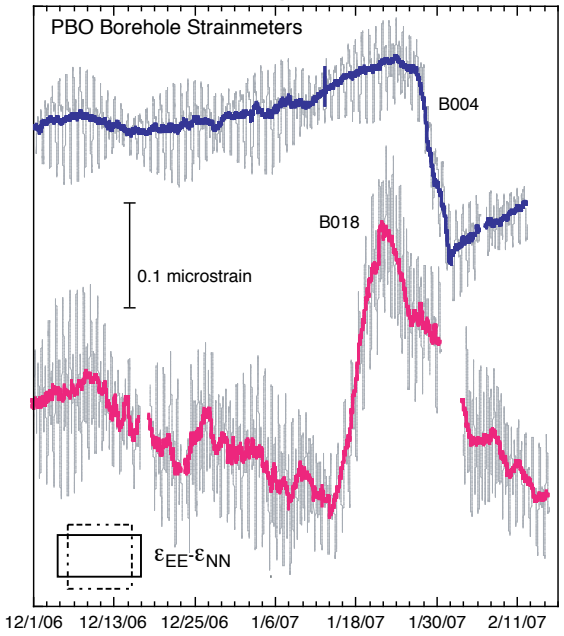

PBO borehole strainmeter data from Washington state (5-minute samples) reveal large strain-rate changes in late January, 2007. A trend has been subtracted from the data shown in gray; data after removing earth-tide variations are superimposed in color.

We acknowledge support from the USGS Earthquake Hazards Reduction Program.

A 70+ STATION GPS RECORDING OF THE JANUARY, 2007 CASCADIA ETS

Timothy Melbourne, Marcelo Santillan, Walter Szeliga, Meghan Miller • Central Washington University

Of the 35 slow slip events that have been recognized to date with GPS in the Cascadia subduction zone, the coverage of the most recent January 2007 transient is unprecedented and reflects the ongoing geodetic instrumentation of the northern Cascadia forearc. Compared with previous events recorded on a handful of stations, this most recent ETS ruptured through more than 70 instruments from the combined PBO and PANGA arrays and shows measurable deformation on 40 of them. Although at this time final orbits are still pending for last few days of the event, many of its characteristics are already measurable. The event nucleated mid-January to the west of the southern Puget Basin and propagated only northwards: transient deformation appears in the southern Puget Basin for at least 14 days prior to its onset around the Strait of Juan de Fuca. The greatest offsets are also found along a swath beneath the eastern Olympic Mountains and overlying the 30 km depth contour, west of the southern Basin. The largest of these measure 6+-1.8 mm and is directed towards the southwest, characteristic of previous Cascadia events. The total effective moment of the event appears to be Mw=6.6, as estimated by inverting transient offsets for thrust-only slip; this number

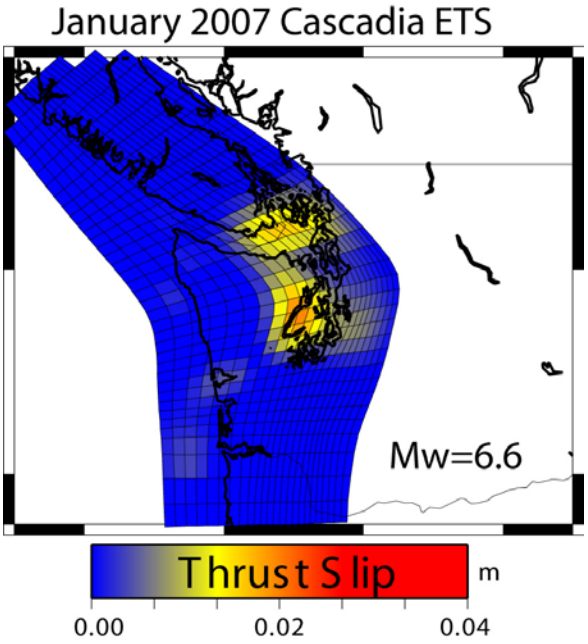

Slip distribution of the January, 2007 Cascadia slow slip event. Slip is pure thrust with average rake of N40E. Maximum slip is ~3 cm, equivalent moment magnitude of 6.6.

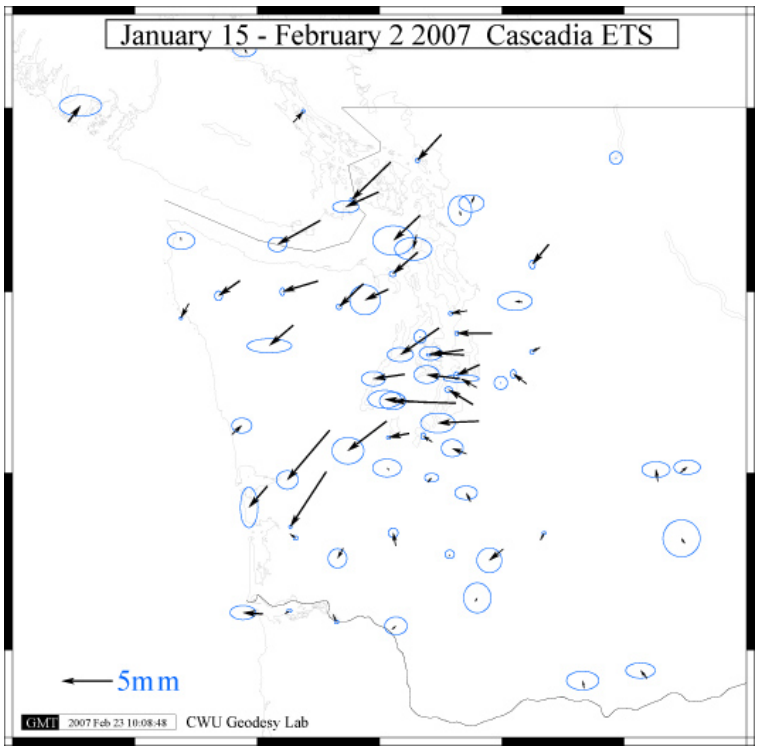

Cumulative transient deformation from the January, 2007 Cascadia slow slip event

is also typical of past events in this region. Slip appears to be more concentrated, with best-fitting inversions yielding 4 cm of slip. Qualitatively, this event looks like the northern half of the Feb-March 2003 ETS, which also nucleated in the SW Puget Basin but propagated bidirectionally to the north and south. Based on the last decade's worth of GPS, at this time it looks as though this region is not bleeding off strain energy as fast as it tectonically accumulates, suggesting this region might seismogenically fail during a megathrust event.

CWU Geodesy Lab

GPS CONSTRAINTS ON 34 SLOW SLIP EVENTS WITHIN THE CASCADIA SUBDUCTION ZONE

Timothy Melbourne, Marcelo Santillan, Meghan Miller • Central Washington University

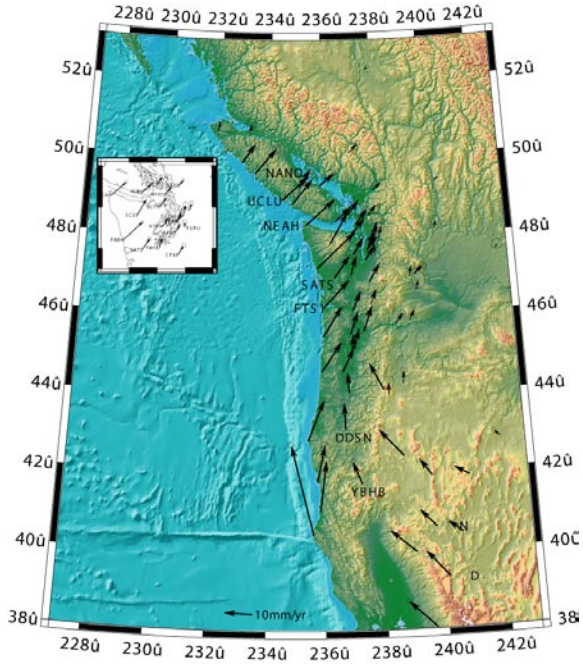

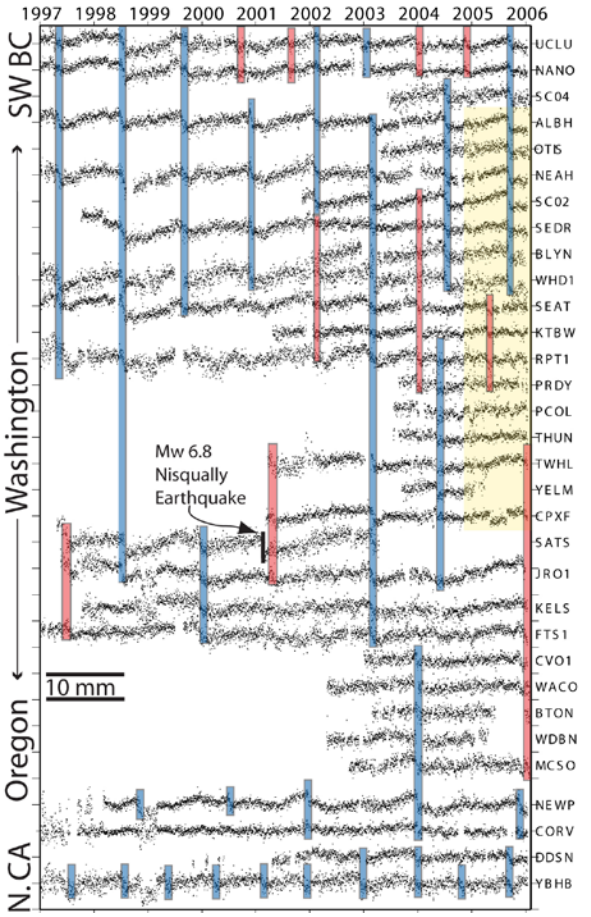

Improvements to analysis techniques of GPS measurements from the Cascadia subduction zone show that 34 slow slip events (SSE) have occurred along the megathrust since 1997 and hint at variable seismogenic coupling along-strike from California to BC. Roughly 30 PBO-NUCLEUS, PANGA, and WCDA continuous GPS stations constrain slow slip events through 2005, with the densest concentration in northwestern Washington State and southwestern British Columbia. In this region, the station distribution permits us to track the creep fronts as they migrate laterally across the plate boundary and reveals a wide variety of slip behavior among these events. To isolate deformation caused by transient creep events, we factor time series into distinct physical bases functions that represent steady-state tectonic deformation, hardware steps, tectonic steps, and annual and semi-annual signals and use these in both reference frame stabilization and time-series filtering.

At the latitude of the northern Washington State and southwestern British Columbia, the 14-month average recurrence interval still holds true, four events after first recognition. Along northern Vancouver Island, a 14-month periodicity is also observed, but six months out of phase with its southern counterpart. Smaller, non-periodic events appear to take place along the central Vancouver region. In southern Washington State, large transient displacements are seen, but lack any obvious periodicity in their recurrence. Many of these events have equivalent moment magnitudes of 6.4 (smallest resolvable with GPS) to 6.8, and 2 to 3 cm of slip. Along central Oregon, there is some evidence of an 18-month recurrence, while in northern California (Yreka) an 11-month periodicity has been proven with both GPS and seismic tremor. Together, these geodetic inferences of temporal and spatial creep distributions along the otherwise enigmatic Cascadia megathrust paint a picture of a wide range of coupling heterogeneity along the margin.

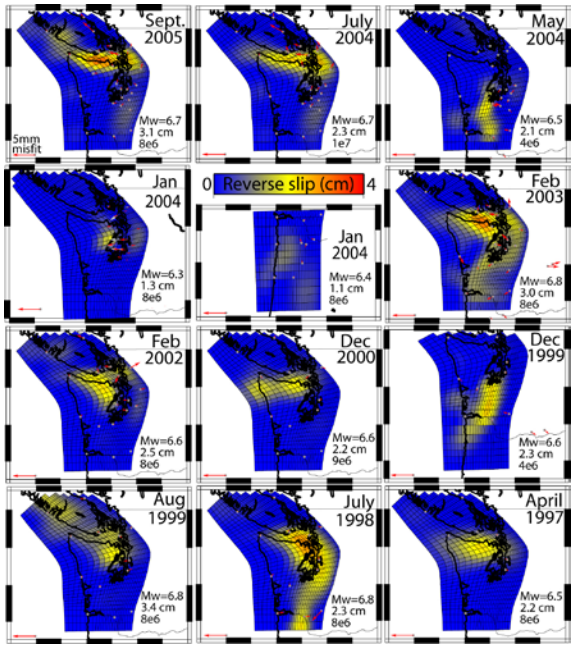

TRACKING THE PROGRESS OF THE USARRAY TRANSPORTABLE ARRAY WITH AMBIENT NOISE TOMOGRAPHY

Morgan Moschetti, Michael Ritzwoller • University of Colorado at Boulder
Nikolai Shapiro • Institut de Physique du Globe de Paris, France

Ambient noise surface wave tomography has been shown to be an effective technique for estimating surface wave dispersion maps at multiple spatial scales over a broad period band. The technique provides a means to make observations of short period surface waves along inter-station paths, which are inaccessible by earthquake tomography. Because earthquakes are primarily limited to plate margins and tectonically-active regions, the tomography of tectonically-quiescent regions requires the observation of teleseisms or the use of active sources. Shorter period surface waves, which are most sensitive to the crust, are preferentially attenuated and scattered, often leading to poor constraints on the crust from teleseismic earthquake observations. However, the resolution of ambient noise tomography is limited by the number and path density of inter-station paths and requires both dense instrumentation and widely-distributed stations.

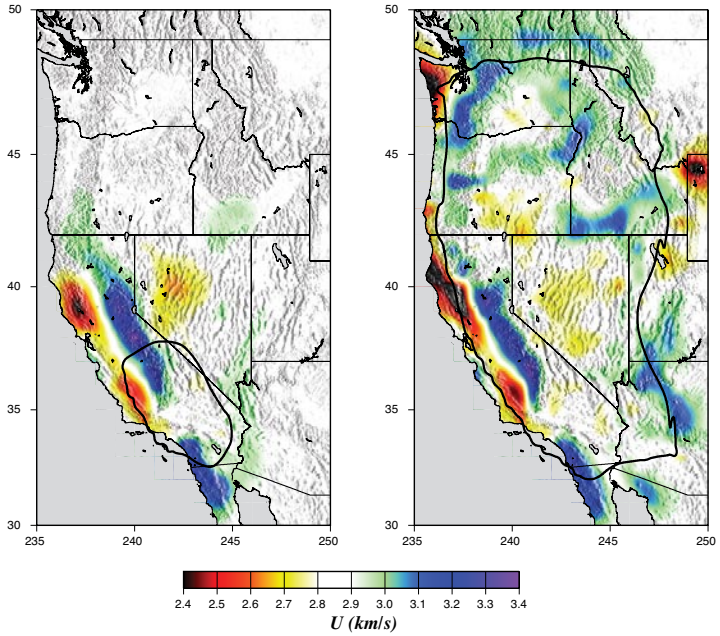

16-seonds period Rayleigh wave group velocity map comparison for October 2004 and December 2006

The emerging EarthScope USArray Transportable Array (TA) provides a nearly ideal network for the application of ambient noise surface wave tomography to provide new information about the crust and uppermost mantle. We have applied ambient noise surface wave tomography to continuously emerging data from the TA over the past two years. Using the seismic records that become available from TA stations in the western United States (US) each month, we have processed available data between October 2004, and December 2006 to assess the effect of the expanding TA network on the estimated group velocity maps. Estimated Green's functions are calculated by cross-correlating noise records between every station pair. We measure the dispersion characteristics of the Rayleigh waves observed in these cross-correlations using frequency-time analysis and invert the group velocities at each period to generate group velocity maps between 6- and 40-second periods.

The figure compares the resulting 16-second period Rayleigh wave group velocity maps from October 2004 and December 2006. The contour defines a region within which the resolution is better than 70 km (the approximate inter-station distance). The increase in the spatial extent of the imaged region is apparent, and the region of high resolution has increased during the operation of the TA by a factor of about six. The area enclosed by the 70 km contour continues to grow as the TA expands to the east across the US. Geological features correlate strongly with velocity anomalies in the group velocity maps. The 16-second period Rayleigh wave group velocity map shown here is most sensitive to structures in the upper and middle crust. At this period, the maps show the plutonic and volcanic rocks of the Sierra Nevada Mountains and the Peninsular Range, and faster anomalies begin to appear for the Cascade Range. The thick sedimentary deposits of the Great Valley are apparent from their low velocities. The Snake River Plain appears as a high velocity anomaly. Both Yellowstone and the accreted terranes of the Olympic Peninsula appear as low velocity anomalies, despite being located outside of the high resolution contour. Monthly and cumulative results from October 2004 through the present are posted at: http://ciei.colorado.edu/~morganm

Moschetti, M.P., M.H. Ritzwoller, and N.M. Shapiro, Ambient noise tomography from the first two years of the USArray Transportable Array: Group speeds in the western US, submitted to Geophys. Res. Lett.

Bensen, G.D., M.H. Ritzwoller, M.P. Barmin, A.L. Levshin, F. Lin, M.P. Moschetti, N.M. Shapiro, and Y. Yang, Processing seismic ambient noise data to obtain reliable broad-band surface wave dispersion measurements, Geophys. J. Int., in press.

Shapiro, N.M. M. Campillo, L. Stehly, and M.H. Ritzwoller, High resolution surface wave tomography from ambient seismic noise, Science, 307(5715), 1615-1618, 11 March 2005.

This research is funded by the EarthScope office of the National Science Foundation - NSF EAR-0450082. MPM acknowledges a National Defense Science and Engineering Graduate Fellowship from the American Society for Engineering Education. The data are principally from the ANSS Backbone and the USArray Transportable Array and were obtained from the IRIS Data Management Center.

A MICROSEISMIC VIEW OF THE IMMEDIATE SAFOD TARGET ZONE

Robert Nadeau • University of California, Berkeley

Monitoring of continuous waveform data from the local borehole High Resolution Seismic Network (HRSN) with pattern scanning methods has revealed over 100 tightly clustered microseismic events within an approximately 100m long by 50m deep zone surrounding the SAFOD primary and secondary target sequences since August of 2001. This provides additional constraints on both the relative event locations of the SAFOD target events and on the detailed fault structure around the targets. The clustered micro-seismicity also exhibits highly systematic patterns of spatio-magnitude clustering with long interevent times that are similar to those of the characteristically repeating SAFOD target sequences.

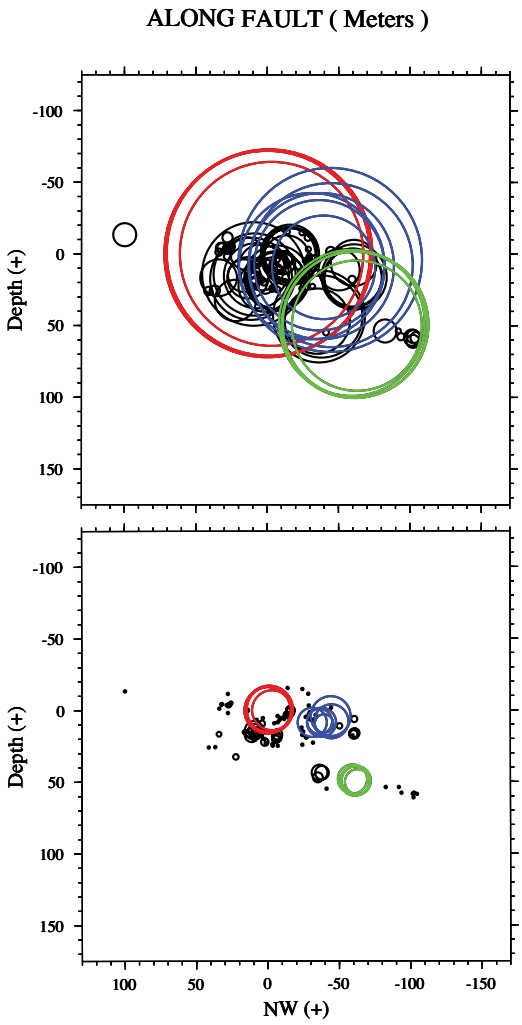

(Top) Along fault section view of the 100+ microseismic events occurring the immediate SAFOD target region between August, 2001 and January of 2007. Dimensions of the circles reflect the inferred rupture dimensions of the events assuming a 3MPa stress drop and circular rupture (i.e., most often used as criteria for repeating earthquake searches and consistent with the constant stress drop hypothesis for earthquakes). Red circles indicate the SAFOD primary target sequence (SF) events, blue the secondary target sequence (LA) events and green the tertiary target sequence (HI) events (which are located on a seismically active strand approximately 150-200m to the southwest and 50 m deeper than the seismicity containing the primary and secondary targets. (Bottom) Same events and sectional view as shown at (Top) but with rupture dimensions inferred from tectonic loading and recurrence interval scaling of repeating earthquakes. The large discrepancy between the inferred rupture dimensions for these events is one manifestation of earthquake properties illustrating our current state of uncertainty in earthquake physics. High-resolution long-term monitoring data from SAFOD will provide information invaluable in helping to resolve this and related issues.

The recurrence behavior of these small sequences mimics that of large characteristic events, but on much shorter time scale. Hence, their recurrence interval statistics have been incorporated into time-dependent earthquake forecast models for larger quakes in the Bay Area of California [WGCEP, 1999, 2002]. The close proximity of the various sequences also appears to give rise to event triggering behavior and occasional simultaneous rupture of asperity patches which have also been of concern in developing earthquake forecast models. However, recurrence interval scaling relationships from the micro- to large earthquake scales has revealed fundamental contradictions between observed source properties and those expected by stress accumulation through tectonic loading.

At the heart of this dilemma is the question of the strength and heterogeneity of earthquake faults, and the SAFOD experiment affords a unique opportunity to resolve this issue through its in-situ long-term monitoring of strength related properties (e.g., deformation and stress accumulation, heat generation, fluid and gas chemistry, and seismic energy release) at unprecedented resolution in the immediate vicinity of a characteristic sequence of events over several seismic cycles.

From a seismological perspective SAFOD's recordings of high-frequency broad-band seismic data in the near-field of an earthquake source and in the extremely low noise environment of the SAFOD main-hole will complement the far-field and relatively low sampling rate data of the HRSN and surface Northern California Seismic Network (NCSN). This will lead to a much more detailed picture of the evolution of seismicity in the SAFOD zone for understanding earthquake triggering, simultaneous rupture and renewal processes, and for understanding how these processes relate to the evolution of the other physical properties occurring in the fault zone. The close-in SAFOD seismic data will also allow for the application of advanced relative source techniques between very closely space earthquakes of diverse magnitudes in the SAFOD zone.

Working Group on California earthquake Probabilities (WGCEP) (1999). Earthquake probabilities in the San Francisco Bay Region: 2000 to 2030--a summary of findings, U.S. Geol. Surv. Open-File Rept. 99-517, 36 pp.

Working Group on California earthquake Probabilities (WGCEP) (2002), Earthquake probabilities in the San Francisco Bay Region: 2002 to 2031, U.S. Geol. Surv. Open-file Rep. 03-214, 1-340 (USGS, Reston, Virginia, 2003).

Support for this research has been provided by: 1) The National Science Foundation through grants EAR-0537641, EAR-0544730, EAR-0337308, and subaward DTM-2025-01 and 2) The USGS NEHRP program through grant number 05HQGR0080.

ONGOING TRANSIENT DEFORMATION FROM A SHALLOW SOCORRO MAGMA BODY?

Andrew V. Newman • Georgia Institute of Technology
Timothy H. Dixon • University of Miami
Dave Love, Richard Chamberlain • New Mexico Bureau of Geology and Mineral Resources

The Socorro Magma Body (SMB), between Socorro and Belen, New Mexico, lies within the central portion of the Rio Grande Rift Valley and is one of the largest known magma bodies in Earth`s continental crust. The SMB is expressed in several geophysical anomalies, including increased local seismicity, low electric conductivity, and surface uplift. Studies of local microseismicity and deep seismic soundings revealed an unusual crustal reflector about 50 to 70 km wide, and about 19 km in depth, and were interpreted as requiring fluids, most likely melt, in the middle crust beneath Socorro. These data have led to a general acceptance of the Socorro reflector as the prime example of a large active sill-like magma intrusion. Using precision leveling and Interferometric Synthetic Aperture Radar, previous studies have found averaged uplift of about 2 to 4 mm/yr centered on the Socorro seismic reflector at 19 km depth.

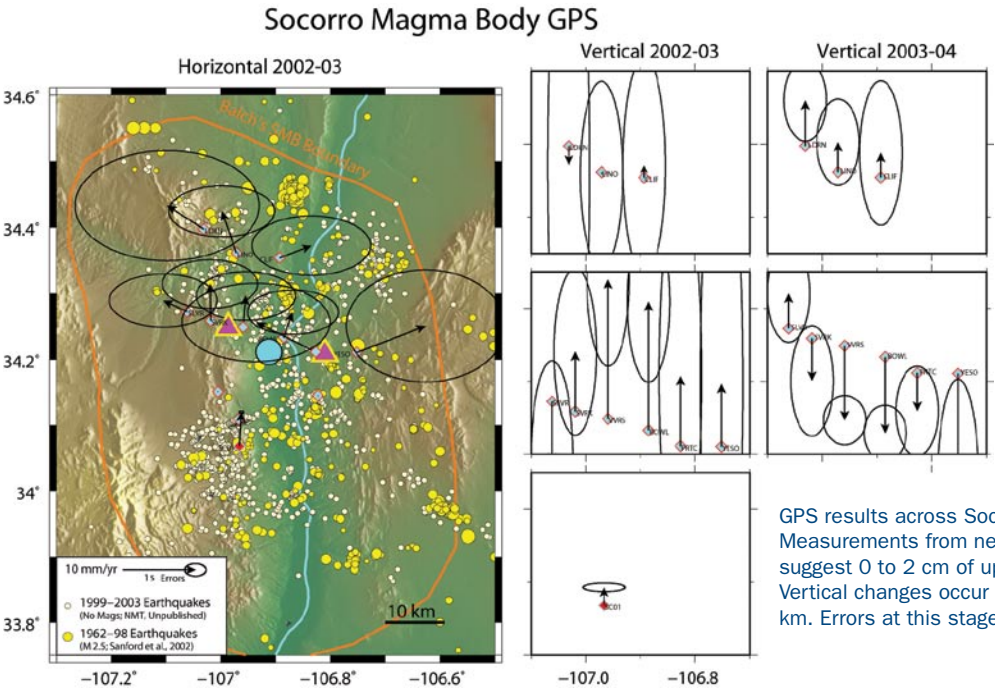

GPS results across Socorro Magma Body, New Mexico. Measurements from new campaign sites (blue diamonds) suggest 0 to 2 cm of uplift, with horizontal spreading. Vertical changes occur rapidly with > 1 cm change over 10 km. Errors at this stage are still large.

We performed three GPS campaigns over 9 to 12 bedrock sites in 2002, 2003, and 2005. Vertical GPS over the southern SMB switch from between +10 and 20 mm with the maximum uplift (20 mm) in 2002, to a similar level deflation the following year. Currently, these data suggest a significant and smaller body transiently inflating at about 5 km depth and corresponding to 0.5 to 5 million m3 between 2002 and 2003. These results indicate that the SMB may have considerable variation in the spatio-temporal pattern of deformation averaging to a slower long-term inflation.

In fall of 2005, with the help of UNAVCO field engineers, we installed two new continuous GPS sites near the center of transient inflation. In collaboration with Los Alamos National Laboratory and New Mexico Tech, these sites are collocated with two continuously recording broadband seismometers aimed at identifying low-frequency tremors associated with migrating fluids.

UNAVCO field engineers Beth Bartel and Nicole Feldl after the completion of short-brace continuous installation of PDBG GPS within the Socorro Magma Body.

Newman, A. V., D. Love, R. Chamberlin, P. LaFemina & T. H. Dixon, Rapid inflation across the central Socorro Magma Body?, Trans. Amer. Geophys. Un. (EOS), 85, Fall 2004.
Newman, A. V., D. Love, R. Chamberlin, P. LaFemina & T. H. Dixon, Rapid inflation across the central Socorro Magma Body?, Geoph. Res. Lett. [In Prep].

The work was supported by LANL-NMT MOU Grant; Georgia Tech, College of Sciences.

THE EARTHSCOPE AUTOMATED RECEIVER SURVEY

Thomas J. Owens, H. Philip Crotwell • University of South Carolina

The EarthScope Automated Receiver Survey (EARS; http://www.seis.sc.edu/EARS) [Crotwell and Owens, 2005] is using data collected by USArray to create crustal thickness and Vp/Vs measurements across the United States. EARS has also mined the historical archive of data at the IRIS DMC to enhance the spatial resolution by incorporating stations from existing permanent networks as well as older PASSCAL deployments. EARS was designed to function in an automated manner, and harvests seismograms for all available stations when it is notified of an earthquake. The products generated by EARS, all available from the EARS website, include the receiver functions, as well as the preprocessed seismograms that were used to generated them, crustal thickness vs Vp/Vs plots, and estimates of crustal thickness and Vp/Vs for each station. The receiver functions and preprocessed seismograms are useful for seismologists wishing to do more detailed receiver function studies or reproduce our results, while the bulk crustal property estimates appeal to a wider audience from seismologists to the general public.

USArray station density allows the creation of a surface of crustal thickness in which broad patterns can be observed. Examination of the trends reveals both the potential for EARS to produce images of the broad variations in crust/upper mantle structure in the region and the need to resist interpretation of all features in terms of continental Moho depth. For example, recent work has shown that there are complexities in the Moho signal in the southern Sierras that are only broadly reveal by EARS. In the Pacific Northwest, recent studies have proposed that serpentinization in the upper mantle in a large area of the Pacific Northwest may complicate, obscure or even invert the signal from the base of the continental crust. Previous work has shown that the the subducted oceanic Moho can generate large converted phases. Detailed analysis of EARS results shows that it provides estimates of the depth to the subducted oceanic moho in the western part of Oregon and Washington and the continental Moho in the east of -123.3°. There is an region of more erratic estimates in between that may be caused complex Moho signals in the serpentized region.

Crotwell, H.P and T.J. Owens (2005). Automated receiver function processing, Seismological Research Letters, 76, 702-708.

EARS is funded by the NSF EarthScope science program through grant EAR-0346114 to the University of South Carolina. Researchers publishing results that incorporate EARS results are requested to reference Crotwell and Owens (2005).

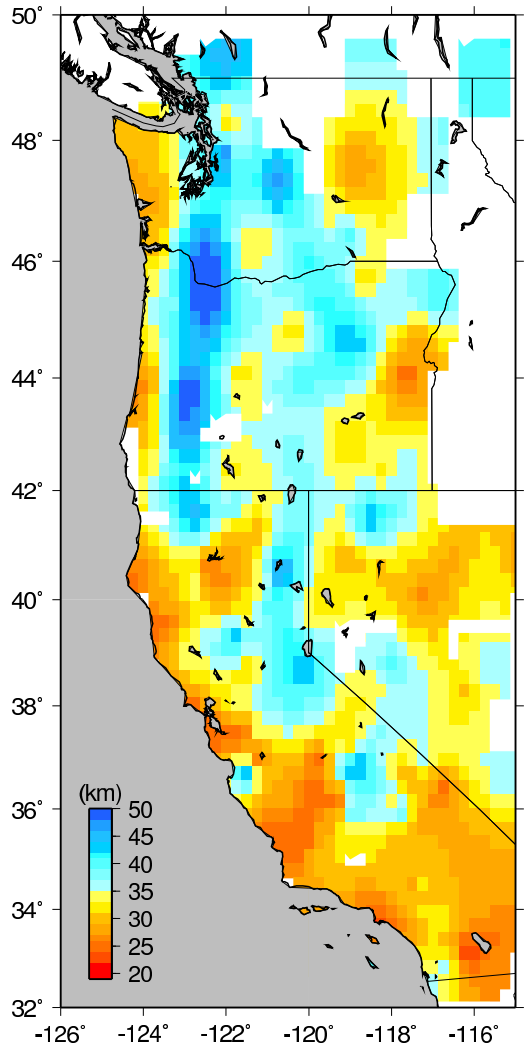

Thickness estimates from EARS within the Western US

ARRAY PROCESSING OF TELESEISMIC BODY WAVES WITH THE EARTHSCOPE TRANSPORTABLE ARRAY

Gary Pavlis • Indiana University
Frank Vernon • University of California, San Diego

The Earthscope Transportable Array is the largest broadband seismic array ever deployed. Its large aperture, large number of sensors, and remarkable data quality open new frontiers in wavefield processing with this facility. One of the simplest examples of wavefield processing is conventional slant-stack array processing. This type of processing has been the foundation of nuclear monitoring since the earliest seismic arrays deployed under project VELA in the 1960s. That early experience led to the widespread use of high frequency phased arrays for nuclear explosion monitoring including the current-generation system now in place for monitoring the comprehensive test band treaty. The USArry facility is very different, however, because it's use of broadband sensors makes it a highly functional long-period array. We have begun the application of routine array processing of the data at the Array Network Facility. We have modified the standard slant-stack approach in two fundamental ways that make it more suitable for the USArray: (1) we assume an approximate location of any event to be processed is known a-priori, and (2) we utilize a novel, nonlinear stacking algorithm that differs drastically from conventional methods. The first assumption follows from a fundamental difference from the goals of this application to that in nuclear monitoring. That is, the goal is not to search for small signals buried in noise, but to provide improved estimates of seismic phase arrival times of teleseismic earthquakes. The second feature of our approach exploits this assumption. The nonlinear stacking algorithm we have developed utilizes robust estimators to automatically discard problem data along with a cross-correlation against an array beam in an iterative refinement of the stack. The algorithm has three main outputs: (1) a robust estimate of the array beam; (2) time residuals relative to a reference earth model computed by cross-correlation; and (3) time domain amplitude correction factors of each station relative to the array beam. The algorithm can process any distinct seismic phase for which we can compute a first order alignment from a predicted arrival time, but the basic approach is only sensible for seismic phases that are coherent across the entire array or at least on a specified subarray scale. The figure below shows an example result for the P phase from a magnitude 6.5 event in Peru. The reults show a clear correlation with subduction processes in the Pacific Northwest. The figures show that a lower amplitude signal arrives relatively early (negative residual) in an area that correlates directly with known higher velocities in the subducting Juan de Fuca plate.

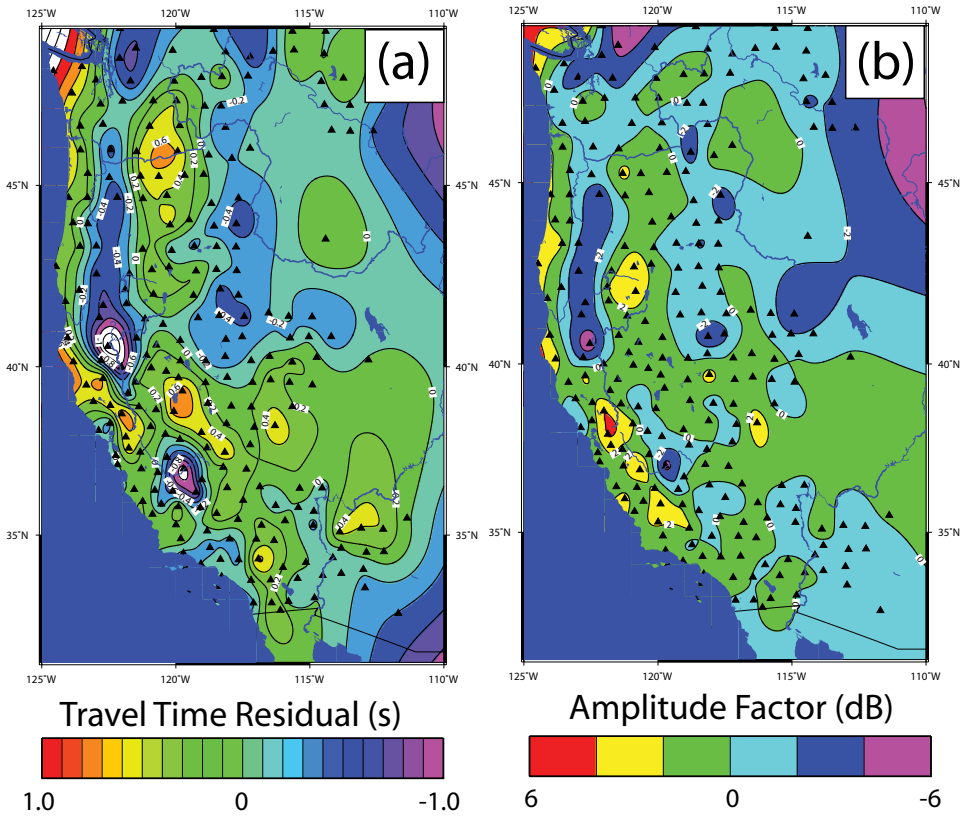

Travel time and relative amplitudes computed by array processing. Results shown are for P waves recorded by a magnitude 6.5 event in Peru. Residuals are computed by cross-correlation with the array beam and plotted in (a). Relative amplitudes (b) are computed in the time domain using the dot product between the normalized array beam and an individuals stations data on a common time gate. Stations used to create each plot are shown as the black triangles.

MICROPLATE DEFORMATION OF THE WESTERN U.S. INTERIOR

C. M. Puskas, R. B. Smith • University of Utah

This study of western U.S. deformation examines the intraplate extension of the Basin-Range (BR) province and the Yellowstone-Snake River Plain volcanic region [Puskas and Smith, 2007]. Microplate motions were modeled using GPS data compiled from multiple studies (many supported by UNAVCO and including the PBO network), Late Quaternary fault-slip rates, and earthquake slip directions from moderate to large earthquakes. The western U.S. was divided into blocks of uniform deformation based on tectonic and volcanic history and the location of active fault zones. The model examined the effects of rotation, internal strain, and block-bounding faults on these microplates. Our results show that western interior is characterized by a clockwise rotation and increase of velocities from east to west. The Yellowstone-Snake River Plain moves southwest at 1.4 ± 0.2 mm/yr. This motion rotates into a westward direction at 2.3 ± 0.1 mm/yr in the eastern Basin-Range. Velocities then rotate to the northwest in the western Basin-Range, accompanied by a velocity increase to 4.6 ± 0.1 mm/yr and the introduction of internal shear-deformation in the western Basin-Range. The total east-west extension across the entire Basin-Range is 12.9 ± 0.1 mm/yr, and velocities in the northwestern region decrease in magnitude and rotate farther to the north.

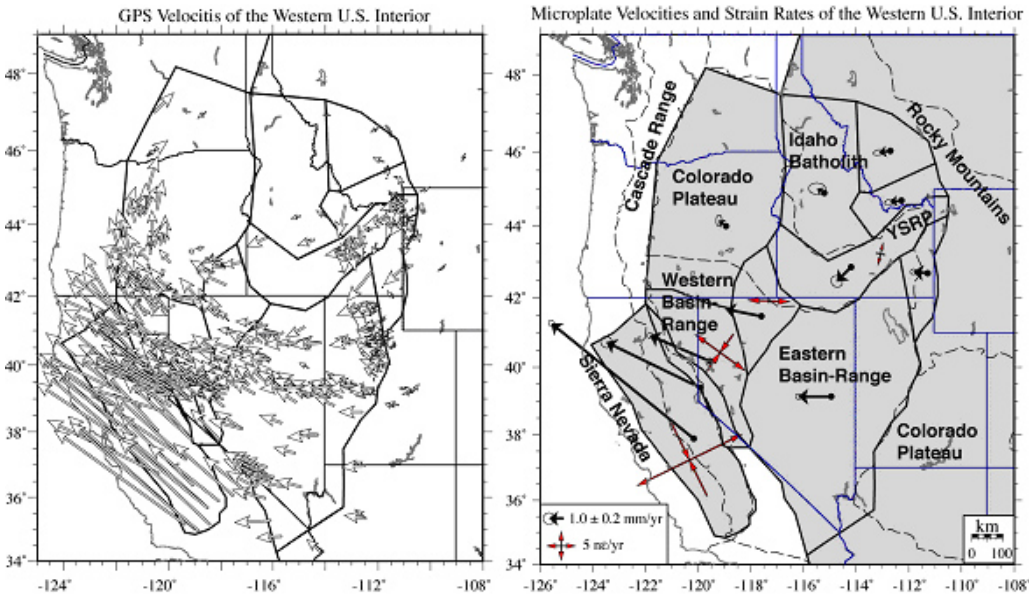

(a) GPS-measured velocities of microplate motions in the western U.S. interior. (b) overview of microplate velocities and strain rates in the western U.S. interior.

The pattern of deformation is considered to be the result of multiple factors. Gravitational potential energy from buoyancy forces associated with the Yellowstone hotspot and Rocky Mountains contributes to southwest motion of the Yellowstone-Snake River Plain microplate [Puskas et al., 2004]. The northwest-moving Sierra Nevada microplate blocks westward extension of the Basin-Range and deflects motion to the northwest. Additional extension of the BR extends north of the Sierra Nevada in Nevada and Oregon.

Puskas, C. M. and R. B. Smith, (2007), Intraplate deformation and block rotations of the western U.S. interior, in preparation.

Puskas, C. M., R. B. Smith, C. M. Meertens, W. L. Chang, (2007), Crustal deformation of the Yellowstone-Snake River Plain volcanic system: campaign and continuous GPS observations, 1987-2004, J. Geophys. Res., 112 doi:10.1029/2006JB004325, in press.

Puskas, C. M., R. B. Smith, G. Waite, L. Flesch, (2004), Kinematic deformation of the Interior Western U.S. Extensional Regime with Mantle Flow, Eos Trans. AGU, 85(47), Fall Meet. Suppl. Abstract T31A-1247.

This research was supported by NSF Grants 314298, 9725431, and 9316289.

KINEMATICS AND CRUSTAL DEFORMATION OF THE YELLOWSTONE HOTSPOT FROM GPS MEASUREMENTS: 1987-2006

C. M. Puskas, R. B. Smith, W. L. Chang • University of Utah
C. M. Meertens • UNAVCO

Campaign and continuous GPS data were acquired from 1987 to 2005 to measure deformation of the Yellowstone-Snake River Plain volcano-tectonic province [Puskas et al., 2006]. The University of Utah, supported by UNAVCO and with collaborators, conducted seven campaigns between 1987 and 2003, occupying 140 stations and installing and operating 15 permanent GPS stations. The University of Utah permanent stations will be incorporated into an expanded EarthScope PBO network, improving coverage of Yellowstone.

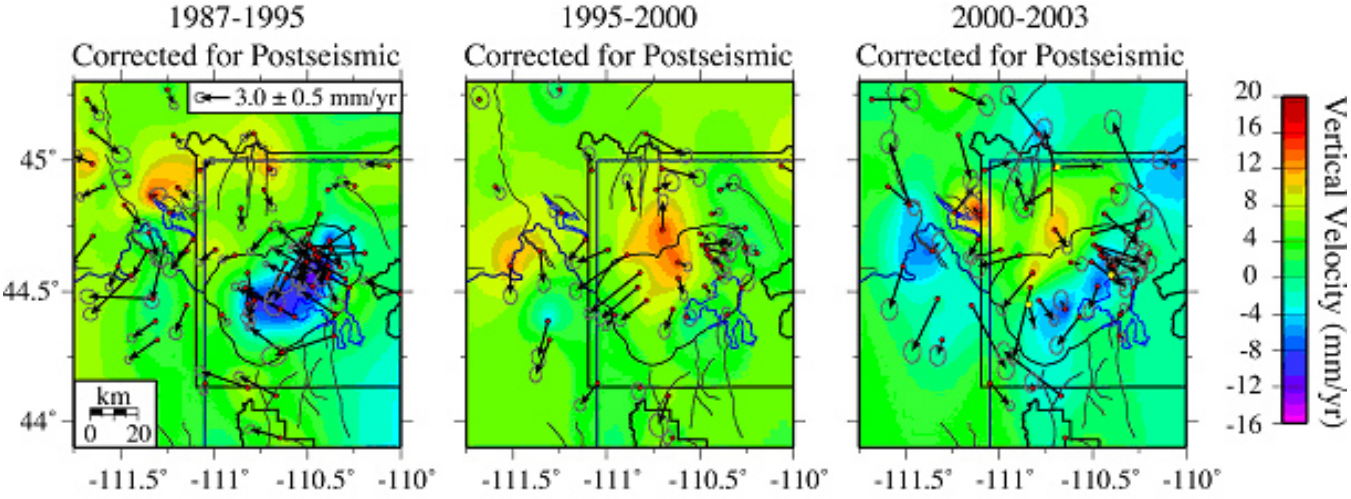

Vertical velocities in the Yellowstone caldera (a) 1987-1995, (b) 1995-2000, and (c) 2000-2003.

The GPS data revealed large and unexpected episodes of vertical deformation of the Yellowstone caldera. The caldera subsided at a maximum rate of 14 ± 3 mm/yr in 1987-1995. Vertical deformation shifted to the NW caldera boundary uplift at 5 ± 4 mm/yr for 1995-2000. For 2000-2003, caldera deformation switched to subsidence of up to 9 ± 6 mm/yr, yielding direct evidence of a restless caldera. Continuous GPS observations revealed a reversal to rapid caldera-wide uplift up to ~6 cm/yr from 2004 to 2006.

These deformation episodes have been modeled [Vasco et al., 2007] by volumetric strain inversion revealing a mid-crustal source (6-10 km deep) of compression and expansion that coincides with the top of the tomographically imaged crustal magma body. Deformation is likely a result of accumulation and/or migration of hydrothermal fluids or magmatic crystallization.

Thirty kilometers west of the Yellowstone caldera, fault-normal extension continued across the Hebgen Lake fault at 3.1 to 5.3 mm/yr during the period 30 to 46 years following the 1959 M7.5 earthquake. Baseline data for 16 years of GPS observations combined with USGS trilateration data were used to model crustal rheology from the viscoelastic relaxation following this large event [Chang and Smith, 2006]. This model predicted post-seismic horizontal motion of 1 mm/yr within 40 km of the fault and uplift up to 2 mm/yr to the north of the fault. Using the rheology model, all of our data were corrected for time-dependent deformation caused by the M7.5 earthquake.

Chang, W. L. and R. B. Smith, (2007), Lithospheric rheology from post-seismic deformation of a M=7.5 normal-faulting earthquake with implications for continental kinematics, J. Geophys. Res., (in revision).

Meertens, C. M., R. B. Smith, C. M. Puskas, (2000), Crustal Deformation of the Yellowstone Caldera from Campaign and Continuous GPS surveys, 1987 – 2000, Eos Trans. AGU, 81(48), Fall Meet. Suppl. Abstract V22F-19.

Puskas, C. M., R. B. Smith, C. M. Meertens, W. L. Chang, (2007), Crustal Deformation of the Yellowstone-Snake River Plain volcanic system: campaign and continuous GPS observations, 1987-2004, J. Geophys. Res., 112 doi:10.1029/2006JB004325, in press.

Puskas, C. M., R. B. Smith, G. Waite, L. Flesch, (2004), Kinematic Deformation of the Interior Western U.S. Extensional Regime with Mantle Flow, Eos Trans. AGU, 85(47), Fall Meet. Suppl. Abstract T31A-1247.

The research was supported by NSF Grants 0314298, 9725431, and 9316289.

STRUCTURE AND PHYSICAL PROPERTIES OF FAULT ROCKS OF THE SAN ANDREAS FAULT-ZONE AT SAFOD BOREHOLE AND EXHUMED, ACTIVE SEGMENTS

Ze'ev Reches, Randy Keller • University of Oklahoma

It was realized during the last two decades that understanding earthquake mechanics requires detailed knowledge of fault-zone properties [Ben-Zion and Sammis, 2002]. For example, the composition/properties of fault rocks (gouge, damaged rocks, cataclasite, pseudotachylites, pulverized rocks), the structure and spatial distribution of fault-rocks (distinct bands, shear zones, cross cutting relations), the processes of slip localization (thin zone versus wide zone), and time-dependent alteration and cementation of active fault-zones are important considerations. However, due to the lack of accessibility, these properties are poorly known for depths of 5-15 km, the nucleation depth of most earthquakes along transform faults. The San Andreas Fault Observatory at Depth (SAFOD) project removes this limitation by drilling across the San Andreas Fault and by long-term monitoring at depth [Zoback et al., 2002].

During Phase 3 of SAFOD (Summer 2007), four multilateral holes will be drilled, each extending 250 m from the main hole. These holes will provide up to 1000 m of continuous core of host rock and fault rocks (cataclasites, gouge, veins and crack-seal feature), including samples from currently active segments. We propose to analyze the microstructure and properties of selected samples of these cores. We will also plan to up-scale the findings in SAFOD fault-zones to field-scale through the analysis of exposed active segments of the San Andreas Fault at Tejon Pass, which is located about 180 km SE of SAFOD along the San Andreas Fault; this area was exhumed to depths of 3-6 km [Reches et al., 2006].

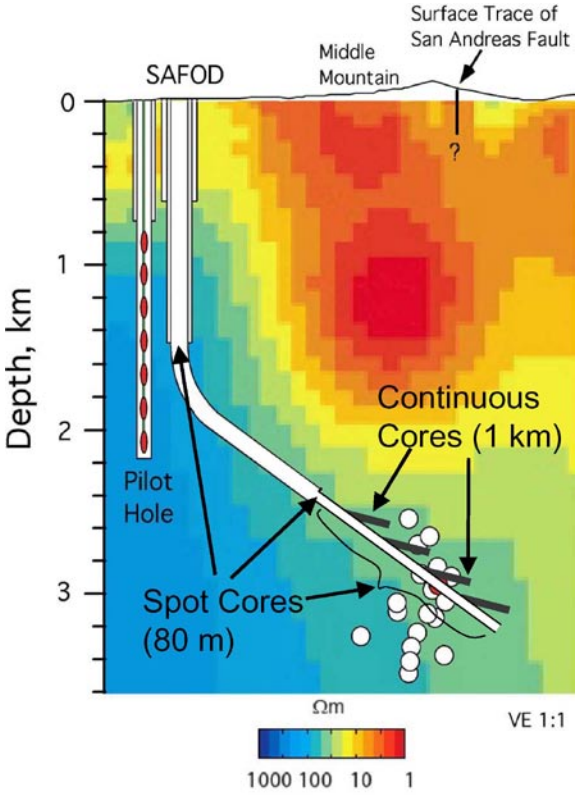

SAFOD Phase 3 Drilling (Summer 2007). Drilling four multilateral core holes extending 250 m from main hole into the active segments of the San Andreas Fault; they will provide up to 1000 m of continuous core of host rocks and fault rocks.

The proposed research includes the following components: (1) Analysis of the texture and composition of fresh gouge samples from SAFOD cores. Gouge from active zones will be of particular importance, yet such zones are difficult to sample. The techniques to be applied include laser particle size analyzer, SEM, TEM, electron- microprobe, and BET; (2) Microstructural analyses of cohesive fault rocks from SAFOD cores by using optical microscopy and electron-micro-probe (including cathodoluminescence). These techniques will constrain the timing and order of fragmentation, alteration, and generation of authigenic phases; (3) Application of measured physical properties of SAFOD cores (by USGS team) to field scale mapping of the exposed fault zone of the San Andreas at Tejon Pass. Successful accomplishment of the project will contribute to several central issues of earthquake physics. First, knowledge on gouge surface area and grain size distribution is central to understanding testing hypotheses for dynamic fault weakening (e.g., pulverization and failure in process zone). Second, knowledge of gouge properties is essential to understanding the energy expenditure and thus the intensity and type of on- and off-fault damage. Third, up-scaling of core and borehole data to the recognition of physical properties of exhumed, seismically active fault-zones in the field (here for Tejon Pass) is essential for seismic hazard evaluation.

Ben-Zion Y, Sammis CG, 2003, Characterization of fault zones. Pure Appl Geophys, 160, 677-715.

Reches, Z. Verrett, JD, Borjes, G., Dewers T., Witten, A, Brune, JN, 2006. Structure, Composition and Strain of the San Andreas Fault-Zone at Tejon Pass, California. Seismological Research Letters, 77 (2) 257.

Zoback, M.D., Hickman, S. & Ellsworth, W. Testing Fundamental Theories of Earthquake Mechanics: The San Andreas Fault Observatory at Depth. http://icdp.gfz-potsdam.de/html/sites/sanandreas/objectives/proposal.html (2002).

Associated grants: Natural Earthquake Laboratory in South African Mines. NSF ($1.6 m for five institutions), 2004-07; Drilling Active Faults in South African Mines, ICDP, Germany, $250,000. Collaborators in proposed work: David London, Preston Larson, and Gregory W. Strout all from the U of Oklahoma, Norman, OK.

HIGH-RESOLUTION 3D ANISOTROPIC STRUCTURE OF THE NORTH AMERICAN UPPER MANTLE FROM INVERSION OF BODY AND SURFACE WAVEFORM DATA

Barbara Romanowicz • Berkeley Seismological Laboratory
Federica Marone • Paul Scherrer Institute, Switzerland

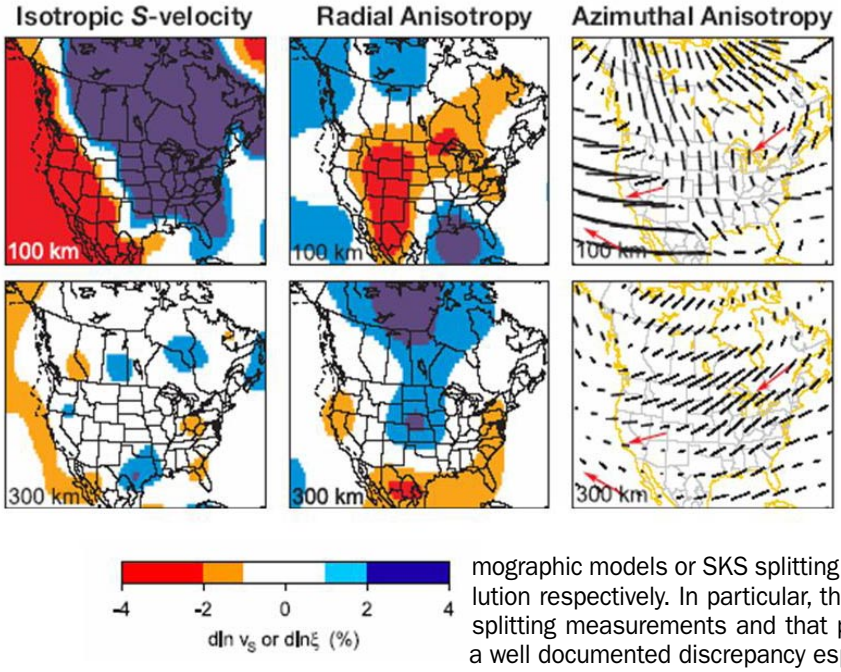

Horizontal slices at depths of 100 and 300 km showing the isotropic and anisotropic parts of our 3D tomographic model of the upper mantle in North America. Left: isotropic Vs structure. Middle: Lateral variations of the radially anisotropic parameter plotted with respect to the PREM model (Dziewonski and Anderson, 1981). Note that PREM is radially anisotropic down to 200 km. The plot at 100 km indicates that the root of the craton is less anisotropic than PREM. Right: azimuthal anisotropy. The black lines give the direction of the fast axis and relative size of azimuthal anisotropy, the red arrows give the direction of absolute plate motion.

Seismic anisotropy provides insight into paleo and recent deformation processes and therefore mantle dynamics. Our knowledge of the upper mantle anisotropic structure under North America is based mainly on global tomographic models or SKS splitting studies which lack horizontal and vertical resolution respectively. In particular, the azimuthal anisotropy derived from local SKS splitting measurements and that predicted from surface wave inversions shows a well documented discrepancy especially under continents. We present here the first 3D regional tomographic model of the North American upper mantle, which simultaneously includes both radial and azimuthal anisotropy and reconciles this discrepancy. The novelty of our approach consists in the joint inversion of fundamental and higher mode surface waveforms together with constraints on azimuthal anisotropy derived from SKS splitting measurements, producing a 3D anisotropic model with enhanced depth resolution down to the transition zone. In a first step, we inverted long period waveform data simultaneously for perturbations in the isotropic S-velocity structure, the anisotropic parameter $x=(Vsh/Vsv)^2$ and the depth to the Moho, in the framework of normal mode asymptotic theory (NACT) [Li and Romanowicz, 1995], correcting for 3D structure outside of the region of study using a global radially anisotropic model of the upper mantle, and correcting for crustal structure using a non-linear approach adapted to the large lateral variations of Moho depth. The resulting 2D broad-band sensitivity kernels allow us to exploit the information contained in long-period seismograms for body, fundamental and higher-mode surface waves at the same time. We have adapted the NACT algorithm for the regional case by implementing a lateral parametrization in terms of spherical splines on an inhomogeneous triangular grid of nodes, with the finest mesh for North America. The inverted dataset consists of more than 100,000 high quality 3-component body, fundamental and overtone surface waveforms, recorded at broad-band seismic stations in North America from teleseismic events.

Notable features of the radially anisotropic part of the model are a positive ξ anomaly down to 300 km under cratons, indicating the presence of horizontal shear in the asthenosphere and a negative ξ anomaly beneath the Basin and Range province, which suggests the presence of mantle upwelling. Our 3D azimuthal anisotropic model indicates the presence of two layers of anisotropy with distinct fast axis directions under the stable part of the North American continent: a deeper layer with the fast axis direction aligned with the absolute plate motion direction suggesting lattice preferred orientation of anisotropic minerals in a present day asthenospheric flow and a shallower lithospheric layer likely showing records of past tectonic events. Under the tectonically active western US, where the lithosphere is thin, the direction of tomographically inferred anisotropy is stable with depth and compatible with the absolute plate motion direction. Synthetic SKS splitting parameters computed for this new 3D azimuthal anisotropic model are in good agreement with observations throughout North America. We believe that previous surface wave based models strongly underestimated the strength of the anisotropy at large depths beneath cratons. The acquisition of USArray data will help progressively obtain a more uniform and dense data distribution, thus improving both lateral and depth constraints.

F. Marone and B. Romanowicz (2007) Non-linear crustal corrections in high-resolution waveform seismic tomography, Geophys. Res. Lett., in press.
F. Marone, Y. Gung and B. Romanowicz (2007) High resolution 3D radial anisotropic structure of the north American upper mantle from inversion of surface waveform
Marone, F. and B. Romanowicz (2007) On the depth distribution of azimuthal anisotropy in the continental lithosphere, Nature, in revision

This work has been supported by the NSF grant NSF/EAR-0345481

IMAGING SUBDUCTION AND RELATED FLUID PROCESSES IN THE PACIFIC NORTHWEST: CASCADIA ARRAYS FOR EARTHSCOPE (CAFE)

Stéphane Rondenay • Massachusetts Institute of Technology
Geoffrey Abers • Boston University
Kenneth Creager, Stephen Malone • University of Washington

Subduction delivers fluids into the Earth's mantle by downward transport of hydrated crust. These fluids are released at depth and may be responsible for a wide variety of phenomena including weakened thrust faults, episodic tremor and slip (ETS), intraslab earthquakes, forearc serpentinization, and arc magmatism. These processes are fundamentally controlled by the thermal structure of the incoming plate. Viewed in this perspective, Cascadia is an important thermal endmember - it is the volcanic arc associated with the youngest subducting plate globally.

In 2006 we launched a major EarthScope-supported project across the Cascadia margin, Cascadia Arrays For Earthscope (CAFE). CAFE explores fluid processes in subduction zones using the tools of seismology, geodesy and petrology, and integrates these results with complementary constraints from geodynamics and geochemistry. In particular, seismic imaging is employed to illuminate (i) the descending oceanic plate, from where fluids are expelled by metamorphism, and (ii) the mantle wedge, where fluids migrate to produce hydrous phases such as serpentine or, beneath the volcanic arc, primary magmas. The experiment targets a section of the Cascadia system where earthquakes extend to nearly 100 km depth, thus permitting an investigation of the relationship between the release of fluids and the generation of Wadati-Benioff-zone earthquakes. The study area is also ideally located to explore the relationship between fluid transport and ETS, a phenomenon that is robustly observed in Cascadia.

The basic experiment has four components: (1) a 47-element broadband imaging array of Flexible Array instruments, integrated with stations from the Earthscope Transportable Array [Figure 1]; (2) three small-aperture seismic arrays with 15 additional short-period instruments near known sources of ETS [Figure 1]; (3) analysis of the PBO and PANGA GPS data sets to define the details of episodic slip events; and (4) integrative modeling. In July 2006, the seismographs were deployed in western Washington along a swath extending from the coast (south of the Olympic Peninsula) to the back-arc across Mt. Rainier, with a variable station spacing of 5 to 20 km. Most of these sites were constructed and deployed over a period of 3 weeks by a field crew of 12, including several graduate students and IRIS interns, an activity that provided training for the next generation of geophysicists. Initial data recovery has been excellent after the first 6 months of deployment. This time window includes an ETS episode in Jan. 2007, which is discussed elsewhere in this volume [Creager et al., this volume]. Given the success of this deployment to date, we expect to make significant progress toward understanding the relationship between subduction, ETS, and fluid cycle.

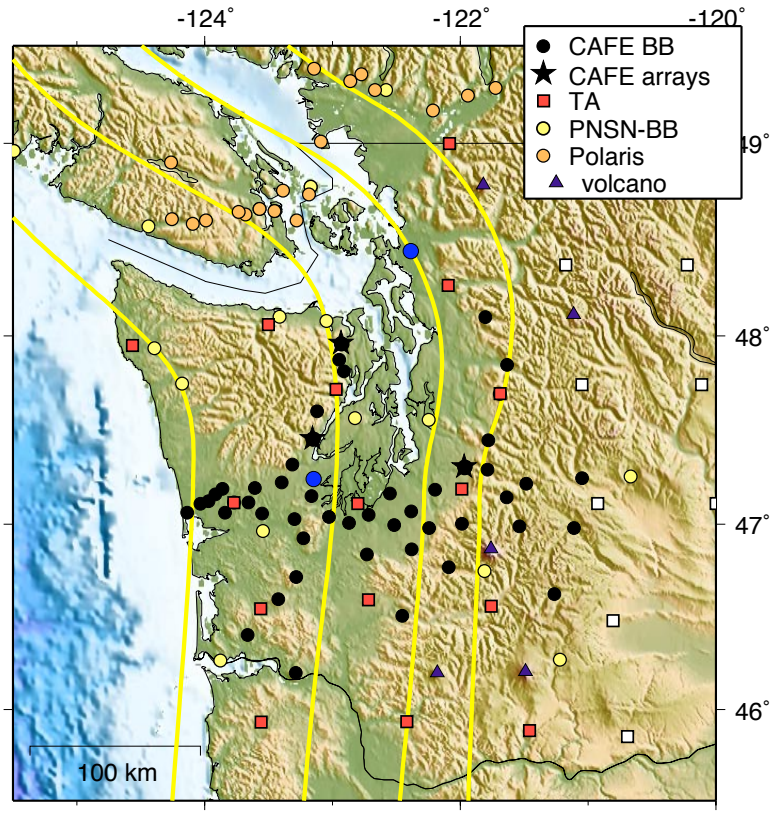

Map of the Pacific Northwest showing the distribution of seismic stations currently in operation in the region. CAFE stations are indicated by black symbols (see legend).

This project is supported financially by NSF-EarthScope grant EAR-0544996. Further support is provided by IRIS-PASSCAL (technical), IRIS-DMS (data archival), and EarthScope-ANF (real-time data). Other collaborators include: T. Melbourne, B. Hacker, A. Wech, and Z. Zhang. We are grateful to everyone who participated in the fieldwork.

EARTHQUAKE NUCLEATION

Allan Rubin • Princeton University

We do not know how earthquakes begin. Efforts to detect a quasi-static nucleation phase observationally have been largely unsuccessful, very likely because the dimensions of most nucleation zones are too small [Dieterich and Kilgore, 1996]. Theoretically, despite three decades of laboratory experiments, we do not even know the proper constitutive equations to use in numerical models. Yet a better understanding of nucleation is important for seismic hazards reduction. Episodic slow slip events in subduction zones in Cascadia and Japan represent times of increased stressing rate on major subduction thrust faults, and can be considered as "nucleation" events that, for reasons yet to be fully understood, do not proceed to instability. A large fraction of earthquakes appear to begin with a "seismic nucleation phase" that scales with the ultimate size of the earthquake [Ellsworth and Beroza, 1995]. Whether this phase reflects a large-scale quasi-static nucleation process or the dynamics of rupture in the presence of material or stress heterogeneity, possibly established by the last major earthquake, is unknown. It has also recently been claimed that the size of large earthquakes can be determined from the first few seconds of the compressional wavetrain, produced well before the earthquake is over [Olson and Allen, 2005]. The relation of this observation to either nucleation or a heterogeneous prestress is uncertain, but it is being actively explored for use in seismic early warning systems.

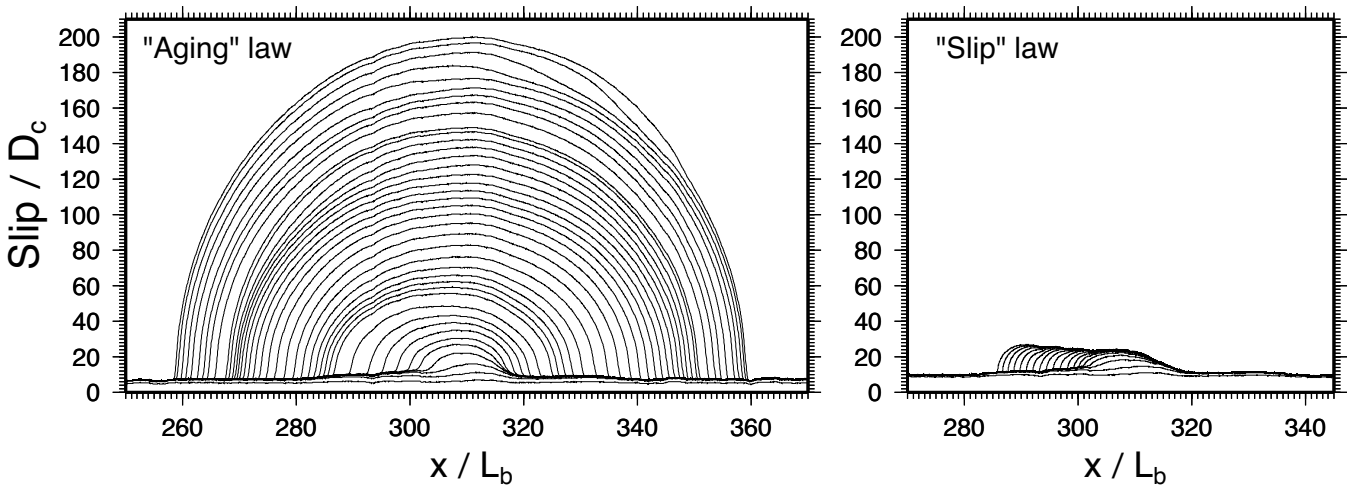

Snapshots of normalized fault slip as a function of normalized position for two simulations of earthquake nucleation that are identical in all respects except in the version of the state evolution law (the two most popular are used). Nucleation may take the form of a quasi-statically expanding crack or a unidirectional pulse. Given a large enough nucleation zone, these styles should de distinguishable from strain measurements made in the near field.

For the last 3 years, Jean-Paul Ampuero and I have been studying earthquake nucleation numerically and analytically [Rubin and Ampuero, 2005; Ampuero and Rubin, in prep.]. Our work has clarified the implications of the standard rate-and-state-dependent friction equations for nucleation on deformable faults, and has identified multiple length scales of nucleation that can interact in important ways, for example so as to produce periodic "slow slip events" where the fault is near velocity-neutral. What we lack is the proper constitutive law for the evolution of the fault "state" variable, which we have shown to control the style of nucleation in a way that can be qualitatively understood. Monitoring known earthquake nucleation sites for precursory strain in the near field, as can be done at SAFOD, might represent our best chance for remedying this situation and for tying together the quasi-static and early seismic nucleation phases.

Rubin and Ampuero's work was supported by NSF awards 0126184 and 0538156.

SOURCE PROCESSES AND EARTHQUAKE TRIGGERING USING SAFOD DATA

Justin Rubinstein • University of Washington

The continued operation of a seismic string within the SAFOD drillhole will offer many opportunities for understanding the physical processes that produce earthquakes. The operation of these seismic instruments at depth offer a great boon because they are below near-surface materials, which have particularly high levels of attenuation, and their proximity to earthquake sources further reduces the effects of attenuation, providing much better resolution on the high frequency component of seismic radiation. This improvement will allow me to identify the generation of aftershocks and triggered earthquakes within the "noise" of body waves and surface waves from nearby and distant earthquakes. This information gleaned from this will assist in understanding how the stresses of nearby earthquakes and/or slow slip events influence seismogenesis and the physical controls on earthquake nucleation and runaway. More uniquely, the instruments will allow me to observe the effects of the changing stress state on faults imposed by earthquake rupture and how that affects earthquake nucleation. This will involve using a method devised by Ampuero and Rubin [in preparation]. This technique relies on the assumption that waveforms from sources with the same focal mechanism and similar locations will be highly similar. Given this, one can use a recording of a single earthquake in a region as an empirical Green's function (EGF), and deconvolve its waveform from the waveforms of highly similar, nearby earthquakes. Deconvolving the EGF leaves a seismogram describing the source properties of the initial earthquake. This technique has been used to identify source complexity in the waveforms of similar earthquakes. From these source characterizations I may be able to determine how the effects of the stress changes from rupture on an adjacent section of the fault influence local rupture. Determining how the stresses from rupture influence further rupture will help reveal the physical processes behind all phases of earthquake rupture, i.e., nucleation, propagation, and termination. A slight modification of this technique may also prove to be useful for identifying earthquake triggering. Using smaller earthquakes as the EGF's for larger events, one can deconvolve their effect from the larger earthquake waveform, in the hope of identifying early aftershocks that occurred nearby to the small earthquake used as an EGF. Events identified using this technique would further supplement my catalog of dynamically triggered events.

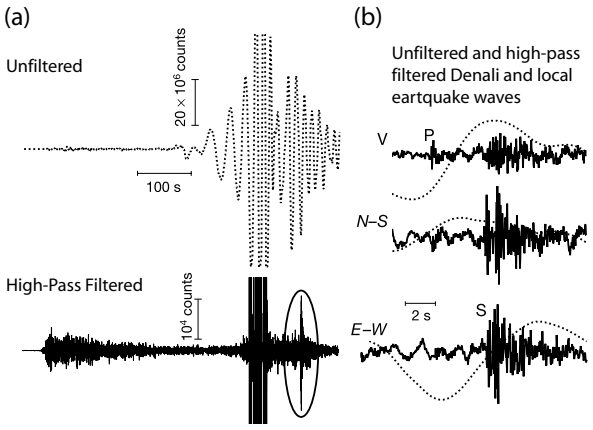

Broadband recordings of the 2002 Denali earthquake from the N-S component of station PNT. (a) A local earthquake is not apparent when examining an unfiltered record of the Denali Earthquake (dotted). Filtering frequencies below ~2Hz (solid trace) reveals a local earthquake (circled). (b) Expanded view of the local earthquake circled in the left for all three components of ground velocity. The arrival of the P and S waves are clearly observable. Figure modified from Gomberg, et al., 2004.

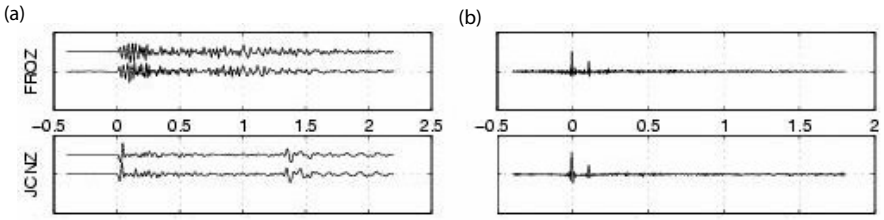

Source complexity revealed by EGF deconvolution of highly similar earthquakes. (a) Seismograms for two similar earthquakes as recorded at stations JCN and FRO. (b) Results of EGF deconvolution for these stations revealing two distinct bursts of energy that occur 0.1s apart. Figure courtesy J-P Ampuero.

INTEGRATING CONTROLLED-SOURCE AND PASSIVE SEISMIC DATASETS

Eva-Maria Rumpfhuber, Randy Keller • University of Oklahoma
Aaron Velasco • University of Texas at El Paso

EarthScope enables geoscientists to address fundamental questions about continental structure, dynamics and evolution by its multidisciplinary nature. In general, models derived from the analysis of individual geological and geophysical datasets indicate the complexity of the Earth's structure and the processes at work. However, all too often these models have discrepancies, mainly due to contrasts in resolution and parameters they target. Thus, it is essential to incorporate geophysical and geological datasets and techniques to produce one consistent earth model and to further understand the Earth's dynamics. We focus on developing a formal integration approach using continental scale controlled-source experiments and passive source experiments in overlapping regions. Controlled source experiments provide the highest resolution for a number of geophysical properties (Vp, Vs, etc.), as well as interfaces and transition zones, but generally can only cover specific regions in detail. Passive Source experiments collect large quantities of data from three-component broadband stations, such as the USArray component of EarthScope, but usually with sparse station coverage. We explore formal integration schemes for the combination of controlled-source seismic data and receiver functions on a lithospheric scale. Our initial attempt stems from a tomography approach using interfaces partly constrained by receiver functions, and we are also investigating ray-tracing as basis for the integration. We use datasets from recent field experiments, and build a framework for adding additional data to the integration scheme.

Rumpfhuber, E., Keller, G.R., Velasco A.A. (2006), Toward an integration of controlled-source and passive seismic datasets, Eos Trans. AGU, 87(52), Fall Meeting. Suppl., Abstract A31A-0871

Rumpfhuber, E., Keller, G.R., Velasco A.A. (2005), Formal integration of controlled-source and passive seismic data: Utilization of the CD-ROM experiment, Eos Trans. AGU, 86(52), Fall Meet. Suppl., Abstract S44A-03

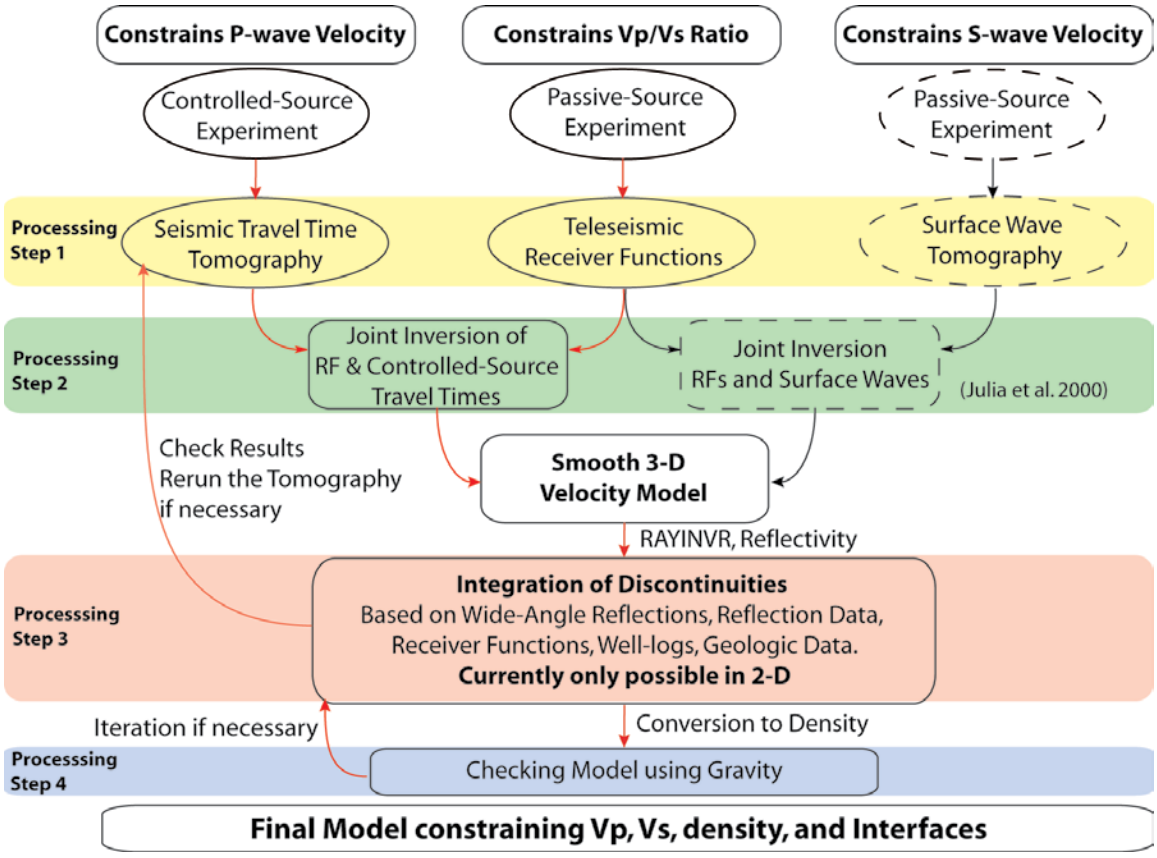

MODELING PLATE BOUNDARY STRESS CHANGES WITH INSAR AND CGPS

David Sandwell, Bridget Konter, Yehuda Bock • University of California, San Diego

The San Andreas Fault System has long been recognized as a natural laboratory for investigating the many facets of plate boundary deformation. The growing archive of space geodetic data now culminating in the Plate Boundary Observatory is providing a detailed synoptic picture of the accumulation of stress and strain along this zone. At best, these measurements can provide a detailed snapshot of the present-day stress accumulation rate. However, an improved understanding of plate boundary physics and seismic hazard will require estimates of absolute stress and accumulated seismic moment that can only be established through model simulations. These simulations must include interseismic, coseismic and postseismic slip history on complex three-dimensional fault systems for the past several earthquake cycles (~1000 years) and also account for viscoelastic relaxation of the asthenosphere and the restoring force of gravity due to vertical loads. We have developed a three-dimensional viscoelastic body force algorithm capable of highly efficient modeling of large-scale plate boundary deformation data by making computations in the spectral domain. Initial model simulations provide a plausible description of large-scale plate boundary deformation and stress for many earthquake cycles and also explore changes in stress due to lake and ocean loading. More importantly, they provide a quantitative prediction of the present-day crustal Coulomb stress field. Model simulations, constrained by improved measurements, can be used to address the following scientific questions: What is the present level of stress on the San Andreas Fault Zone and how has it evolved since the availability (circa 1992) of InSAR and continuous GPS? What processes influence the spatial and temporal pattern of earthquake occurrence? Is the earthquake cycle modulated by lake and ocean loads on 100-10,000 year timescales? How is strain relieved during the interseismic period at shallow depths on mature faults? Another outcome of this study is a robust crustal deformation model for addressing the epoch-date surveying problem for the California Spatial Reference Center (CSRC).

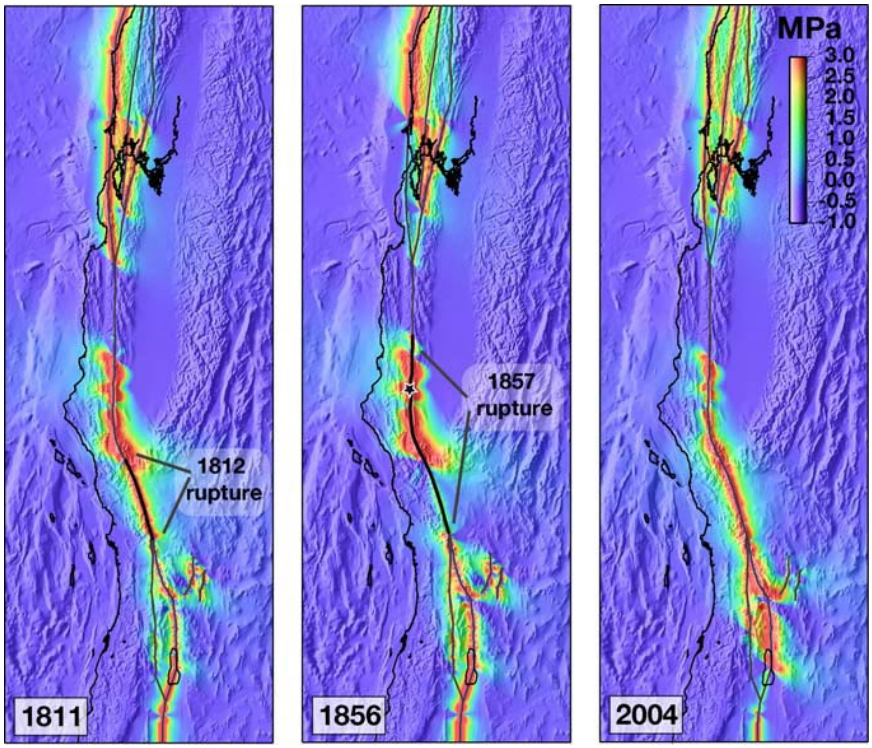

Coulomb stress in MPa for the San Andreas Fault System for three snapshots in time. (left) 1811 calendar year model, representing the stress field prior to the 1812 M~7 Wrightwood earthquakes. (center) 1856 calendar year model, representing the stress field prior to the M7.9 1857 Great Fort Tejon earthquake. (right) 2004 calendar year model, representing stress of ~ present day [Smith and Sandwell, 2006].

Langbein, J. and Y. Bock, (2004) High-rate real-time GPS network at Parkfield; Utility for detecting fault slip and seismic displacements, Geophys. Res. Lett., 31.

Lyons, S. N., Y. Bock, and D. Sandwell (2002), Creep along the Imperial fault, southern California, from GPS measurements, J. Geophys. Res., 107(B10), 2249.

Lyons, S. and D. Sandwell (2003), Fault creep along the southern San Andreas from InSAR, permanent scatterers, and stacking, J. Geophys. Res., 108 (B1), 2047.

Prawirodirdjo, L., Y. Ben-Zion, and Y. Bock (2006), Observation and modeling of thermoelastic strain in Southern California Integrated GPS Network daily position time series, J. Geophys. Res., 111, B02408.

This work was supported by EAR0105896 and NASA/JPL REASoN contract 1258722.

CRUSTAL DEFORMATION AND THE SEISMIC CYCLE ACROSS THE KODIAK ISLANDS, ALASKA

Jeanne Sauber, Steven Cohen • National Aeronautics and Space Administration, Goddard Space Flight Center
Gary Carver • Humboldt University
Robert King • Massachusetts Institute of Technology

The Kodiak Islands are located approximately 120 to 250 km from the Alaska-Aleutian Trench. At this location, the Pacific plate is underthrusting the North American plate at a rate of about 57 mm/yr. The southern extent of the 1964 Prince William Sound (Mw = 9.2) earthquake rupture occurred offshore and beneath the eastern portion of the Kodiak Islands. In this study we report global positioning system (GPS) results for 1993 to 2001 from Kodiak Island. The results span the transition between the 1964 uplift region along the eastern coast and the region of coseismic subsidence farther inland. We used these geodetic results to look at the amount of slip near Kodiak during the great 1964 earthquake and we examined the relation of the coseismic slip to crustal deformation measured in the 30 years following the great earthquake. In addition to strain accumulating that will be released in the next large subduction earthquake, we suggest that 4-8 mm/yr of slip is accumulating that will be released as left-lateral strike-slip motion across the inland faults of Kodiak Island. Based on the pre-1964 and post-1964 earthquake history, as well as the pattern of interseismic earthquakes across the plate boundary zone, we hypothesize that in southern Kodiak some strain is released in moderate to large earthquakes between the occurrences of great earthquakes like the 1964 event. In northern Kodiak, however, the main thrust zone is locked and will eventually be relieved in another large subduction zone earthquake in the future.

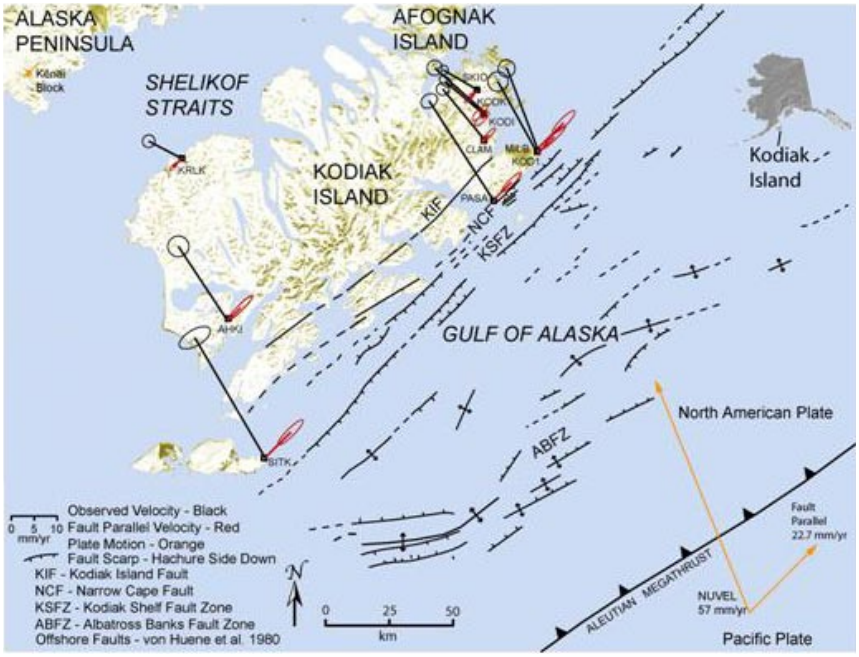

Map showing representative GPS station velocities from the northeastern Kodiak and the USGS Katmai network in southwestern Kodiak processed by R. King using GAMIT/GLOBK [Sauber et al., 2006; Carver et al., Alaska Seismic Hazard Chapman conference, May, 2006]. UNAVCO instruments were used for campaign observations between 1993 and 2001 and at the permanent IGS station KODK.

Sauber, J., Carver, G., Cohen, S., and King, R. Crustal deformation and the seismic cycle across the Kodiak Islands, Alaska, J. Geophys. Res., 111, B02403, doi:10.1029/2005JB003626.

This research was supported by NASA's Solid and Natural Hazards Program, SRTM investigation (921-622-74-10-04).

CLAY MINERAL REACTIONS IN THE SAFOD DRILLHOLE AND THEIR INFLUENCE ON THE SEISMIC BEHAVIOR OF THE SAN ANDREAS FAULT

Anja M. Schleicher • Universität Würzburg, Germany
Laurence N. Warr • Centre de Géochimie de la Surface, France
Ben A. van der Pluijm, Sara Tourscher • University of Michigan

The clay mineralogy of two fault segments of the SAFOD drill hole is investigated in detail by electron microscopy (SEM, HRTEM), X-ray diffraction and X-ray texture goniometry (XRD, XTG), element-chemistry (ICP-OES, ICP-MS), differential thermal analysis (DTA), and 40Ar-39Ar dating. The diverse clay phases present in the rock matrix and on fracture surfaces at 3064 and 3436 m measured depths (MD) occur in zones characterized by recent creep and faulting events. The mudrocks contain detrital grains of chlorite and biotite, along with a range of authigenic illite, illite-smectite, chlorite, chlorite-smectite, smectite and occasional serpentinite fragments [Solum et al. 2006; Schleicher et al. 2006]. The dominant authigenic clay minerals in the matrix are illite, illite-smectite and chlorite. The illite-smectite particles are 20-30 nm in thickness and mainly of the 1Md polytype. At greater depths (3436 m MD), these illite show less ordering and a higher proportion of smectite in the mixed-layer particles. Additionally, some veins are filled with smectite. The illite-smectite in the shallower part (3067 m MD) consists of ~75% illite and 25% smectite layers, with long-range ordering ($R \geq 3$). These mineral phases were likely formed during the movement of aqueous fluids along permeable fractures and veins by dissolution-precipitation reactions, and partly at the expense of larger (~150 nm thick), deformed, detrital packets. Elemental composition of a range of plucked fault rock cuttings at these depths also indicate extensive mobility and mass transfer has occurred along these mineralized structures and implies extensive circulation of low temperature fluids of varying composition accompanied dissolution of the detrital rock components [Tourscher et al. 2006]. Based on textural observations, the timing of authigenic clay mineral growth in the matrix is considered coeval or older than the mineralization along fractures and grain boundaries. The fractures show distinct polished surfaces and striations with thin film coatings and slickenfiber formation that are notably smectite rich. The alignment and widespread occurrence of these coatings along small-scale displacement surfaces indicate a direct relationship between slip and mineral formation [Schleicher et al. 2006]. Illite-rich grain-size separates (8 fractions in total) are currently been analyzed to determine the absolute age of illite clay growth by 40Ar/39Ar dating techniques.

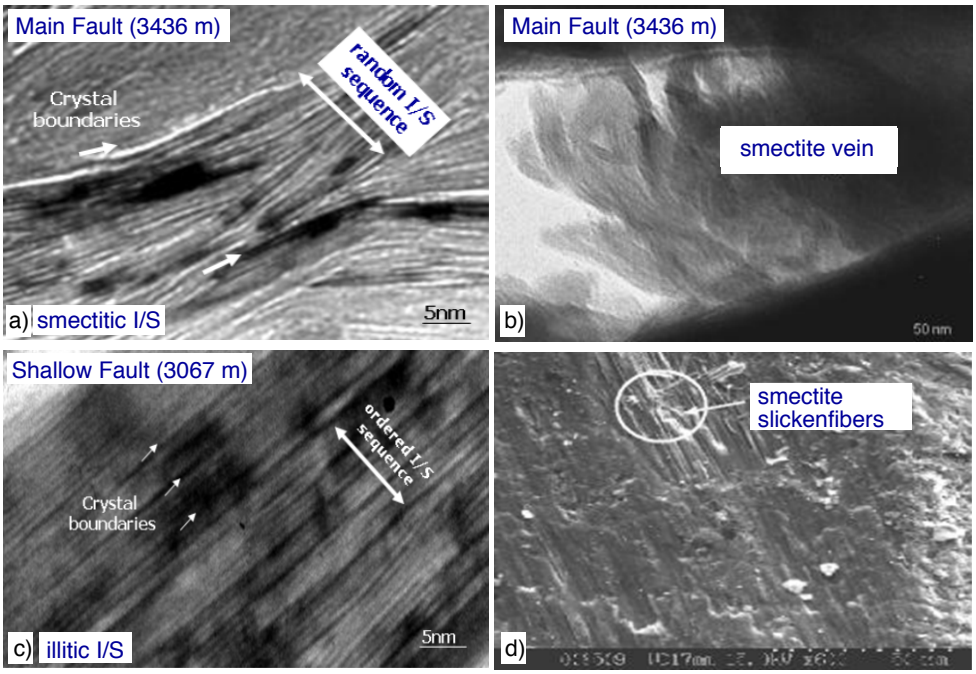

Illite-smectite mixed-layering and smectite occurrence in the SAFOD mud-rocks. a) smectitic illite-smectite at 3436 m MD with a low degree of ordering, b) smectite vein-fillings, c) illitic illite-smectite at 3067 m MD with a high degree of ordering, d) Newly-formed smectite as slickenfibers and coatings on grains and fractures are most abundant in the Main Fault.

Schleicher A.M., van der Pluijm B.A., Solum J.G., Warr L.N. (2006): The origin and significance of clay-coated fractures in mudrock fragments of the SAFOD borehole (Parkfield, California); Geophysical Research Letters 33, LI 6313, DOI: 10.1029/2006GL02650

Solum, J. G., Hickman, S. H., Lockner. D. A., Moore, D. E., van der Pluijm, B. A., Schleicher, A., and Evans, J. P. (2006): Mineralogical characterization of protolith and fault rocks from the SAFOD main hole, Geophysical Research Letters, 33, L21314, DOI

Tourscher S., Schleicher A.M., van der Pluijm B.A., Warr L.N. (2006) Elemental Geochemistry of samples from fault segments of the San Andreas Fault Observatory at Depth (SAFOD) drill hole, Eos Trans. AGU, 87(52), Fall Meet. Suppl., Abstract T21C-0433

The study is funded through the US National Science Foundation (EAR-0345985) and the Deutsche Forschungsgemeinschaft DFG (International continental drilling project ICDP). We thank Steve Hickman, Mark Zoback, and Bill Ellsworth for SAFOD coordination and for providing the sample material, John Solum and Sarah Draper for help in sample collection.

INVESTIGATIONS OF SLOW SLIP ALONG THE CASCADIA SUBDUCTION ZONE USING GPS AND STRAINMETER TIME SERIES

David Schmidt, Haiying Gao • University of Oregon

We are studying the kinematic slip history of slow slip events on the Cascadia Subduction zone. Since the first discovery of transient slow slip by Dragert et al. (2001), several more recent aseismic slip events have been observed. GPS time series data are analyzed using the Extended Network Inversion Filter, which is an implementation of a Kalman filter (Segall and Matthews, 1997). The Extended Network Inversion Filter estimates a time-dependent signal on a buried dislocation by filtering uncorrelated station displacements. We have analyzed GPS time series for slip transients from 2003 to 2005 (Gao and Schmidt, 2006; Schmidt, 2006a). Initial results indicate that the release of strain from one event to the next is not uniform along-strike. In addition, the regular recurrence interval observed beneath southern Vancouver Island is not observed with a slip patch located beneath southern Puget Sound.

Prior to the 2005 event, PBO installed tensor strainmeters on the northern Olympic Peninsula. The observed strain transients are compared to predicted strain time series to cross-validate these new instruments. Generally, the magnitude and sign of the transient is in rough agreement between the observed and predicted time series (see figure below). Based on simulations, the rollback from -0.15 to -0.1 microstrain late in the observed time series can be explained by the passage of a nodal plane in the strain field over the instrument. This finding indicates that the strainmeters provide greater resolution of slip propagation on the plate interface (Schmidt, 2006b).

Dragert, H., Wang, K., and T. S. James (2001), A silent slip event on the deeper Cascadia subduction interface, Science, 292, 1525-1528.

Gao, H., and D. A. Schmidt (2006), The slip history of the 2004 slow slip event on the northern Cascadia subduction zone, EOS Trans. AGU, 87 (52), Fall Meet. Suppl., Abstract T41A-1540.

Schmidt, D. A. (2006a), Comparative study of recent aseismic slip events on the Cascadia subduction zone from GPS, US-Japan Research Panel on Earthquake Research, Tokushima, Japan, Abstract with Program.

Schmidt, D. A. (2006b), The 2005 Cascadia ETS event inferred from PBO tensor strainmeters and GPS, EOS Trans. AGU, 87 (52), Fall Meet. Suppl., Abstract T41A-1545.

This work was supported by NSF Grant EAR-0346037.

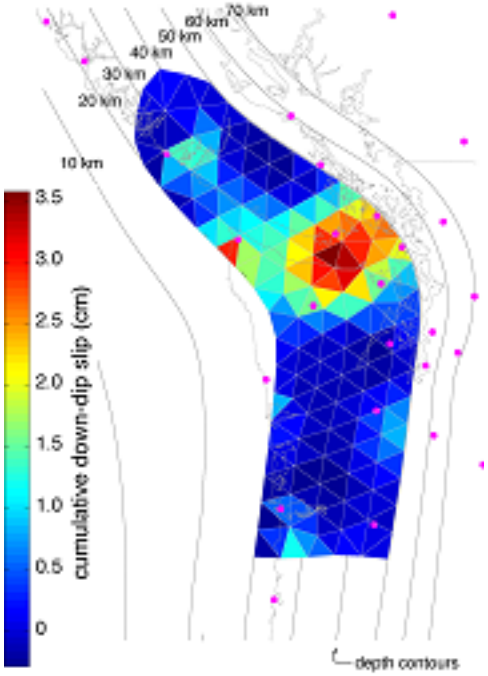

(Left) Cumulative slip distribution of the 2005 slow slip event inferred from GPS time series data. The event is centered below Port Angeles, WA. Fine lines show the depth contours of the subduction interface. Pink circles indicate the locations of GPS benchmarks.

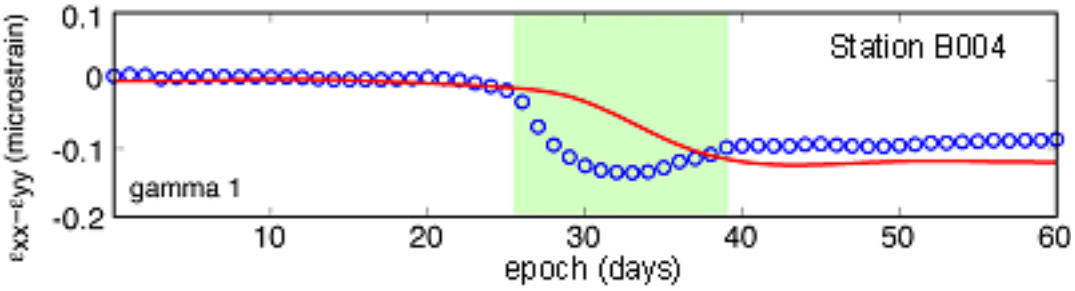

Comparison of observed tensor strain (blue circles) for station B004 compared to predicted strain (red line) inferred from the slip model shown to the left. The green background indicates the period when transient displacement was identified on the GPS time series.

EARTHSCOPE ENGAGES AMERICAN INDIAN STAKEHOLDERS IN ARIZONA

Steven Semken, Peterson Zah, Matthew Fouch, Edward Garnero • Arizona State University

EarthScope is taking up residence in Arizona, where planned deployments place USArray and Plate Boundary Observatory stations on or near the lands of seven different American Indian nations. In concert with the research, the EarthScope education and outreach (E&O) plan calls for direct affiliations with Native stakeholders and school systems. For the past eighteen months we have been collaborating with American Indian communities in Arizona to facilitate USArray deployment and EarthScope E&O activities in a culturally appropriate manner. The collaboration began with a fall 2005 workshop at Arizona State University (Native American Perspectives and Preferences Bearing on EarthScope Deployments in the Southwest, NAPP-ES) for decision-makers and experts in cultural resources and education from the nations that would be affected. The workshop embodied a successful cross-cultural exchange: EarthScope researchers provided Tribal representatives with an introduction to the scientific and educational components of the project, while the American Indian participants shared critical information on relevant cultural and jurisdictional issues. These included sacredness of lands, the significance of ancestral homelands, multi-agency clearance procedures, and best approaches to community-based outreach. Outcomes of the NAPP-ES workshop, including direct connections established with five American Indian nations, guided a successful siting and permitting plan for USArray in Arizona carried out in 2006 and early 2007. The program has also initiated E&O partnerships with six K-14 schools on the Navajo, San Carlos Apache, and Gila River Pima-Maricopa Nations. Results and findings of this two-year project will be offered to inform subsequent EarthScope deployment and E&O activities across American Indian nations in the Rocky Mountain and Northern Plains regions.

Organizers of and participants in the November 2005 NAPP-ES conference at Arizona State University, standing by a full-sized mockup of a Transportable Array station used by presenters to explain the deployment procedure.

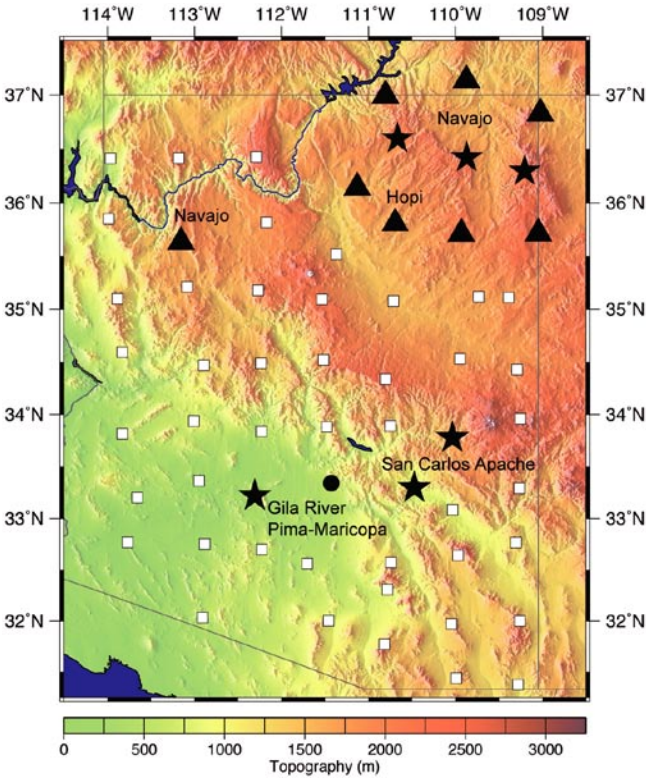

Location map of USArray (Transportable Array) sites in Arizona. Collaborating American Indian nations are named. Black symbols indicate sites on or adjoining American Indian lands: Stars indicate K-14 school hosts, Triangles indicate other American Indian sites, Circle indicates a school outside Tribal jurisdiction. White squares indicate other USArray sites.

Semken, S., Fouch, M., Garnero, E., Zah, P., and Parrish, J. (2006), Native American perspectives and preferences bearing on EarthScope deployments in the Southwest, Geological Society of America Abstracts with Programs, 38, 251.

Semken, S. (2005), Sense of place and place-based introductory geoscience teaching for American Indian and Alaska Native undergraduates, Journal of Geoscience Education, 53, 149-157.

The workshop and activities are supported by the NSF (grant EAR-0454502) and the IRIS E&O Program. We are grateful for the efforts of Jaynie Parrish, ASU; Don Lippert, USArray; Rena Martin, Dinetahdoo CRM; Ron Maldonado, Navajo Nation; Arnold Taylor, Hopi Tribe; Robert Evans and Tamera Dawes, Gila River; David Pastor, San Carlos HS; John Taber, IRIS.

INTERFEROMETRIC TECHNIQUES FOR FAULT ZONE IMAGING AND MONITORING

Roel Snieder, Ivan Vasconcelos, Alexandre Gret • Colorado School of Mines

Seismic interferometry is of increasing importance for monitoring the subsurface. Coda wave interferometry is a tool for monitoring small changes in the subsurface. The seismic waveforms shown are recorded on the wall of a mine pillar, and are excited by a hammer source in the experimental mine of the Colorado School of Mines. With a hydraulic jack the stress state in the pillar was changed and the waveforms before and after the stress change is shown in different colours. We used coda wave interferometry to extract a velocity change of about 0.2% from a comparison of these waveforms.

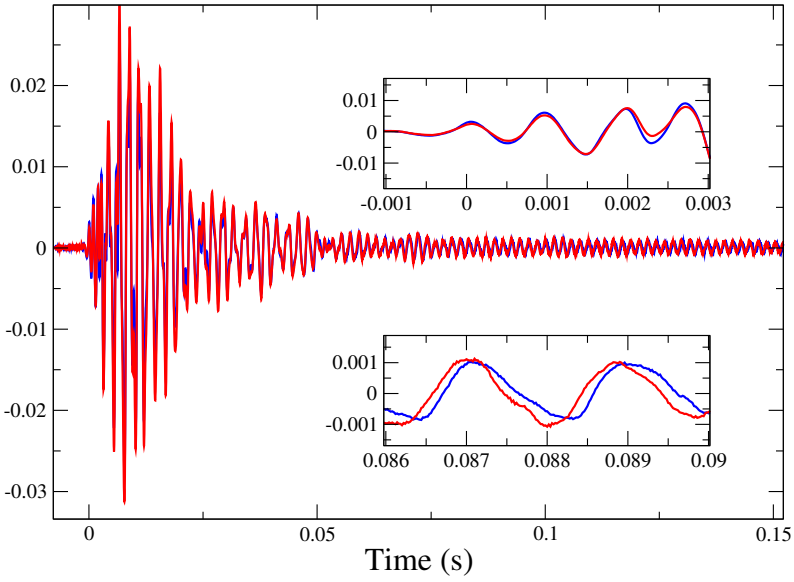

The waveforms recorded with hammer source seismics on the mine pillar for a pressure of 4.14 MPa and 12.41 MPa in the jack (blue and red curves, respectively).

Another variation of seismic interferometry makes it possible to extract the impulse response of a system from ambient fluctuations. With seismic interferometry we used drill-bit noise generated during the drilling of the SAFOD main-hole to determine the waves that propagate from receivers in the pilot hole to the San Andreas Fault and back to other receivers in the pilot hole. The fault-zone reflected waves thus extracted gave the image shown in the gray scale. This image is superposed on an image obtained earlier. Reflection 2 coincides with the surface expression of the San Andreas fault.

A promising line of research is to combine the extraction of the Green's function from ambient noise with the detection of change. As shown in the example of the data recorded in mine, stress changes can be extracted from high-frequency seismic data. By combining these two forms of seismic interferometry using down-hole data, it is possible to carry out long-term in-situ monitoring of the structural properties and stress of fault zone, notably the San Andreas fault.

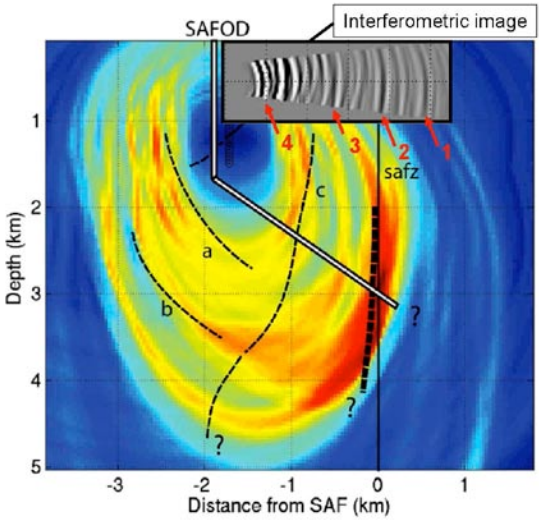

Image obtained from drill bit noise recorded in the pilot hole (grey scale in image), and an earlier model of the region near the San Andreas fault (color).

Curtis, A., P. Gerstoft, H. Sato, R. Snieder, R. and K. Wapenaar, Seismic interferometry -- turning noise into signal, The Leading Edge, 25, 1082-1092, 2006

Grêt, A., R. Snieder, and U. Ozbay, Monitoring in-situ stress changes in a mining environment with coda wave interferometry, Geophys. J. Int., 167, 504-508, 2006

Sens-Schonfelder, C. and U. Wegler, U., Passive image interferometry and seasonal variations at Merapi volcano, Indonesia}, Geophys. Res. Lett., 33, L21302, doi:10.1029/2006GL027797, 2006

Snieder, R., A. Grêt, H. Douma, and J. Scales, Coda wave interferometry for estimating nonlinear behavior in seismic velocity, Science, 295, 2253-2255, 2002

This work is supported by the National Science Foundation through grants EAR-0106668 and EAR-0609595.

CONSTRAINING THE COMPOSITION AND BEHAVIOR OF FAULT ZONES AT SAFOD

John Solum • Sam Houston State University
David Lockner, Stephen Hickman, Diane Moore • U.S. Geological Survey

The San Andreas Fault Observatory at Depth (SAFOD) provides a continuous set of samples through the active San Andreas Fault (SAF) zone. These samples help address decades-old questions about the behavior of the SAF, and provide the unparalled opportunity to constrain the processes that control the behavior of large faults. Serpentine is present in <2 wt % in cuttings collected near a region at ~ 3.3 km measured depth (MD), where casing is actively deforming due to fault creep. The low abundance of serpentine in the cuttings suggests that if it is rheologically important then it occurs as very thin veins. The spatial distribution of serpentine is one of the issues that will be addressed during Phase III coring in 2007. Some faults penetrated during drilling contain clay-rich fault rocks, including several that contain smectitic clays. The weakness of smectites has been proposed as a mechanism to explain the weakness of the SAF, at least at shallow crustal levels (<~3 km), and plucked grains of clay-rich fault rocks have coefficients of friction, mu, as low as 0.3-0.35 for a fault at 2.5 km MD, and 0.4-0.49 for the active fault at 3.3 km MD. These results suggest that the weakness of the SAF is due in part to the growth of weak phases. Neomineralization requires fluid activity, providing another motivation for constraining fault-related fluids. In addition recent work indicates that the frictional properties of smectites are strongly influenced by fluid chemistry.

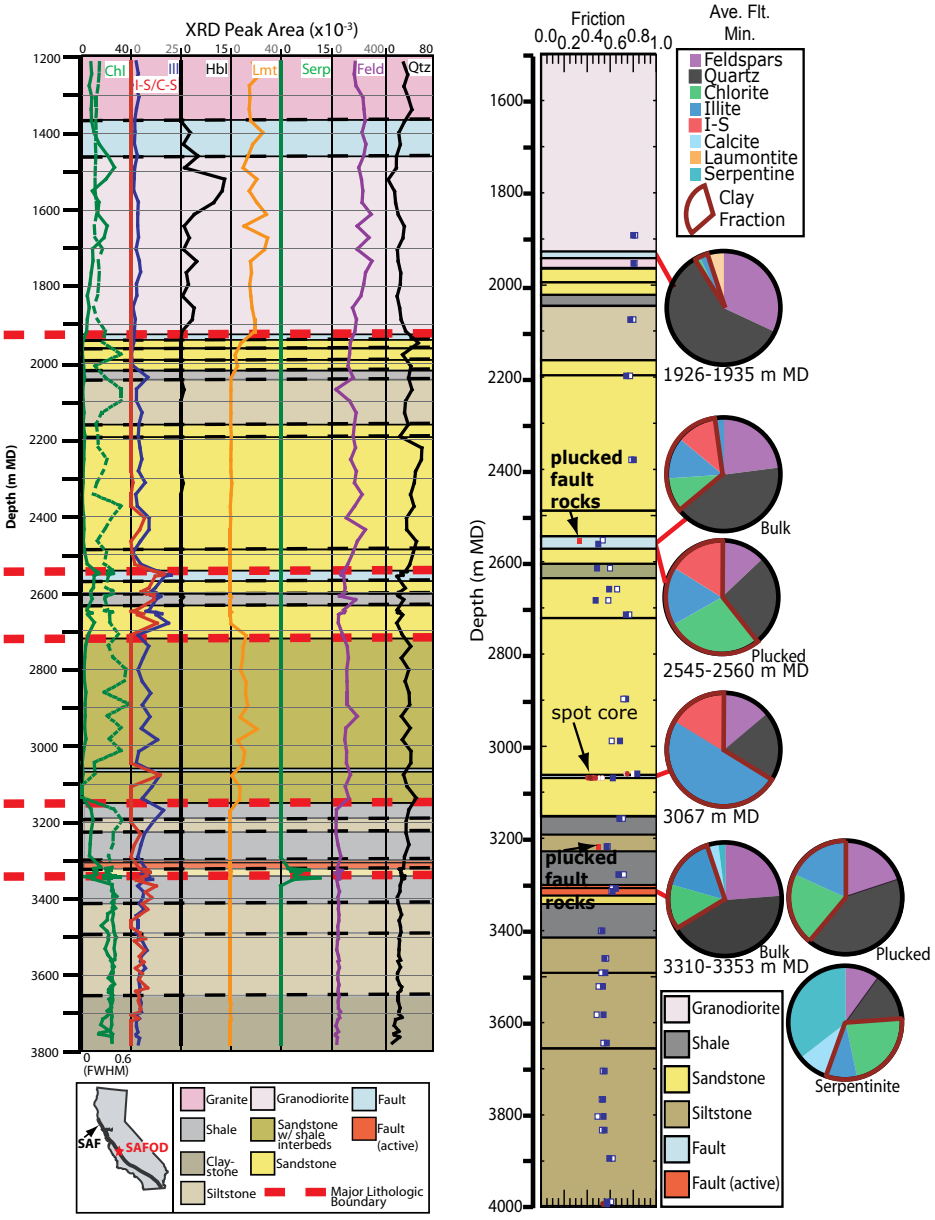

Mineral assemblages measured using washed cuttings from the SAFOD main hole. Red lines denote boundaries of major mineralogical zones. From Solum et al., 2006 (GRL)

Morrow, C., Solum, J., Tembe, S., Lockner, D., and T. –f. Wong, Using drill cutting separates to estimate the strength of narrow shear zones at SAFOD, to be submitted to Geophys. Res. Lett.

Schleicher, A. M., B. A. van der Pluijm, J. G. Solum, and L. N. Warr (2006), Origin and significance of clay-coated fractures in mudrock fragments of the SAFOD borehole (Parkfield, California), Geophys. Res. Lett., 33, L16313, doi:10.1029/2006GL026505.

Solum, J. G., S. H. Hickman, D. A. Lockner, D. E. Moore, B. A. van der Pluijm, A. M. Schleicher, and J. P. Evans (2006), Mineralogical characterization of protolith and fault rocks from the SAFOD Main Hole, Geophys. Res. Lett., 33, L21314, doi:10.1029/200

Tembe, S., D. A. Lockner, J. G. Solum, C. A. Morrow, T. Wong, and D. E. Moore (2006), Frictional strength of cuttings and core from SAFOD drillhole phases 1 and 2, Geophys. Res. Lett., 33, L23307, doi:10.1029/2006GL027626.

Funding: Partially supported by the U.S. Geological Survey Mendenhall Program. Carried out in collaboration with W. Calvin, S. Tourscher, D. C. Barton, K. Bradbury, M. Mayer, D. Kirschner, F. Chester, J. Chester

GPS CONSTRAINTS ON CONTINENTAL INTRAPLATE EARTHQUAKES AND HAZARDS

Seth Stein • Northwestern University

GPS data have significantly advanced understanding of intraplate earthquakes in eastern North America and other continental interiors. They constrain deformation rates to be < 1-2 mm/yr, corresponding approximately to a magnitude 7 earthquake every 500-1000 years. Thus for the New Madrid Seismic Zone, they exclude the previously-common assumption that the area experienced M 8 earthquakes about every 500 years, unless the past 2,000 years of seismicity are non-steady state, with moment release exceeding the long-term loading rate. This result is consistent with the earthquake recurrence history once biases in the paleoseismic data are corrected.

Hence instead of viewing New Madrid as an extraordinary region, it is more useful to view it as typical of other continental intraplate seismic zones (Rhine Graben, Pannonian Basin, Australia) with similar deformation and earthquake recurrence rates. It appears that essentially all of the geodetically observed deformation is released seismically, in contrast to continental plate boundary zones, some of which appears to have significant aseismic deformation.

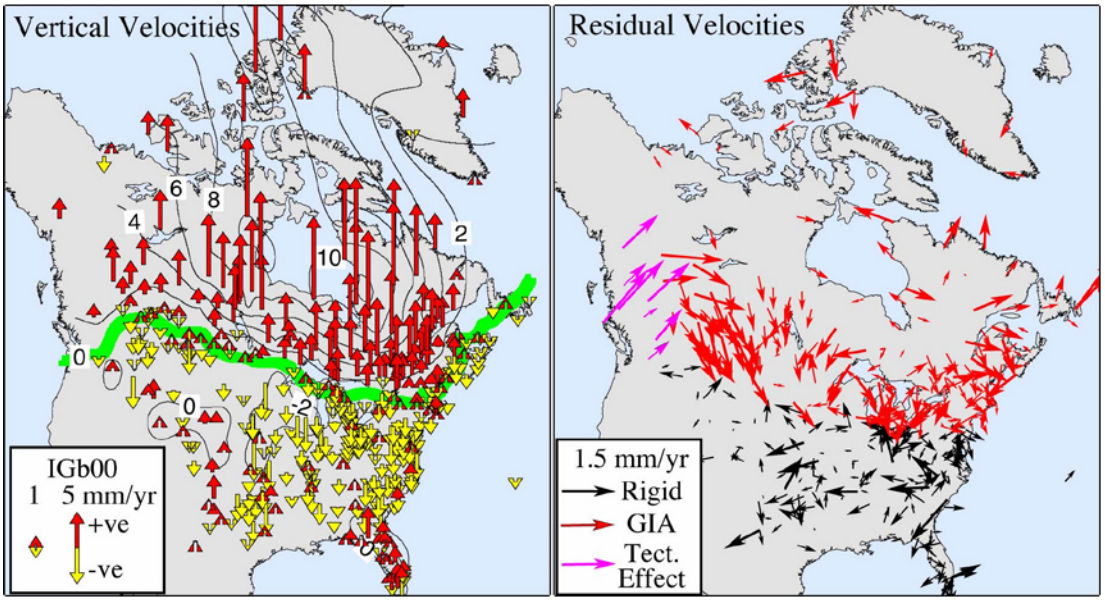

Left: Vertical GPS site motions. Note large uplift rates around Hudson Bay, and subsidence to the south. Green line shows observed "hinge line" separating uplift from subsidence.

Right: Horizontal motion site residuals after subcontracting best fit rigid plate rotation.

The GPS data also provide new insight into earthquake hazards and can be used to help develop cost-effective hazard mitigation strategies. At New Madrid, they do not support USGS hazard maps showing the area to be as hazardous as California, and thus suggest that the proposed upgrade of New Madrid zone building codes to California-level is likely to impose societal costs exceeding the benefits. More generally, because GPS data do not show concentrated deformation at present intraplate seismic zones, they favor a model in which large earthquakes occur almost randomly in a continent containing many long-lived fossil weak zones. Minor stress variations stress due to platewide driving forces and local stresses such as from glacial-isostatic adjustment and other density variations cause transient seismicity as the locus of strain release migrates. In this scenario, much of the present seismicity in regions like New Madrid is likely long aftershock sequences, consistent with concepts from rate-and-state rock friction. If so, present regions of seismicity do not significantly differ from similar weak zones that are less active. This view is consistent with the fact that heat flow data show that the New Madrid region is at most slightly warmer and hence weaker than its surroundings. Hence seismic hazard from large earthquakes in continental plate interiors should be viewed as relatively diffuse, rather than concentrated in areas of recent seismicity.

Newman, A., S. Stein, J. Weber, J. Engeln, A. Mao, and T. Dixon, Slow deformation and low seismic hazard at the New Madrid seismic zone, Science, 284, 619-621, 1999.

A. Newman, J. Schneider, S. Stein, and A. Mendez, Uncertainties in seismic hazard maps for the New Madrid Seismic Zone, Seis. Res. Lett., 72, 653-667, 2001.

Stein, S., J. Tomasello, and A. Newman, Should Memphis build for California`s earthquakes? EOS, 84, 177,184-185, 2003.

Stein, S. and A. Newman, Characteristic and uncharacteristic earthquakes as possible artifacts: applications to the New Madrid and Wabash seismic zones, Seis. Res. Lett., 75, 170-184, 2004.

MAPPING THE PV-PPV BOUNDARY BENEATH CENTRAL AMERICA

Daoyuan Sun, Don Helmberger • California Institute of Technology

A lower mantle S-wave triplication with a Scd branch occurring between S amd ScS appears to be explained by a recently discovered Perovskite (PV) to Post-Perovskite (PPV) phase-change. It is predicted to have a positive Clapeyron slope between 5 to 13 MPa/K with a small S-velocity jump (1.5 to 4%) and an even smaller 1 to 2% jump in P-velocity. Seismic observations indicate that Scd arrives earlier and stronger beneath fast regions (circum-Pacific) than slow regions (super plumes) indicating a positive Clapeyron slope. However, it proves difficult to separate effects produced by downwelling (slab debris) from upwelling (plumes) in refining the actual physical properties. Here we model dense record sections collected from USArray and existing PASSCAL data to isolate effects produced by lower mantle structure as evidenced by P and S tomographic models, to better define the seismic phase-change properties beneath Central America. We find that the PV-PPV velocity jump is twice as strong beneath slow regions as fast regions requiring distinct reference heights indicative of changing chemistry. Moreover, the edges of the supposed buckled slabs deliminated by both P and S-waves display very rapid changes in phase-boundary heights producing Scd multipathing. These features can explain the unstable nature of this phase with easy detection to no detection commonly observed. The fine structure at the base of the mantle beneath these edges contains particularly strong reflections indicative of local ultralow velocity zones, which is predicted by some dynamic models.

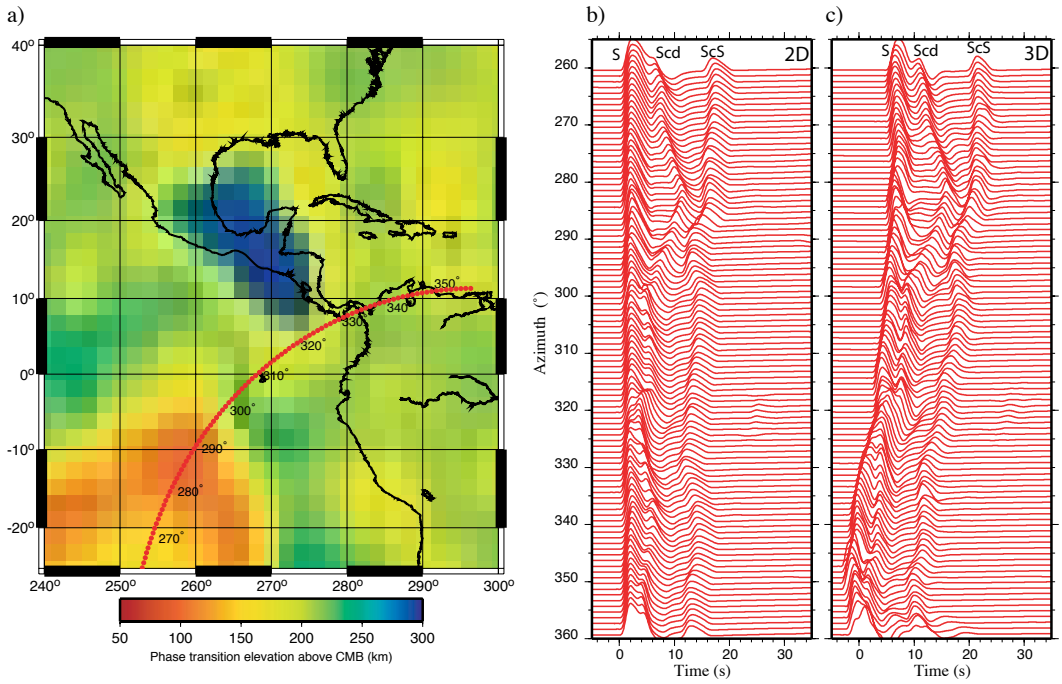

MULTI-PARAMETER SEISMIC IMAGING OF THE CRUST AROUND SAFOD, PARKFIELD, CALIFORNIA

Clifford Thurber, Haijiang Zhang, Ninfa Harrington • University of Wisconsin, Madison
Steven Roecker • Rensselaer Polytechnic Institute

Using seismic data collected by the pre-EarthScope arrays PASO-UNO and PASO-DOS, the USArray Flexible Array deployment PASO-TRES, SAFOD borehole instruments, and active-source experiments, we are developing high-resolution, three-dimensional (3D) models of velocity structure (Vp and Vs), attenuation structure (Qp and Qs), and shear wave anisotropy for the upper crust immediately surrounding the SAFOD drill site near Parkfield, California. The goal is to provide a comprehensive seismological context for interpreting downhole geophysical measurements and integrating geological inferences from cores and cuttings. Structural discontinuities at the SAF in all seismic characteristics are obvious. In addition to imaging the high-Vp Salinian rocks directly beneath the SAFOD site and the low-Vp sediments that the SAFOD borehole penetrated soon after it was deviated, a deeply penetrating fault-zone low velocity zone is evident, in direct association with the earthquakes that define the fault plane at depth. This model was obtained using the recently developed method of double-difference seismic tomography, and it represents the highest-resolution 3D seismic model of a fault zone at seismogenic depths ever obtained.

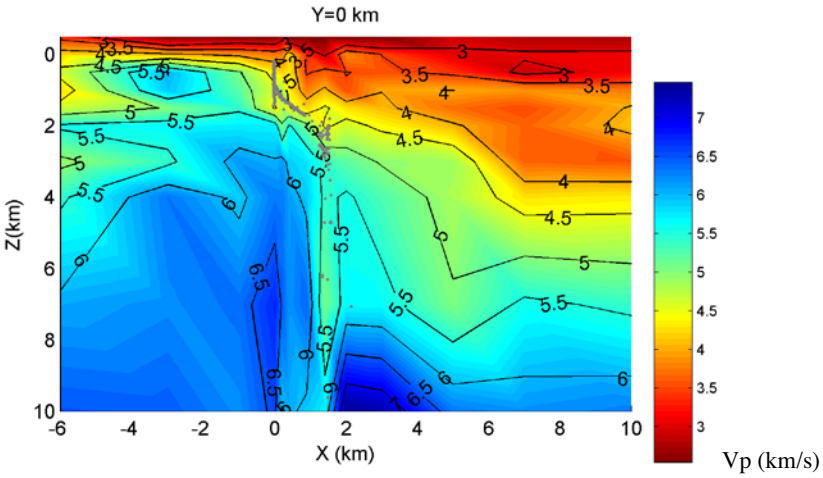

P-wave velocity (Vp) model for a cross-section normal to the San Andreas fault through the SAFOD well-head (at X = 0 km). Contours are in km/s, and the gray dots are earthquakes or "virtual earthquakes" (receiver gathers from surface shots relocated as if they were earthquakes). Z = 0 corresponds to mean sea level, +X points 50° east of north.

We interpret a low Qs feature at shallow depths (< 2 km) on the southwest side of the SAF to be due to late Cenozoic sedimentary rocks overlying weathered and fractured Salinian granitic rocks. A moderate to high Qs feature beneath it can be attributed to Salinian basement rocks with less fracturing (or simply closed cracks) at depth. A low Qs feature along the SAF coincides with the low Vp zone. A low to moderate Qs region on the northeast side of the fault, which extends to depths of 2 to 3 km, coincides with the low velocity basin and the Eastern Conductor imaged in the resistivity model of Unsworth and Bedrosian [2004]. One feature that remains unexplained at present is a high-Qs "finger" just northeast of the SAF trace that extends relatively close to the surface.

In general, the orientations of measured polarization directions in the region of the SAF zone and to the northeast are parallel or subparallel to the SAF, while those on the southwest side of the fault are generally oriented in the direction of the regional maximum compressional stress. There are some areas in which the measurements do not conform to this general pattern. This reveals the extreme complexity of the shear wave anisotropy in the area.

Roecker, S., C. Thurber, and D. McPhee, Joint inversion of gravity and arrival time data from Parkfield: new constraints on structure and hypocenter locations near the SAFOD drill site, Geophys. Res. Lett., 31, L12S04, doi 10.1029/ 2003GL019396, 2004.

Thurber, C., S. Roecker, H. Zhang, S. Baher, and W. Ellsworth, Fine-scale structure of the San Andreas fault and location of the SAFOD target earthquakes, Geophys. Res. Lett., 31, L12S02, doi 10.1029/2003GL019398, 2004.

Unsworth, M., and P.A. Bedrosian (2004), Electrical resistivity structure at the SAFOD site from magnetotelluric exploration, Geophys. Res. Lett., 31, L12S05, doi:10.1029/ 2003GL019405.

This material is based upon work supported by National Science Foundation grants EAR-9814192 (Continental Dynamics), EAR-0346105 (EarthScope), and EAR-0454511 (EarthScope) to UW-Madison and grants EAR-9814155 (Continental Dynamics), EAR-0346032 (EarthScope), and EAR-0454463 (EarthScope) to RPI; additional support provided by USGS grant 06HQGR0105.

LOCATING THE SAFOD DRILLING TARGET EARTHQUAKES

Clifford Thurber, Haijiang Zhang, Yunfeng Liu • University of Wisconsin, Madison
Steven Roecker • Rensselaer Polytechnic Institute

One of the important goals of the SAFOD drilling plan is to core across the San Andreas fault at a point which falls within the rupture patch of a repeating magnitude ~2 earthquake, and to compare the physical properties of the materials in that core to another core taken from a fault patch that undergoes stable sliding (creep). Analysis of these cores is expected to provide significant insight into what controls the nature of fault slip, causing some patches to fail in an unstable, brittle manner (earthquake) versus other patches that undergo stable slip. Because the size of a magnitude ~2 rupture patch is on the order of several tens of meters, knowing the location of the earthquake with a commensurate degree of accuracy is vital to the success of this aspect of the SAFOD project. Seven years of field work, data collection, and data analysis by the UW and RPI seismology groups is being brought to bear on achieving the highest possible accuracy and precision in the location of the target earthquakes. A high-resolution P-wave velocity model has been developed using the new double-difference seismic tomography technique. This image represents the highest-resolution 3D seismic model of a fault zone at seismogenic depths ever obtained, due in large part to the availability of SAFOD borehole recordings. In addition to recording ambient seismicity simultaneously with instruments in the SAFOD borehole and permanent and temporary stations in the area, signals from surface shots have be recorded downhole in order to calibrate seismic wave velocities and estimate absolute location accuracy. The latter is achieved by treating the borehole sensors as "virtual earthquakes" (borehole receiver gathers from surface shots), and using them to test our absolute location capability. Relative location techniques using the target earthquakes, which can be clustered into subgroups based on waveform similarity, in combination with the virtual earthquakes are being used to improve the accuracy and precision of the target locations.

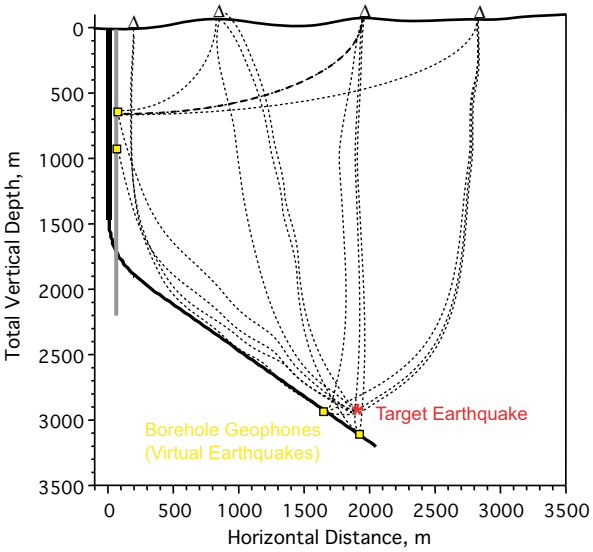

Cartoon showing the strategy for using relative locations of the target earthquake (red star) and "virtual earthquakes" (yellow squares - borehole receiver gathers from surface shots at stations) to determine the position of the target earthquake relative to the SAFOD borehole.

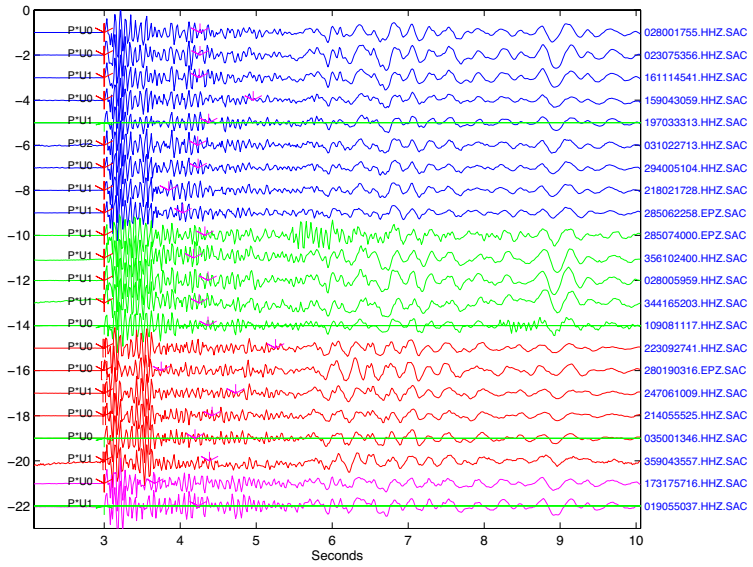

Example of aligned vertical-component waveforms for target-area events at PASO station CRAK. The different colors correspond to events from different subregions within the target zone.

Roecker, S., C. Thurber, and D. McPhee, Joint inversion of gravity and arrival time data from Parkfield: new constraints on structure and hypocenter locations near the SAFOD drill site, Geophys. Res. Lett., 31, L12S04, doi 10.1029/ 2003GL019396, 2004.

Thurber, C., S. Roecker, H. Zhang, S. Baher, and W. Ellsworth, Fine-scale structure of the San Andreas fault and location of the SAFOD target earthquakes, Geophys. Res. Lett., 31, L12S02, doi 10.1029/2003GL019398, 2004.

This material is based upon work supported by National Science Foundation grants EAR-9814192 (Continental Dynamics), EAR-0346105 (EarthScope), and EAR-0454511 (EarthScope) to UW-Madison and grants EAR-9814155 (Continental Dynamics), EAR-0346032 (EarthScope), and EAR-0454463 (EarthScope) to RPI.

EARTHQUAKE SOURCE STUDIES USING ANZA AND PBO BOREHOLE DATA

Frank Vernon • University of California, San Diego

The ANZA Seismic Network (http://eqinfo.ucsd.edu) utilizes broadband and strong motion sensors with 24-bit dataloggers combined with real-time telemetry to monitor local and regional seismicity in southernmost California . The goal of this project is to provide on-scale digital recording of high-resolution three-component seismic data for earthquakes occurring in southern California.

As part of EarthScope, about 100 PBO strainmeters will be installed in regions of scientific interest; in particular seven stations have been installed in the region of the Anza seismic gap along the San Jacinto Fault. PBO brought a drill rig to drill the 150-meter deep borehole and install a Gladwin Tensor Strainmeter. Other scientific instruments installed in PBO strainmeter boreholes include a three-component short period seismometer, a pore pressure monitor and, in some cases, a two-component tiltmeter. The short period seismometer will be installed 6 m above the strainmeter and cemented in place. Each of the PBO borehole stations will have real-time data telemetry provided.

Dr. Jamie Steidl from UCSB received funding from SCEC to augment the seven PBO borehole seismometers with microelectromechanical systems accelerometers, with high frequency response and the high dynamic range.

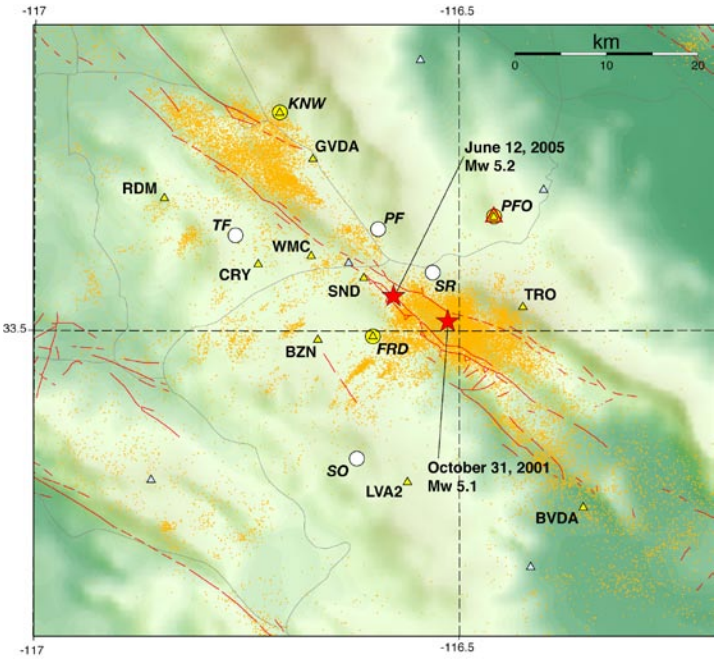

Map illustrating the distribution of four Plate Boundary Observatory (PBO) borehole sites and co-located ANZA/PBO sites. The area of interest is concentrated on the San Jacinto Fault Zone. PBO stations (large white circles and italicized station codes); TF - Trip Flats, PF - Path Finder, SO- Sky Oaks, SR - Santa Rosa. ANZA broadband stations are represented by yellow triangles. Co-located ANZA/PBO sites are represented by large yellow circles (behind the yellow triangle ANZA station symbol) with italicized station codes. Seismicity from October 1st 2000 to September 30th 2005 is represented by orange dots.

Given the presence of large number of stations close to the very active San Jacinto Fault region we have been able to extract information about the earthquake source. Using the Empirical Green Functions (EGF) method and spectral stacking [Prieto et al., 2004; Shearer et al., 2006] we have analyzed hundreds of spectra from the Anza network and thousands of spectra from Southern California (including the Anza network stations). From this analysis we have concluded that at least for the smaller earthquakes there is a large variability of estimated stress drops (0.2 to 30 MPa) with no clear dependence with earthquake magnitude. The new PBO borehole stations will allow us to extent this analysis to both smaller and larger earthquakes.

We have also analyzed the problem of uncertainties of the earthquake source spectrum using EGFs [Prieto et al., 2007]. To remove the effects of the propagation of the seismic waves through the earth, it is necessary to use a small earthquake as an approximate Green function, and deconvolve it from the earthquake that we are interested in characterizing. However, using this method can introduce uncertainties and the deconvolved spectrum has larger variability. Using data from the aftershock sequence of the M5.1 2001 Anza Earthquake, we study the errors associated with EGF methods and introduce a way to estimate confidence intervals of some source parameters and reduce the uncertainties. The new PBO borehole stations will allow us to extend this analysis to a wider range of earthquakes.

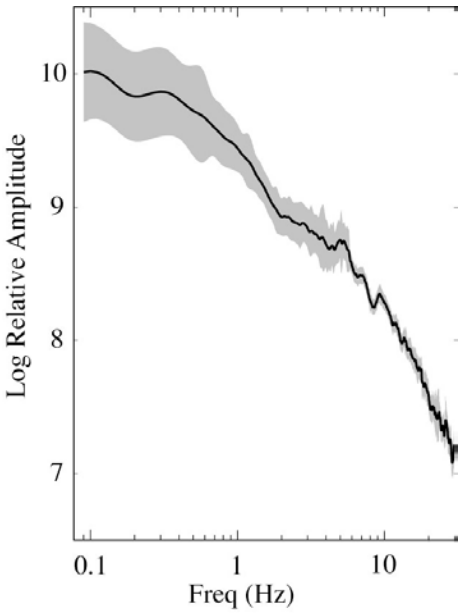

Example taken from Prieto, et al. (2007) using ANZA network data shows the mean source spectrum over eight stations with 95% confidence intervals (gray area) for the M5.1 target.

Prieto, G. A., P. M. Shearer, F. L. Vernon, and D. Kilb (2004). Earthquake source scaling and self-similarity estimation from stacking P and S spectra. J. Geophys. Res., 109, No. B8, B08310 10.1029/2004JB003084.

Prieto, G. A., R. L. Parker, F. L. Vernon, P. M. Shearer and D. J. Thomson (2007). Uncertainties in Earthquake Source Spectrum Estimation using Empirical Green Functions. AGU Monograph on Radiated Energy and the Physics of Earthquake Faulting , R. E. Abercrombie, A. McGarr, H. Kanamori, and G. di Toro eds. Doi: 10.1029/170GM08 69-74.

Shearer, P. M., Prieto, G. A., Hauksson, E., Comprehensive analysis of earthquake source spectra in southern California, J. Geophys. Res., 111, B06303, doi:10.1029/ 2005JB003979, 2006.

This work was supported by USGS 01HQAG0018 & NSF EAR04-17983.

USARRAY HELPS UPGRADE THE PACIFIC NORTHWEST SEISMIC NETWORK

John Vidale, Paul Bodin, Steve Malone • University of Washington

We at the Pacific Northwest Seismograph Network (PNSN) successfully proposed to the Murdock Trust, a regional philanthropy, for $480K to purchase 15 state-of-the-art broadband and strong-motion seismic stations. This purchase leverages the substantial USArray investment in temporary installations to retain their best sites in our region.

The PNSN since 1969 has been the primary seismograph network covering the states of Washington and Oregon. It has the responsibility for monitoring all earthquakes in the region as part of the Advanced National Seismic System. The mission of the PNSN is to assist with the mitigation of geologic hazards related to earthquakes, volcanoes, landslides and tsunami.

The Pacific Northwest is host to many of the most interesting plate tectonic processes, and its rich geological history documents the necessity of surveillance and preparedness. Examples include the stunning eruption of Mt. St. Helens in 1980, its recent renewed activity starting in 2004, an earthquake in 1700 of magnitude 9 that devastated the entire coastlines of Oregon and Washington, and the prehistoric 900 AD magnitude 7.2 earthquake directly under what is now Seattle. Timely information about such geophysical natural events is imperative. The need for improved earthquake information products is underlined by the disastrous December 2004 earthquake and tsunami near Sumatra in a geological setting similar to the Pacific Northwest, the ongoing discovery of recently-active crustal faults under western Washington, and volcanic hazards of Mount St. Helens and Mount Rainier. Both real-time seismic monitoring for public information products and high-quality seismic data for basic seismological research into the nature and causes of catastrophic geophysical events depend on modern instrumentation capable of recording on-scale from the smallest detectable events to the biggest expected ones.

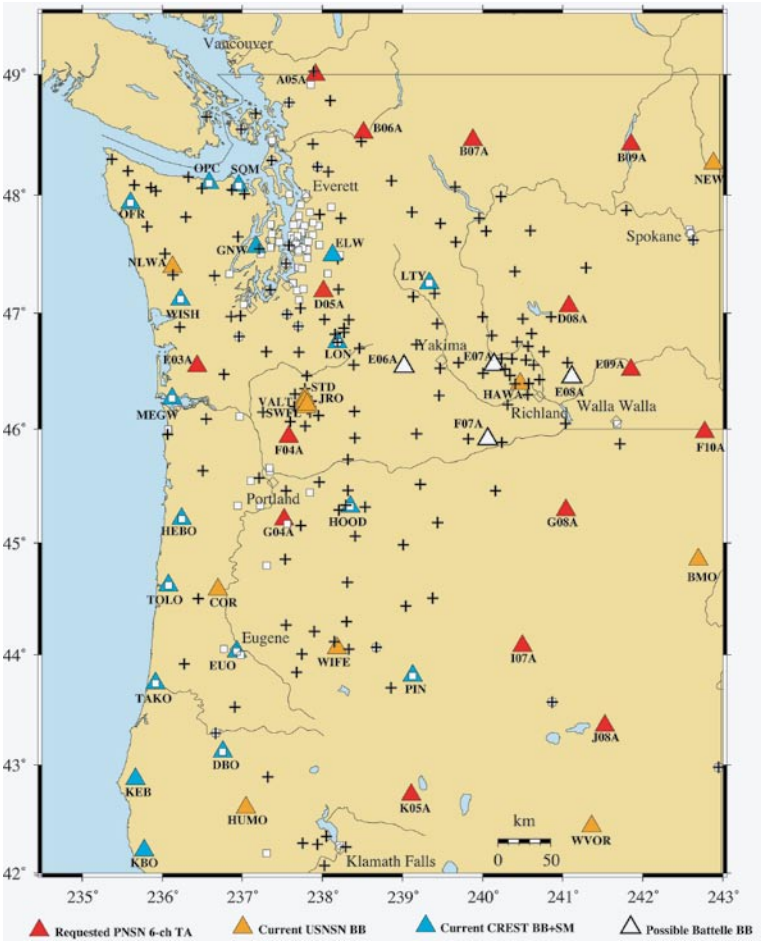

Map of the seismic stations in the PNSN. The red triangles show the locations of the new stations paid for by the Murdock Trust and installed by the USArray.

Major but temporary additions and upgrades of our regional seismic stations were part of the USArray experiment. USArray installed about 80 modern, broadband seismographs in Washington and Oregon. However, around 2008 these instruments will be removed and moved to other sites in the US as the USArray slowly marches across the country over a ten-year period. Thus, for almost two years we will have had a full-blown network of high-quality instruments but would have lost all of those stations at the end of the local deployment period. Thus, by purchasing 15 stations, the PNSN has accrued the substantial value of USArray's sites and vaults, as well as the results of our experience recording and using the data to assess these temporary stations. These new stations have dramatically improved both the quantity and quality of the PNSN's coverage in Washington and Oregon, enhancing earthquake detection and location everywhere in this large region, and improving bandwidth and signal quality. These advances allow new and novel research into earthquakes and volcanoes by geophysicists in the Pacific Northwest and elsewhere. The new stations along with the current high-quality broadband stations will, in effect, form the new backbone of the network, replacing out-dated and worn out equipment, some dating from the 1970's. As citizens of the Pacific Northwest, we will be both protected by the greatly improved monitoring and most likely enchanted by the unexpected discoveries from the successful upgrade to the Pacific Northwest Seismic Network.

The expansion of the PNSN is due to a combination of support from the Murdock Trust, USArray, the UW, the State of Washington, and the USGS.

ALONG-STRIKE VARIATION IN LOCKING ON THE CASCADIA SUBDUCTION ZONE, OREGON AND NORTHERN CALIFORNIA

Ray Weldon, David Schmidt, Reed Burgette • University of Oregon

The tectonic uplift rate along the Cascadia subduction zone provides a constraint on the magnitude and distribution of plate coupling. Observations of sea level change at six permanent NOAA tide gauges (Crescent City, California to Astoria, Oregon) over the past 73 to 81 years provide measurements of uplift rate along the Cascadia subduction zone in a geocentric reference frame, once the rate of regional sea level change is removed from the time series. We use a satellite-based estimate of regional sea level rise to place the relative tidal uplift rates in an absolute vertical reference frame. Repeated high quality leveling lines add a dense network of point observations along the coastal route between the tide gauges, as well as five trench-perpendicular transects (Burgette et al., 2005). We anchor the leveling estimates of uplift rate into the absolute reference frame by using a weighted least-squares adjustment that accounts for errors in both the tidal and leveling data. Absolute uncertainties in uplift rate range from 0.3 to 1 mm/yr. In recent years we have collected GPS observations along the leveling lines in an attempt to better anchor the inland endpoints.

The first deployment of the EarthScope GPS Campaign Systems occurred along the Oregon coast in the summer of 2005.

The first order pattern of uplift rate decays from maximum values near the coast to zero inland, in a pattern consistent with models of elastic strain accumulation above a locked subduction zone. To investigate the along-strike variation in uplift rate pattern, we divide the region into northern, central, and southern sections. Because subduction coupling is believed to be fundamentally a function of depth, and the dip of the interface varies along strike, we compare uplift rates between sections using the plate interface geometry of McCrory et al. (2004). Preliminary modeling results indicate that the along-strike 3D geometry of the coastline and plate interface are not sufficient to explain variations in uplift rate. This finding suggests that the width of the locked zone and degree of coupling must vary along-strike. The data are best fit by a decrease in the width of locking below Oregon near Astoria (Weldon et al., 2006).

McCrory, P.A., J. L. Blair, D.H. Oppenheimer, and S. R. Walter (2004), Depth to the Juan de Fuca slab beneath the Cascadia subduction margin – A 3–D model for sorting earthquakes, U.S. Geological Survey Data Series 91, http://pubs.usgs.gov/ds/91.

Burgette, R. J., R. J. Weldon, D. Livelybrooks, D. A. Schmidt, S. K. Alba, and B. A. Wisely (2005), Constraints on the Extent of Subduction Zone Locking Along the Central Oregon Coast From Leveling and Sea Level Observations, Eos Trans. AGU, 86(52), Fall Meet. Suppl., Abstract S51C-1017.

Weldon, R. J., R. J. Burgette, and D. A. Schmidt (2006), Along-Strike Variation in Locking on the Cascadia Subduction Zone, Oregon and Northern California, EOS Trans. AGU, 87 (52), Fall Meet. Suppl., Abstract T41A-1556.

This work was supported by USGS Grant 05HQR0053.

SUBCONTINENTAL-SCALE STRAIN WAVES ACROSS THE PACIFIC-NORTH AMERICA PLATE BOUNDARY DEFORMATION ZONE: A JOINT EARTHSCOPE-TECTONICS OBSERVATORY STUDY IN CENTRAL NEVADA

B. Wernicke, K. Mahan, M. Simons, R. Briggs • California Institute of Technology

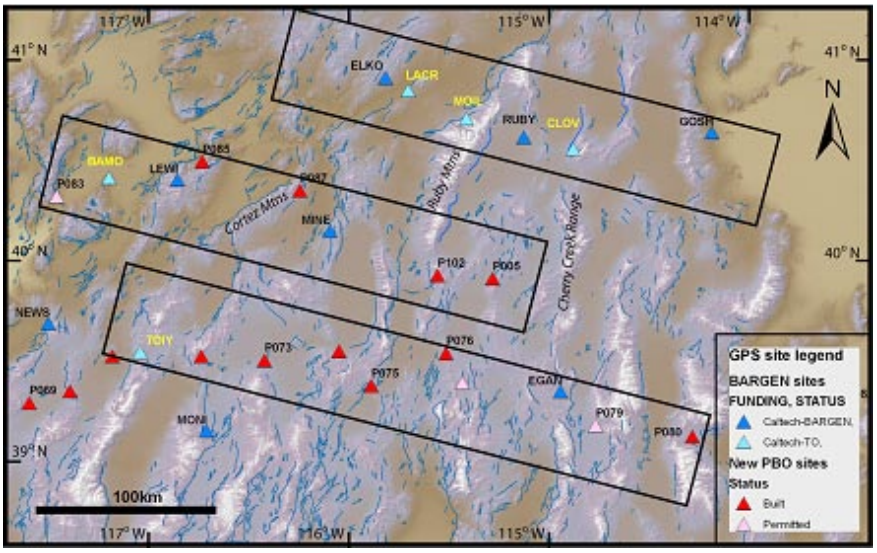

Map near Elko, NV showing Caltech and PBO continuous GPS sites.

The Nevada GPS project represents a strategic augmentation of planned Earthscope continuous GPS sites in the Basin and Range, with the objective of producing dense enough coverage to observe and model apparent migratory strain in north-central and eastern Nevada. This region of the Basin and Range forms a boundary zone between accelerating sites in the western Basin and Range and non-accelerating sites to the east (Davis et al., 2006). These large-aperture observations over the last decade are the first to suggest efficient anelastic energy transfer at the subcontinental scale across a deforming plate boundary zone at human timescale. This anelastic energy transfer is in turn is likely to be a major control on the seismic cycle and rheological properties of the lithosphere.

The original BARGEN network (begun in 1996) included site spacing across central Nevada of about 80 km (Figure 1A). The network measured significant (1-2 mm/yr) velocity variations for sites near latitude 40°N. This result is surprising because overall this part of Nevada is not systematically deforming (red curve, Figure 1B). The simplest hypothesis to explain these variations is rapid, transient creep on the deep portions of Basin and Range normal faults in the area. Calculations of surface deformation due to deep crustal creep on a Basin and Range fault (Figure 1C) show that at 80 km spacing we are sampling at less than half the Nyquist frequency for the waveforms predicted by fault creep at depth. With the strategic augmentation of new Caltech Tectonics Observatory continuous GPS sites and sites from EarthScope's PBO, we will have about 14 sites at ~40 km spacing covering the geodetically complex region of contractile and extensional strain near BARGEN sites TUNG, LEWI, MINE, ELKO, RUBY, and GOSH. These stations form en echelon arrays oriented at right angles to the major normal faults in the region. With this station spacing, we will be able to identify and test physical models that might explain such waveforms. With the high velocity accuracy we expect after about two years, the GPS data will rigorously limit the range of possible models.

Davis, J.L., Wernicke, B.P., Bisnath, S., Niemi, N.A., Elosequi, P., 2006, Subcontinental-scale Transient Deformation along Pacific-N. America Boundary, Nature 441: 1131-1134.

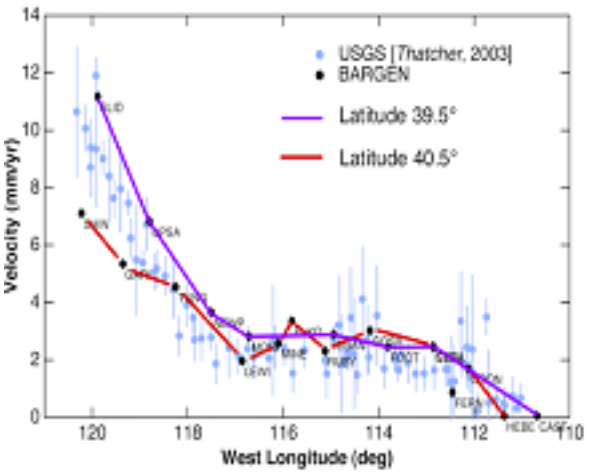

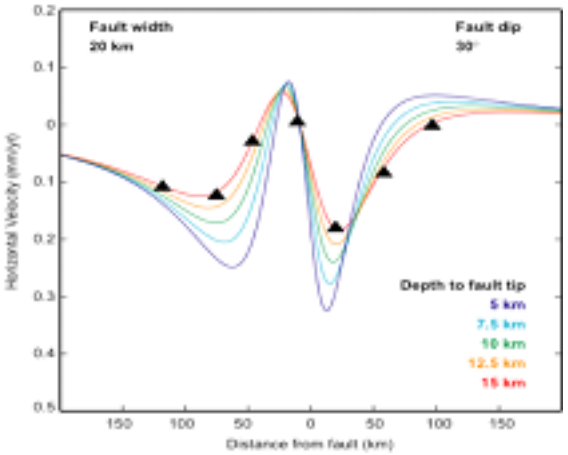

Top: West velocities as a function of longitude.

Bottom: Model calculations of surface deformation for creeping mid-crustal normal faults, showing prediction velocities of red curve for 40-km station spacing (black triangles).

ON THE ORIGIN, CONCENTRATION AND SPATIAL DISTRIBUTION OF GASES AT SEISMOGENIC DEPTHS

Thomas Wiersberg, Jörg Erzinger • GeoForschungsZentrum Potsdam, Germany

Studies on the geochemistry of gases at seismogeinic depths of the SAF by monitoring, sampling, and analyzing gases extracted from returning drill mud were very successful and revealed a wealth of data [Erzinger et al., 2004; Wiersberg and Erzinger, 2007; Wiersberg and Erzinger, subm.]. The most abundant gases at seismogenic depths are CO2, hydrocarbons, and hydrogen, from which CO2 and hydrocarbons are clearly derived from a nearby organic-rich strata, whereas hydrogen is probably due to mechanochemical reaction of fresh mineral surfaces generated by tectonic forces. The distinct composition of mud gas on both sites of the fault as well as the helium isotope composition imply the presence of two distinct fluid regimes, separated by a low-permeable fault core. The low contribution of mantle-derived helium (max. 6% on the Pacific Plate and max 12% on the North American Plate, respectively) shows that the SAF intersect by SAFOD plays only a minor role as conduit for fluids from the mantle at the time of drilling.

However, some key aspects addressed to the role of fluids and gases at the SAF cannot be resolved by mud gas analysis alone. In particular, mud gas monitoring cannot reveal quantitative data on the concentrations of gases entering the borehole at depth. Such data, in combination with data on the permeability and porosity of the host rocks, are essential to quantify the fluid flow at fault core in time and space. Furthermore, interpretation of drill mud gas is restriced to gases low abundant in air, because the drill mud always contains a high contribution of atmospheric gases, such as N2 or Ar, which hampers the identification of these gases from a different than atmospheric source. At present, there is a lack of information regarding these gases. For the Phase 3 of SAFOD, we propose on-line monitoring of drill mud gas and in addition on-site gas extraction and analysis of newly drilled core samples from both seismogenic and creeping fault sections. In order to interpret gas data and to understand the regional fluid systems better, we need long-term monitoring data of in situ fluid pressure and seismicity of both the fault core and fault margins.

Erzinger, J., T. Wiersberg, and E. Dahms (2004), Real-time mud gas logging during drilling of the SAFOD Pilot Hole in Parkfield, CA, Geophys. Res. Lett., 31, L15S18, doi:10.1029/2003GL019395.

Wiersberg, T., and J. Erzinger (2007), A helium isotope cross-section study through the San Andreas Fault at seismogenic depths, Geochem. Geophys. Geosyst., 8, Q01002, doi:10.1029/2006GC001388.

Wiersberg, T., and J. Erzinger, On the origin and spatial distribution of gas at seismogenic depths of the San Andreas Fault from drill mud gas analysis, submitted to Applied Geochemistry.

Funding for this project is provided by the Deutsche Forschungsgemeinschaft (grant ER 123/14 & 17, ICDP priority program) and the GeoForschungsZentrum Potsdam. We thank SAFOD PIs Steve Hickman, Mark Zoback, and Bill Ellsworth for their valuable help and assistance while conducting this project.

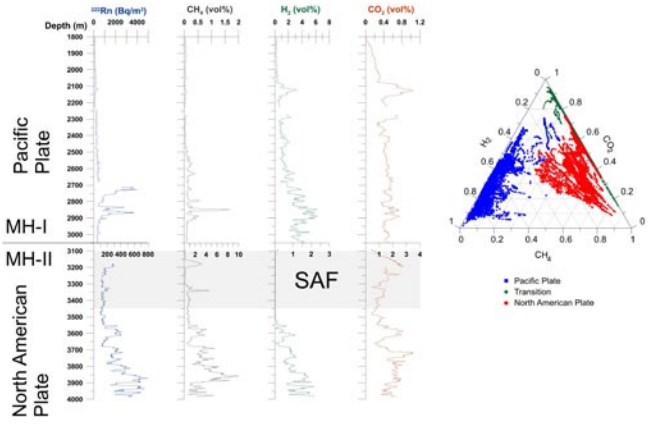

Down hole distribution of mud gas composition in SAFOD Main Hole

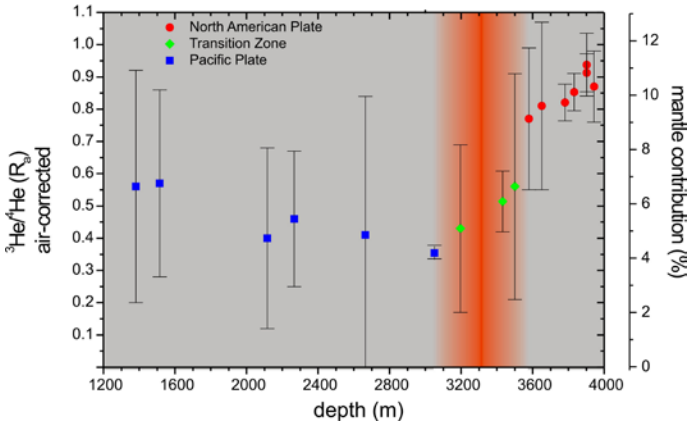

Air-corrected helium isotope composition vs. borehole depth (SAFOD Main Hole).

SEISMIC TRAVEL TIMES AND ATTENUATION MEASUREMENTS: AN EARTHSCOPE DATA PRODUCT

Michael Wysession • Washington University

A project is underway to provide a (1) USArray seismic database of attenuation measurements and attenuation-corrected cross-correlated travel times for major seismic body wave phases, and (2) 3-D attenuation tomograms of the sub-North America mantle. These will constitute EarthScope data products that will be used by other geophysicists in developing other EarthScope products at both the data and knowledge levels.

An important part of the goals of EarthScope involve an understanding of the structure, composition, temperature and dynamics of the earth beneath North America. Seismic imaging will play an important part in achieving this understanding. This project involves the creation of a standardized, normalized, complete dataset of the travel times and attenuation measurements from all USArray stations for major earthquakes during its deployment. A vital part of the analysis involves the determination of differential attenuation between different seismic phases on the same seismogram, which in turn leads to much more accurate cross-correlation measurements of the differential travel times between these seismic phases. Because measurements are made separately for SH and SV phases, this database also provides the basis for investigations of anisotropic earth structure. The development of 3D mantle models of seismic attenuation beneath the North American USArray seismic stations will be of great help in addressing many geophysical questions including the structure of the asthenosphere, the temperature and composition of the mantle (including the presence of water), and the manner of subduction of the Farallon slab beneath North America.

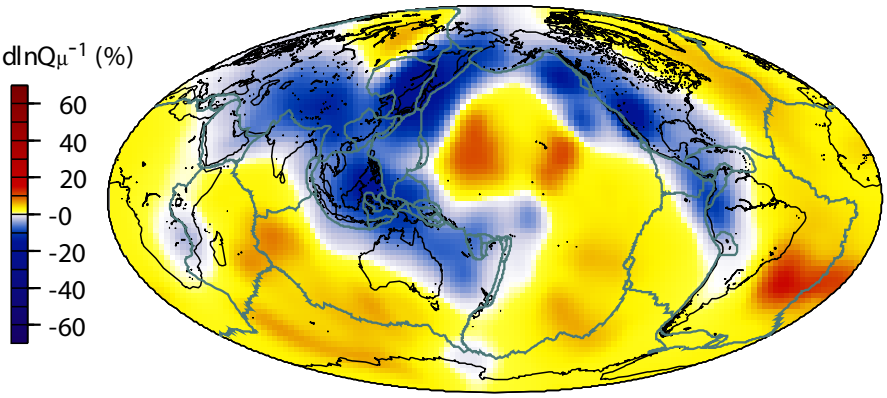

A map of the shear-wave attenuation anomalies (shown as anomalous Q values) at a depth of 2000 kilometers in the mantle [Lawrence and Wysession, 2006b]. The inclusion of EarthScope data will significantly improve the resolution beneath North America and allow for a high-resolution regional tomographic mapping of both S- and P-wave attenuation crust-to-core.

Based upon the report of the Workshop on Data Products for Education and Research from the USArray (Portland, OR, October, 2004), attenuation measurements and tomograms as well as cross-correlation travel times are important Level 3 (to be carried out by PI-driven grants) data products, and they provide an important foundation for Level 4 (knowledge-based) data products. For instance, knowledge of attenuation with distance is critical for a number of applications, from the estimation of ML to prediction of peak ground acceleration for ANSS products such as ShakeMap. In addition, the inclusion of many different seismic phases into tomographic inversions and other types of seismic modeling will greatly enhance our understanding of the structure of North America, crust-to-core: images will have greater resolution and accuracy. This increase in quality of our geophysical modeling will carry down to better research by other earth scientists, and better educational products for classrooms and public arenas.

The algorithms used for the generation of the differential velocity and attenuation data for the examination of structure beneath North America have been developed over a series of studies [Wysession et al., 1994; Fisher et al., 2003; Lawrence and Wysession, 2006a,b]. The current project using EarthScope data can be seen as an extension of the study of whole-mantle attenuation tomography developed in Lawrence and Wysession [2006b], which is shown with an example in the accompanying figure.

Wysession, M. E., L. Bartkó, and J. Wilson, Mapping the lowermost mantle using core-reflected shear waves, J. Geophys. Res., 99, 13,667-13,684, 1994.

Fisher, J. L., M. E. Wysession, K. M. Fischer, Small-scale lateral variations in D" attenuation and velocity structure, Geophys. Res. Lett., 30,10.1029/2002GL016179, 26 April 2003.

Lawrence, J. F., and M. E. Wysession, QLM9: A new radial quality factor (Q) model for the mantle, Earth Planet. Sci. Lett., 241, 962-971, 2006a.

Lawrence, J. F., and M. E. Wysession, Seismic evidence for subduction-transported water in the lower mantle, in Earth's Deep-Water Cycle, AGU Monograph, 251-261, 2006b.

AMBIENT NOISE AND TELESEISMIC TOMOGRAPHY TO INFER THE PHYSICAL STATE AND STRUCTURE OF THE CRUST AND UPPER MANTLE IN THE WESTERN US

Yingjie Yang, Michael Ritzwoller, Morgan Moschetti • University of Colorado at Boulder
Donald Forsyth • Brown University

In this study, we apply two powerful new complementary methods of surface wave tomography to infer the physical state and structure of the crust and upper mantle in the western US using seismic data predominantly from the Transportable Array (TA) component of EarthScope/USArray. The two methods are ambient noise tomography and two-plane wave teleseismic tomography. Ambient noise tomography (ANT) is based on the extraction of surface-wave Green functions by cross-correlating long sequences of ambient or background seismic noise. Two plane-wave tomography (TPWT) interprets the variation in amplitude and phase of teleseismic surface waves observed across a regional seismic array in terms of phase velocity variations within the foot-print of the array and, importantly, also models corrugations in the incoming wavefield caused by scattering that occurs between the earthquake and array. Both methods measure surface wave dispersion, but in complementary period bands: ANT (6 - 40 sec) and TPWT (25 - 150 sec). Used in combination, the methods are able to produce dispersion curves across the entire western US from about 6 sec to 150 sec period on a 25-50 km geographic grid.

We compare phase velocity maps at overlapped periods from the two methods, and find phase velocity is similar for both methods. We performed a preliminary 3-D shear velocity inversion using the combined phase velocity dispersion results at

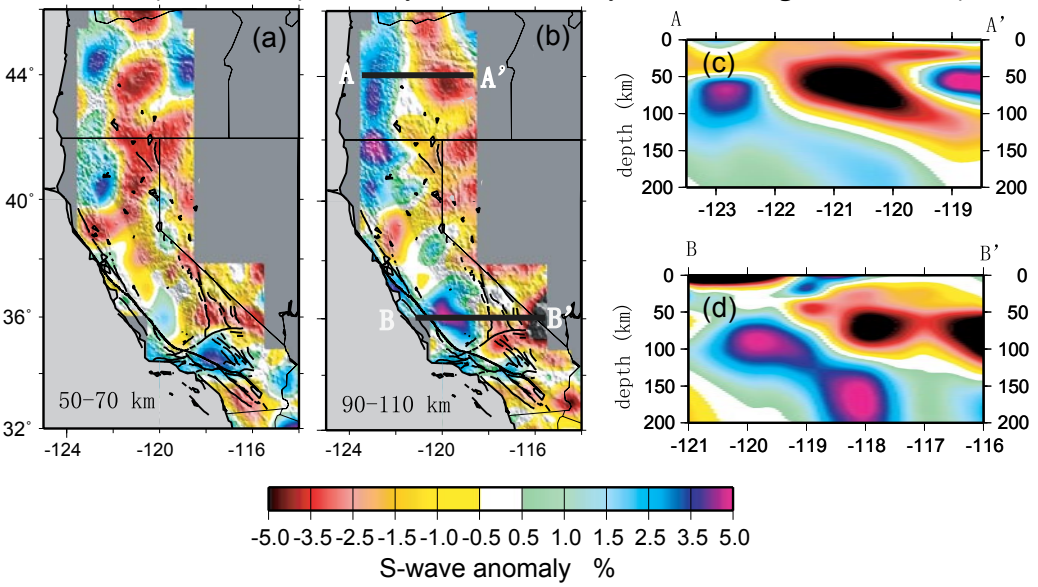

Example model slices from a preliminary joint inversion of phase velocities obtained from ambient noise and two-plane wave tomography. (a) and (b) Horizontal slices in the upper mantle at about 60 km and 100 km depth, respectively. (c) and (d) Vertical east-west oriented profiles across (A-A') the Cascades in central Oregon and (B-B') the Great Valley and the southern Sierra Nevada Mountains in south-central California.

periods from 6 sec to 150 sec to obtain a high-resolution shear velocity model from the surface to 200 km depth in the western US. The model possesses a wealth of velocity features. We touch on only three examples here. (1) The high velocity slab subducting beneath the Cascades in northern California and Oregon is seen in the vertical cross-section A-A' shown in Figure 1c overlain by a low velocity upper mantle wedge. The slab initiates in the south near the Mendocino transform. (2) In the uppermost mantle in south-central California, there is a low velocity anomaly beneath the eastern edge of the southern Sierra Nevada and the adjoining Walker Lane region. The vertical cross-section B-B' shows that this anomaly is directly underlain by a high velocity anomaly which may or may not be connected to a shallower high velocity anomaly beneath the southern Central Valley. (3) The well know high velocity anomaly associated with downwelling lithosphere beneath the Transverse Range is also clearly visible.

Yang, Yingjie, Ritzwoller, M.H, Moschetti, M. P., Forsyth D.W (2006), High-resolution 3-D shear velocity model of the crust and upper mantle beneath southern California: surface wave tomography combining ambient seismic noise and teleseismic data, Eos Trans. AGU, 87(52), Fall Meet. Suppl., Abstract S43A-1364.

Yang, Y., and D.W. Forsyth, Rayleigh wave phase velocities, small-scale convection and azimuthal anisotropy beneath southern California, J. Geophys. Res., 111, B07306, doi:10.1029/2005JB004180, 2006

Moschetti, M.P., M.H. Ritzwoller, and N.M. Shapiro, Ambient noise tomography from the first two years of the USArray Transportable Array: Group speeds in the western US, submitted to Geophys. Res. Lett.

TESTING THE FIVE SIMPLEST UPPER MANTLE ANISOTROPIC VELOCITY PARAMETERIZATIONS USING TELESEISMIC S AND SKS DATA FROM THE BILLINGS, MONTANA PASSCAL ARRAY

Huaiyu Yuan, Ken Dueker, Derek Schutt • University of Wyoming

The five simplest parameterizations of upper mantle anisotropy are tested and ranked by the F-test to determine model significance. These five hexagonal symmetry anisotropy models are: a single layer with a horizontal fast velocity axis (FVA), a single layer with a dipping FVA, two layers with a horizontal FVA, two layers with one dipping and one flat FVA, and two layers with dipping FVA. These five velocity models are fit to data from a 30 broad-band station array that operated around Billings, Montana for ten months. This array recorded fifteen high quality direct S and SKS arrivals whose recordings across the array are stacked to provide accurate waveforms and error estimates to model. Source normalization is accomplished using the cross-convolution technique. The stack traces are fit to the five anisotropic model parameterizations using the Neighborhood Algorithm to map the posteriori model probability density (PPD) volume. The F-test shows that the two models which do not permit a dipping FVA can be rejected at >91% confidence. The best model is a two layer dipping FVA parameterization, albeit the two layer model with one flat and one dipping FVA can only be rejected at 68% confidence. The 2-D marginal PPD for most of our models are compact and show little model parameter correlation. The best model (Figure 1) has an upper layer with a N13°W FVA strike and a 47° FVA dip and a lower layer with a N65°E FVA strike and a 12° dip down to the southwest. The N13°W FVA strike of the upper (lithospheric) layer is broadly consistent with the FVA strike found by several other studies [Currie, et al., 2004 ; Fox and Sheehan, 2005; Marone and Romanowicz, 2006], and is readily interpreted as fossil fabric in the lithosphere. The bottom (asthenospheric) layer FVA strike is parallel to North American absolute plate motion and the dip is opposite of that predicted for a quiescent asthenosphere [Bokelmann, 2002]. Comparison of the PPD modeling of a SKS-only dataset with respect to the full-dataset PPD shows that the direct S waves improve resolution of the anisotropic model parameters.

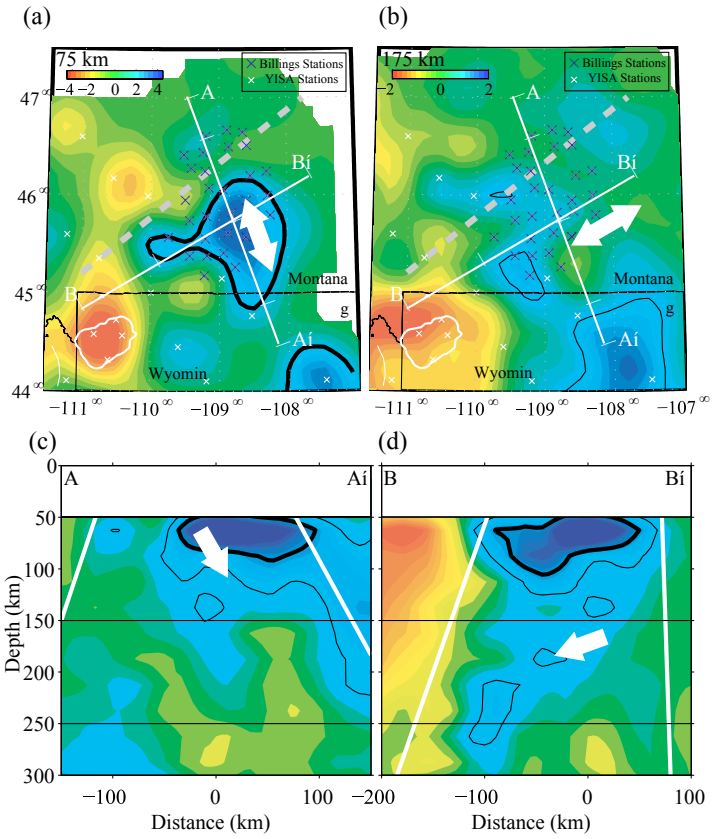

Correlation of our best model P5 and P-wave tomographic results of Yuan and Dueker [2005]. (a) Map views at the 75 km. The percent P-wave velocity perturbation is color-coded. The thick black lines contour the 2% velocity perturbation. The white contour denotes the Yellowstone Caldera. Gray dash line approximates the location of the Madison Mylonite zone. Thick blacks contours the 2% velocity purturbation. The two-head white arrow shows the strike of the FVA in the top layer. Two profiles shown in (c) and (d) are labeled as A-Aí and B-Bí. (b) Map view at 175 km. Thin blacks contours the 1% velocity perturbation. (c) Profile view along A-Aí. The white arrow shows the FVA dip in the top layer. Two thick white straight lines show approximately the extent of the SKS and S ray paths. (d) Profile view along B-Bí. The white arrow shows the FVA dip in the bottom layer.

Bokelmann, G. H. R. (2002), What forces drive North America?, Geology, 30, 1027-1030.

Currie, C., et al. (2004), Shear wave anisotropy beneath the Cascadia subduction zone and western North American craton, Geophys. J. Int., 157, 341-353.

Fox, O., and A. F. Sheehan (2005), Shear wave splitting beneath the CDROM transects, in The Rocky Mountain region--an evolving lithosphere: tectonics, geochemistry, and geophysics, edited by G. Randy and K. E. Karlstrom, American Geophysical Union, Washington DC.

Marone, F., and B. Romanowicz (2006), On the depth distribution of azimuthal anisotropy in the continental upper mantle, submitted to Nature.

SEISMIC IMAGING OF SOUTHERN CALIFORNIAN CRUST USING DEFORMABLE-LAYER TOMOGRAPHY AND PRESTACK DEPTH MIGRATION: INNOVATIVE APPLICATIONS FOR EARTHSCOPE/USARRAY PROJECTS

Hua-wei Zhou, Michael Thornton, Li Li, Chris Gantela, Tom Bjorklund • University of Houston

To better understand the crustal structure and geodynamics of southern California, we are applying new subsurface imaging methods to map the regional 3D crustal velocity structure and major reflection events across the San Andres fault system. The data for this study include earthquake readings compiled by the Southern California Earthquake Center (SCEC) and seismic reflection records from the Los Angeles Regional Seismic Experiment (LARSE). We are using deformable-layer tomography to directly map the geometry of P-wave and S-wave velocity discontinuities in the crust and uppermost mantle, which are constrained by independently-derived crustal thickness variations. We have also applied an advanced wave equation prestack depth migration technology to develop new reflection images for the LARSE profiles.

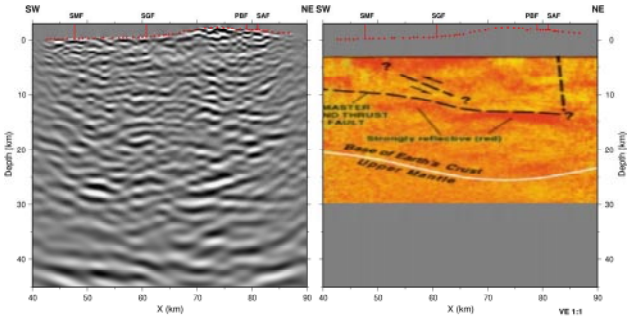

Comparison between (Left) prestack depth migration (Thornton and Zhou, 2007) and (Right) stacked image with interpretations (Henyey et al., 1999) of 1994 LARSE I profile. Red dots along the surface denote LARSE II shots. Faults are: Sierra Madre (SMF), San Gabriel (SGF), and San Andreas (SAF).

ously published analyses of LARSE data, the LARSE reflection images from this study indicate that prestack depth migration can better treat lateral velocity variations in the shallow crust and improve the resolution of reflection events. Our results suggest that prestack depth imaging is much better than simple CMP stack techniques to process 2D seismic data in the presence of high noise level, strong lateral velocity heterogeneity and crooked survey geometry. The innovative seismic imaging techniques from this study are directly applicable to EarthScope/USArray projects planned to study the structure of the crust and mantle.

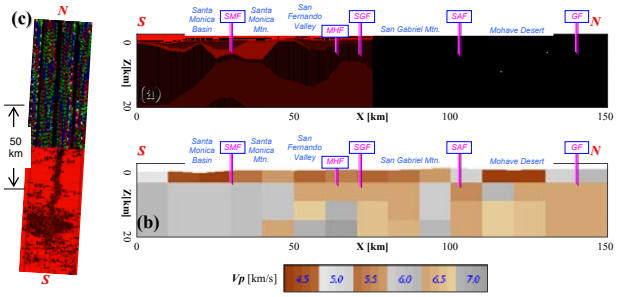

Comparison between cross sections of: (a) deformable-layer tomography and (b) cell tomography along 1999 LARSE II profile. These tomography models were based on the same P-wave arrivals from local earthquakes and the LARSE II profile. Faults (pink) are: Sierra Madre (SMF), Mission Hills (MHF), San Gabriel (SGF), San Andreas (SAF), and Garlock (GF). (c) Map showing earthquakes (purple crosses), stations (green triangles), LARSE II shots (red circles) and LARSE receivers (black triangles).

The preliminary results from this analysis indicate that deformable-layer tomography produces sharper vertical resolution of velocity discontinuities and realistic representations of lens-shaped geologic features such as the edges of basins and lithologic pinchouts, which cannot be achieved by fixed-in-space mesh grids with conventional tomography. Compared to previ-

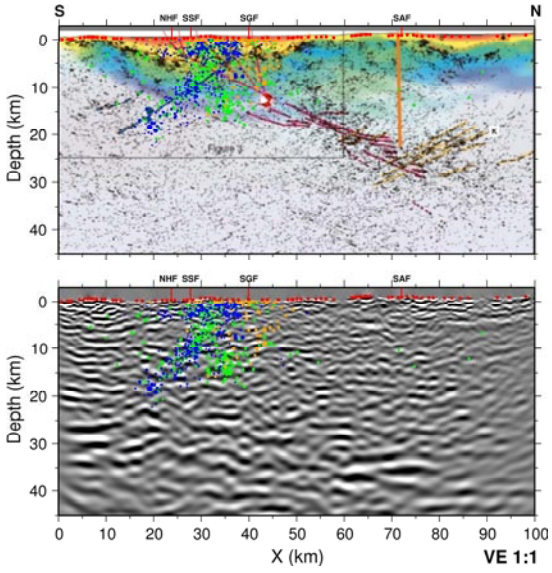

Comparison between (Upper) stacked image with interpretations and tomographic velocities in color (Fuis et al., 2003) and (Lower) prestack depth migration (Thornton and Zhou, 2007) of 1999 LARSE II profile. Red dots along the surface denote LARSE II shots, other color dots are earthquake foci. Faults are: Northridge Hills (NNF), Santa Susana (SSF), San Gabriel (SGF), and San Andreas (SAF).